

# **Regulation of Microtubule Dynamics by Protein Interaction Networks at Microtubule Tips**

**Babet van der Vaart**

© B. van der Vaart

This thesis was printed by CPI-Wörhmann Print Service, Zutphen

The research presented in this thesis was performed at the Department of Cell Biology of the Erasmus Medical Center in Rotterdam, The Netherlands.

This research was supported by the Netherlands Organization for Scientific Research ALW open program and ALW-VICI grants.

Cover: Geometric shape representing an interaction network surrounding a plus

# **Regulation of Microtubule Dynamics by Protein Interaction Networks at Microtubule Tips**

**Regulatie van microtubuli dynamiek door eiwit interactie netwerken op microtubuli uiteinden**

**Proefschrift**

ter verkrijging van de graad van doctor aan de  
Erasmus Universiteit Rotterdam op gezag van de  
rector magnificus

Prof.dr. H.G. Schmidt

en volgens besluit van het College voor Promoties

De openbare verdediging zal plaatsvinden op  
woensdag 8 juni 2011 om 13:30 uur

door

**Babet van der Vaart**  
geboren te Vlaardingen



**Promotiecommissie:**

Promotoren: Prof.dr. F. G. Grosveld  
Prof.dr. A. Akhmanova

Overige leden: Prof.dr. C.C. Hoogenraad  
Dr.ir. N.J. Galjart  
Dr. M.O. Steinmetz



<b>Scope of this thesis</b>	<b>7</b>
<b>Chapter 1. Introduction: Regulation of microtubule dynamic instability</b> <i>Biochemical Society Transactions. 2009 Oct;37(Pt 5):1007-13.</i>	<b>11</b>
<b>Chapter 2. STIM1 is a MT-plus-end tracking protein involved in remodelling of the ER</b> <i>Current Biology. 2008 18:177-82</i>	<b>21</b>
<b>Chapter 3. SLAIN2 links microtubule plus-end tracking proteins and controls microtubule growth in interphase</b> <i>The Journal of Cell Biology. 2011</i>	<b>37</b>
<b>Chapter 4. Microtubule plus-end tracking proteins SLAIN1/2 and ch-TOG promote neurite outgrowth</b> <i>Manuscript in preparation</i>	<b>75</b>
<b>Chapter 5. Regulation of microtubule dynamics by a liprin-<math>\alpha</math>1/<math>\beta</math>1-mediated cortical attachment complex of KANK2 and KIF21A</b> <i>Manuscript in preparation</i>	<b>91</b>
<b>Chapter 6. General Discussion: Building protein interaction networks at microtubule tips</b>	<b>119</b>
<b>Summary</b>	<b>143</b>
<b>Samenvatting</b>	<b>147</b>
<b>Portfolio</b>	<b>151</b>
<b>Curriculum vitae</b>	<b>155</b>
<b>Publications</b>	<b>159</b>
<b>Dankwoord</b>	<b>163</b>

## **Scope of this thesis**

Microtubules are cytoskeletal filaments, which play essential roles in cell division, morphology, migration and organization of intracellular organelles. Many of these functions are regulated by the association of microtubule plus ends with a group of structurally diverse and unrelated proteins - the microtubule plus-end tracking proteins (+TIPs). This thesis describes how +TIPs influence microtubule dynamics, how the assembly of interaction networks from a large number of +TIPs at the relatively small MT end is regulated both in space and time, and how this contributes to the cellular functions. In addition, this thesis addresses the identification and characterization of proteins that control local microtubule dynamics at the cell cortex.

**Chapter 1** introduces the key players in the field of microtubule dynamic instability.

**Chapter 2** describes the role of the transmembrane protein STIM1 in the remodelling of the endoplasmic reticulum through its interaction with microtubule tips.

**Chapter 3** describes in detail the function of SLAIN proteins in the formation of +TIP networks and in regulation of microtubule dynamics by interacting with the microtubule polymerase ch-TOG.

**Chapter 4** reports on the role of the microtubule tip-associated complex of SLAIN and ch-TOG in regulation of neurite extension in primary cultures of rat hippocampal neurons.

**Chapter 5** focuses on newly identified cell cortex-associated members of the microtubule tip attachment complex. This chapter also provides new molecular insights into the role of KIF21A in CFEOM1 syndrome.

**Chapter 6** discusses the experimental data presented in the previous chapters and their implications for future research.







# Chapter 1

## **Introduction: Regulation of microtubule dynamic instability**

Babet van der Vaart, Anna Akhmanova and Anne Straub

*Biochemical Society Transactions. 2009 Oct;37(Pt 5):1007-13.*





# Regulation of microtubule dynamic instability

Babet van der Vaart\*, Anna Akhmanova\* and Anne Straube†<sup>1</sup>

\*Department of Cell Biology, Erasmus Medical Center, 3000 CA Rotterdam, The Netherlands, and †Cytoskeletal Organization Laboratory, Marie Curie Research Institute, Oxted RH8 0TL, U.K.

## Abstract

Proper regulation of MT (microtubule) dynamics is essential for various vital processes, including the segregation of chromosomes, directional cell migration and differentiation. MT assembly and disassembly is modulated by a complex network of intracellular factors that co-operate or antagonize each other, are highly regulated in space and time and are thus attuned to the cell cycle and differentiation processes. While we only begin to appreciate how the concerted action of MT stabilizers and destabilizers shapes different MT patterns, a clear picture of how individual factors affect the MT structure is emerging. In this paper, we review the current knowledge about proteins that modulate MT dynamic instability.

## Introduction

MTs (microtubules) form a cytoplasmic network composed of hollow tubes that assemble from  $\alpha/\beta$ -tubulin heterodimers. Due to the polarized nature of the tubulin dimer, the generated MT is also polarized:  $\beta$ -tubulin is exposed at the plus end, whereas the  $\alpha$ -subunit is exposed at the minus end. MTs are dynamic and can rapidly switch between phases of growth and shrinkage, a process called dynamic instability [1]. MTs play an essential role in separating sister chromatids during mitosis and have multiple functions in non-dividing cells, for example in intracellular transport, positioning of intracellular organelles, cell migration and differentiation [2]. All these processes require the organization of MTs into arrays with different geometry and density, which depends on the generation of new MTs as well as on the proper regulation of their dynamic behaviour. New MT ends can be formed by two main types of mechanisms: *de novo* MT nucleation [3] and mechanical or enzymatic breakage of pre-existing MTs. The latter mechanism depends on severing proteins such as spastin and katanin, the AAA (ATPase associated with various cellular activities) family ATPases that use ATP as a source of energy necessary for their action ([4] and references therein).

Free MT ends can elongate or shorten, and even mild suppression of MT dynamics by low doses of MT-stabilizing or -destabilizing drugs has a profound effect on the organization of the mitotic apparatus, directional migration and even synaptogenesis in neuronal cells [5–7]. Cells express an arsenal of MT-modulating factors, some of which promote assembly [such as XMAP215 (*Xenopus* microtubule-associated protein 215)] or disassembly [kinesin-13s and stathmin/SCG10 (superior cervical ganglion-10 protein) proteins], while others have more specific roles only on a subset of MTs. In the

present review, we summarize the current knowledge about factors modulating MT dynamic instability (see Figure 1).

MT dynamics is determined largely by four parameters: (i) the speed of MT growth, (ii) the speed of MT shrinkage, (iii) the frequency of catastrophes (transitions from growth to shrinkage phase) and (iv) the frequency of rescues (transitions from shrinkage to growth phase) [8]. In addition, MT pausing can be frequently observed in animal cells. It is unclear whether pauses represent a truly undynamic and thus stable state or whether they are phases of growth and shrinkage that occur at either a very low speed or with very high transition frequencies that cannot be resolved spatially and/or temporally with the current imaging technologies. Owing to uncertainties in pause definition, the data on pauses obtained in different studies are difficult to compare and will not be discussed here.

Purified tubulin can self-assemble under certain conditions to form MT filaments that exhibit dynamic behaviour at both ends [9]. However, in intact cells and cell extracts, MT plus ends assemble and disassemble at much higher speeds than *in vitro* at the same tubulin concentration [10]. In contrast, although MT minus ends show dynamic instability, albeit at a lower rate than the plus ends *in vitro*, they are usually capped and anchored at MT organizing centres in cells. Even in specialized cell types where minus ends are free (such as most of the lamellar MTs in migrating epithelial cells [11]), growth at the minus end has never been reported (reviewed in [12]). Capping of MT minus ends requires specialized factors such as  $\gamma$ -tubulin and the components of the  $\gamma$ -TuRC ( $\gamma$ -tubulin ring complex), and anchoring at centrosomal or non-centrosomal sites involves ninein and/or Nezhha [13–15]. However, MT minus ends can serve as sites of depolymerization in cells; their shrinkage often being regulated by the same factors that also affect plus end dynamics.

MT dynamics-modulating factors can largely be divided into MT-stabilizing and -destabilizing factors. MTs are stabilized in several ways: (i) by preventing catastrophe (this ensures MT growth persistency or prolonged interaction with target sites), (ii) by rescuing a depolymerizing MT and

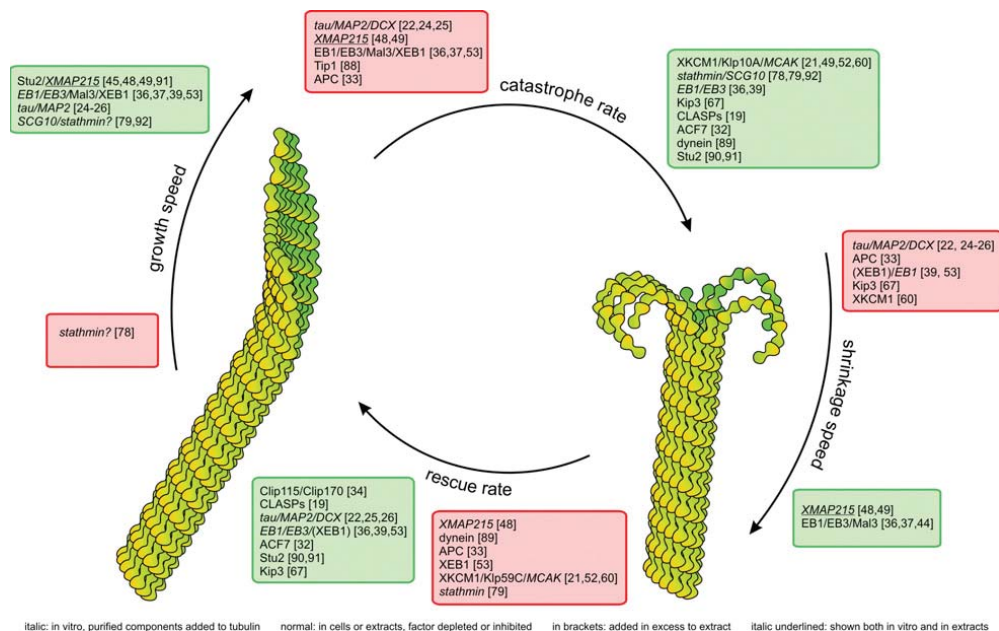
**Key words:** dynamic instability, kinesin-13, microtubule-associated protein, microtubule dynamics, microtubule assembly and disassembly regulation, tau protein.

**Abbreviations used:** CLIP, cytoplasmic linker protein; EB, end-binding protein; MCAK, mitotic centromere-associated kinesin; MAP, microtubule-associated protein; MT, microtubule; SCG10, superior cervical ganglion-10 protein; +TIP, MT plus-end tracking protein; XKCM1, *Xenopus* kinesin catastrophe modulator-1; XMAP215, *Xenopus* microtubule-associated protein 215.

<sup>1</sup>To whom correspondence should be addressed (email a.straube@mcri.ac.uk).

**Figure 1 | Factors that modulate parameters of MT dynamic instability**

MT stability can be described by four parameters: speed of growth and shrinkage and frequency of transitions (catastrophe and rescue rate). Different MT-modulating factors affect distinct parameters either positively, hence increasing the frequency or speed (green boxes), or negatively, suppressing transitions or reducing the speed (red boxes). Factors that were shown to affect certain parameters directly on purified tubulin *in vitro* are shown in italic. Where activity shown was based on phenotypes resulting after depletion or inhibition of factors in complex extracts or cells, factors are shown in normal font. If the activity could be demonstrated in extracts as well as *in vitro*, factors are shown in italic and underlined. If the effect was only apparent when a factor was added in excess to extracts, it is shown in round brackets). Supporting data can be found in the references indicated (square brackets).



thereby decreasing shortening phases, or (iii) by decreasing shrinkage speeds. Likewise, MTs are destabilized by inducing catastrophes, preventing rescues or increasing shrinkage speeds. MT growth rate also has an effect on MT stability: increase of MT polymerization efficiency can increase the amount of MT polymer, and growth-promoting factors are often associated with MT stability. However, more rapid MT growth can also increase the frequency of catastrophes because MTs reach the cell border more rapidly. We only start to understand the mechanisms underlying these dynamic parameter changes. Assembly and disassembly rates can be modulated by catalytic activity that stabilizes a transition state of tubulin heterodimer addition/release, a strategy XMAP215 seems to apply [16]. Other proteins modify the conformation of tubulin heterodimers and introduce kinks that favour MT depolymerization and thus induce catastrophes, mechanisms that kinesin-13s and stathmin appear to employ [17,18]. Finally, changing the concentration of available tubulin heterodimers has an impact on growth speed and persistence. Thus MT destabilization due to a

loss of MT-stabilizing factors can increase the free tubulin concentration and raise MT polymerization rate [19]. On the other hand, proteins that sequester tubulin heterodimers (such as stathmin and kinesin-13s) can reduce available subunits and limit polymerization efficiency [20,21].

## Regulating MT assembly

Structural MAPs (MT-associated proteins) such as tau protein, MAP2, MAP4 and DCX (doublecortin) decorate the MT lattice and stabilize it [22,23]. They strongly suppress catastrophes, but also promote growth and reduce shrinkage speeds [23–26]. Tau protein can antagonize the MT-destabilizing activity of XKCM1 (Xenopus kinesin catastrophe modulator-1) [27] and can also protect MTs against katanin-dependent severing [28]. The phosphorylation status of MAPs such as tau protein is crucial for their function, because phosphorylation causes their dissociation from the lattice, making the MT accessible to severing activity or MT shrinkage [29].

**Table 1** | MT stabilizers of the ch-TOG/XMAP215 family

Organism	Name	Description
Mammals	Ch-TOG/CKAP5	Colonic and hepatic tumour overexpressed/cytoskeleton-associated protein 5
Frog	XMAP215	<i>Xenopus</i> MAP of 215 kDa
Fruitfly	Msp5	Mini-spindles
Nematode worm	ZYG-9	Zygote defective 9
Plant ( <i>Arabidopsis</i> )	MOR1	Microtubule organization 1
Budding yeast	Stu2p	Suppressor of tubulin 2
Fission yeast	Dis1p/Alp14p	Distorted trichomes 1/altered growth polarity protein 14
Slime mould	Ddcp224	<i>Dictyostelium discoideum</i> centrosomal protein of 224 kDa

A particular class of MAPs is the +TIPs (MT plus-end tracking proteins). This is a group of evolutionarily unrelated proteins that share the ability to specifically bind to growing MT plus ends [30]. Association of +TIPs with the MT end can greatly influence MT dynamics. Many +TIPs have been implicated in stabilizing MTs by connecting them to the cell cortex (reviewed in [31]). For instance, CLASPs (cytoplasmic linker protein-associated proteins) and ACF7 (ATP-dependent chromatin assembly and remodelling factor 7) act as MT rescue and stabilizing factors at the cell cortex [19,32], whereas APC (adenomatous polyposis coli) reduces catastrophes at a subset of MTs in cellular protrusions [33]. Both of these strategies stabilize specifically those MTs that reach certain cortical domains. CLIPs (cytoplasmic linker proteins) act as cytosolic rescue factors [19,34]; the mechanism underlying their activity is enigmatic, since they preferentially associate with growing rather than depolymerizing MTs. An intriguing possibility is that the action of CLIPs and other rescue factors could be related to GTP-tubulin remnants, which are small MT lattice regions with incomplete GTP hydrolysis that were recently implicated in rescue events [35].

In addition, EB (end-binding) 1, EB3 and the fission yeast homologue Mal3 allow persistent MT growth in cells by preventing catastrophes [36,37]. EB proteins directly and autonomously interact with the tips of growing MTs [38] and it is likely that their binding coincides with the stabilization of the growing tubulin sheets [39], the lattice seam [40] or possibly even an overall effect on MT lattice structure [41]. This may not only explain how EBs prevent catastrophes, but also why EBs can increase MT growth speeds under certain conditions *in vitro* [36,39]. It should be noted that other *in vitro* studies found no effect of the EBs on MT growth rate [42,43], in line with *in vivo* observations [36,44].

The most potent protein shown to increase MT polymerization speeds is XMAP215, a widely expressed and highly conserved protein found in all eukaryotic cells (see Table 1). XMAP215 can boost the assembly by a factor of 10 *in vitro* [45]; in agreement with this observation, ZYG-9

**Table 2** | MT-destabilizing kinesins

Organism	Kinesin-13	Kinesin-8	Kinesin-14
Mammals	Kif2A, Kif2B, Kif2C/MCAK	Kif18A	
Frog	XKif2, XKCM1		
Fruitfly	Klp59C, Klp59D, Klp10A	Klp67A	Ncd
Budding yeast	-	Kip3p	Kar3p
Fission yeast	-	Klp5/Klp6	Klp2

(zygote defective 9) is the major MT growth-promoting factor in worms [46]. Stu2 as well as XMAP215 wraps round a tubulin heterodimer and facilitate its incorporation into a growing plus end [16,47]. This activity is purely catalytic and does not involve ATP hydrolysis; therefore XMAP215 can also promote the reverse reaction under conditions that favour depolymerization. Thus XMAP215 increases both growth and shrinkage rates and prevents phase transitions *in vitro* and in cell extracts [48,49]. Consistently, the *Arabidopsis* MOR1 (microtubule organization 1) promotes rapid MT growth and shrinkage [50].

Although XMAP215 is able to bind MT plus ends directly *in vitro*, *in vivo* conditions differ due to the presence of other MAPs that could regulate and/or compete with the association of XMAP215 with the MT tip. Binding to EBs, the core proteins of the +TIP complex, is often essential for +TIPs to accumulate at the MT plus end and for plus-end tracking [38,42,51,52]. An interaction between XMAP215 family members and EBs has been reported to occur in yeast and *Xenopus* egg extracts [53,54]. This interaction appears to be regulated in a cell cycle-dependent manner [53] and probably involves intermediary factors that remain to be identified. These and other observations suggest that *in vivo*, XMAP215 and its homologues might be regulated by their association with different targeting factors such as +TIPs or TACC (transforming acidic coiled-coil) proteins [55].

In mammalian cells, depletion of ch-TOG (colonic and hepatic tumour overexpressed) has a profound effect on mitotic spindle formation, whereas no strong interphase phenotypes have been reported so far [56]. This raises the question of whether there are additional factors responsible for the high MT growth rate in mammals.

## Regulating MT disassembly

MT destabilizing proteins induce MT catastrophes, inhibit polymerization and promote disassembly. The best understood and most potent MT depolymerizers are the non-motile kinesins from the kinesin-13 family, which includes three members in mammals: Kif2A, Kif2B and Kif2C/MCAK (mitotic centromere-associated kinesin) (see Table 2).

Kinesin-13s probably have both an ATP-dependent catastrophe-promoting activity and an ATP-independent tubulin-sequestration activity [21]. MCAK binds both plus and minus ends *in vitro* [57,58] and shows the highest affinity for curved protofilaments that resemble shrinking MTs [17].

Also the crystal structure of kinesin-13 motors fits best to a curved protofilament [59,60]. Thus MCAK binding to MT ends is thought to accelerate the rate of transition to catastrophe by destabilizing the lateral interaction of protofilaments. This activity requires the consumption of ATP and it was shown that MCAK is a processive depolymerase: one MCAK dimer can remove 20 tubulin subunits before detaching [58].

In somatic vertebrate cells, MCAK has no or only minor effects on the organization of interphase MT arrays [56,61]: inhibition of MCAK in PtK2 cells led to slightly increased MT stability due to a 2-fold decrease in catastrophe frequency, a 2-fold increase in rescue frequency and, surprisingly, a mild increase in shrinkage rates [61]. Another kinesin-13, Kif2A, is strongly expressed in neuronal cells [62], and the brains of *kif2a*<sup>-/-</sup> mice show multiple phenotypes, including aberrantly long axonal branching and migratory defects [63]. MTs in *kif2a*<sup>-/-</sup> cells frequently fail to stop growing after reaching the cell edge, resulting in bent and overextended MTs; this suggests that Kif2A promotes catastrophes at the cell cortex. During mitosis, different kinesin-13 family members share the workload: whereas Kif2A and Kif2B are primarily associated with the centrosome, Kif2C/MCAK predominates at the kinetochores [64,65]; therefore these proteins are likely to affect diverse MT subpopulations differently ([5] and references therein).

Differential activities of kinesin-13 may be at least in part due to association with different partners. For example, MCAK and *Drosophila* Klp10A preferentially track growing MT plus ends [52,66] through a direct interaction with EB1 [51,52]. In contrast, Kif2A and Klp59C do not bind to EB1; and Klp59C tracks depolymerizing rather than growing MT ends [52,66].

Besides kinesin-13s, members of the kinesin-8 family (see Table 2) also promote MT depolymerization in cells. Kinesin-8s, namely Kip3 and Kif18A, disassemble MTs exclusively from the plus end in a length-dependent manner, depolymerizing long MTs more efficiently than short ones. This is explained by the fact that they are motile and exhibit a slow plus-end-directed motor activity and thus use the MT as an 'antenna' to accumulate at the plus end [67–69]; the longer the MT, the more kinesin would accumulate at its end. This characteristic would enable kinesin-8s to act as a part of the MT length-control mechanism that might be important for the alignment of chromosomes at the centre of the mitotic spindle [68,69]. Loss of kinesin-8 activity results in aberrant long spindles with hyperstable MTs in various organisms [69–72].

Another kinesin family implicated in MT destabilization is kinesin-14s. The budding yeast Kar3, which forms a heterodimer with a non-motor polypeptide Cik1, has been shown to be a minus-end-directed motor and to slowly depolymerize taxol-stabilized MTs from the plus end [73]. It is thought that shortening of cortex-anchored MT plus ends by Kar3Cik1 is crucial for karyogamy during mating of budding yeast. Also the *Drosophila* kinesin-14 Ncd promotes MT shortening *in vitro* [73], and the deletion of Klp2 from fission yeast results in long spindles [74], suggesting an evolutionarily conserved

role in negatively regulating MT stability. However, the kinesin-14 homologues HSET (human spleen, embryonic tissue and testes) and XCTK2 (*Xenopus* C-terminal kinesin 2) control spindle length, but, in contrast with Klp2, spindle length positively correlates with their presence [75]. It therefore remains to be elucidated whether MT-destabilizing activity is conserved in all kinesin-14 family members.

A completely different type of a negative regulator of MT stability is Op18/stathmin. Recent structural and thermodynamic studies on the complex formed between stathmin and tubulin provide a mechanistic model of how stathmin acts on MTs (for a recent review, see [76]). Essentially, stathmin possesses two binding sites with equal affinity for tubulin heterodimers, and occupation of both binding sites leads to the ternary tubulin–stathmin complex [20,77]. Capping of  $\alpha$ -tubulin by the N-terminal domain of stathmin as well as the kinked structure of the ternary complex that is maintained by the C-terminal helical domain of stathmin prevents the incorporation of the sequestered tubulin subunits into protofilaments [18]. If stathmin were able to introduce such a bent conformation into tubulin subunits at the ends of MTs, this would explain the catastrophe-inducing activity of stathmin that has been reported in several studies [78–80]. Similarly to MCAK that is thought to depolymerize MTs via introducing protofilament curvature, stathmin is able to induce catastrophes at the plus as well as the minus ends of MTs [79].

During interphase, stathmin inactivation or depletion causes extensive MT polymerization and increased MT polymer content [80,81]. Long-term interference with stathmin levels revealed that stathmin acts as a positive and reversible regulator of tubulin expression, acting on the level of tubulin mRNA stability [81,82]. Further, there is a strong positive correlation between stathmin expression and cell proliferation (reviewed in [83]). The importance of the careful regulation of stathmin activity is illustrated by the observations that inhibition as well as overexpression of stathmin leads to mitotic arrest [84,85]. Mice lacking stathmin are viable, but show neurological defects in adults [86]. Neuronal cells express stathmin and three structurally related proteins [SCG10, SCLIP (SCG10-like protein) and RB3]. The regulation of MT dynamics by stathmin/SCG10-family destabilizers is thought to be crucial for neural development and plasticity (reviewed in [87]).

## Concluding remarks

Regulation of MT assembly and disassembly has to be tightly controlled by multiple factors. While we begin to decipher the activities of individual factors, we are still missing the picture of how these often antagonistic activities work together to generate a certain type of MT array. For example, both XMAP215 and tau protein can antagonize the MT-destabilizing activity of XKCM1. XMAP215 does this by strongly promoting assembly and counteracting the net polymer loss, whereas tau has only minor effects on the growth speed, but is very potent in suppressing the catastrophe-promoting activity of XKCM1 [27]. Also EB

proteins probably suppress catastrophes by counteracting MT destabilizers [36]. The three-component system of tubulin, XMAP215 and XKCM1 mimics physiological MT dynamics values [10], indicating that this basic set of factors could be largely responsible for MT dynamics in cells. However, in interphase vertebrate cells, neither XMAP215 nor XKCM1/MCAK was shown to play a major role in regulating MT dynamics, suggesting that another set of factors might be performing a similar function. The development of high-throughput protein depletion technologies makes it possible to identify the molecules responsible for different aspects of MT dynamic behaviour in different systems and settings. In combination with improved imaging techniques, automated image analysis and modelling, this approach should enable us to develop a comprehensive understanding of the mechanisms governing the generation of MT arrays during cell division, polarization and differentiation.

## Funding

B.v.d.V. and A.A. are supported by the Netherlands Organization for Scientific Research NWO Vici and Open programme grants. A.S. is funded by a Marie Curie Cancer Care programme grant.

## References

- Kirschner, M.W. and Mitchison, T. (1986) Microtubule dynamics. *Nature* **324**, 621
- Desai, A. and Mitchison, T.J. (1997) Microtubule polymerization dynamics. *Annu. Rev. Cell Dev. Biol.* **13**, 83–117
- Wiese, C. and Zheng, Y. (2006) Microtubule nucleation:  $\gamma$ -tubulin and beyond. *J. Cell Sci.* **119**, 4143–4153
- Salinas, S., Carazo-Salas, R.E., Proukakis, C., Schiavo, G. and Warner, T.T. (2007) Spastin and microtubules: functions in health and disease. *J. Neurosci. Res.* **85**, 2778–2782
- Rizk, R.S., Bohannon, K.P., Wetzel, L.A., Powers, J., Shaw, S.L. and Walczak, C.E. (2009) MCAK and Paclitaxel have differential effects on spindle microtubule organization and dynamics. *Mol. Biol. Cell* **20**, 1639–1651
- Jaworski, J., Kapitein, L.C., Gouveia, S.M., Dortland, B.R., Wulf, P.S., Grigoriev, I., Camera, P., Spangler, S.A., Di Stefano, P., Demmers, J. et al. (2009) Dynamic microtubules regulate dendritic spine morphology and synaptic plasticity. *Neuron* **61**, 85–100
- Liao, G., Nagasaki, T. and Gundersen, G.G. (1995) Low concentrations of nocodazole interfere with fibroblast locomotion without significantly affecting microtubule level: implications for the role of dynamic microtubules in cell locomotion. *J. Cell Sci.* **108**, 3473–3483
- Walker, R.A., O'Brien, E.T., Pryer, N.K., Soboeiro, M.F., Voter, W.A., Erickson, H.P. and Salmon, E.D. (1988) Dynamic instability of individual microtubules analyzed by video light microscopy: rate constants and transition frequencies. *J. Cell Biol.* **107**, 1437–1448
- Lee, J.C. and Timasheff, S.N. (1975) The reconstitution of microtubules from purified calf brain tubulin. *Biochemistry* **14**, 5183–5187
- Kinoshita, K., Arnal, I., Desai, A., Drechsel, D.N. and Hyman, A.A. (2001) Reconstitution of physiological microtubule dynamics using purified components. *Science* **294**, 1340–1343
- Waterman-Storer, C.M. and Salmon, E.D. (1997) Actomyosin-based retrograde flow of microtubules in the lamella of migrating epithelial cells influences microtubule dynamic instability and turnover and is associated with microtubule breakage and treadmilling. *J. Cell Biol.* **139**, 417–434
- Dammermann, A., Desai, A. and Oegema, K. (2003) The minus end in sight. *Curr. Biol.* **13**, R614–R624
- Dammermann, A. and Merdes, A. (2002) Assembly of centrosomal proteins and microtubule organization depends on PCM-1. *J. Cell Biol.* **159**, 255–266
- Mogensen, M.M., Malik, A., Piel, M., Bouckson-Castaing, V. and Bornens, M. (2000) Microtubule minus-end anchorage at centrosomal and non-centrosomal sites: the role of ninein. *J. Cell Sci.* **113**, 3013–3023
- Meng, W., Mushika, Y., Ichii, T. and Takeichi, M. (2008) Anchorage of microtubule minus ends to adherens junctions regulates epithelial cell–cell contacts. *Cell* **135**, 948–959
- Brouhard, G.J., Stear, J.H., Noetzel, T.L., Al-Bassam, J., Kinoshita, K., Harrison, S.C., Howard, J. and Hyman, A.A. (2008) XMAP215 is a processive microtubule polymerase. *Cell* **132**, 79–88
- Moore, C.A., Yu, M., Guo, J., Beraud, C., Sakowicz, R. and Milligan, R.A. (2002) A mechanism for microtubule depolymerization by Kif1 kinesins. *Mol. Cell* **9**, 903–909
- Steinmetz, M.O., Kammerer, R.A., Jahnke, W., Goldie, K.N., Lustig, A. and van Oostrum, J. (2000) Op18/stathmin caps a kinked protofilament-like tubulin tetramer. *EMBO J.* **19**, 572–580
- Mimori-Kiyosue, Y., Grigoriev, I., Lansbergen, G., Sasaki, H., Matsui, C., Severin, F., Galjart, N., Grosveld, F., Vorobjev, I., Tsukita, S. and Akhmanova, A. (2005) CLASP1 and CLASP2 bind to EB1 and regulate microtubule plus-end dynamics at the cell cortex. *J. Cell Biol.* **168**, 141–153
- Jourdain, L., Curmi, P., Sobel, A., Pantaloni, D. and Carlier, M.F. (1997) Stathmin: a tubulin-sequestering protein which forms a ternary T25 complex with two tubulin molecules. *Biochemistry* **36**, 10817–10821
- Newton, C.N., Wagenbach, M., Ovechikina, Y., Wordeman, L. and Wilson, L. (2004) MCAK, a Kin I kinesin, increases the catastrophe frequency of steady-state HeLa cell microtubules in an ATP-dependent manner *in vitro*. *FEBS Lett.* **572**, 80–84
- Dehmelt, L. and Halpain, S. (2005) The MAP2/Tau family of microtubule-associated proteins. *Genome Biol.* **6**, 204
- Moore, C.A., Perderiset, M., Kappeler, C., Kain, S., Drummond, D., Perkins, S.J., Chelly, J., Cross, R., Houdusse, A. and Francis, F. (2006) Distinct roles of doublecortin modulating the microtubule cytoskeleton. *EMBO J.* **25**, 4448–4457
- Drechsel, D.N., Hyman, A.A., Cobb, M.H. and Kirschner, M.W. (1992) Modulation of the dynamic instability of tubulin assembly by the microtubule-associated protein tau. *Mol. Biol. Cell* **3**, 1141–1154
- Kowalski, R.J. and Williams, Jr, R.C. (1993) Microtubule-associated protein 2 alters the dynamic properties of microtubule assembly and disassembly. *J. Biol. Chem.* **268**, 9847–9855
- Pryer, N.K., Walker, R.A., Skeen, V.P., Bourns, B.D., Soboeiro, M.F. and Salmon, E.D. (1992) Brain microtubule-associated proteins modulate microtubule dynamic instability *in vitro*: real-time observations using video microscopy. *J. Cell Sci.* **103**, 965–976
- Noetzel, T.L., Drechsel, D.N., Hyman, A.A. and Kinoshita, K. (2005) A comparison of the ability of XMAP215 and tau to inhibit the microtubule destabilizing activity of XKCM1. *Philos. Trans. R. Soc. London Ser. B* **360**, 591–594
- Qiang, L., Yu, W., Andreadis, A., Luo, M. and Baas, P.W. (2006) Tau protects microtubules in the axon from severing by katanin. *J. Neurosci.* **26**, 3120–3129
- Ebneth, A., Drewes, G., Mandelkow, E.M. and Mandelkow, E. (1999) Phosphorylation of MAP2c and MAP4 by MARK kinases leads to the destabilization of microtubules in cells. *Cell Motil. Cytoskeleton* **44**, 209–224
- Schuyler, S.C. and Pellman, D. (2001) Microtubule 'plus-end-tracking proteins': the end is just the beginning. *Cell* **105**, 421–424
- Gundersen, G.G., Gomes, E.R. and Wen, Y. (2004) Cortical control of microtubule stability and polarization. *Curr. Opin. Cell Biol.* **16**, 106–112
- Kodama, A., Karakesisoglou, I., Wong, E., Vaezi, A. and Fuchs, E. (2003) ACF7: an essential integrator of microtubule dynamics. *Cell* **115**, 343–354
- Kita, K., Wittmann, T., Nathke, I.S. and Waterman-Storer, C.M. (2006) Adenomatous polyposis coli on microtubule plus ends in cell extensions can promote microtubule net growth with or without EB1. *Mol. Biol. Cell* **17**, 2331–2345
- Komarova, Y.A., Akhmanova, A.S., Kojima, S., Galjart, N. and Borisov, G.G. (2002) Cytoplasmic linker proteins promote microtubule rescue *in vivo*. *J. Cell Biol.* **159**, 589–599
- Dimitrov, A., Quesnoit, M., Moutel, S., Cantaloube, I., Pous, C. and Perez, F. (2008) Detection of GTP-tubulin conformation *in vivo* reveals a role for GTP remnants in microtubule rescues. *Science* **322**, 1353–1356
- Komarova, Y., De Groot, C.O., Grigoriev, I., Gouveia, S.M., Munteanu, E.L., Schober, J.M., Honnappa, S., Buey, R.M., Hoogenraad, C.C., Dogterom, M. et al. (2009) Mammalian end binding proteins control persistent microtubule growth. *J. Cell Biol.* **184**, 691–706

- 37 Busch, K.E. and Brunner, D. (2004) The microtubule plus end-tracking proteins mal3p and tip1p cooperate for cell-end targeting of interphase microtubules. *Curr. Biol.* **14**, 548–559
- 38 Bieling, P., Laan, L., Schek, H., Munteanu, E.L., Sandblad, L., Dogterom, M., Brunner, D. and Surrey, T. (2007) Reconstitution of a microtubule plus-end tracking system *in vitro*. *Nature* **450**, 1100–1105
- 39 Vitre, B., Coquelle, F.M., Heichette, C., Garnier, C., Chretien, D. and Arnal, I. (2008) EB1 regulates microtubule dynamics and tubulin sheet closure *in vitro*. *Nat. Cell Biol.* **10**, 415–421
- 40 Sandblad, L., Busch, K.E., Tittmann, P., Gross, H., Brunner, D. and Hoenger, A. (2006) The *Schizosaccharomyces pombe* EB1 homolog Mal3p binds and stabilizes the microtubule lattice seam. *Cell* **127**, 1415–1424
- 41 des Georges, A., Katsuki, M., Drummond, D.R., Osei, M., Cross, R.A. and Amos, L.A. (2008) Mal3, the *Schizosaccharomyces pombe* homolog of EB1, changes the microtubule lattice. *Nat. Struct. Mol. Biol.* **15**, 1102–1108
- 42 Dixit, R., Barnett, B., Lazarus, J.E., Tokito, M., Goldman, Y.E. and Holzbaur, E.L. (2009) Microtubule plus-end tracking by CLIP-170 requires EB1. *Proc. Natl. Acad. Sci. U.S.A.* **106**, 492–497
- 43 Manna, T., Honnappa, S., Steinmetz, M.O. and Wilson, L. (2008) Suppression of microtubule dynamic instability by the +TIP protein EB1 and its modulation by the CAP-Gly domain of p150<sup>glued</sup>. *Biochemistry* **47**, 779–786
- 44 Straube, A. and Merdes, A. (2007) EB3 regulates microtubule dynamics at the cell cortex and is required for myoblast elongation and fusion. *Curr. Biol.* **17**, 1318–1325
- 45 Gard, D.L. and Kirschner, M.W. (1987) A microtubule-associated protein from *Xenopus* eggs that specifically promotes assembly at the plus-end. *J. Cell Biol.* **105**, 2203–2215
- 46 Srayko, M., Kaya, A., Stamford, J. and Hyman, A.A. (2005) Identification and characterization of factors required for microtubule growth and nucleation in the early *C. elegans* embryo. *Dev. Cell* **9**, 223–236
- 47 Al-Bassam, J., van Breugel, M., Harrison, S.C. and Hyman, A. (2006) Stu2p binds tubulin and undergoes an open-to-closed conformational change. *J. Cell Biol.* **172**, 1009–1022
- 48 Vasquez, R.J., Gard, D.L. and Cassimeris, L. (1994) XMAP from *Xenopus* eggs promotes rapid plus end assembly of microtubules and rapid microtubule polymer turnover. *J. Cell Biol.* **127**, 985–993
- 49 Tournebise, R., Popov, A., Kinoshita, K., Ashford, A.J., Rybina, S., Pozniakovskiy, A., Mayer, T.U., Walczak, C.E., Karsenti, E. and Hyman, A.A. (2000) Control of microtubule dynamics by the antagonistic activities of XMAP215 and XKCM1 in *Xenopus* egg extracts. *Nat. Cell Biol.* **2**, 13–19
- 50 Kawamura, E. and Wasteneys, G.O. (2008) MOR1, the *Arabidopsis thaliana* homologue of *Xenopus* MAP215, promotes rapid growth and shrinkage, and suppresses the pausing of microtubules *in vivo*. *J. Cell Sci.* **121**, 4114–4123
- 51 Lee, T., Langford, K.J., Askham, J.M., Bruning-Richardson, A. and Morrison, E.E. (2008) MCAK associates with EB1. *Oncogene* **27**, 2494–2500
- 52 Mennella, V., Rogers, G.C., Rogers, S.L., Buster, D.W., Vale, R.D. and Sharp, D.J. (2005) Functionally distinct kinesin-13 family members cooperate to regulate microtubule dynamics during interphase. *Nat. Cell Biol.* **7**, 235–245
- 53 Niethammer, P., Kronja, I., Kandels-Lewis, S., Rybina, S., Bastiaens, P. and Karsenti, E. (2007) Discrete states of a protein interaction network govern interphase and mitotic microtubule dynamics. *PLoS Biol.* **5**, e29
- 54 Wolyniak, M.J., Blake-Hodek, K., Kosco, K., Hwang, E., You, L. and Huffaker, T.C. (2006) The regulation of microtubule dynamics in *Saccharomyces cerevisiae* by three interacting plus-end tracking proteins. *Mol. Biol. Cell* **17**, 2789–2798
- 55 Peset, I. and Vernos, I. (2008) The TACC proteins: TACC-ling microtubule dynamics and centrosome function. *Trends Cell Biol.* **18**, 379–388
- 56 Holmfeldt, P., Stenmark, S. and Gullberg, M. (2004) Differential functional interplay of Topp/XMAP215 and the Kint kinesin MCAK during interphase and mitosis. *EMBO J.* **23**, 627–637
- 57 Desai, A., Verma, S., Mitchison, T.J. and Walczak, C.E. (1999) Kin I kinesins are microtubule-destabilizing enzymes. *Cell* **96**, 69–78
- 58 Hunter, A.W., Caplow, M., Coy, D.L., Hancock, W.O., Diez, S., Wordeman, L. and Howard, J. (2003) The kinesin-related protein MCAK is a microtubule depolymerase that forms an ATP-hydrolyzing complex at microtubule ends. *Mol. Cell* **11**, 445–457
- 59 Ogawa, T., Nitta, R., Okada, Y. and Hirokawa, N. (2004) A common mechanism for microtubule destabilizers-M type kinesins stabilize curling of the protofilament using the class-specific neck and loops. *Cell* **116**, 591–602
- 60 Shipley, K., Hekmat-Nejad, M., Turner, J., Moores, C., Anderson, R., Milligan, R., Sakowicz, R. and Fletterick, R. (2004) Structure of a kinesin microtubule depolymerization machine. *EMBO J.* **23**, 1422–1432
- 61 Kline-Smith, S.L. and Walczak, C.E. (2002) The microtubule-destabilizing kinesin XKCM1 regulates microtubule dynamic instability in cells. *Mol. Biol. Cell* **13**, 2718–2731
- 62 Noda, Y., Sato-Yoshitake, R., Kondo, S., Nangaku, M. and Hirokawa, N. (1995) KIF2 is a new microtubule-based anterograde motor that transports membranous organelles distinct from those carried by kinesin heavy chain or KIF3A/B. *J. Cell Biol.* **129**, 157–167
- 63 Homma, N., Takei, Y., Tanaka, Y., Nakata, T., Terada, S., Kikkawa, M., Noda, Y. and Hirokawa, N. (2003) Kinesin superfamily protein 2A (KIF2A) functions in suppression of collaterally branch extension. *Cell* **114**, 229–239
- 64 Ganem, N.J. and Compton, D.A. (2004) The Kint kinesin Kif2a is required for bipolar spindle assembly through a functional relationship with MCAK. *J. Cell Biol.* **166**, 473–478
- 65 Manning, A.L., Ganem, N.J., Bakhoum, S.F., Wagenbach, M., Wordeman, L. and Compton, D.A. (2007) The kinesin-13 proteins Kif2a, Kif2b, and Kif2c/MCAK have distinct roles during mitosis in human cells. *Mol. Biol. Cell* **18**, 2970–2979
- 66 Moore, A.T., Rankin, K.E., von Dassow, G., Peris, L., Wagenbach, M., Ovechkina, Y., Andrieux, A., Job, D. and Wordeman, L. (2005) MCAK associates with the tips of polymerizing microtubules. *J. Cell Biol.* **169**, 391–397
- 67 Gupta, M.L., Jr., Carvalho, P., Roof, D.M. and Pellman, D. (2006) Plus end-specific depolymerase activity of Kip3, a kinesin-8 protein, explains its role in positioning the yeast mitotic spindle. *Nat. Cell Biol.* **8**, 913–923
- 68 Varga, V., Helenius, J., Tanaka, K., Hyman, A.A., Tanaka, T.U. and Howard, J. (2006) Yeast kinesin-8 depolymerizes microtubules in a length-dependent manner. *Nat. Cell Biol.* **8**, 957–962
- 69 Mayr, M.I., Hummer, S., Bormann, J., Gruner, T., Adio, S., Woehlke, G. and Mayer, T.U. (2007) The human kinesin Kif18A is a motile microtubule depolymerase essential for chromosome congression. *Curr. Biol.* **17**, 488–498
- 70 Cottingham, F.R. and Hoyt, M.A. (1997) Mitotic spindle positioning in *Saccharomyces cerevisiae* is accomplished by antagonistically acting microtubule motor proteins. *J. Cell Biol.* **138**, 1041–1053
- 71 Gandhi, R., Bonaccorsi, S., Wentworth, D., Doxsey, S., Gatti, M. and Pereira, A. (2004) The *Drosophila* kinesin-like protein KLP67A is essential for mitotic and male meiotic spindle assembly. *Mol. Biol. Cell* **15**, 121–131
- 72 West, R.R., Malmstrom, T., Troxell, C.L. and McIntosh, J.R. (2001) Two related kinesins, *kfp5+* and *kfp6+*, foster microtubule disassembly and are required for meiosis in fission yeast. *Mol. Biol. Cell* **12**, 3919–3932
- 73 Sproul, L.R., Anderson, D.J., Mackey, A.T., Saunders, W.S. and Gilbert, S.P. (2005) Cik1 targets the minus-end kinesin depolymerase kar3 to microtubule plus ends. *Curr. Biol.* **15**, 1420–1427
- 74 Troxell, C.L., Sweezy, M.A., West, R.R., Reed, K.D., Carson, B.D., Pidoux, A.L., Cande, W.Z. and McIntosh, J.R. (2001) *pk11+* and *kfp2+*: two kinesins of the Kar3 subfamily in fission yeast perform different functions in both mitosis and meiosis. *Mol. Biol. Cell* **12**, 3476–3488
- 75 Cai, S., Weaver, L.N., Ems-McClung, S.C. and Walczak, C.E. (2009) Kinesin-14 family proteins HSET/XCTK2 control spindle length by cross-linking and sliding microtubules. *Mol. Biol. Cell* **20**, 1348–1359
- 76 Steinmetz, M.O. (2007) Structure and thermodynamics of the tubulin-stathmin interaction. *J. Struct. Biol.* **158**, 137–147
- 77 Curmi, P.A., Andersen, S.S., Lachkar, S., Gavet, O., Karsenti, E., Knossow, M. and Sobel, A. (1997) The stathmin/tubulin interaction *in vitro*. *J. Biol. Chem.* **272**, 25029–25036
- 78 Belmont, L.D. and Mitchison, T.J. (1996) Identification of a protein that interacts with tubulin dimers and increases the catastrophe rate of microtubules. *Cell* **84**, 623–631
- 79 Manna, T., Thrower, D., Miller, H.P., Curmi, P. and Wilson, L. (2006) Stathmin strongly increases the minus end catastrophe frequency and induces rapid treadmilling of bovine brain microtubules at steady state *in vitro*. *J. Biol. Chem.* **281**, 2071–2078
- 80 Howell, B., Deacon, H. and Cassimeris, L. (1999) Decreasing oncoprotein 18/stathmin levels reduces microtubule catastrophes and increases microtubule polymer *in vivo*. *J. Cell Sci.* **112**, 3713–3722
- 81 Sellin, M.E., Holmfeldt, P., Stenmark, S. and Gullberg, M. (2008) Global regulation of the interphase microtubule system by abundantly expressed Op18/stathmin. *Mol. Biol. Cell* **19**, 2897–2906
- 82 Fletcher, G. and Rorth, P. (2007) *Drosophila* stathmin is required to maintain tubulin pools. *Curr. Biol.* **17**, 1067–1071



- 83 Rubin, C.I. and Atweh, G.F. (2004) The role of stathmin in the regulation of the cell cycle. *J. Cell. Biochem.* **93**, 242–250
- 84 Marklund, U., Osterman, O., Melander, H., Bergh, A. and Gullberg, M. (1994) The phenotype of a 'Cdc2 kinase target site-deficient' mutant of oncoprotein 18 reveals a role of this protein in cell cycle control. *J. Biol. Chem.* **269**, 30626–30635
- 85 Luo, X.N., Mookerjee, B., Ferrari, A., Mistry, S. and Atweh, G.F. (1994) Regulation of phosphoprotein p18 in leukemic cells: cell cycle regulated phosphorylation by p34cdc2 kinase. *J. Biol. Chem.* **269**, 10312–10318
- 86 Schubart, U.K., Yu, J., Amat, J.A., Wang, Z., Hoffmann, M.K. and Edelmann, W. (1996) Normal development of mice lacking metablastin (p19), a phosphoprotein implicated in cell cycle regulation. *J. Biol. Chem.* **271**, 14062–14066
- 87 Mori, N. and Morii, H. (2002) SCG10-related neuronal growth-associated proteins in neural development, plasticity, degeneration, and aging. *J. Neurosci. Res.* **70**, 264–273
- 88 Brunner, D. and Nurse, P. (2000) CLIP170-like tip1p spatially organizes microtubular dynamics in fission yeast. *Cell* **102**, 695–704
- 89 Adamikova, L., Straube, A., Schulz, I. and Steinberg, G. (2004) Calcium signaling is involved in dynein-dependent microtubule organization. *Mol. Biol. Cell* **15**, 1969–1980
- 90 Kosco, K.A., Pearson, C.G., Maddox, P.S., Wang, P.J., Adams, I.R., Salmon, E.D., Bloom, K. and Huffaker, T.C. (2001) Control of microtubule dynamics by Stu2p is essential for spindle orientation and metaphase chromosome alignment in yeast. *Mol. Biol. Cell* **12**, 2870–2880
- 91 Usui, T., Maekawa, H., Pereira, G. and Schiebel, E. (2003) The XMAP215 homologue Stu2 at yeast spindle pole bodies regulates microtubule dynamics and anchorage. *EMBO J.* **22**, 4779–4793
- 92 Manna, T., Grenningloh, G., Miller, H.P. and Wilson, L. (2007) Stathmin family protein SCG10 differentially regulates the plus and minus end dynamics of microtubules at steady state *in vitro*: implications for its role in neurite outgrowth. *Biochemistry* **46**, 3543–3552

Received 13 March 2009  
doi:10.1042/BST0371007



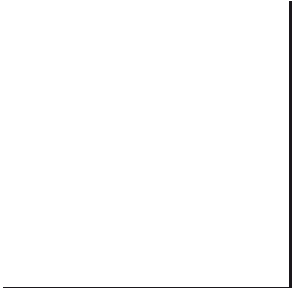


## Chapter 2

### **STIM1 is a MT-Plus-End-Tracking Protein Involved in Remodeling of the ER**

Ilya Grigoriev, Susana Montenegro Gouveia, Babet van der Vaart,  
Jeroen Demmers, Jeremy T. Smyth, Srinivas Honnappa, Daniël  
Splinter, Michel O. Steinmetz, James W. Putney, Jr., Casper C.  
Hoogenraad, and Anna Akhmanova

*Current Biology. 2008 18:177-82*





# STIM1 Is a MT-Plus-End-Tracking Protein Involved in Remodeling of the ER

Ilya Grigoriev,<sup>1,6</sup> Susana Montenegro Gouveia,<sup>1,6</sup>  
Babet van der Vaart,<sup>1</sup> Jeroen Demmers,<sup>2</sup>  
Jeremy T. Smyth,<sup>3</sup> Srinivas Honnappa,<sup>4</sup> Daniël Splinter,<sup>1</sup>  
Michel O. Steinmetz,<sup>4</sup> James W. Putney, Jr.,<sup>3</sup>  
Casper C. Hoogenraad,<sup>5</sup> and Anna Akhmanova<sup>1,\*</sup>

<sup>1</sup>Department of Cell Biology and

<sup>2</sup>Department of Biochemistry

Erasmus Medical Center

3000 CA Rotterdam

The Netherlands

<sup>3</sup>Laboratory of Signal Transduction

National Institute of Environmental Health Sciences

Department of Health and Human Services

Research Triangle Park, North Carolina 27709

<sup>4</sup>Biomolecular Research

Structural Biology

Paul Scherrer Institut

CH-5232 Villigen PSI

Switzerland

<sup>5</sup>Department of Neuroscience

Erasmus Medical Center

3000 CA Rotterdam

The Netherlands

## Summary

Stromal interaction molecule 1 (STIM1) is a transmembrane protein that is essential for store-operated  $\text{Ca}^{2+}$  entry, a process of extracellular  $\text{Ca}^{2+}$  influx in response to the depletion of  $\text{Ca}^{2+}$  stores in the endoplasmic reticulum (ER) (reviewed in [1–4]). STIM1 localizes predominantly to the ER; upon  $\text{Ca}^{2+}$  release from the ER, STIM1 translocates to the ER-plasma membrane junctions and activates  $\text{Ca}^{2+}$  channels (reviewed in [1–4]). Here, we show that STIM1 directly binds to the microtubule-plus-end-tracking protein EB1 and forms EB1-dependent comet-like accumulations at the sites where polymerizing microtubule ends come in contact with the ER network. Therefore, the previously observed tubulovesicular motility of GFP-STIM1 [5] is not a motor-based movement but a traveling wave of diffusion-dependent STIM1 concentration in the ER membrane. STIM1 overexpression strongly stimulates ER extension occurring through the microtubule “tip attachment complex” (TAC) mechanism [6, 7], a process whereby an ER tubule attaches to and elongates together with the EB1-positive end of a growing microtubule. Depletion of STIM1 and EB1 decreases TAC-dependent ER protrusion, indicating that microtubule growth-dependent concentration of STIM1 in the ER membrane plays a role in ER remodeling.

## Results and Discussion

### STIM1 Binds Directly to EB1

We used the fact that the majority of microtubule (MT)-plus-end-tracking proteins (+TIPs) directly bind to EB1 or its homologs

(reviewed in [8]) to identify novel +TIPs. We performed glutathione S-transferase (GST) pull-down assays with cell extracts by using GST-EB1, -EB2, and -EB3 fusions and analyzed the isolated proteins by mass spectrometry. Among the proteins that were highly enriched in the GST-EB pull-downs but did not bind to GST alone, we found many known +TIPs (Table S1 available online; [8]). One of the most abundant potential new partners of EB1 and EB3 was STIM1; its homolog STIM2 was also present in the GST-EB1/-EB3 pull-downs (Table S1). The association of STIM1 with the EB family members was specific: Although GFP alone did not interact with any GST fusions, GFP-STIM1 strongly associated with the GST-EB1 and GST-EB1 C terminus but not with GST alone or with the GST-EB1 N terminus (Figure 1A). Compared to GST-EB1, GFP-STIM1 showed reduced binding to GST-EB3 and GST-EB2, in line with the mass spectrometry data (Table S1). The interaction between EB1 and STIM1 is direct because purified EB1 bound to the purified GST fusion of the STIM1 C terminus (Figures 1B and 1G). The fact that EB1 and STIM1 associate with each other under physiological conditions was confirmed by coimmunoprecipitation of endogenous proteins (Figure 1E).

GFP-STIM1, expressed in HeLa cells at low levels, localized in an ER-like pattern, as shown before [5, 9] (Figure 1C). Within this pattern we observed comet-like structures that coincided with some of the MT ends that were positive for the endogenous EB1 (Figure 1C). This explains the previously described partial colocalization of GFP-STIM1 with MTs [5, 10].

STIM1 is a multidomain transmembrane protein, with the N terminus located in the ER lumen and the C terminus in the cytoplasm (Figure 1G) (reviewed in [11]). By expressing GFP-fused deletion mutants of STIM1, we mapped the minimal domain of STIM1 required for MT-plus-end association to a part of the C terminus, including a portion of the ezrin-radixin-moesin (ERM) domain and the basic serine-proline (S/P)-rich region (fragment STIM1-C3, amino acids 392–652) (Figures 1D and 1G). This fragment was efficiently pulled down by the GST-EB1 and the EB1-C terminus, similar to the full-length STIM1 (Figure 1F). It is likely that the positively charged S/P-rich region of STIM1 is involved in binding to EB1 because similar domains of other +TIPs also perform this function [12].

### STIM1 Associates with Growing MT Ends

By using live-cell imaging, we observed that in HeLa cells GFP-STIM1 highlighted the ER network through which comet-like structures traveled with an average velocity of  $0.22 \pm 0.07 \mu\text{m/s}$  (mean  $\pm$  SD, calculated from five cells) (Movie S1). These comets coincided with growing MT ends visualized with EB3-mRFP, a MT-plus-end marker [13] (Figures S1A and S1B and Movie S2). Comet-like behavior of GFP-STIM1 was also observed in MRC5-SV fibroblasts, which have a sparse MT array and are therefore better suited for distinguishing individual ER tubules and MT tips. Also in these cells GFP-STIM1 localized to the ER (visualized with a luminal ER marker) and mobile comets within the ER network (Figure 2A, Movie S3). In addition, we also observed immobile accumulations of GFP-STIM1, which likely represented an overexpression artifact in this cell type (Movies S3 and S4). All GFP-STIM1 comets coincided with EB3-mRFP-positive MT ends (Figures 2B and 2C

\*Correspondence: a.akhmanova@erasmusmc.nl

<sup>6</sup>These authors contributed equally to this work.

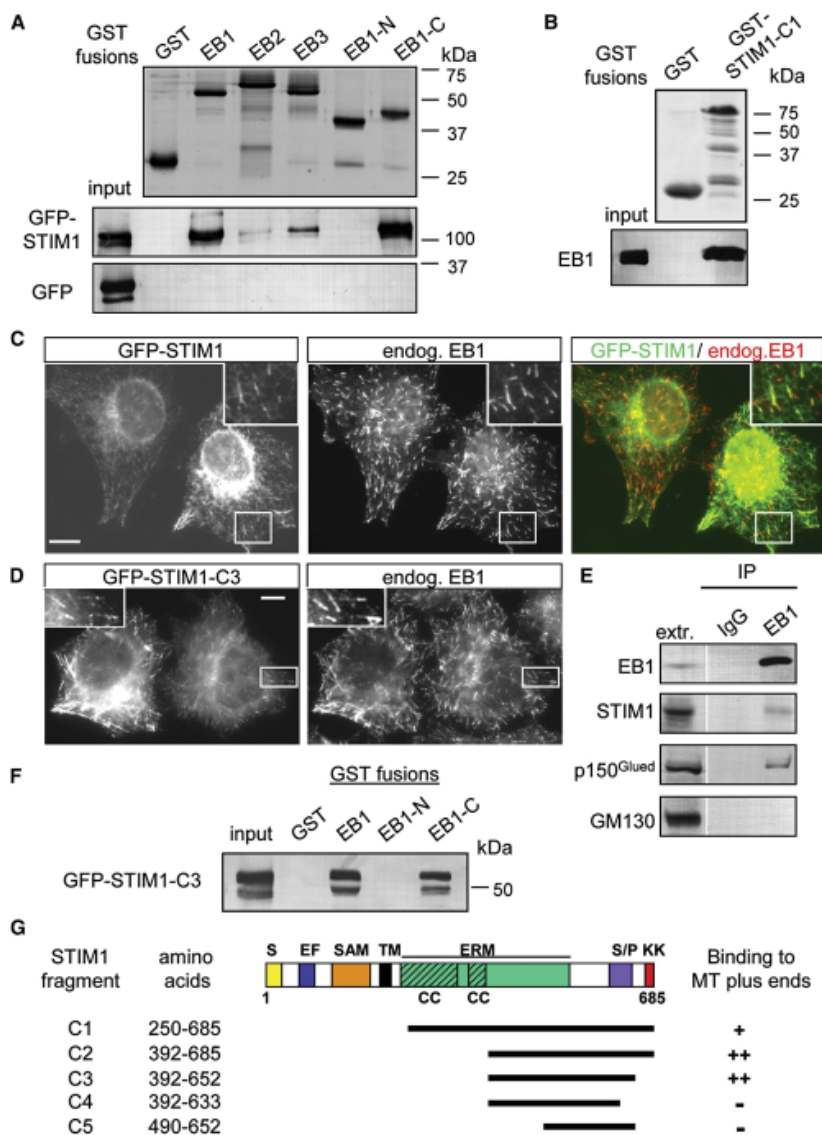


Figure 1. STIM1 Interacts with EB1

(A, B, and F) GST pull-down assays with the indicated GST fusions; extracts of HEK293 cells overexpressing GFP-STIM1, GFP-STIM1-C3 mutant, or GFP alone were used in (A) and (F), and the purified full-length EB1 protein was used in (B). Coomassie-stained gels are shown for GST fusions; other proteins were detected by Western blotting with antibodies against GFP (A and F) or EB1 (B).

(C and D) HeLa cells were transfected with GFP-STIM1 or GFP-STIM1-C3 mutant, fixed, and stained for the endogenous EB1. The insets show enlargements of the boxed areas. In the overlay GFP-STIM1 is shown in green and EB1 in red. The bars represent 10  $\mu$ m.

(E) Immunoprecipitation from extracts of HeLa cells with the rabbit polyclonal antibody against EB1 or a control rabbit serum. The lane marked "extr." shows 5% of the input. Dynactin subunit p150<sup>Glued</sup>, a known EB1 partner, was used as a positive control, and GM130, a protein associated with the cytoplasmic side of the Golgi, was used as a negative control.

(G) Mapping of the minimal MT-plus-end binding domain of STIM1 by colocalization with EB1 in fixed HeLa cells. A scheme of STIM1 protein structure and the deletion mutants is shown. Abbreviations: S, signal peptide; EF, EF hand; SAM, sterile  $\alpha$  motif domain; TM, transmembrane domain; ERM, ezrin-radixin-moesin domain; CC, coiled coil; S/P, serine-proline-rich domain; KK, lysine-rich domain.

and Movie S4). When a growing MT tip arrived at the edge of the ER network, an ER tubule with a STIM1-positive accumulation at its tip often extended together with the growing MT. When the connection between the MT end and the ER tubule

was lost, the ER tubule retracted while the MT end usually continued growing (Figure 2C). Once a growing MT end came in contact with another ER tubule, STIM1 accumulation at the MT tip reappeared. This dynamic behavior explains why only

**STIM1 Tracks Growing Microtubule Ends**  
179

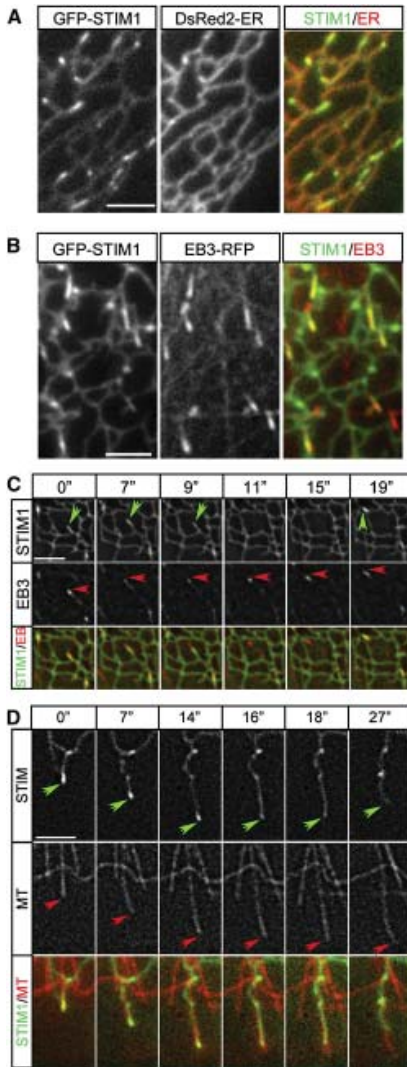


**Figure 2. GFP-STIM1 Colocalizes with ER and MT Plus Ends in Live Cells**  
(A) Simultaneous imaging of GFP-STIM1 (green in overlay) and DsRed2-ER (red in overlay) in a transiently transfected MRC5-SV cell.  
(B and C) Simultaneous imaging of GFP-STIM1 (green in overlay) and EB3-mRFP (red in overlay) in a transiently transfected MRC5-SV cell; a single frame is shown in (B). Successive frames from Movie S4 are shown in (C) (time is indicated above the panels). GFP-STIM1 comets are indicated by green arrows, and EB3-mRFP comets are highlighted by red arrows.  
(D) Simultaneous imaging of GFP-STIM1 (green in overlay) and mCherry- $\alpha$ -tubulin (red in overlay) in a transiently transfected MRC5-SV cell. Successive frames are shown; time is indicated above the panels. Tips of extending/retracting ER tubules and MTs are indicated by green and red arrows, respectively. The bars represent 3  $\mu$ m.

some of the EB1/EB3-labeled MT ends are GFP-STIM1 positive: GFP-STIM1 comets are present only at the sites of physical contact between MT ends and ER membranes.

These observations were confirmed by simultaneous imaging of GFP-STIM1 and MTs (Figure 2D, Figure S2, and Movie

S5). Accumulations of GFP-STIM1 were detected only at the ends of growing, but not shortening or pausing, MTs (Figure 2D and Figure S2). Again we observed simultaneous extension of MTs and ER tubules with GFP-STIM1 comets at their tips; these comets were lost either after the MT underwent a catastrophe (Figure S2) or because the ER tubule lost connection with the MT end (Figure 2D). MT polymerization-dependent ER tubule extension was described previously in *Xenopus* extracts and in newt lung epithelial cells; this type of ER tubule formation was named “tip attachment complex” (TAC) mechanism as opposed to ER sliding along preexisting MTs [6, 7].

The fact that GFP-STIM1 comets disappeared once the contact between MT tips and the ER was lost and reappeared soon after this contact was re-established suggested that individual GFP-STIM1 molecules do not undergo processive MT-based transport. Analysis of GFP-STIM1 fluorescence recovery after photobleaching (FRAP) showed that GFP-STIM1 diffuses in the ER slower than EB3-mRFP in the cytoplasm (Figures 3A and 3B). Recovery of the diffuse GFP-STIM1 signal in the ER network in the bleached region always preceded the appearance of MT tip-associated GFP-STIM1 comets (Figure 3A), supporting the idea that GFP-STIM1 molecules arrive at the growing MT end by diffusion. Therefore, the observed “movement” of GFP-STIM1 concentration at the sites of the EB1-positive MT end and ER-membrane interaction.

**Ca<sup>2+</sup> Release from the ER Abolishes STIM1 Plus-End-Tracking Behavior**

Previous studies showed that when Ca<sup>2+</sup> stores in the ER are depleted by the addition of thapsigargin, STIM1 oligomerized and redistributed to peripheral foci [2–4, 11, 14]. Indeed, thapsigargin treatment caused rapid relocalization of GFP-STIM1 into immobile ER-associated puncta (Movie S6). FRAP experiments showed, in line with previous publications [14], that the exchange of GFP-STIM1 in thapsigargin-induced foci was strongly diminished (Figure 3B). In MRC5-SV fibroblasts, the dynamics of EB-positive MT ends was not significantly affected by thapsigargin and EB1 and EB3 were only weakly associated with the immobile GFP-STIM1 (Figure 3C, Movie S7, and data not shown). In contrast, in HeLa cells a proportion of the endogenous and overexpressed EB proteins still displayed colocalization with the immobile GFP-STIM1 accumulations (Figure S3 and data not shown); FRAP assay showed that EB3-mRFP underwent rapid exchange at these sites (Figure 3B). The difference between the two cell types might be due to the differential expression of additional EB and/or STIM1-binding partners. These data suggest that STIM1 oligomerization after Ca<sup>2+</sup> release from the ER does not preclude its association with the EBs. However, in the oligomerized state, STIM1 diffuses within the ER much more slowly ([14], Figure 3B) and, as a result, it can no longer track growing MT tips (Figure 3C and Movie S7).

**Comet-like Behavior of STIM1 Depends on EB1 and Is Not Essential for Store-Operated Ca<sup>2+</sup> Entry**

EB1 is the predominant EB species in HeLa cells (A.A., unpublished data), and its knockdown was sufficient to significantly reduce the accumulation of other +TIPs at the MT ends [15]. GFP-STIM1 still showed ER-like distribution after EB1 depletion, but its accumulation in mobile comets was abolished (Figures 4A and 4B, Figure S1C, Movie S8, and data not shown), indicating that it is EB1 dependent. Also blocking MT dynamics by the addition of nocodazole or taxol, which abolish MT end

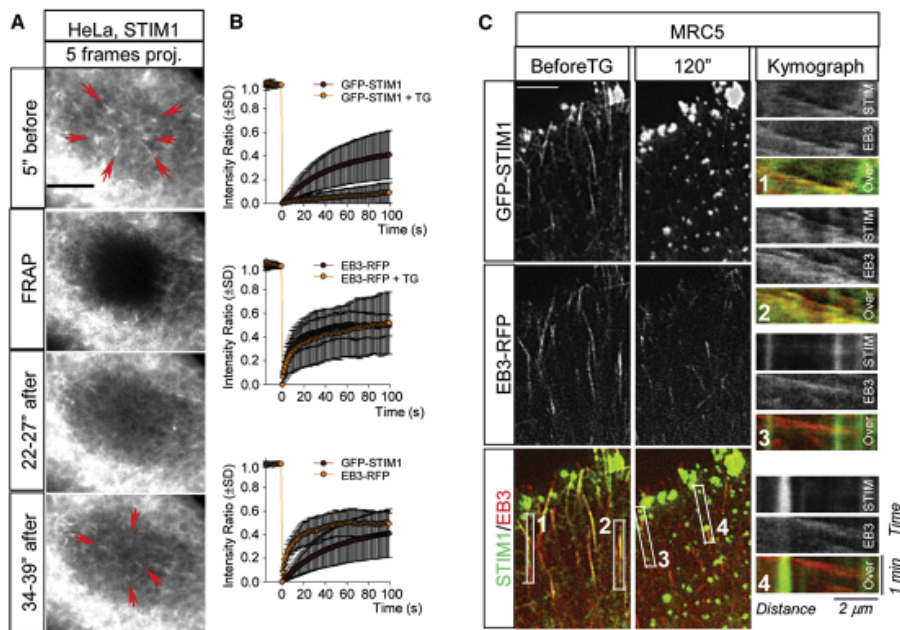


Figure 3. Analysis of GFP-STIM1 Dynamics in Control Cells and after  $\text{Ca}^{2+}$  Store Depletion

(A) FRAP analysis of GFP-STIM1 behavior. Each panel, with the exception of the panel marked "FRAP" (which shows a single frame), represents superimposition of five successive frames with a 1 s interval. Note that recovery of diffuse ER signal in the bleached area precedes the appearance of GFP-STIM1 comets (indicated by red arrows).

(B) The average GFP-STIM1 intensity ratio of two regions inside and outside of the photobleached area in HeLa cells (calculated as described in [14]). Top: control cells,  $n = 20$ ; cells after addition of  $2 \mu\text{M}$  thapsigargin (TG),  $n = 13$  cells. Middle: control cells,  $n = 7$ ;  $2 \mu\text{M}$  thapsigargin  $n = 12$  cells. Bottom: GFP-STIM1,  $n = 20$  cells; EB3-mRFP,  $n = 7$  cells. Error bars represent SD.

(C) Representative frames of simultaneous two-color video of an MRC5-SV cell expressing GFP-STIM1 and EB3-RFP before and 120 s after the addition of  $2 \mu\text{M}$  thapsigargin in normal culture medium. Kymographs illustrating the changes of fluorescent intensity over time in the indicated boxed areas are shown on the right. In the kymographs motile comets appear as slopes and immobile structures as vertical lines. The bars represent  $5 \mu\text{m}$ .

accumulation of the mammalian +TIPs [13, 16], completely abrogated the comet-like localization of GFP-STIM1 (Figure 4C and Figures S1D and S1E).

GFP-STIM1 puncta induced by  $\text{Ca}^{2+}$  release still formed in EB1-depleted cells (data not shown); moreover, EB1 knockdown or the inhibition of MT dynamics by taxol had no significant influence on thapsigargin-induced store-operated  $\text{Ca}^{2+}$  entry (SOCE) in HeLa cells, whereas STIM1 siRNA transfection had a significant inhibitory effect (Figure S4). Therefore, it appears that MT growth-dependent concentration of STIM1 is not necessary for STIM1-mediated activation of SOCE when intracellular  $\text{Ca}^{2+}$  stores are depleted with thapsigargin.

#### STIM1 and EB1 Are Required for TAC-Mediated ER Tubule Extension

Observation of the ER dynamics with luminal ER markers together with MTs showed that TAC-mediated tubule formation does occur in MRC5-SV cells but is rare compared to the sliding of new ER tubules along preexisting MTs (Table S2). TAC-associated and sliding events occurred with clearly different velocities: MT-tip attached ER tubules grew at  $\sim 0.2 \mu\text{m}/\text{s}$ , which corresponds to the MT growth rate in these cells, whereas ER sliding occurred with velocities up to  $\sim 5 \mu\text{m}/\text{s}$ . Remarkably, in GFP-STIM1-expressing cells, the frequency of TAC-driven ER tubule formation events increased  $\sim 12$ -fold (Table S2).

Because TAC-mediated ER protrusion events are infrequent in MRC5-SV fibroblasts, these cells are not a convenient model to study the TAC mechanism. We therefore turned to HeLa cells, where TAC-mediated tubule formation constitutes  $\sim 21\%$  of all ER tubule extension events (among  $18.5 \pm 6.7$  new ER tubule formation events detected per  $200 \mu\text{m}^2$  per 1 min,  $3.9 \pm 2.2$  were TAC-mediated;  $n = 20$  cells; Figures 4D and 4E and Movie S9). We inhibited the expression of EB1 and STIM1 by siRNA transfection and found that although the knockdown of either protein had no effect on the expression of the other (Figure 4A), individual depletion of each protein reduced the frequency of TAC-dependent ER protrusions without significantly affecting the number of sliding events or the MT density (Figures 4D and 4E and Figure S5). In contrast, the expression of GFP-STIM1 increased the number of TAC-mediated events; this effect was not observed in EB1-depleted cells, indicating that it is EB1 dependent (Figure 4D). It appears, therefore, that STIM1 in the ER membrane and EB1 at the growing MT tip participate in forming the molecular link responsible for MT polymerization-dependent ER tubule extension. It should be noted that the suppression of TAC-dependent ER protrusion by STIM1 and EB1 depletion was not complete; the residual events can be explained by the incomplete knockdown of the two proteins and by the potential participation of their homologs, STIM2 and EB3, in ER protrusion.



**STIM1 Tracks Growing Microtubule Ends**  
181

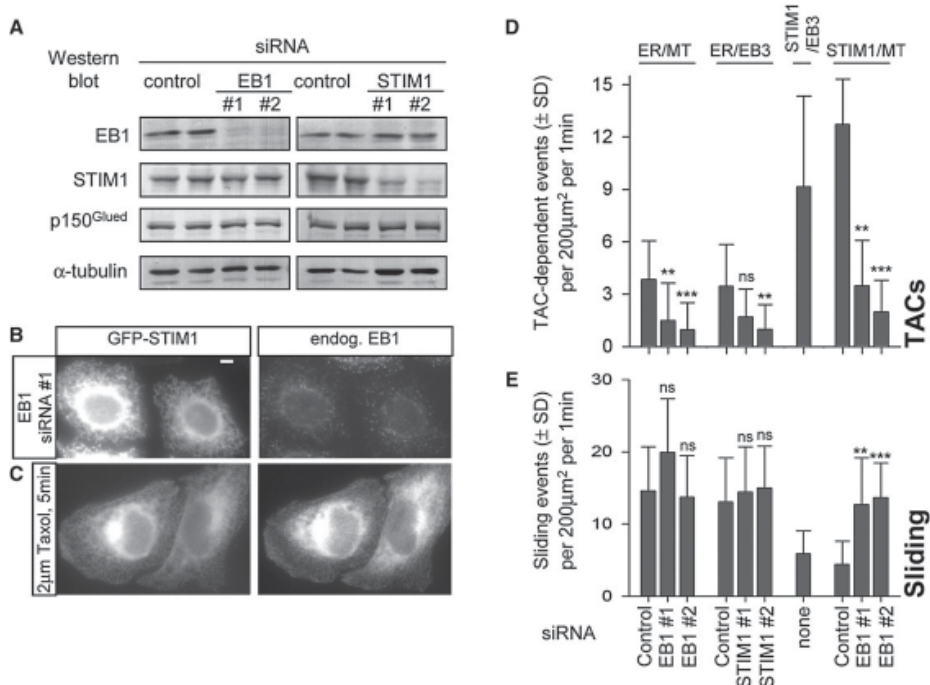


**Figure 4. EB1 and STIM1 Are Required for TAC-Mediated ER Extension**

(A) Western blot analysis of extracts of HeLa cells 3 days after transfection with the indicated siRNAs. (B) HeLa cells were transfected with the siRNA EB1 #1; two days later the cells were transfected with GFP-STIM1, cultured for 1 more day, fixed, and stained for EB1. The bar represents 5 µm. (C) HeLa cells transfected with GFP-STIM1 were treated with taxol, fixed, and stained for EB1. (D and E) HeLa cells were transfected with the indicated siRNAs. One day later cells were transfected with plasmid DNA, cultured for 2 more days, and used for dual color imaging. The following combinations of fluorescent markers were used: mCherry- $\alpha$ -tubulin (stably expressed in HeLa cells) together with transiently expressed YFP-ER; transiently expressed EB3-mRFP and YFP-ER; transiently expressed EB3-mRFP and GFP-STIM1; and mCherry- $\alpha$ -tubulin (stably expressed in HeLa cells) together with transiently expressed GFP-STIM1. Error bars represent SD. (D) Number of TACs, determined as the events of colocalization of ER tubule protrusion (detected with YFP-ER or GFP-STIM1) with EB3 comets or with growing MT plus ends. (E) Number of sliding events, determined as the events of ER protrusion (detected with YFP-ER or GFP-STIM1), which did not colocalize with EB3 comets or with growing MT plus ends. In (D) and (E), the number of analyzed cells were as follows. ER-MT: control, n = 20; EB1 #1, n = 20; EB1 #2, n = 15. ER-EB3: control, n = 20; STIM1 #1, n = 20; STIM1 #2, n = 20. STIM1-EB3: n = 20. STIM1-MT: control, n = 10; EB1 #1, n = 15; EB1 #2, n = 15. Values obtained in EB1 or STIM1 siRNA-treated cells that were significantly different from the corresponding values in cells treated with the control siRNAs are indicated by asterisks (\*\*p < 0.001, \*p < 0.01, and \*p < 0.05, p > 0.05, n.s.; Kolmogorov-Smirnov test).

Interestingly, both in MRC5-SV and HeLa cells, the frequency of ER tubule sliding was reduced after GFP-STIM1 expression, whereas sliding velocity was not affected (Table S2 and Figure 4E). GFP-STIM1 expression did not suppress ER tubule sliding in EB1-depleted cells, where no upregulation of TAC-driven ER protrusion was observed. As a result, in all conditions tested the total number of ER tubule formation events remained relatively constant (Figure S5A), suggesting that it may depend on some intrinsic properties of the ER network.

**Conclusions**

We have identified STIM1 as a MT-plus-end binding protein. Its dynamics are similar to those of other mammalian +TIPs: It is based on diffusion combined with transient accumulation at the freshly polymerized MT end. However, in contrast to all other known +TIPs, STIM1 is diffusing not in the cytoplasm but in the ER membrane. Our data show that a MT tip growing along a membrane can continuously remodel it by concentrating certain molecules for which it has affinity. Furthermore, our

findings suggest that a specific interaction of membrane-embedded molecules with the growing MT ends can create forces that are sufficient to cause membrane deformation and tubule extension, similar to motor-based pulling of membrane tubules along stabilized MTs [17].

Although a recent study showed that complete MT depolymerization affects Ca<sup>2+</sup> release-activated Ca<sup>2+</sup> currents [10], our experiments failed to find an effect of MT stabilization or EB1 depletion on SOCE, indicating that comet-like behavior of STIM1 plays no significant role in regulating Ca<sup>2+</sup> influx when Ca<sup>2+</sup> stores are fully depleted by thapsigargin treatment. Still, it is possible that in physiological conditions MT-growth-dependent ER remodeling and STIM1 concentration could be important for the formation of ER-plasma membrane junctions and the spatial organization of Ca<sup>2+</sup> signaling.

**Supplemental Data**

Supplemental Experimental Procedures, two tables, five figures, and nine movies are available at <http://www.current-biology.com/cgi/content/full/18/3/177/DC1/>.

## Acknowledgments

We thank K. Bezstarosti and P. Wulf for technical assistance. We are grateful to R. Tsiens and R. Lewis for the gift of materials. This work was supported by the Netherlands Organization for Scientific Research grants 814.02.005 and 816.02.016 to A.A., the Dutch Ministry of Economic Affairs, a Fundação para a Ciência e a Tecnologia fellowship to S.M.G., the Netherlands Organization for Scientific Research (NWO-ZonMw-VIDI) and the European Science Foundation (European Young Investigators) awards to C.C.H., the Swiss National Science Foundation through grant 3100A0-109423 to M.O.S., and the Intramural Research Program of the National Institutes of Health, National Institute of Environmental Health Sciences (J.T.S and J.W.P.).

Received: September 8, 2007

Revised: December 19, 2007

Accepted: December 19, 2007

Published online: January 31, 2008

## References

1. Luik, R.M., and Lewis, R.S. (2007). New insights into the molecular mechanisms of store-operated Ca<sup>2+</sup> signaling in T cells. *Trends Mol. Med.* *13*, 103–107.
2. Putney, J.W., Jr. (2007). New molecular players in capacitative Ca<sup>2+</sup> entry. *J. Cell Sci.* *120*, 1959–1965.
3. Hogan, P.G., and Rao, A. (2007). Dissecting ICRAC, a store-operated calcium current. *Trends Biochem. Sci.* *32*, 235–245.
4. Wu, M.M., Luik, R.M., and Lewis, R.S. (2007). Some assembly required: Constructing the elementary units of store-operated Ca(2+) entry. *Cell Calcium* *42*, 163–172.
5. Baba, Y., Hayashi, K., Fujii, Y., Mizushima, A., Watarai, H., Wakamori, M., Numaga, T., Mori, Y., Iino, M., Hikida, M., and Kurosaki, T. (2006). Coupling of STIM1 to store-operated Ca<sup>2+</sup> entry through its constitutive and inducible movement in the endoplasmic reticulum. *Proc. Natl. Acad. Sci. USA* *103*, 16704–16709.
6. Waterman-Storer, C.M., and Salmon, E.D. (1998). Endoplasmic reticulum membrane tubules are distributed by microtubules in living cells using three distinct mechanisms. *Curr. Biol.* *8*, 798–806.
7. Waterman-Storer, C.M., Gregory, J., Parsons, S.F., and Salmon, E.D. (1995). Membrane/microtubule tip attachment complexes (TACs) allow the assembly dynamics of plus ends to push and pull membranes into tubulovesicular networks in interphase *Xenopus* egg extracts. *J. Cell Biol.* *130*, 1161–1169.
8. Lansbergen, G., and Akhmanova, A. (2006). Microtubule plus end: A hub of cellular activities. *Traffic* *7*, 499–507.
9. Wu, M.M., Buchanan, J., Luik, R.M., and Lewis, R.S. (2006). Ca<sup>2+</sup> store depletion causes STIM1 to accumulate in ER regions closely associated with the plasma membrane. *J. Cell Biol.* *174*, 803–813.
10. Smyth, J.T., Dehaven, W.I., Bird, G.S., and Putney, J.W., Jr. (2007). Role of the microtubule cytoskeleton in the function of the store-operated Ca<sup>2+</sup> channel activator STIM1. *J. Cell Sci.* *120*, 3762–3771.
11. Dziadek, M.A., and Johnstone, L.S. (2007). Biochemical properties and cellular localisation of STIM proteins. *Cell Calcium* *42*, 123–132.
12. Galjart, N. (2005). CLIPs and CLASPs and cellular dynamics. *Nat. Rev. Mol. Cell Biol.* *6*, 487–498.
13. Stepanova, T., Slemmer, J., Hoogenraad, C.C., Lansbergen, G., Dortmund, B., De Zeeuw, C.I., Grosveld, F., van Cappellen, G., Akhmanova, A., and Galjart, N. (2003). Visualization of microtubule growth in cultured neurons via the use of EB3-GFP (end-binding protein 3-green fluorescent protein). *J. Neurosci.* *23*, 2655–2664.
14. Liou, J., Fivaz, M., Inoue, T., and Meyer, T. (2007). Live-cell imaging reveals sequential oligomerization and local plasma membrane targeting of stromal interaction molecule 1 after Ca<sup>2+</sup> store depletion. *Proc. Natl. Acad. Sci. USA* *104*, 9301–9306.
15. Watson, P., and Stephens, D.J. (2006). Microtubule plus-end loading of p150(Glued) is mediated by EB1 and CLIP-170 but is not required for intracellular membrane traffic in mammalian cells. *J. Cell Sci.* *119*, 2758–2767.
16. Perez, F., Diamantopoulos, G.S., Stalder, R., and Kreis, T.E. (1999). CLIP-170 highlights growing microtubule ends in vivo. *Cell* *96*, 517–527.
17. Koster, G., VanDuijn, M., Hofs, B., and Dogterom, M. (2003). Membrane tube formation from giant vesicles by dynamic association of motor proteins. *Proc. Natl. Acad. Sci. USA* *100*, 15583–15588.

# Supplemental Data

S1

## STIM1 Is a MT-Plus-End-Tracking Protein Involved in Remodeling of the ER

Ilya Grigoriev, Susana Montenegro Gouveia, Babet van der Vaart, Jeroen Demmers, Jeremy T. Smyth, Srinivas Honnappa, Daniël Splinter, Michel O. Steinmetz, James W. Putney, Jr., Casper C. Hoogenraad, and Anna Akhmanova

### Supplemental Experimental Procedures

#### Cell Culture, Expression Constructs, and Transfection of Plasmids and siRNAs

HeLa, MRC5-SV, B16F1, and HEK293 cells were cultured as described previously [S1]. The GFP-STIM1 fusion [S2] was a gift of Dr. R. Lewis (Stanford University, Stanford, CA), mCherry- $\alpha$ -tubulin [S3] was a gift of Dr. R. Tsien (University of California, San Diego, La Jolla, CA), and pDsRed2-ER and pYFP-ER were purchased from Clontech. EB3-mRFP was generated by substituting the GFP-encoding part of EB3-GFP [S4] for mRFP (a gift of Dr. R. Tsien). FuGENE 6 (Roche) reagent was used for plasmid transfection of HeLa and MRC5-SV cells; HEK293 cells were transfected with Lipofectamine 2000 (Invitrogen). A HeLa cell line stably expressing mCherry- $\alpha$ -tubulin was generated as described previously [S5]. siRNAs were synthesized by Ambion and were directed against the following target sequences: EB1 #1, AUUCCAAGCUAAGCUAGAA and EB1 #2, UUCGUUCAGUGGUUC AAGA [S6]; STIM1 #1, GGCUCUGGAUACAGUCUC [S7]; and STIM1 #2, GGGGAAGACCUCAAUACCA [S8]. We used two control siRNAs, with the sequences GCACUCAUUAUGACUCCAU [S5] and CGUACGCGGAAUACUU CGA (luciferase GL2, QIAGEN); both gave the same phenotypes in the assays described in this study. Synthetic siRNAs were transfected by using HiPerFect (QIAGEN) at a concentration 5 nM. Cells were analyzed by different methods 3 days after siRNA transfection and 1–3 days after plasmid transfection.

#### GST Pull-Down Assays and Mass Spectrometry

GST fusions of EB1, EB2, EB3, EB1-N, and EB1-C; expression and purification of the GST-tagged proteins from *E. coli*, and Western blotting were performed as described by [S9]. Purified untagged EB1 was prepared as described previously [S10]. Lysates of untransfected B16F1 cells or transfected HEK293 cells were prepared in a buffer containing 20 mM Tris-HCl (pH 7.5), 100 mM NaCl, 1% Triton X-100, 1 mM DTT, and protease inhibitors (Complete, Roche). Cell lysates were centrifuged at 16,000  $\times$  g for 15 min at 4°C, and the supernatant was incubated with individual GST fusion proteins for 2 hr at 4°C. Beads were washed four times with a buffer containing 20 mM Tris-HCl (pH 8), 150 mM NaCl, 0.05% Triton X-100, and 1 mM DTT. The proteins retained on the beads were analyzed by Western blotting or mass spectrometry.

#### Antibodies, Immunofluorescent Staining, and Immunoprecipitation

We used rabbit polyclonal antibodies against GFP (Abcam) and EB1 [S5], mouse monoclonal antibodies against EB1, p150<sup>GluEed</sup> and GM130 (BD Biosciences), and STIM1 (Abnova) and rat monoclonal antibodies against EB1

Table S1. Identification of STIM1 and STIM2 as Potential EB Partners by Mass Spectrometry in B16F1 Mouse Melanoma Cell Extract

Identified Proteins	NCBI Identification Score	Mascot			% Coverage			Unique Peptides		
		EB1	EB2	EB3	EB1	EB2	EB3	EB1	EB2	EB3
CLIP-115	gij85662406	3143	1652	3140	45	28.3	48.9	39	24	42
CLASP 1	gij82881262	1560	160	1027	23.8	11.7	15.7	27	5	19
CLASP 2	gij58037445	2349	363	2133	36	12.9	32.5	34	8	31
CLIP-170	gij23821025	1698	252	2087	23.9	8	26.6	29	5	33
Dynactin 1 (p150 <sup>GluEed</sup> )	gij74186248	2321		1126	35.6		20.8	31		18
melanophilin	gij87080831	488		551	19.3		23.4	7		8
STIM 1	gij17368305	1234		614	31.7		17.7	17		9
STIM 2	gij94374457	232		368	14.1		12.5	5		6

Only proteins that were absent from control pull-downs with GST alone are included in the table. Several known EBs binding +TIPs are included in this table for comparison. A complete list of all proteins identified in this experiment will be published elsewhere (S.M.G., unpublished data).

(clone KT51, Absea) and  $\alpha$ -tubulin (Abcam). Secondary Alexa 594-conjugated goat antibodies against rat and mouse IgG were purchased from Molecular Probes. Cells were fixed with -20°C methanol fixation for 15 min, postfixed in 4% paraformaldehyde in PBS for 15 min at room temperature, and rinsed with 1% Triton X-100 in PBS; subsequent washing and staining steps were carried out in PBS supplemented with 1% bovine serum albumin and 0.15% Tween-20. Immunoprecipitation of the endogenous EB1 was performed with rabbit polyclonal antibodies as described previously [S5].

#### Image Acquisition and Processing

Images of fixed cells were collected with a Leica DMRBE microscope equipped with a PL Fluotar 100 $\times$  1.3 N.A. oil objective, a FITC/EGFP filter 41012 (Chroma), a Texas Red filter 41004 (Chroma), and an ORCA-ER-1394 CCD camera (Hamamatsu). Twelve-bit images were projected onto the CCD chip at a magnification of 0.1  $\mu$ m/pixel. Images of fixed samples were prepared with Adobe Photoshop by converting them to 8-bit images and linear adjustment of "levels"; no image filtering was performed.

Simultaneous dual-color (green and red), time-lapse live-cell imaging was performed on the inverted research microscope Nikon Eclipse TE2000E (Nikon) with a CFI Apo TIRF 100 $\times$  1.49 N.A. oil objective (Nikon), equipped with

Table S2. Parameters of ER Dynamics in MRC5-SV Cells

Type of Elongation	Control		GFP-STIM1 Expression	
	Sliding ER Tubule	TACs	Sliding ER Tubule	TACs
Elongation rate, $\mu$ m/s	1.39 $\pm$ 0.69	0.22 $\pm$ 0.17	1.38 $\pm$ 0.76	0.22 $\pm$ 0.09
Total n in total cells	71 in 5	4 in 5	45 in 5	50 in 5
Frequency of new tubule formation events, per 100 $\mu$ m <sup>2</sup> per 1 min	5.31 $\pm$ 1.94	0.31 $\pm$ 0.20	3.65 $\pm$ 1.41*	3.88 $\pm$ 2.60**
Ratio sliding/TACs	17.13		0.94	

The events of de novo ER tubule formation were identified by observing a luminal ER marker (YFP-ER in control cells or DsRed2-ER in GFP-STIM1-expressing cells). In control cells, ER tubule sliding along pre-existing MTs was distinguished from TAC-mediated tubule formation by simultaneous imaging with MTs, which were visualized with mCherry- $\alpha$ -tubulin. In GFP-STIM1-expressing cells, TAC-dependent tubules were distinguished from the sliding ones by the presence of a GFP-STIM1 comet at their tip (this was possible because all motile GFP-STIM1 comets correspond to the growing MT ends, and the interaction of a growing MT tip with the ER membrane induces a GFP-STIM1 comet). Values indicate mean  $\pm$  SD; values significantly different in GFP-STIM1-expressing cells compared to control cells are marked with asterisks.

\*p < 0.05, \*\*p < 0.001; Mann-Whitney U test.

S2

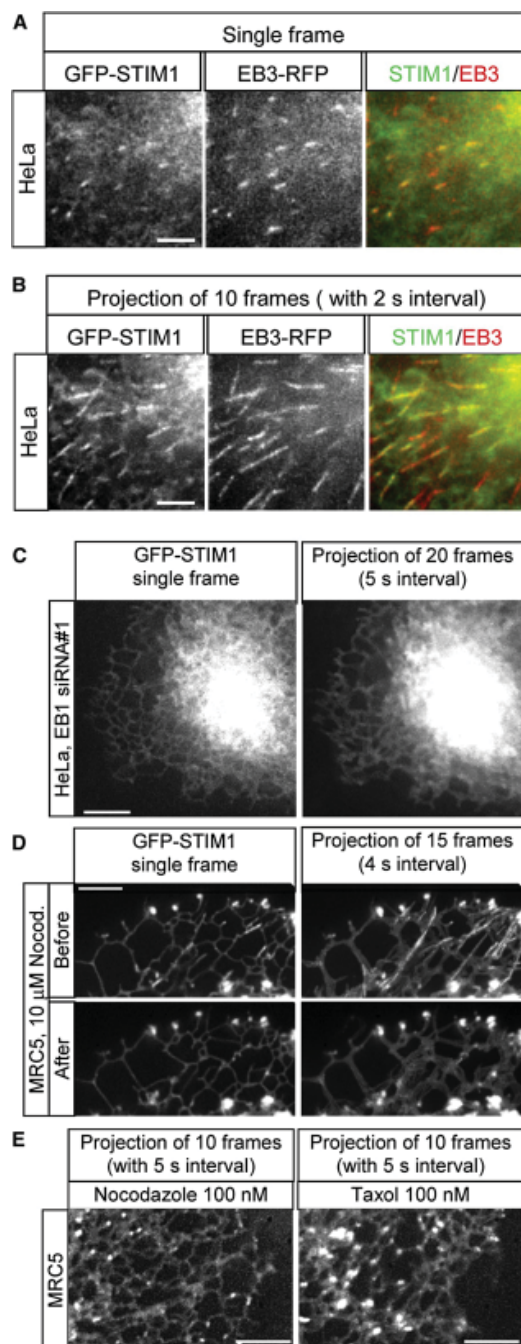


Figure S1. GFP-STIM1 Localizes to the Growing MT Tips in an EB1-Dependent Manner

(A and B) Simultaneous imaging of GFP-STIM1 (green in overlay) and EB3-mRFP (red in overlay) in a transiently transfected HeLa cell. A single frame of Movie S2 is shown in (A) and projection analysis is shown in (B). The bars represent 3  $\mu\text{m}$ .

QuantEM EMCCD camera (Roper Scientific) controlled by MetaMorph 7.1 software (Molecular Devices). For excitation we used a HBO 103 W/2 Mercury Short Arc Lamp (Osram) and a Chroma ET-GFP/mCherry filter cube. For separation of emissions we used DualView (Optical Insight) with emitters HQ530/30M and HQ630/50M (Chroma) and the beam splitter 565DCXR (Chroma). The same set-up was used for dual-color total internal reflection fluorescence microscopy (TIRFM). For excitation we used simultaneously the 113 mW, 488 nm laser line of an argon laser (Spectra-Physics Lasers) and an 11 mW, 561 nm diode-pumped solid-state laser (Melles Griot) and Chroma ET-GFP/mCherry filter cube. The 16-bit images were projected onto the CCD chip at a magnification of 0.067  $\mu\text{m}/\text{pixel}$ , with intermediate magnification of 2.5 $\times$ . FRAP assay was performed on the same microscope with the FRAP scanning head FRAP L5 D - CURIE (Curie Institute) and the 113 mW, 488 nm laser line of an argon laser (Spectra-Physics Lasers). During imaging cells were maintained at 37 $^{\circ}\text{C}$  in the standard culture medium in a closed chamber. All live images, with the exception of those used for the analysis of ER extension events in HeLa cells (Figures 4D and 4E, Figure S5, and Movie S9) were acquired with wide-field fluorescence microscopy. To improve contrast of dual-color images of HeLa cells, which are rather thick and have a dense microtubule system, we used the TIRFM set-up in a semi-TIRF mode, which allowed optimal visualization of the  $\sim 0.5\text{-}1 \mu\text{m}$  thick part of the cell proximal to the coverslip. Images of live cells were adjusted with MetaMorph and Adobe Photoshop software as described in the supplemental data. Image analysis was performed by using MetaMorph software.

#### Intracellular $\text{Ca}^{2+}$ Measurements

Intracellular  $\text{Ca}^{2+}$  concentration was measured in individual cells with a microscope-based imaging system as previously described [S11, S12]. Briefly, cells were loaded with the  $\text{Ca}^{2+}$  indicator dye Fura-5F/AM, and fluorescence emission intensity at 510 nm was measured when cells were sequentially excited at 340 nm and 380 nm. Data representing relative intracellular  $\text{Ca}^{2+}$  concentrations are reported as 340/380 ratios.

#### Mass Spectrometry Analysis

For mass spectrometry analysis, proteins bound to the beads were separated on a 3%–8% NuPAGE tris-acetate gel and stained with the Colloidal Blue staining kit (Invitrogen). Gel lanes were cut into 2 mm slices with an automatic gel slicer and subjected to in-gel reduction with dithiothreitol, alkylation with iodoacetamide, and digestion with trypsin (Promega, sequencing grade), essentially as described previously [S13]. Nanoflow LC-MS/MS was performed on an 1100 series capillary LC system (Agilent Technologies) coupled to an LTQ linear ion trap mass spectrometer (Thermo) operating in positive mode and equipped with a nanospray source. Peptide mixtures were trapped on a ReproSil C18 reversed phase column (Dr. Maisch GmbH, Tübingen, Germany; column dimensions 1.5 cm  $\times$  100  $\mu\text{m}$ , packed in-house) at a flow rate of 8  $\mu\text{l}/\text{min}$ . Peptide separation was performed on ReproSil C18 reversed phase column (Dr. Maisch GmbH, Tübingen, Germany; column dimensions 15 cm  $\times$  50  $\mu\text{m}$ , packed in-house) with a linear gradient from 0 to 80% B (A = 0.1 M acetic acid; B = 80% (v/v) acetonitrile, 0.1 M acetic acid) in 70 min and at a constant flow rate of 200 nl/min with a splitter. The column eluent was directly sprayed into the ESI source of the mass spectrometer. Mass spectra were acquired in continuum mode; fragmentation of the peptides was performed in data-dependent mode. Peak lists were automatically created from raw data files by using Mascot Distiller software (version 2.1; MatrixScience). The Mascot search algorithm (version 2.1, MatrixScience) was used for searching against the NCBI nr database (release NCBI nr\_20070217; taxonomy: *Mus musculus*). The peptide tolerance was typically set to 2 Da and the fragment ion tolerance to 0.8 Da. A maximum number of two missed cleavages by trypsin were allowed and carbamidomethylated cysteine and oxidized methionine were set as fixed and variable modifications, respectively. The Mascot score cutoff

(C) HeLa cells were transfected with the siRNA EB1 #1; two days later the cells were transfected with GFP-STIM1, cultured for 1 more day, and used for live imaging. A single frame from Movie S8 is shown on the left, and projection analysis is shown on the right. The bar represents 10  $\mu\text{m}$ . (D) MRC5-SV cells were transfected with GFP-STIM1 and imaged before and 18 s after nocodazole addition. Single frames are shown on the left, projection analysis is shown on the right. The bar represents 5  $\mu\text{m}$ . (E) MRC5-SV cells were transfected with GFP-STIM1 and imaged after the addition of low dosages of nocodazole or taxol. Images show superimposition of ten successive frames. The bar represents 5  $\mu\text{m}$ .

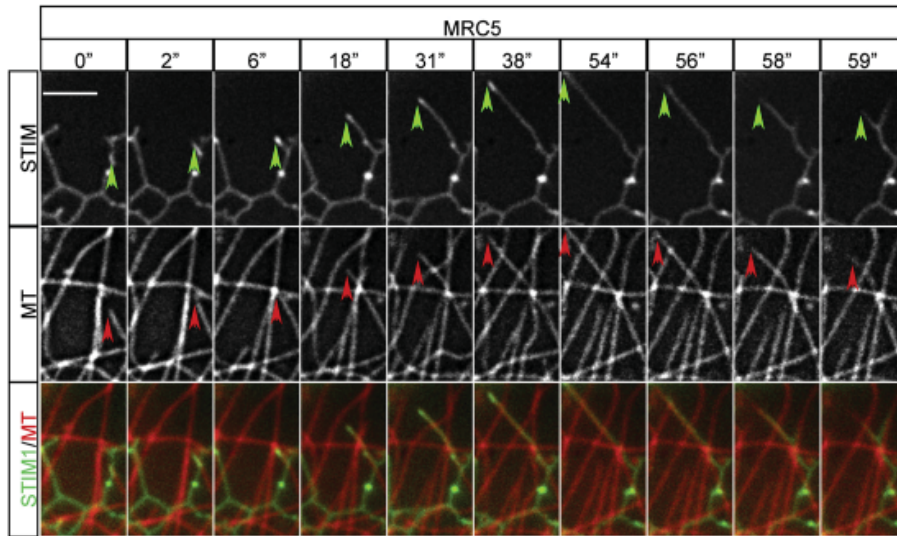


Figure S2. GFP-STIM1 Accumulates at the Tips of Extending ER Tubules in a MT Polymerization-Dependent Manner

Simultaneous imaging of GFP-STIM1 (green in overlay) and mCherry- $\alpha$ -tubulin (red in overlay) in transiently transfected MRC5-SV cells. Successive frames are shown; time is indicated above the panels. Tips of extending/retracting ER tubules and MTs are indicated by green and red arrows, respectively. The bars represent 3  $\mu$ m.

value for a positive protein hit was set to 60. Individual peptide MS/MS spectra with Mowse scores below 40 were checked manually and either interpreted as valid identifications or discarded.

**Details of Acquisition and Processing for Live-Cell Images Shown in Figures 2 and 3 and Figures S1–S3**

**Figure 2A**

Cells were imaged with 1 s exposure time without delay between frames. The following image adjustments were performed in Adobe Photoshop: levels and blur filter (sensitivity 0.3).

**Figure 2B**

Cells were imaged with 1 s exposure time without delay between frames. The following image adjustments were performed in Adobe Photoshop: unsharp mask filter (amount, 100%; radius 4.0 pixels; threshold, 0 levels), and levels and blur filter (sensitivity 0.3) for the red channel.

**Figure 2C**

Cells were imaged with 1 s exposure time without delay between frames. The following image adjustments were performed in MetaMorph: low-pass filter (horizontal size, 24; vertical size, 24), subtraction of low-pass-filtered image from the original one (plus value 10,000), blur filter (sensitivity 1), and equalize light (average, by multiplication). The following image adjustments were performed in Adobe Photoshop: unsharp mask filter (amount, 100%; radius, 4.0 pixels; threshold, 0 levels), levels and blur filter (sensitivity 0.3) for the green channel, and levels and blur filter (sensitivity 0.3) for the red channel.

**Figure 2D**

Cells were imaged with 1 s exposure time without delay between frames. The following image adjustments were performed in Adobe Photoshop: unsharp mask filter (amount, 100%; radius 4.0 pixels; threshold, 0 levels), blur filter (sensitivity 0.3) and levels for the green channel, and unsharp mask filter (amount, 100%; radius, 4.0 pixels; threshold 0 levels), blur filter (sensitivity 0.3), unsharp mask filter (amount, 100%; radius, 4.0 pixels; threshold, 0 levels), blur filter (sensitivity 0.3), and levels for the red channel.

**Figure 3A**

Cells were imaged with 1 s exposure time without delay between frames. The following image adjustments were performed in Adobe Photoshop: unsharp mask filter (amount, 100%; radius, 4.0 pixels; threshold, 0 levels), blur filter (sensitivity 0.3), and levels.

**Figure 3C**

Cells were imaged with 1 s exposure time and a 2 s delay between frames. The following image adjustments were performed in Adobe Photoshop: unsharp mask filter (amount, 100%; radius, 4.0 pixels; threshold, 0 levels), blur filter (sensitivity 0.3), and levels.

**Figure S1A**

Cells were imaged with 0.5 s exposure time and a 2 s delay between frames. The image was adjusted in MetaMorph by applying the blur filter (sensitivity 1). Levels were adjusted in Adobe Photoshop.

**Figure S1B**

The image was adjusted in MetaMorph by applying the blur filter (sensitivity 1). The following image adjustments were performed in Adobe Photoshop: levels and projection of ten adjacent frames. The blending mode for each layer was "lighten," opacity 100%, and fill 100%.

**Figure S1C**

Cells were imaged with 1 s exposure time without delay between frames. The following image adjustments were performed in Adobe Photoshop: unsharp mask filter (amount, 100%; radius, 4.0 pixels; threshold, 0 levels), blur filter (sensitivity 0.3), and levels.

For the right side of the figure, the following image adjustments were performed in Adobe Photoshop: unsharp mask filter (amount, 100%; radius, 4.0 pixels; threshold, 0 levels), blur filter (sensitivity 0.3), levels, and projection of 20 frames (every fifth frame). The blending mode for each layer was "lighten," opacity 100%, and fill 100%.

**Figure S1D**

For the left side of the figure, the following image adjustments were performed in Adobe Photoshop: unsharp mask filter (amount, 100%; radius 4.0 pixels; threshold, 0 levels), blur filter (sensitivity 0.3), and levels.

For the right side of the figure, the following image adjustments were performed in Adobe Photoshop: unsharp mask filter (amount, 100%; radius, 4.0 pixels; threshold, 0 levels), blur filter (sensitivity 0.3), levels, and projection of 15 frames (every second frame). The blending mode for each layer was "lighten," opacity 100%, and fill 100%.

**Figure S1E**

For the left side of the figure, cells were imaged with 1s exposure time without delay between frames. The following image adjustments were performed in Adobe Photoshop: unsharp mask filter (amount, 100%; radius, 4.0 pixels; threshold, 0 levels), blur filter (sensitivity 0.3), levels, and projection of ten frames (every fifth frame). The blending mode for each layer was "lighten," opacity 100%, and fill 100%.

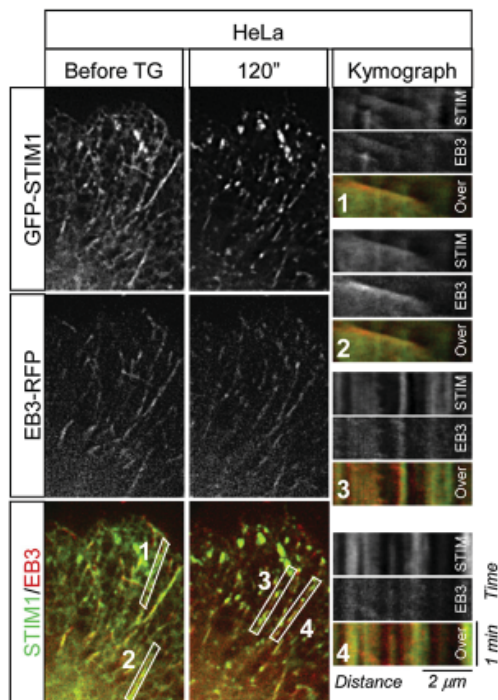


**Figure S3. Analysis of GFP-STIM1 Dynamics after  $\text{Ca}^{2+}$  Store Depletion**  
Representative frames of simultaneous two-color videos of a HeLa cell expressing GFP-STIM1 and EB3-RFP before and 120 s after the addition of 2  $\mu\text{M}$  thapsigargin in normal culture medium. Kymographs illustrating the changes of fluorescent intensity over time in the indicated boxed areas are shown on the right. In the kymographs motile comets appear as slopes and immobile structures as vertical lines.

For the right side of the figure, cells were imaged with 1 s exposure time without delay between frames. The following image adjustments were performed in Adobe Photoshop: unsharp mask filter (amount, 100%; radius, 4.0 pixels; threshold, 0 levels), blur filter (sensitivity 0.3), levels, and projection of ten frames (every fifth frame). The blending mode for each layer was "lighten," opacity 100%, and fill 100%.

#### Figure S2

Cells were imaged with 1 s exposure time without delay between frames. The following image adjustments were performed in Adobe Photoshop: unsharp mask filter (amount, 100%; radius, 4.0 pixels; threshold, 0 levels), blur filter (sensitivity 0.3), and levels for the green channel, and unsharp mask filter (amount, 100%; radius, 4.0 pixels; threshold 0 levels), blur filter (sensitivity 0.3), and levels for the red channel.

#### Figure S3

Cells were imaged with 1 s exposure time and a 2 s delay between frames. The following image adjustments were performed in Adobe Photoshop: unsharp mask filter (amount, 100%; radius, 4.0 pixels; threshold, 0 levels), blur filter (sensitivity 0.3), and levels.

#### Supplemental References

- S1. Lansbergen, G., Grigoriev, I., Mimori-Kiyosue, Y., Ohtsuka, T., Higa, S., Kitajima, I., Demmers, J., Galjart, N., Houtsmuller, A.B., Grosveld, F., and Akhmanova, A. (2006). CLASPs attach microtubule plus ends to the cell cortex through a complex with LL5beta. *Dev. Cell* **11**, 21–32.
- S2. Wu, M.M., Buchanan, J., Luik, R.M., and Lewis, R.S. (2006).  $\text{Ca}^{2+}$  store depletion causes STIM1 to accumulate in ER regions closely associated with the plasma membrane. *J. Cell Biol.* **174**, 803–813.
- S3. Shaner, N.C., Campbell, R.E., Steinbach, P.A., Giepmans, B.N., Palmer, A.E., and Tsien, R.Y. (2004). Improved monomeric red, orange

and yellow fluorescent proteins derived from *Discosoma* sp. red fluorescent protein. *Nat. Biotechnol.* **22**, 1567–1572.

- S4. Stepanova, T., Slemmer, J., Hoogenraad, C.C., Lansbergen, G., Dortland, B., De Zeeuw, C.I., Grosveld, F., van Cappellen, G., Akhmanova, A., and Galjart, N. (2003). Visualization of microtubule growth in cultured neurons via the use of EB3-GFP (end-binding protein 3-green fluorescent protein). *J. Neurosci.* **23**, 2655–2664.
- S5. Mimori-Kiyosue, Y., Grigoriev, I., Lansbergen, G., Sasaki, H., Matsui, C., Severin, F., Galjart, N., Grosveld, F., Vorobjev, I., Tsukita, S., and Akhmanova, A. (2005). CLASP1 and CLASP2 bind to EB1 and regulate microtubule plus-end dynamics at the cell cortex. *J. Cell Biol.* **168**, 141–153.
- S6. Watson, P., and Stephens, D.J. (2006). Microtubule plus-end loading of p150(Glued) is mediated by EB1 and CLIP-170 but is not required for intracellular membrane traffic in mammalian cells. *J. Cell Sci.* **119**, 2758–2767.
- S7. Roos, J., DiGregorio, P.J., Yeromin, A.V., Ohlsen, K., Liudyno, M., Zhang, S., Safrina, O., Kozak, J.A., Wagner, S.L., Cahalan, M.D., et al. (2005). STIM1, an essential and conserved component of store-operated  $\text{Ca}^{2+}$  channel function. *J. Cell Biol.* **169**, 435–445.
- S8. Peel, S.E., Liu, B., and Hall, I.P. (2006). A key role for STIM1 in store operated calcium channel activation in airway smooth muscle. *Respir. Res.* **7**, 119.
- S9. Komarova, Y., Lansbergen, G., Galjart, N., Grosveld, F., Borisy, G.G., and Akhmanova, A. (2005). EB1 and EB3 control CLIP dissociation from the ends of growing microtubules. *Mol. Biol. Cell* **16**, 5334–5345.
- S10. Honnappa, S., John, C.M., Kostrewa, D., Winkler, F.K., and Steinmetz, M.O. (2005). Structural insights into the EB1-APC interaction. *EMBO J.* **24**, 261–269.
- S11. Baba, Y., Hayashi, K., Fujii, Y., Mizushima, A., Watarai, H., Wakamori, M., Numaga, T., Mori, Y., Iino, M., Hikida, M., and Kurosaki, T. (2006). Coupling of STIM1 to store-operated  $\text{Ca}^{2+}$  entry through its constitutive and inducible movement in the endoplasmic reticulum. *Proc. Natl. Acad. Sci. USA* **103**, 16704–16709.
- S12. Smyth, J.T., Dehaven, W.I., Bird, G.S., and Putney, J.W., Jr. (2007). Role of the microtubule cytoskeleton in the function of the store-operated  $\text{Ca}^{2+}$  channel activator STIM1. *J. Cell Sci.* **120**, 3762–3771.
- S13. Wilm, M., Shevchenko, A., Houthaeve, T., Breit, S., Schweigerer, L., Fotsis, T., and Mann, M. (1996). Femtomole sequencing of proteins from polyacrylamide gels by nano-electrospray mass spectrometry. *Nature* **379**, 466–469.

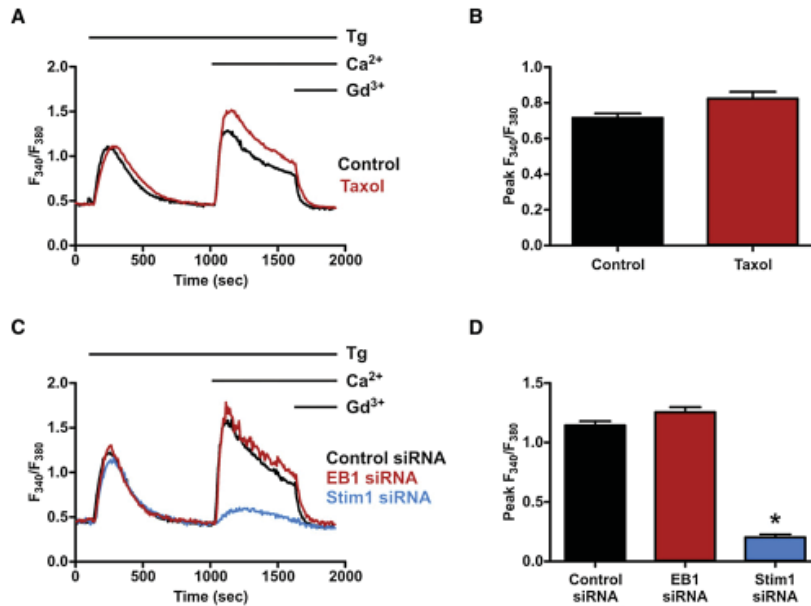


Figure S4. EB1 Depletion or Inhibition of MT Dynamics with Taxol Have No Effect on Thapsigargin-Induced SOCE

Single-cell  $Ca^{2+}$  concentrations were measured in live cells plated on glass coverslips and mounted in Teflon chambers. Prior to experiments, cells were incubated in 1  $\mu$ M Fura-5F/AM (Invitrogen) for 25 min at 37°C. Cells were then bathed in room temperature HEPES-buffered saline solution (HBSS; 120 mM NaCl, 5.4 mM KCl, 0.8 mM  $MgCl_2$ , 11 mM glucose, and 20 HEPES [pH 7.4]) throughout the course of the experiments. Fura-5F/AM fluorescence emission at 510 nm was measured when cells were excited consecutively at 340 nm and 380 nm by using a microscope-based digital fluorescence imaging system (InCyt Im2; Intracellular Imaging Inc.), and relative  $Ca^{2+}$  concentrations are reported as the ratio of fluorescence emission at the two excitation wavelengths. At the end of each experiment, Fura-5F/AM fluorescence was quenched by treating cells with 10  $\mu$ M ionomycin and 20 mM  $MnCl_2$  to obtain background fluorescence values; these background values were subtracted from each experimental measurement. To monitor SOCE, HeLa cells were treated with 2  $\mu$ M thapsigargin (Tg) in nominally  $Ca^{2+}$ -free extracellular medium to deplete intracellular  $Ca^{2+}$  stores. Fifteen minutes later, extracellular  $Ca^{2+}$  was restored to 1.8 mM to reveal SOCE. Gadolinium (5  $\mu$ M), which inhibits SOCE, was added in the continued presence of 1.8 mM extracellular  $Ca^{2+}$  at the end of each experiment to demonstrate the specificity of the SOCE response.

(A) SOCE was monitored in cells pretreated for 20 min with 500 nM taxol (red trace) or in cells left untreated (control; black trace). For taxol-treated cells, the drug was present throughout the course of the experiment. Each trace represents the average response of all the cells measured in a single experiment. (B) The peak SOCE responses above baseline from experiments performed as described in (A) were averaged for untreated control cells (n = 104 cells, three experiments) and for taxol-treated cells (n = 81 cells, three experiments). Data are reported as mean  $\pm$  SEM.

(C) SOCE responses of cells treated with siRNA targeted to EB1 (red trace), STIM1 (blue trace), or control siRNA (black trace).

(D) The peak SOCE responses above baseline from experiments performed as described in (C) were averaged for cells treated with control siRNA (n = 107 cells, three experiments), EB1 siRNA (n = 115 cells, three experiments), and STIM1 siRNA (n = 106 cells, three experiments). Data are reported as mean  $\pm$  SEM; An asterisk (\*) indicates significant difference ( $p < 0.01$ ) compared to control siRNA based on one-way ANOVA.

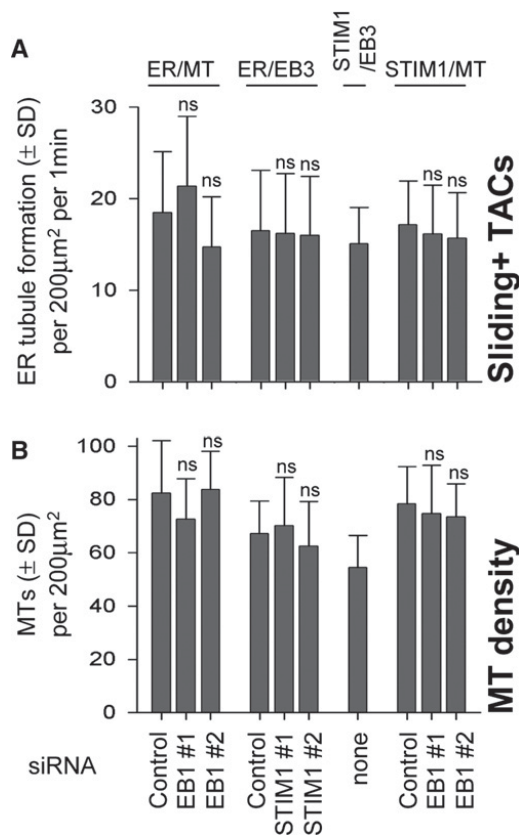


Figure S5. Quantification of ER Protrusion Events and MT Density after STIM1 and EB1 Depletion

HeLa cells were transfected with the indicated siRNAs; 1 day later cells were transfected with plasmid DNA, cultured for 2 more days, and used for dual-color imaging. The following combinations of fluorescent markers were used: mCherry- $\alpha$ -tubulin (stably expressed in HeLa cells) together with transiently expressed YFP-ER; transiently expressed EB3-mRFP and YFP-ER together with transiently expressed EB3-mRFP and GFP-STIM1; and mCherry- $\alpha$ -tubulin (stably expressed in HeLa cells) together with transiently expressed GFP-STIM1.

(A) Total number of ER protrusion events (a sum of TAC and sliding events). Error bars represent SD.

(B) MT density, determined by projecting all frames of 50 s long movies, with either mCherry- $\alpha$ -tubulin or EB3-mRFP as markers. Because most of the MTs underwent elongation during the 50 s period, the numbers of MTs visualized by the two markers are not significantly different. Error bars represent SD.

Number of analyzed cells. ER-MT: control,  $n = 20$ ; EB1 #1,  $n = 20$ ; EB1 #2,  $n = 15$ . ER-EB3: control,  $n = 20$ ; STIM1 #1,  $n = 20$ ; STIM1 #2,  $n = 20$ . STIM1-EB3:  $n = 20$ . STIM1-MT: control,  $n = 10$ ; EB1 #1,  $n = 15$ ; EB1 #2,  $n = 15$ . Values obtained in EB1 or STIM1 siRNA-treated cells that were significantly different from the corresponding values in cells treated with the control siRNAs are indicated by asterisks (\*\*\*)  $p < 0.001$ , \*\*  $p < 0.01$ , \*  $p < 0.05$ ;  $p > 0.05$ , n.s.; Kolmogorov-Smirnov test).









# Chapter 3

## **SLAIN2 links microtubule plus-end tracking proteins and controls microtubule growth in interphase**

Babet van der Vaart, Cristina Manatschal, Ilya Grigoriev, Vincent Olieric, Susana Montenegro Gouveia, Saša Bjelić, Jeroen Demmers, Ivan Vorobjev, Casper C. Hoogenraad, Michel O. Steinmetz and Anna Akhmanova

*The Journal of Cell Biology. 2011*





## **Abstract**

Growing microtubules accumulate at their ends a set of diverse factors known as microtubule plus end tracking proteins (+TIPs), which control microtubule dynamics and organization. Here, we identified SLAIN2 as a key component of +TIP interaction networks. We showed that the C-terminal part of SLAIN2 binds to EBs, CLIPs and CLASPs, and characterized in detail the interaction of SLAIN2 with EB1 and CLIP-170. Further, we found that the N-terminal part of SLAIN2 interacts with ch-TOG, the mammalian homologue of the microtubule polymerase XMAP215. Through its multiple interactions, SLAIN2 enhances ch-TOG accumulation at microtubule plus ends and, as a consequence, strongly stimulates processive microtubule polymerization in interphase cells. Depletion or disruption of the SLAIN2-ch-TOG complex leads to disorganization of the radial microtubule array. During mitosis, SLAIN2 becomes highly phosphorylated, and its interaction with EBs and ch-TOG is inhibited. Our study provides new insights into the molecular mechanisms underlying cell-cycle-specific regulation of microtubule polymerization and the organization of the microtubule network.

## **Introduction**

Microtubules (MTs) are filamentous structures required for various cellular processes such as intracellular transport, cell division and locomotion. The remodeling of MT networks depends on MT dynamic instability – spontaneous switching between episodes of growth and shortening (Desai and Mitchison, 1997). Numerous cellular factors control MT polymerization, depolymerization and pausing, or transitions between different states (catastrophes and rescues) (Desai and Mitchison, 1997; van der Vaart et al., 2009).

MTs are intrinsically asymmetric, and in cells only one of the two MT ends, the plus end, can grow. Not surprisingly, it is an important site for the regulation of MT dynamics (Howard and Hyman, 2003). Among MT regulators, MT plus end tracking proteins (+TIPs) are distinguished by their ability to form comet-like accumulations at the ends of growing MTs (Schuyler and Pellman, 2001). +TIPs can influence MT dynamics in various ways: CLIPs and CLASPs stimulate rescues (Komarova et al., 2002; Mimori-Kiyosue et al., 2005), EBs promote MT dynamicity and growth, and suppress catastrophes (Komarova et al., 2009; Tirnauer and Bierer, 2000), while the MT depolymerase MCAK induces catastrophes (Howard and Hyman, 2007).

Although many +TIPs can interact with MTs directly, most of them target growing MT ends by binding to members of the EB family, which can autonomously localize to growing MT tips (Akhmanova and Steinmetz, 2008). The N-terminal part of the EBs consists of a calponin homology domain, which is the primary determinant of MT tip recognition (Komarova et al., 2009). The C-terminal part of the EBs includes an EB homology (EBH) domain that encompasses a coiled-coil and a four-helix bundle, and an acidic tail with a conserved terminal tyrosine residue reminiscent of the ones of  $\alpha$ -tubulin and CLIP-170 (Akhmanova and Steinmetz, 2008). To date two types of interactions between the EBs and their partners have been characterized in detail. Proteins containing CAP-Gly domains such as CLIPs interact with the EEY/F motifs of the EB tails whereby the C-terminal tyrosine is required for efficient binding (Honnappa et al., 2006; Weisbrich

et al., 2007). A large number of other EB partners, including CLASPs and MCAK, associate with a hydrophobic cavity of the EBH domain through basic and serine-rich regions containing the short linear motif SxIP (Honnappa et al., 2009). +TIP interactions with the EBs are transient and competitive, as EB dimers can associate with only two CAP-Gly domains or SxIP motifs at the same time. Additional enrichment of +TIPs at the MT ends can be achieved by binding to other +TIPs (Akhmanova and Steinmetz, 2008). For example, CLASPs associate with the coiled-coil part of CLIPs independently of EB binding (Akhmanova et al., 2001). +TIPs thus form an intricate and dynamic protein network at growing MT plus ends (Akhmanova and Steinmetz, 2008).

A highly conserved and essential +TIP family is represented by XMAP215 in *Xenopus* and Dis1 in fission yeast (Slep, 2009). XMAP215 was shown to track MT ends processively and autonomously, and to act as a MT polymerase (Brouhard et al., 2008). Experiments in *Xenopus* egg extracts indicated that XMAP215 is a major MT stabilizing factor in both mitosis and interphase (Tournebize et al., 2000). In addition to promoting MT polymerization, XMAP215 can also counteract the MT-destabilizing activity of the MT depolymerase XKCM1 (Kinoshita et al., 2001; Tournebize et al., 2000). The mammalian homologue of XMAP215, ch-TOG, also promotes MT assembly *in vitro* (Bonfils et al., 2007; Charrasse et al., 1998). The cellular function of ch-TOG has been predominantly studied in mitosis, where it is essential for proper spindle assembly and organization (Barr and Gergely, 2008; Cassimeris et al., 2009; Cassimeris and Morabito, 2004; Gergely et al., 2003; Holmfeldt et al., 2004). However, the role of ch-TOG in interphase cells has not been addressed in detail, and it is unknown whether this protein behaves as an authentic +TIP.

In this study we identified SLAIN as a new +TIP that associates with EBs, CLASPs, CLIPs and ch-TOG. We provide evidence that the SLAIN2-ch-TOG complex, enriched at MT ends through association with EBs and possibly other +TIPs, strongly promotes processive MT growth. During cell division, SLAIN2 is phosphorylated and thereby its interaction with the EBs and ch-TOG is inhibited. Therefore, the disruption of the SLAIN2-ch-TOG complex has a profound effect on MT growth and organization in interphase, but it does not affect mitotic progression. Our study provides new insights into the control of MT plus end dynamics during the cell cycle.

## Results

### *Identification of SLAIN1 and SLAIN2 as EB-dependent +TIPs*

To identify new EB interacting partners we performed glutathione S-transferase (GST) pull-down assays combined with mass spectrometry using GST-EB1 and different cell extracts (Fig. S1A,B). Among the new potential EB partners was SLAIN2, which was initially described as a homologue of SLAIN1, a protein named after an amino acid stretch in the C-terminus that reads “SLAIN” (Hirst et al., 2006). SLAINs are present in all vertebrates, and two SLAIN homologues exist in mammalian genomes (Hirst et al., 2006). Sequence analysis of SLAIN1 and SLAIN2 predicts a short coiled-coil domain at their N-termini (Fig.S1C). Analysis of a purified SLAIN2 N-terminal fragment (residues 1-43) by circular dichroism spectroscopy, thermal unfolding and multi-angle light scattering showed that it indeed folds into a dimeric  $\alpha$ -helical coiled-coil structure (Fig. S1D-F).

The remaining SLAIN1/2 sequence is rich in serines, prolines and basic residues, encompasses no conserved sequence regions and is predicted to be largely unstructured.

Mass spectrometry results were validated by GST-EB pull-down assays with the extracts of cells overexpressing GFP-tagged SLAIN1/2 (Fig. 1A). Next, we performed GST-EB pull-down assays with different deletion mutants of SLAIN2 (Fig. 1B,C). The C-terminal part of SLAIN2 contains four SxIP-like sequence motifs, as well as a more distantly related motif RSLP, which are potential EB1-binding sites and MT plus end localization signals (Honnappa et al., 2009) (Fig. S1C). Indeed, two short non-overlapping C-terminal fragments of SLAIN2 could interact with EB1 in GST pull down assays, indicating that SLAIN2 has several tandemly arranged EB1 binding sites (Fig. 1B,C). Both GFP-SLAIN1 and 2, as well as short EB1-binding fragments of SLAIN2 colocalized with EB-positive MT ends (Fig. 1B,D, Movie 1 and data not shown).

To investigate whether the SxIP-like sites in SLAIN2 are required for MT tip tracking, the IP/LP dipeptides within the identified sites were mutated to asparagines (Fig. 1B, Fig.S1C). Mutation of the first four sites considerably diminished but did not abolish plus end tracking of the C-terminal SLAIN fragment (Movie 2). Next, we introduced additional mutations in the fifth, more divergent site RSLP as well as two other, even more deviant potential EB1-binding sites containing a hydrophobic residue followed by a proline (Fig. S1C and data not shown). These mutations further reduced plus end tracking (with the RSLP site at position 560 having the strongest contribution to plus end tracking, Fig.S1C and Movie 2), but we still observed a very weak association of the resulting mutants with the growing MT ends, as well as binding to EB1 (Movie 2 and data not shown). We conclude that SxIP-like sites in SLAIN2 strongly contribute to its plus end tracking behavior, but that additional weak EB1- and MT tip-binding sites that do not match the SxIP consensus are present within the SLAIN2 C-terminus.

To study endogenous SLAINs we raised an antibody that recognized both GFP-SLAIN1 and GFP-SLAIN2 (Fig. S1G). On Western blots of different cell lines, this antibody recognizes protein bands of 75-85 kDa (Fig. S1H), which is in agreement with the predicted molecular weight of SLAIN1/2. The presence of multiple bands is likely explained by the existence of alternatively spliced isoforms, phosphorylation and/or degradation (see below). Endogenous SLAIN1/2 co-precipitates with EB1 (Fig. 1E) and colocalizes with it at MT plus ends (Fig. 1F). The accumulation of SLAINs at MT tips depends on EBs as it is strongly reduced after siRNA-mediated knockdown of EB1 and EB3 (Fig. 1G,H). Based on these findings, we conclude that SLAIN1/2 accumulate at MT plus ends in an EB-dependent manner.

#### *SLAINs associate with CLIPs*

While at low expression levels exogenous SLAINs decorated only MT plus ends, at high expression levels GFP-SLAIN2 bound along MTs and formed bundles of acetylated MTs (Fig. S2A). The formation of these bundles was dependent on the presence of EB proteins, because in EB1/3 depleted cells SLAIN2 did not associate with MTs but formed aggregates (Fig.S2B). In line with these data, we could not detect a direct interaction between SLAIN2 and MTs in MT pelleting assays (data not shown), indicating that SLAIN2 has no high intrinsic affinity for MTs.

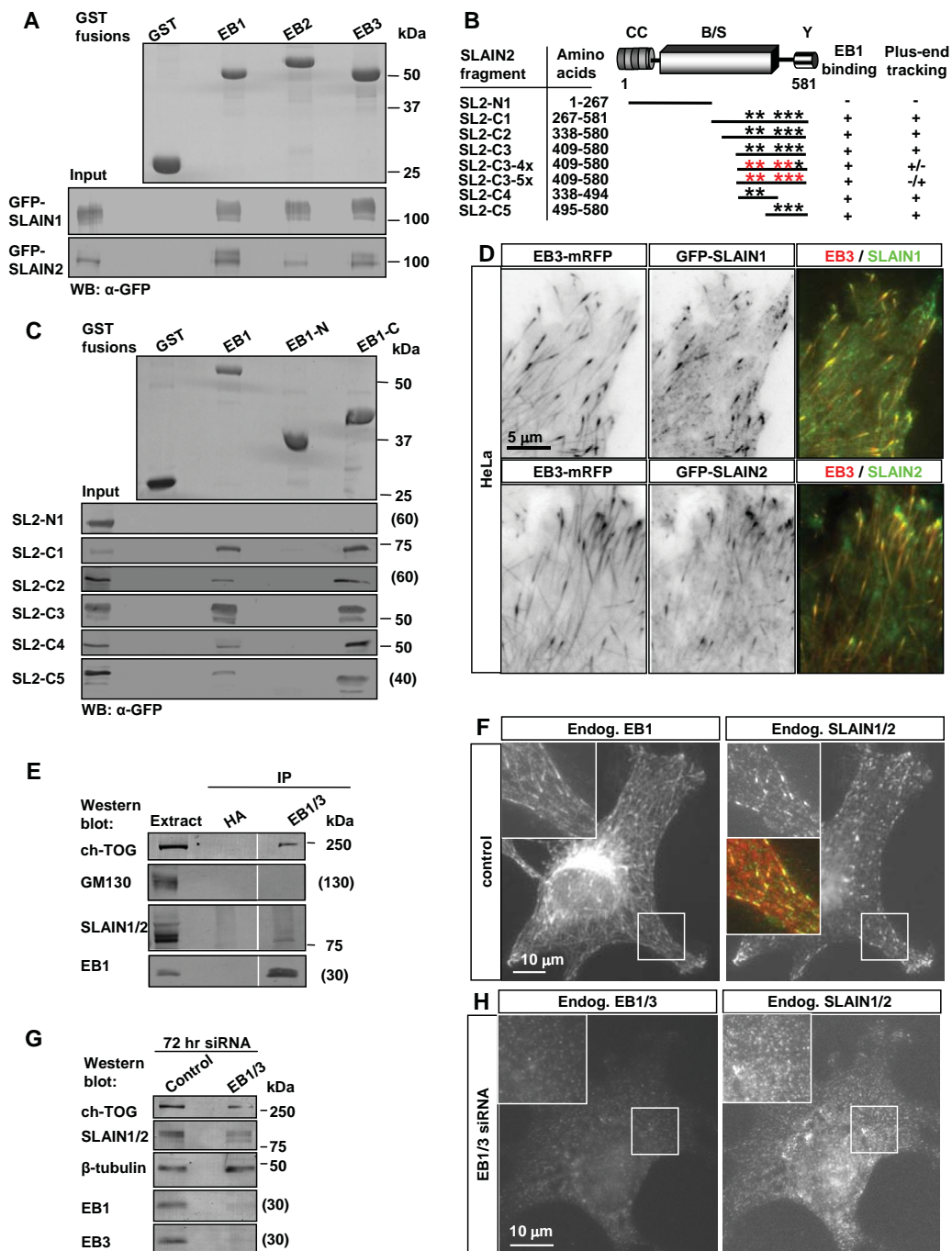


**Figure 1. SLAIN1 and SLAIN2 are EB-dependent +TIPs**

**A,C.** GST pull-down assays were performed with the indicated GST fusions and lysates of cells expressing different GFP-SLAIN1/2 fusions. Coomassie-stained gels are shown for GST fusions, and Western blots with anti-GFP antibodies for GFP fusions.

**B.** Mapping of the minimal MT plus end binding domain of SLAIN2 based on GST-EB1 binding and MT plus end tracking in live cells. CC, coiled-coil; B/S, basic and serine rich; Y, C-terminal tyrosine; asterisks, SxIP-like motifs. Mutations in the SxIP-like sites are indicated by red asterisks (see Fig. S1C for the sequence of SLAIN2).

**D.** Live cell imaging of HeLa cells transiently transfected with EB3-mRFP (red in overlay) and GFP-SLAIN1/2 (green in overlay). Red and green images were collected simultaneously with a beam splitter and 0.5 s interval; 5 consecutive



Interestingly, CLASPs and CLIP-170 were also recruited to MT bundles induced SLAIN2 overexpression (Fig. 2A, Fig. S2A). Previous studies have shown that +TIPs compete for EB binding, and that their simultaneous recruitment to MT bundles is observed only when they can interact with each other in an EB-independent manner (Mimori-Kiyosue et al., 2005; Weisbrich et al., 2007). This suggests a direct interaction between SLAIN2 and CLIP-170 and/or CLASPs.

To test this possibility, we performed pull-down assays using GST fusions of SLAIN2 N- and C-termini, but found no significant interaction with full-length CLIP-170 (Fig. 2B). We hypothesized that this was due to the formation of an auto-inhibitory loop within CLIP-170 blocking the binding of CAP-Gly domains with their partners (Lansbergen et al., 2004). To test this, we performed GST pull-down assays with GFP-CLIP-170 N-terminus or full-length GFP-CLIP-115, two proteins that contain CAP-Gly domains but lack the inhibitory C-terminus of CLIP-170 (Lansbergen et al., 2004). We found that both associated with the SLAIN2 C-terminus (Fig. 2B). Purified biotinylated and GFP-tagged SLAIN2 (BioGFP-SLAIN2) bound to purified GST-CLIP-170 N-terminus as well as GST-EB3 (Fig. 2C), confirming that the interactions of SLAIN2 with CLIP170 and EBs are direct and do not depend on the presence of each other or additional +TIPs.

A conspicuous feature of SLAIN sequences is the presence of a highly conserved tyrosine at the outmost C-terminus, similar to that of  $\alpha$ -tubulin, EBs and CLIP-170 (Fig. 2D). In the latter proteins the C-terminal aromatic residue of the EEY/F motif is essential for binding to CAP-Gly domains (Honnappa et al., 2006; Komarova et al., 2005; Mishima et al., 2007; Weisbrich et al., 2007). To determine if this is also true for the SLAIN2-CLIP-170 interaction, we generated GFP-SLAIN2 deletion mutants lacking the last 20 amino acids (GFP-SLAIN2- $\Delta$ C) or only the C-terminal tyrosine (GFP-SLAIN2- $\Delta$ Y). Both mutants colocalized with endogenous EB1 at MT plus ends and interacted with GST-EB3 in pull down experiments, but displayed no binding to GST-CLIP-170-N (Fig. S2C, Fig. 2C). Moreover, MT bundles induced by these SLAIN2 mutants failed to recruit CLIP-170, indicating that the C-terminal tyrosine in SLAIN2 is important for the interaction with CLIP-170 in cells (Fig. S2C, and data not shown).

#### *Biophysical and structural analysis of the SLAIN2-CLIP-170 interaction reveals a new CAP-Gly domain-binding mode*

To investigate the SLAIN2-CLIP-170 interaction in more detail we performed isothermal titration calorimetry (ITC) experiments with a 13 amino acid peptide of SLAIN2 C-terminus (SLAIN2c) and with the CAP-Gly domains of CLIP-170 (CLIPCG1 and CLIPCG2). Analysis of the data yielded equilibrium dissociation constants,  $K_D$ , in the micromolar range (Fig. 2E, Fig. S2D). A comparable  $K_D$  was obtained for the double CAP-Gly construct CLIPCG12, which bound two SLAIN2c peptides (Fig. 2E, Fig. S2D). In contrast, only very weak binding was observed between SLAIN2c and the

#### **Legend Figure 1 continued**

frames were averaged.

**E.** IPs from HeLa cell extracts with rat monoclonal antibodies against HA tag (control) or EB1 and EB3 were analyzed by Western blotting with the indicated antibodies.

**F, H.** 3T3 cells were transfected with the indicated siRNAs, fixed and stained with the indicated antibodies. The insets show enlargements of the boxed areas. In the overlay EB1 is shown in green and SLAIN2 in red.

**G.** Extracts of 3T3 cells transfected with the indicated siRNAs analyzed by Western blotting with the indicated antibodies.

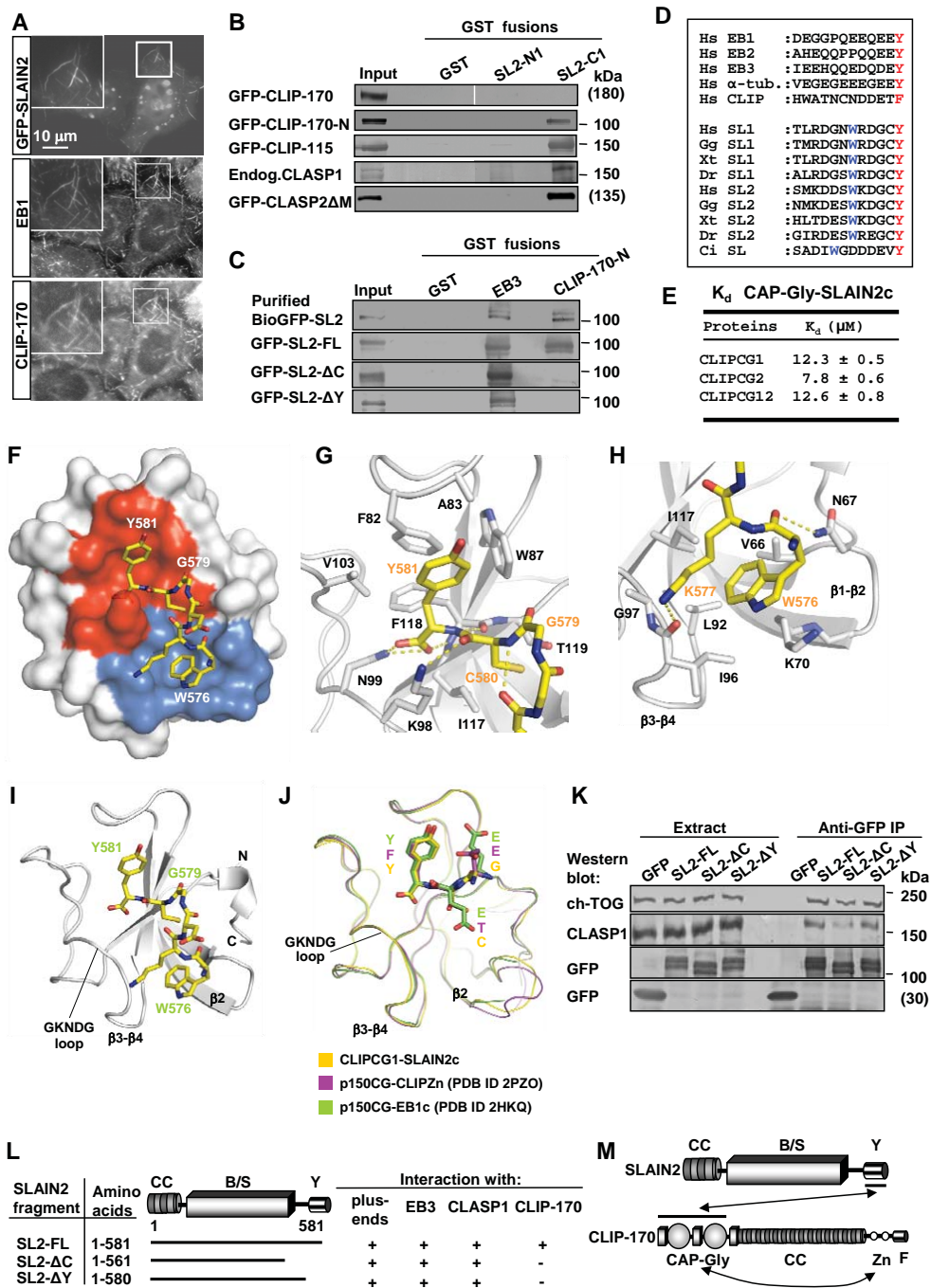


**Figure 2. SLAIN2 interacts with CLIPs and CLASPs**

**A.** HeLa cells were transiently transfected with GFP-SLAIN2, fixed and labeled with the indicated antibodies. Insets show enlargements of the boxed areas.

**B, C.** GST pull-down assays were performed with the indicated GST fusions and lysates of untransfected HeLa cells or cells expressing the indicated GFP fusions (SLAIN2 is abbreviated as SL2). Western blots were performed using the antibodies against GFP or CLASP1. The upper lane of panel C shows a GST pull-down assay with BioGFP-SLAIN2 purified from HEK293 cells.

**D.** Alignment of the C-terminal tails of human EB1, EB2, EB3, α-tubulin, CLIP-170 and SLAIN1 and SLAIN2 from different species. Hs, *Homo sapiens*, Gg, *Gallus gallus*, Xt, *Xenopus tropicalis*, Dr, *Danio rerio*, Ci, *Ciona intestinalis*. The conserved

CAP-Gly domain of the dynactin large subunit p150<sup>Glued</sup> (p150CG) (Fig. S2D), indicating that the C-terminal regions of SLAINs specifically target the CAP-Gly domains of the CLIPs.

Next, we solved the structure of the SLAIN2c-CLIPCG1 complex by X-ray crystallography (Table S1). As illustrated in Fig. 2F-J, the overall structure reveals a heterodimeric complex formed between one CLIPCG1 and one SLAIN2c molecule. The CLIPCG1 subunit displays all features of the CAP-Gly fold (Steinmetz and Akhmanova, 2008). The 6 C-terminal SLAINc residues are tightly packed against the CLIPCG1 fold and assume a loop-like conformation (Fig. 2F-J, Fig. S2E).

Analysis of the SLAIN2c-CLIPCG1 binding interface reveals two contact sites, referred to as A and B. Contact A (Fig. 2G) involves residues from a distinct groove shaped by hydrophobic and polar side chains of CLIPCG1 and the last two C-terminal residues, Cys580 and Tyr581, of SLAIN2c. The side chain of Tyr581, including its  $\alpha$ -carboxylate group, is inserted at one end of the CLIPCG1 groove and is specifically recognized by a set of amino acid residues that are highly conserved across CAP-Gly domain homologues (Steinmetz and Akhmanova, 2008). The binding mode of contact A is nearly identical to the ones seen between the CAP-Gly domain of p150<sup>Glued</sup> and the C-terminal domains of EB1 (Honnappa et al., 2006) and CLIP-170 (Weisbrich et al., 2007), respectively, and between the second CAP-Gly domain of CLIP-170 and a peptide derived from the C-terminus of  $\alpha$ -tubulin (Mishima et al., 2007) (Fig. 2J). The importance of the tyrosine residue for the interaction of the C-terminal SLAIN2 peptide with the two CAP-Gly domains of CLIP-170 was confirmed by ITC (Fig. S2D).

Contact B (Fig. 2H) involves residues from a second, distinct groove shaped by hydrophobic and polar side chains of CLIPCG1 and Trp576 and Lys577 of SLAIN2c (Fig. S2E). The side chain of Trp576, which is highly conserved among SLAIN orthologues (Fig. 2D), is inserted into this groove and is further buried by the hydrophobic moiety of Lys577. Substitution of alanine for Trp576 abrogates binding of the mutant SLAIN2c peptide (SLAIN2c-W576A) to CLIPCG1 and CLIPCG2 (Fig. S2D), demonstrating the importance of this conserved residue for binding to the CAP-Gly domains of CLIP-170. Interestingly, the CLIPCG1 residues that contact Trp576 as well as the  $\beta$ 1- $\beta$ 2 loop, which establishes one wall of the groove are only partially conserved in p150CG (Fig.

**Legend Figure 2 continued**

C-terminal aromatic and the tryptophan residues are highlighted.

**E.** Equilibrium dissociation constants obtained by ITC for the complexes of the human SLAIN2 peptide (SLAIN2c) with either the first (CLIPCG1), second (CLIPCG2) or both (CLIPCG12) CAP-Gly domains of CLIP-170.

**F.** Overall view of the heterodimeric complex formed between CLIPCG1 (surface representation) and SLAIN2c (sticks representation). Contact modes A and B are shown in red and blue, respectively (see text for details).

**G,H.** Close up views of the interaction network seen in the complex formed between SLAIN2c (yellow carbon atoms) and CLIPCG1 (gray carbon atoms) in cartoon (main chain) and sticks (contacting residues) representation. Panels **G** and **H** depict contact modes A and B, respectively (see text for details).

**I, J.** Overall view of the heterodimeric complex formed between CLIPCG1 (ribbon representation) and SLAIN2c (sticks representation) (**I**) and superposition of complexes formed between CAP-Gly domains and C-terminal tyrosine or phenylalanine containing sequence regions (**J**). For simplicity only the last three C-terminal residues of the respective CAP-Gly ligands are shown in sticks representation.

**K.** IP with anti-GFP antibodies from extracts of HeLa cells expressing GFP or GFP-SLAIN2 fusions were analyzed by Western blotting with the indicated antibodies.

**L.** Mapping of the SLAIN2 interaction site with CLIP-170, EB3, CLASP1, and MT plus ends.

**M.** Schematic overview of SLAIN2-CLIP-170 interaction. Abbreviations: CC, coiled-coil; B/S, basic and serine-rich; Y, C-terminal tyrosine; Zn, zinc knuckles, F, C-terminal phenylalanine.

S2F) and other CAP-Gly domain homologues (Steinmetz and Akhmanova, 2008). Since p150CG binds SLAIN2c much weaker than the two CAP-Gly domains of CLIP-170 (Fig. S2D), we propose that these residues play an important role in determining the specificity of CAP-Gly domains for tryptophan side chains that precede C-terminal aromatic residues.

#### *SLAINs associate with CLASPs and ch-TOG*

Next, we investigated the association of SLAIN2 with CLASPs. Endogenous CLASPs were pulled down by GST-SLAIN2-C1 (Fig. 2B and data not shown). Although this interaction might be indirect, it was not mediated by EB1, as CLASP2- $\Delta$ M, a CLASP2 deletion mutant lacking the EB1-binding site (Komarova et al., 2002; Mimori-Kiyosue et al., 2005), could still bind to GST-SLAIN2-C1 (Fig. 2B). The CLASP-SLAIN2 interaction was also independent of CLIP-170, as immunoprecipitation experiments showed that both GFP-SLAIN2 C-terminal mutants that do not bind CLIP-170 could still co-precipitate CLASP1 (Fig. 2K). Taken together, our results show that the SLAIN2 C-terminus binds to EBs, CLIPs and CLASPs (Fig. 2L,M). Targeting of SLAIN2 to the MT plus ends depends on EBs (Fig. 1F,H), while GFP-SLAIN2 still localizes to MT tips in cells depleted of CLIP-170 and CLASPs (Fig. S2G). The interactions with CLIPs and CLASPs are likely needed to avoid competition between these proteins at MT tips.

To identify additional SLAIN partners, we performed streptavidin-based pull-down assays of BioGFP-SLAIN1/2 from HeLa cells (Fig. 3A) and analyzed the resulting proteins by mass spectrometry. The experimental set-up was validated by the identification of CLASP1 among the proteins associated with BioGFP-SLAIN2 (Fig. S3A). Further, on a Coomassie-stained gel, a prominent band of ~220 kDa was visible in both SLAIN1 and SLAIN2 lanes (Fig. 3A). This protein was identified as ch-TOG (Fig. S3A).

Although it is generally accepted that XMAP215 and its homologues act at MT tips (Brouhard et al., 2008), the vertebrate members of XMAP215/Dis1 family have not been shown to form comet-like accumulations at MT ends in cells. Using live cell imaging, we could detect GFP-tagged ch-TOG at the growing MT ends, where it colocalized with SLAIN1/2 and EBs (Fig. 3B, Movie 3, and data not shown). Endogenous SLAIN and ch-TOG were co-precipitated with endogenous EB1 and with each other (Fig. 1E, 3C). Endogenous ch-TOG was also co-precipitated with full length GFP-SLAIN2 and with its mutants deficient in CLIP-170 binding, demonstrating that the SLAIN2-ch-TOG interaction does not require CLIP-170 (Fig. 2K).

#### *EBs and SLAIN2 promote ch-TOG accumulation at MT tips*

In agreement with previous studies, we found that endogenous ch-TOG localized to centrosomes in interphase and to spindle poles and MTs in mitosis (Gergely et al., 2003; Tournebize et al., 2000) (data not shown). In addition, ch-TOG colocalized with endogenous EBs at MT plus ends of interphase cells (Fig. 3D). By performing a double knockdown of EB1 and EB3 we found that ch-TOG requires EBs for efficient comet-like accumulation at the MT plus ends, but not at the centrosome (Fig. 3E, and data not shown).

Next, we investigated the hierarchy of SLAIN and ch-TOG interactions with MT plus

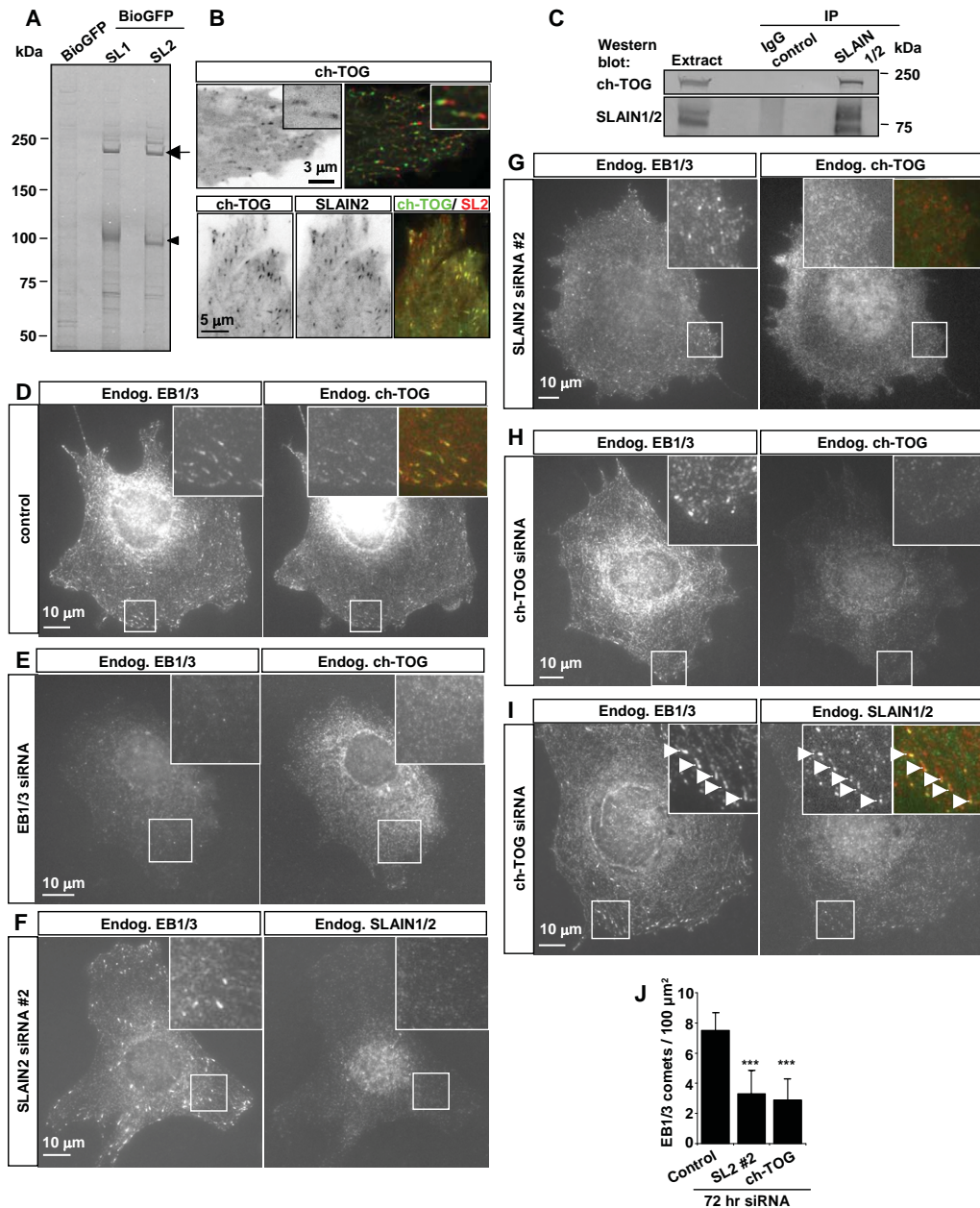


**Figure 3. SLAIN2 interacts with ch-TOG and promotes its MT plus end accumulation**

**A.** Streptavidin pull-down assay from HeLa cells expressing BioGFP or BioGFP-SLAIN1 or -2 together with BirA. Proteins were analyzed by Coomassie staining. Arrow indicates ch-TOG and arrowhead indicates BioGFP-SLAIN1/2.

**B.** Live imaging of HeLa cells transiently expressing GFP-ch-TOG alone (upper panel) or in combination with mCherry-SLAIN 2 (bottom panel), collected as described for Fig.1D. Upper right panel shows maximum intensity projection of two consecutive averaged frames displayed in green and red.

**C.** IPs from HeLa cell extracts with either IgG control or SLAIN1/2 antibody were analyzed by Western blotting with the indicated antibodies.

**D-I.** 3T3 cells were transiently transfected with different siRNAs, fixed and stained with the indicated antibodies. The insets show enlargements of the boxed areas. Arrowheads in I indicate MT plus ends. In the overlay in **D,G** and **I** EB1/3 is in red and ch-TOG or SLAIN1/2 is in green.

**J.** Quantification of the number of EB1/3-positive comets per 100 μm<sup>2</sup> surface area in control 3T3 cells or cells depleted of SLAIN2 or ch-TOG (11-14 cells were analyzed for each condition). Values significantly different from control are indicated with asterisks, p<0.001.

ends. In HeLa cells, all SLAIN-specific bands could be depleted by different siRNAs against SLAIN2 while SLAIN1-specific siRNAs had no effect. This result suggests that HeLa cells do not express SLAIN1, a conclusion supported by RT-PCR analysis (Fig. S3B,C). Using the SLAIN2 siRNA#2, we could efficiently deplete SLAIN2 also from mouse 3T3 cells (Fig. S3D, Fig. 3F). Interestingly, in cells depleted of SLAIN2, EB1/3 comets displayed little ch-TOG labeling (Fig. 3G), indicating that SLAIN2 participates in ch-TOG recruitment to MT ends. In contrast, both CLASPs and CLIPs could still be detected at the plus ends of SLAIN2-depleted cells (Fig. S3E,F).

Next, we used siRNAs to deplete endogenous ch-TOG. Because of the strong mitotic arrest caused by ch-TOG knockdown (Cassimeris and Morabito, 2004; Gergely et al., 2003), we enriched interphase cells by applying a thymidine block for 2 days. Knockdown of ch-TOG in HeLa and 3T3 cells could be confirmed both by Western blotting (Fig. S3D,G) and by immunostaining (Fig. 3H). Although SLAIN2 levels were somewhat reduced in ch-TOG depleted cells, it could still be detected at the EB1/3-positive MT tips (Fig. 3H,I), indicating that SLAIN2 acts upstream of ch-TOG with respect to MT tip localization.

Both SLAIN2 and ch-TOG depletion strongly reduced the number of EB1/3-positive comets (Fig. 3J), as well as the length of EB-positive comets (see below), suggesting a defect in MT growth. An overall disorganization of the MT network was also observed: instead of the radial array typical for 3T3 fibroblasts, MTs often appeared to be circularly arranged and entangled (Fig. S3H and see below).

#### *SLAIN2 promotes the interaction between EB1 and ch-TOG*

To characterize the SLAIN2-ch-TOG interaction in more detail, we performed pull down experiments with deletion mutants of the two proteins. We found that the whole N-terminal half of SLAIN2 (N1), but not its shorter fragments bound to ch-TOG; this interaction depended on the C-terminal domain of ch-TOG (Fig. 4A-D). Using GST pull-down assays we found that, as expected, GFP-SLAIN2 but not GFP-SLAIN2-N1 was pulled down by GST-EB1 (Fig. 4E). Endogenous ch-TOG also interacted with GST-EB1, in line with our mass spectrometry data (Fig. 4E, Fig.S1A). This interaction was increased when GFP-SLAIN2 was overexpressed (Fig. 4E, Fig. S4A), suggesting that full-length SLAIN2 stabilizes the binding between ch-TOG and EB1. In agreement with this idea, we found that GFP-ch-TOG-C1, which localized at centrosomes and in the cytosol of control cells (Fig. S4B) was recruited to MT plus ends when SLAIN2 levels were elevated by expressing mCherry-SLAIN2 (Fig. S4C). On the other hand, when GFP-SLAIN2-N1 was overexpressed, endogenous ch-TOG could no longer be detected at the MT plus ends and its interaction with GST-EB1 was strongly reduced (Fig. 4E,F, S4A), indicating that the SLAIN2 N-terminus uncouples ch-TOG from EB1.

Next, we examined the functional consequences of the disruption of the ch-TOG-EB1 interaction caused by overexpression of GFP-SLAIN2-N1, and found that it induced a strong reduction in the number of EB1-positive MT tips while MT density remained unchanged (Fig. 4G,H, Fig. S4D). Overexpression of the SLAIN1 N-terminus caused an identical phenotype (Fig. 4H, Fig. S4D), suggesting that the functions of SLAIN1 and SLAIN2 are similar. Reduction in the number of EB1 comets was also observed in cells overexpressing the ch-TOG C-terminus, which is

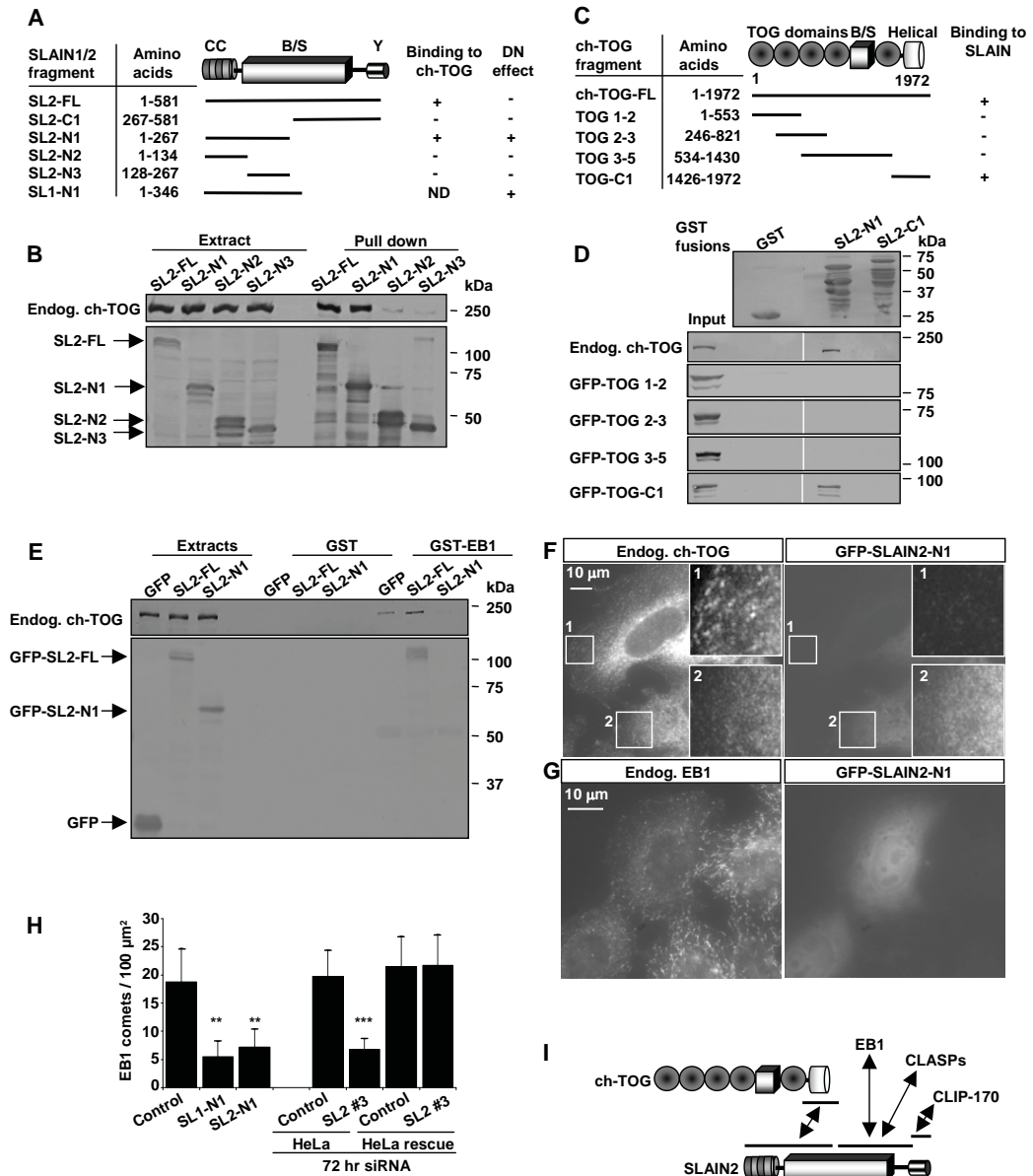


**Figure 4. SLAIN2 links ch-TOG to EB1**

**A.** Mapping of the ch-TOG binding domain of SLAIN1 and 2 (SL1 and SL2). Abbreviations are the same as in Fig. 1B. The ability to exert a dominant negative (DN) effect on the number of EB1-positive MT tips is indicated. ND, not determined.

**B.** Streptavidin pull-down assay were performed with extracts of HEK293 cells co-expressing BioGFP-SLAIN2 mutants and BirA, and analyzed by Western blotting with the indicated antibodies.

**C.** Mapping of the SLAIN2 binding domain of ch-TOG. B/S, basic and serine-rich region.

**D,E.** GST pull-down assays were performed with the indicated GST fusions and lysates of HEK293 cells expressing GFP fusions of ch-TOG or SLAIN2. Coomassie-stained SDS-PAGE are shown for GST fusions. Western blots with anti-GFP antibodies are shown for GFP fusions and with ch-TOG antibodies for endogenous ch-TOG.

**F,G.** 3T3 (**F**) or HeLa cells (**G**) were transfected with GFP-SLAIN2-N1, fixed and labeled with the indicated antibodies. In panel **F**, the insets show enlargements of the boxed areas where (1) is an untransfected control cell and (2) is a GFP-SLAIN2-N1 transfected cell.

**H.** Quantification of the number of EB1-positive comets per 100  $\mu\text{m}^2$  surface area in control or GFP-SLAIN1/2-N1 expressing HeLa cells. ~10-50 cells were analyzed in each experiment. Statistically significant differences are indicated (\*\*  $p < 0.01$ , \*\*\*  $p < 0.001$ ).

**I.** A scheme of the identified interactions between SLAIN2, ch-TOG, EB1, CLASPs and CLIP-170.

also expected to uncouple endogenous ch-TOG from SLAIN and EB1 (Fig. S4B,E), as well as after SLAIN2 and ch-TOG depletion (Fig. 3J, Fig 4H, Fig. S4D). Importantly, the number of growing MT ends was fully rescued by stable expression of low levels of GFP-SLAIN2 in SLAIN2-depleted cells (Fig. 4H), confirming the specificity of the SLAIN2 siRNA.

Taken together, these results indicate that SLAIN2 can promote the binding between ch-TOG and EB1 and potentially other +TIPs (Fig. 4I), and help to recruit ch-TOG to MT plus ends and to maintain the normal number of growing MTs.

#### *SLAIN2-ch-TOG complex is required for persistent MT growth and radial MT organization*

To analyze the effect of the loss or disruption of the SLAIN2-ch-TOG complex on MT growth we used HeLa cells stably expressing fluorescently tagged tubulin. We followed the dynamics of freshly polymerized MTs in the internal cytoplasm after photobleaching of the pre-existing MTs (Fig. 5A). We found that the length of MT stretches polymerized after FRAP was dramatically reduced in cells that were depleted of SLAIN2 and ch-TOG or that were expressing the dominant negative SLAIN1/2-N1 mutants (Fig. 5A,B). The average MT elongation rate, determined using fluorescently tagged tubulin or EB3-GFP without taking into account short pauses or depolymerization events, was reduced approximately two-fold (Fig. 5C,D, and data not shown). This change in rate was primarily due to a 2 to 3-fold increase in the catastrophe frequency (Table S2, Fig. S5A). While in control cells MT growth episodes were relatively “smooth”, in SLAIN2 and ch-TOG depleted cells they were continuously interrupted by short depolymerization events or pauses, an effect that was particularly obvious in kymograph analysis (Fig. 5E, Table S2, Fig. S5A). Interestingly, although the instantaneous rate of MT growth bursts was not significantly changed (Fig. S5B), EB3-GFP comets became shorter (Fig. 5F,G, Movie 4), suggesting an altered state of the MT plus end. The MT depolymerization rate was not significantly affected, and the rescue frequency remained high (it was even elevated in SLAIN2- but not in ch-TOG depleted cells (Fig. S5A, Table S2)). The frequent switching between short episodes of growth and depolymerization led to a strong overall decrease in MT elongation (Fig. 5C-E).

An increased catastrophe frequency was also observed after depletion of SLAIN2 and ch-TOG in 3T3 and CHO cells (Fig. S5A, Table S2). We have shown previously that in the latter cell type, most of the growing MTs emerging from the centrosome extend persistently to the cell periphery and that ~80% of the MT growth tracks visualized by EB3-GFP are longer than half of the average cell radius (7.5  $\mu\text{m}$ ) (Komarova et al., 2009). Depletion of SLAIN2 and ch-TOG reduced this value to less than 10% (Fig. 5F,H), consistent with a strong increase in catastrophe frequency. The depletion of ch-TOG and SLAIN2 might also cause a reduction in the number of growing MT ends by affecting MT nucleation, as XMAP215/Dis1 proteins play an important role at the centrosome (see Cassimeris et al., 2009, and references therein). Indeed, MT nucleation frequency determined with EB3-GFP was significantly reduced after SLAIN2 and ch-TOG knockdown (Fig. 5I). The involvement of the SLAIN2-ch-TOG complex in MT nucleation was further supported by the fact that its disruption by overexpressing SLAIN1/2-N-termini strongly delayed MT recovery after nocodazole treatment: 10 minutes after the drug washout, the MT network was almost completely



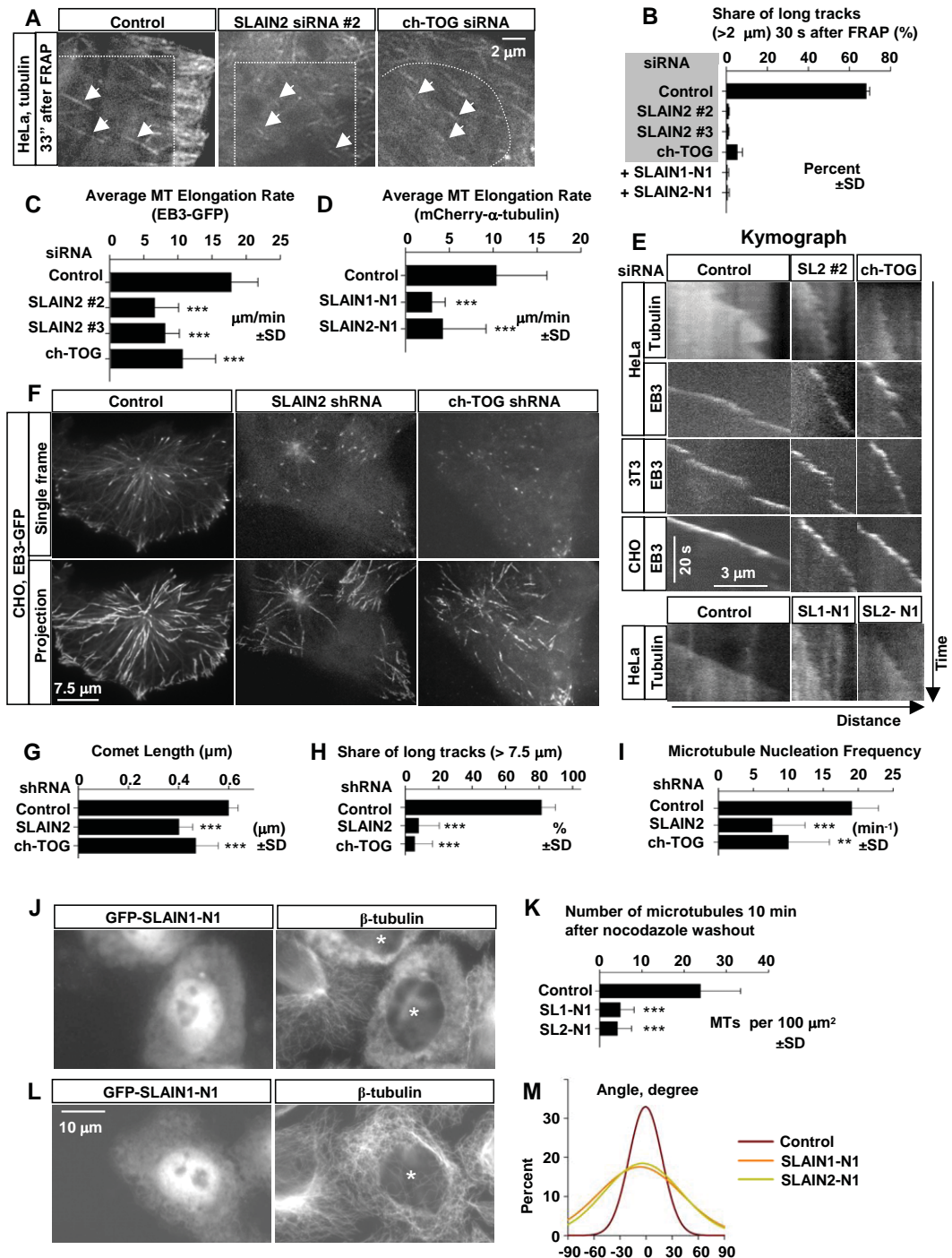


**Figure 5. SLAIN2 and ch-TOG promote MT growth**

**A.** HeLa cells stably expressing GFP- or mCherry- $\alpha$ -tubulin were transfected with the indicated siRNAs. FRAP assay was performed 72 hr later in an internal part of the lamella indicated by a stippled line. Movie frames at 33 s after FRAP are shown; newly polymerized MTs are indicated by arrows.

**B.** Share of freshly polymerized MT segments longer than 2  $\mu\text{m}$  30 s after FRAP. ~230-300 growth episodes were analyzed in 15-20 cells for each condition.

**C,D.** Average MT elongation rate was measured in internal cytoplasm over periods of 10-50 s from the moment of appearance of the growing MT end until the end of the movie or until a catastrophe leading to a processive MT shortening

episode with the length of more than 1  $\mu\text{m}$ . Analysis was performed in HeLa cells stably expressing EB3-GFP that were transfected with the indicated siRNAs (C) or in HeLa cells stably expressing mCherry- $\alpha$ -tubulin, transfected with GFP or GFP-SLAIN1/2-N1 (D). ~70-100 growth episodes in 10-20 cells were analyzed for each condition.

E. Kymographs illustrating MT growth using mCherry- $\alpha$ -tubulin or EB3-GFP after different siRNA treatments or in cells expressing GFP alone (control) or GFP-SLAIN1/2-N1.

F. CHO cells were transiently transfected with EB3-GFP and the indicated shRNAs. Live images were collected with 0.5 s time interval. Single frames (top) and maximum intensity projections of 100 frames (bottom) are shown.

G. Length of EB3-GFP comets in control, SLAIN2 or ch-TOG depleted cells, determined from live imaging experiments shown in panel F. ~300 MT tips were analyzed in ~15 cells per condition.

H, I. Proportion of MT tracks originating from the centrosome with the length exceeding 7.5  $\mu\text{m}$  (H) and MT nucleation frequency from the centrosome in CHO cells transiently transfected with EB3-GFP and the indicated shRNAs (I). In (H), ~100 MT growth episodes were analyzed in ~15 cells per condition. In (I), ~10 cells were analyzed per condition.

J,K. MT recovery after nocodazole washout. HeLa cells expressing GFP or GFP-SLAIN1/2-N1 for 1 day were treated with 10  $\mu\text{M}$  nocodazole for 2 hr, the drug was washed out with fresh medium and cells were fixed and stained 10 min later (J). Number of MTs per 100  $\mu\text{m}^2$  was counted in 20 cells for each condition (K).

L,M. MT organization in HeLa cells transiently expressing GFP or GFP-SLAIN1/2-N1 1 day after transfection. Cells were stained for  $\beta$ -tubulin (L) and the angles of MT segments in relation to the long axis of the lamella were measured; Gaussian fits of the angle distributions measured in 10 cells are shown for each condition (M). Transfected cells are indicated by asterisks in panels J and L. In panels C, D, G-I and K, the values significantly different from controls are indicated with asterisks (\*\*  $p < 0.01$ , \*\*\*  $p < 0.001$ ).

restored in control cells but was virtually absent in cells expressing SLAIN1/2 N-termini (Fig. 5J,K). We further found that in all situations when the SLAIN2-ch-TOG complex was depleted or disrupted, MTs were severely disorganized: instead of running from the cell center to the cell periphery, MTs were arranged at random angles and strongly entangled (Fig. S3H, Fig. 5L,M, Fig. S5C). Taken together, these data show that SLAIN2 and ch-TOG act as major MT growth-promoting factors by stimulating MT nucleation and growth, and suppressing catastrophes. They further indicate that SLAIN2 and ch-TOG-dependent processive MT polymerization is an important factor for maintaining normal interphase MT array.

#### *Mitotic phosphorylation of SLAIN2 disrupts the EB-SLAIN2-ch-TOG complex*

Depletion of ch-TOG causes severe mitotic defects (Cassimeris and Morabito, 2004; Gergely et al., 2003; Holmfeldt et al., 2004). Indeed, ch-TOG knockdown induced a strong increase in the mitotic index of HeLa cells (Fig. 6A). In contrast, two of the three SLAIN2 siRNAs that efficiently deplete SLAIN2 (Fig. S3B) caused no increase in the proportion of mitotic cells (Fig. 6A), and no apparent abnormalities of the mitotic apparatus (data not shown). Localization studies using a HeLa cell line stably expressing GFP-SLAIN2 showed that it dissociated from MT plus ends and the centrosome early in prophase and remained cytosolic until late telophase (Fig. 6B, Movies 5-7).

Western blot analysis of extracts of cells blocked in mitosis showed that endogenous SLAIN2 and GFP-SLAIN2 protein bands are very strongly up-shifted (Fig. 6C,D). Incubation of immunoprecipitated SLAIN2 with lambda phosphatase completely reversed this shift, indicating that it is caused by phosphorylation (Fig. 6C,D). The presence of multiple phosphorylated sites in SLAIN2 isolated from mitotic cells was confirmed by mass spectrometry (Fig. S1C).

In agreement with the absence of GFP-SLAIN2 at the MT plus ends in mitosis, hyperphosphorylated GFP-SLAIN2 did not associate with GST-EB1 in a GST pull-down assay (Fig. 6E). Furthermore, mitotic phosphorylation also inhibited co-precipitation of SLAIN2 and ch-TOG (Fig. 6C,D). In line with these observations, both SLAIN2 N- (the ch-TOG binding domain) and C-termini

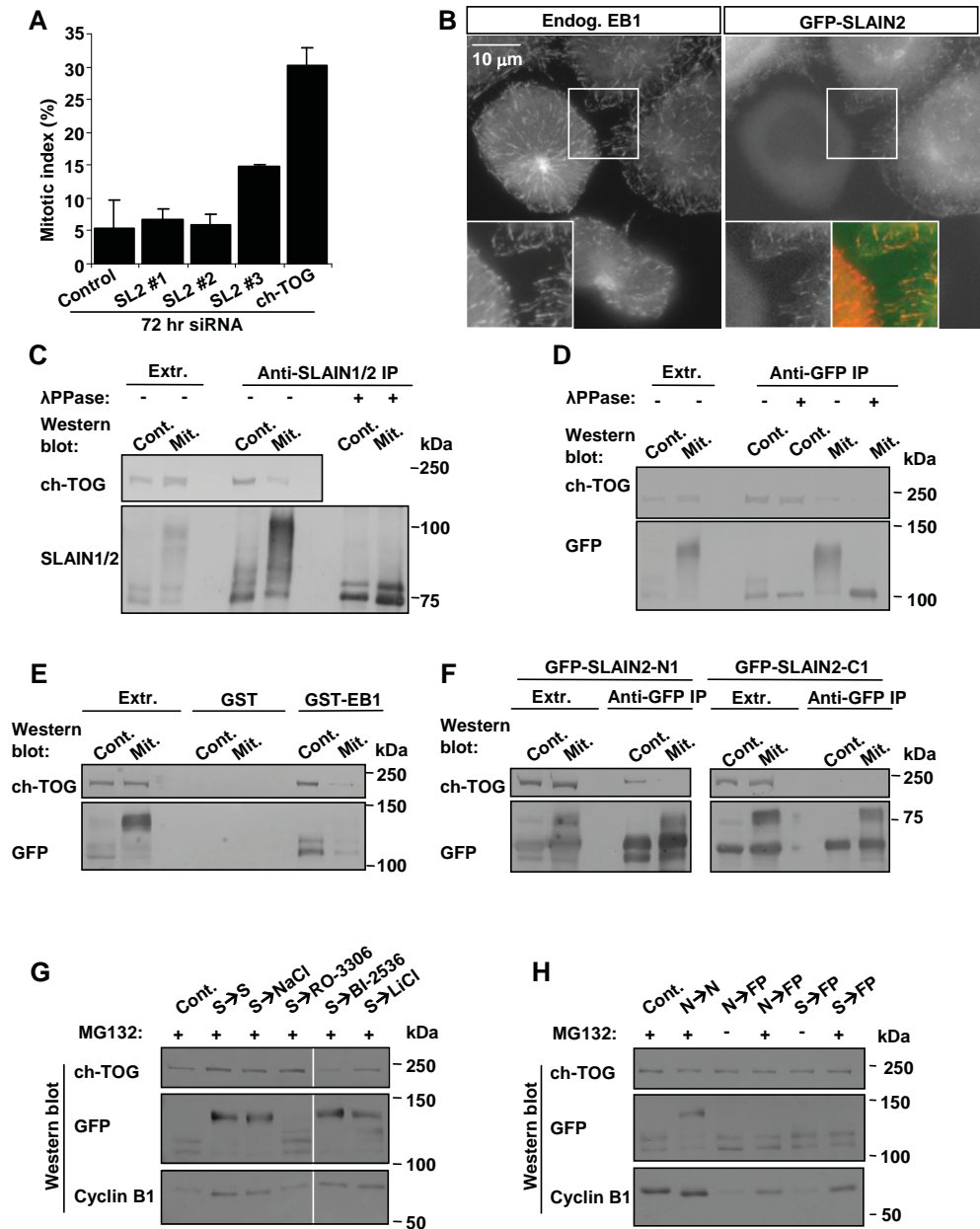


**Figure 6. Mitotic phosphorylation disrupts SLAIN2 interaction with MTs, EB1 and ch-TOG**

**A.** Proportion of mitotic HeLa cells, identified by staining with antibodies against histone H3 phosphorylated at serine 10 after transfection with the indicated siRNAs.

**B.** HeLa cells stably expressing GFP-SLAIN2 were fixed and stained with an anti-EB1 antibodies. The prophase cell was distinguished by the strong increase in centrosomal MT nucleation. Insets show enlargements of the boxed areas.

**C.** IPs with anti-SLAIN1/2 antibodies from control HeLa cells or cells blocked in mitosis with 0.1  $\mu$ M nocodazole. Where indicated, immunoprecipitated material was treated on beads with lambda phosphatase. Western blotting was performed with the indicated antibodies.

**D.** The same experiment as in (C), but using a GFP-SLAIN2 stable HeLa cell line and anti-GFP antibodies.

**E.** GST pull-down assays were performed with GST or GST-EB1 and cell extracts prepared as in (D).

**F.** The same experiment as in (C), but using HeLa cells transiently expressing N- and C-terminal fragments of SLAIN2.

**G,H.** HeLa cells stably expressing GFP-SLAIN2 were blocked in mitosis with 7.5  $\mu$ M STLC (G) or 0.1  $\mu$ M nocodazole (H), and released for 1 h into medium containing either the indicated inhibitors, 20 mM NaCl, or 20 mM LiCl, respectively. S, STLC; N, nocodazole; FP, flavopiridol.

(the EB1, CLIP- and CLASP-binding domain) showed strongly reduced electrophoretic mobility in mitotically blocked cells (Fig. 6F). These results indicate that mitotic hyperphosphorylation inhibits the interaction of SLAIN2 with EB1 and ch-TOG.

To investigate which kinase is responsible for SLAIN2 phosphorylation, HeLa cells stably expressing GFP-SLAIN2 were blocked in mitosis and subsequently released for 1 h in the presence of different kinase inhibitors. Inhibition of cyclin-dependent kinase 1 (CDK1) using RO-3306 or flavopiridol caused a strong downward shift of GFP-SLAIN2 protein bands on Western blots (Fig. 6G,H). This increase in GFP-SLAIN2 electrophoretic mobility was not due to proteasome activity as it was also observed in the presence of the proteasome inhibitor MG132 (Fig. 6G,H). Inhibitors of other kinases, such as Plk1 or GSK3 $\beta$  had no effect (Fig. 6G). Sequence analysis of SLAIN2 predicts multiple major (S/TPxPK/R) and minor (S/TP) CDK1 consensus sites, and several of them are indeed phosphorylated based on mass spectrometry analysis (Fig. S1C), suggesting that SLAIN2 might be a direct target of CDK1.

Collectively, these data show that in mitosis the interaction of SLAIN2 with EB1 and ch-TOG is inhibited by phosphorylation and that SLAIN2-dependent recruitment of ch-TOG to MT tips is thus confined to interphase cells.

## Discussion

In this study we identified SLAINs as MT plus end tracking proteins and showed that SLAIN2 plays an important role in regulating MT growth and organization by interacting with multiple +TIPs and targeting ch-TOG to growing MT plus ends.

Similar to many +TIPs (Akhmanova and Steinmetz, 2008), SLAINs bind to EB proteins and depend on them for MT tip accumulation. In addition, the C-terminal part of SLAIN2 interacts with the CLASPs and the CLIPs. The SLAIN2-CLIP interaction involves the C-terminal tail of SLAINs and the CAP-Gly domains of CLIPs. Notably, the conserved terminal tyrosine residue of SLAIN2 is recognized by the CAP-Gly fold in exactly the same way as the ones of the EEY/F motifs of EBs,  $\alpha$ -tubulin and CLIP-170. However, while in EBs,  $\alpha$ -tubulin and CLIP-170 the acidic residues of EEY/F contribute to the stability of the complexes through electrostatic interactions (Mishima et al., 2007), a conserved tryptophan in SLAIN2 interacts with a distinct hydrophobic cavity present in the CAP-Gly domains of CLIP-170. Our structural data therefore extend the specificity portfolio of CAP-Gly domains and explain the functional role of the evolutionary conserved SLAIN C-terminus.

SLAINs combine different and multiple copies of major +TIP elements, such as SxIP-like and EEY/F-like motifs in one molecule (Fig.7). This unique property of SLAINs is expected to enable them to associate simultaneously with several different +TIPs and thus promote formation of +TIP interaction networks with multiple and partly redundant binding nodes (Fig. 7). The functional significance of each particular interaction might be relatively small; however, their overall effect would be to enable SLAINs to act as 'adhesive +TIP factors' which have a continuous access to growing MT ends, enhance +TIP interactions and promote their access to the MT ends.

Importantly, we found that SLAINs use their adhesive properties to robustly target ch-TOG to growing MT plus ends. ch-TOG binds to SLAINs through its C-terminal part, which is

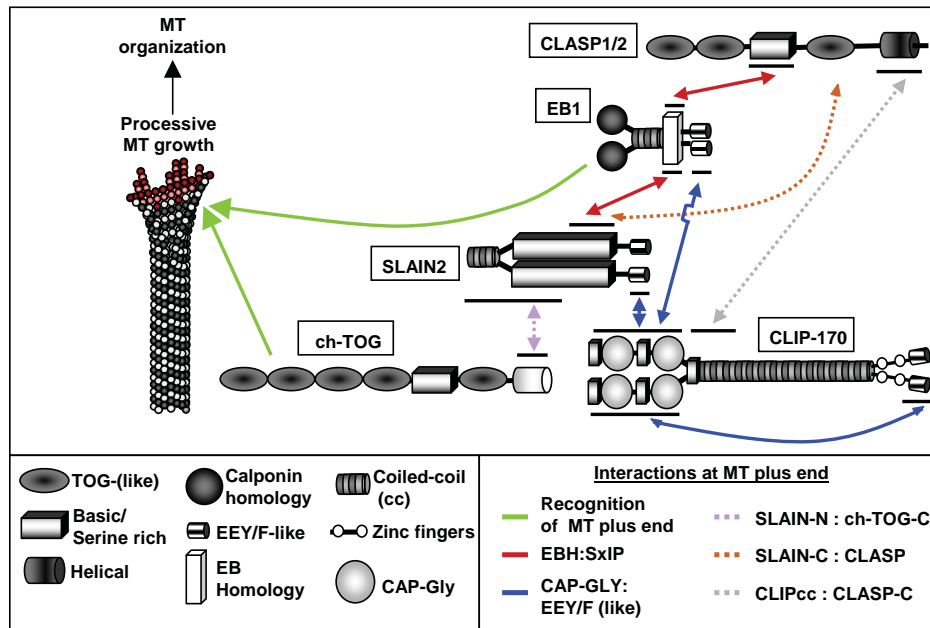


**Figure 7. A scheme of SLAIN2-linked +TIP network and its biological role**

Different types of +TIP interactions are indicated by different colors. The potential direct EB1-ch-TOG interaction based on the data from other species (Kronja et al., 2009; Rehberg and Graf, 2002; Wolyniak et al., 2006) is not shown. SLAIN2-dependent interactions enhance ch-TOG accumulation at the MT tip. ch-TOG, in turn, promotes processive MT growth that is required for proper MT organization.

distinct from its tubulin-binding TOG domains, necessary for MT polymerase activity (Slep, 2009). SLAINs likely promote the activity of ch-TOG by positioning it close to growing MT ends. However, *in vitro* XMAP215 can autonomously track MT plus ends (Brouhard et al., 2008) and stimulate MT growth in the absence of other +TIPs (Kinoshita et al., 2001). So why would the members of the XMAP215/Dis1 family need an accessory factor *in vivo*? We propose that in cells, the ability of XMAP215/Dis1 family members to interact with EB proteins and other +TIPs is needed to gain access to growing MT tips that are strongly occluded by EBs and their numerous partners.

While SLAINs are conserved in vertebrates and tunicates, we could identify no apparent SLAIN counterparts in other taxa, possibly due to a low degree or absence of sequence conservation. Alternatively, lower organisms might not need accessory factors for XMAP215/Dis1 homologues because they are expressed at higher levels or because their +TIP networks are less complex.

Since SLAINs localize to MT tips by interacting with EBs and EB partners (Fig. 7) one could expect that EB depletion should have a MT growth phenotype similar to that of ch-TOG or SLAIN2. Our previous study showed that the depletion of EBs indeed increased the catastrophe frequency (Komarova et al., 2009), but the effect was relatively mild. This difference could be due to the difficulty to completely deplete all three mammalian EBs (Komarova et al., 2009). Alternatively, EBs can concentrate not only MT stabilizing proteins such as CLASPs, but also destabilizing factors, such as MCAK at MT tips (Montenegro Gouveia et al., 2010). Therefore, when EBs are knocked down, the balance of regulatory activities at MT ends might not be significantly shifted. In contrast, SLAIN2 or ch-TOG depletion affects only growth-promoting but not destabilizing activities at MT

tips, and MT polymerization is inhibited.

Overall, our functional data are consistent with the view that in interphase cells SLAIN2 primarily acts as a ch-TOG cofactor at growing MT ends. Remarkably, SLAIN-ch-TOG as well as SLAIN-EB partnership is disrupted during cell division. As the cell proceeds from interphase into mitosis, MT dynamics drastically changes and MT turnover strongly increases (Wittmann et al., 2001). Our data suggest that phosphorylation of SLAIN2 at the onset of mitosis is part of this mitosis-specific regulatory switch in MT dynamics. It remains to be investigated whether in mitosis ch-TOG targets MT tips autonomously or uses some additional partners.

In conclusion, our study identifies SLAIN2 as an important component of a complex MT plus end targeting mechanism and reveals the function of SLAIN2 in the cell-cycle regulated control of MT dynamics.

## Materials and Methods

### *Constructs*

GFP-SLAIN1 and SLAIN2 expression constructs and their deletion mutants were generated using the mouse cDNA IMAGE clone 6811096, and the human cDNA KIAA1458 (a gift of Kazusa DNA Research Institute) in pEGFP-C1 by PCR-based strategies. In BioGFP fusions, a linker encoding the sequence MASGLNDIFEAQKIEWHEGGG, which is the substrate of biotin ligase BirA is inserted into the NheI and AgeI sites in front of the GFP (pBioGFP-C1). The BirA ligase expression construct was a gift from D. Meijer (Erasmus MC, Rotterdam, The Netherlands). mCherry-SLAIN1/2 were made by re-cloning SLAIN1/2 into MluI/EcoRI sites of a modified pEGFP vector in which the GFP open reading frame was substituted for that of mCherry (a gift of R. Tsien, University of California, San Diego, USA). GFP-ch-TOG was a gift from L. Wordeman (University of Washington, Seattle, USA); this construct was used for generating ch-TOG deletion fragments in pBioGFP-C1 by a PCR-based strategy. We also used the previously described constructs GFP-CLIP-115 (De Zeeuw et al., 1997), GFP-CLIP-170 (Hoogenraad et al., 2000), GFP-CLIP-170-N (Komarova et al., 2002) and GFP-CLASPΔM (Mimori-Kiyosue et al., 2005). Point mutations in GFP-SLAIN2-C3 fragment were introduced by overlapping PCR.

pSuper-based shRNA vectors (Brummelkamp et al., 2002) were directed against the following target sequences: mouse/rat ch-TOG AGAGTCCAGAATGGTCCAA; mouse/rat/human SLAIN2 CTCTATAGATAGTGAGTTA.

### *Cell culture, stable cell lines and transfection of DNA constructs*

HeLa, Swiss 3T3, CHO and HEK293 were cultured as described previously (Akhmanova et al., 2001). HeLa cell lines stably expressing GFP- $\alpha$ -tubulin and EB3-GFP were described by (Mimori-Kiyosue et al., 2005; Splinter et al., 2010). mCherry- $\alpha$ -tubulin, GFP-SLAIN2 and GFP-SLAIN2 #3 rescue stable HeLa cell lines and EB3-GFP stable 3T3 cell line were selected using Fluorescence Activated Cell Sorting and cultured in the presence of 0.4 mg/ml G418 (Roche). PolyFect (Qiagen), FuGENE 6 (Roche) or Lipofectamine 2000 (Invitrogen) reagents were used for plasmid transfection.

### *siRNAs*

siRNAs were synthesized by Ambion or Dharmacon; they were directed against the following target sequences: SLAIN1 #1: GACAUGUAGUGAACAAAGAA, SLAIN1 #2: GUAACAUGCCUUAUCAAA, SLAIN1#3: GCAGCAACAGUAUUUUC, SLAIN2 #1: GCGCAGUUCUGGUUCAUCU, SLAIN2 #2: CUCUAUAGAUAGUGAGUUA, and SLAIN2 #3: GGAACUUGAUGCACAAAGU, control: GCACUCAUUUGACUCCA (Mimori-Kiyosue et al., 2005), human ch-TOG: GAGCCCAGAGUGGUCCAAA (Cassimeris and Morabito, 2004). Mouse ch-TOG ON-TARGETplus SMARTpool L-0470, EB1: AUUCCAAGCUAAGCUAGAA (Watson and Stephens, 2006). EB3: CUAUGAUGGAAAGGAUUAC (Komarova et al., 2005); CLIP-170: GGAGAAGCAGCAGCACAUU (Lansbergen et al., 2004); CLASP1: GCCAUUAUGCCAACUAUCU; CLASP2: GUUCAGAAAGCCCUUGAUG (Mimori-Kiyosue et al., 2005). Synthetic oligos were transfected using HiPerFect (Qiagen) at a concentration of 5 nM. Cells were analyzed 72 hr after transfection.

### *Drug treatments*

In case of siRNA-mediated ch-TOG and SLAIN2 knockdown, 3T3 and HeLa cells were blocked in interphase one day after transfection by adding 2 mM thymidine (Sigma-Aldrich) to culture medium for 2 days. HeLa cells were blocked in mitosis by a 16 hr treatment with 0.1  $\mu$ M nocodazole (Sigma-Aldrich) or with 7.5  $\mu$ M STLC (Eg5 inhibitor, Sigma-Aldrich). Cells were released from the mitotic block for 60 min in the presence of the following inhibitors: RO-3306 (10  $\mu$ M) (Calbiochem), BI-2536 (100 nM) (Selleck), LiCl (20 mM), Flavopiridol (10  $\mu$ M) (Sigma-Aldrich), MG132 (20  $\mu$ M) (Sigma-Aldrich). Nocodazole washout experiments were performed by applying 10  $\mu$ M nocodazole for 2 h followed by washout of the drug for 5-20 minutes.

### *RT-PCR*

Total RNA was isolated from HeLa cells using RNA-Bee (Tel-Test Inc.) according to manufacturer's protocol. cDNA was generated using First-Strand cDNA synthesis SuperScript II RT (Invitrogen). Human brain cDNA was a gift of Dr. E. Mientjes (Dept. Clinical Genetics, Erasmus MC, Rotterdam, The Netherlands). Primers used for amplification of SLAIN2 were as follows; forward: TAAGTGCTTCAGAATTAGAT and reverse: CATCATGCAGTATACCTG. SLAIN1 primers were previously described (Smith et al., 2010).

### *Protein purification, peptide preparation, pull-down assays, protein analysis and mass spectrometry*

GST fusions of the N-terminal and C-terminal fragments of SLAIN2 were generated in pGEX-4T-1. GST-EB1, -EB2, -EB3, -EB1-N, -EB1-C, GST-CLIP-170-N and GST-CLIP-115 were described previously (Komarova et al., 2005; Lansbergen et al., 2004). GST pull-downs, IPs and Western blotting were performed according to (Komarova et al., 2005; Lansbergen et al., 2004). Treatments with lambda phosphatase (New England Biolabs) were performed on beads after GST pull-down assays or IP. All GST fusions were expressed in BL21 *E. coli* and purified with glutathione-Sepharose 4B (GE Healthcare) according to protocol of the manufacturer. His6-tagged SLAIN2 fragment (amino acids 1-43) was inserted in the vector PSTCm1 (Olieric et al., 2010). It was expressed in BL21 (DE3)

(Stratagene) and purified by immobilized metal-affinity chromatography on Ni<sup>2+</sup>-Sepharose (GE Healthcare) followed by size exclusion chromatography using a Superdex 200 10/300 GL column (GE Healthcare). Identity of the protein was confirmed by LC/MS. BioGFP-SLAIN2 was purified from HEK293T cells. 70% confluent HEK293T cells were co-transfected with the constructs BioGFP-SLAIN2 and BirA using Lipofectamine 2000. One day after transfection cells were lysed in a buffer containing 20 mM Tris-HCl, 100 mM KCl, 1% Triton X-100 and protease inhibitors (Complete, Roche) and purified with Mutein beads (Roche) according to the protocol of the manufacturer.

Cloning and protein purification of the human CLIP-170 and p150<sup>Glued</sup> fragments CLIPCG1 (residues 56-128), CLIPCG2 (residues 210-282), CLIPCG12 (residues 48-300) and p150CG (residues 18-111) is described in (Weisbrich et al., 2007). In brief, transformed *E. coli* strains BL21 (DE3) (Invitrogen; for CLIPCG1, CLIPCG2 and p150CG) and C41(DE3) (Lucigen; for CLIPCG12) were grown at 37°C in LB media to an OD<sub>600</sub> of 0.7. Expression was induced with 1mM IPTG and performed overnight at 20°C. The His6-tagged fusion proteins were affinity purified by immobilized metal-affinity chromatography on Ni<sup>2+</sup> sepharose (Amersham) at 4°C. Proteolytic cleavage to remove the His6-tag was carried out at 4°C using human thrombin (Sigma). Cleaved proteins were subjected to a second Ni<sup>2+</sup> sepharose column and further purified by size exclusion chromatography on Superdex-75 (CLIPCG1, CLIPCG2, p150CG) or Superdex-200 columns (CLIPCG12; Amersham) equilibrated in PBS (137 mM NaCl, 2.7 mM KCl, 8.3 mM Na<sub>2</sub>HPO<sub>4</sub>, 1.47 mM KH<sub>2</sub>PO<sub>4</sub> pH 7.4). Throughout the CG12 purification reducing conditions (1 mM beta-Mercaptoethanol) were maintained. The homogeneity of the recombinant proteins was assessed by SDS-PAGE and their identity was confirmed by mass spectral analysis.

The SLAIN2c (residues 569-581 of human SLAIN2), SLAIN2c-W576A and SLAIN2c-ΔY581 peptides were assembled on an automated continuous-flow synthesizer employing standard methods. The purity of the peptides was verified by reversed-phase analytical HPLC and their identities were assessed by mass spectral analysis.

#### Protein analysis

Size-exclusion chromatography coupled to multi-angle light scattering was performed on a DAWN EOS 18-angle detector followed by an Optilab Rex refractometer (Wyatt). Protein solutions (100 μl of 1-15 mg/ml) were injected on a Superdex 200 10/300 GL size exclusion chromatography column equilibrated with PBS. Molecular weights were calculated by using the Wyatt ASTRA V version 5.3.4.19 software package.

Far-UV CD spectroscopy was carried out on a Chirascan-plus (Applied Photophysics; Cort-Ir variants) spectropolarimeter equipped with a temperature-controlled quartz cell of 0.1 cm path length. A ramping rate of 1°C per min was used to record thermal unfolding profiles. Midpoints of the transitions, T<sub>m</sub>s, were taken as the maximum of the derivative d[θ]<sub>222</sub>/dT.

#### Isothermal titration calorimetry (ITC)

ITC experiments were performed in PBS at 25 °C on an iTC200 (MicroCal) machine. The sample cell was filled with 160-240 μM CAP-Gly solutions. The syringe was filled with 2.2-2.6 mM SLAIN2c peptide solutions. In the experiment with CLIPCG12 the buffer was supplemented with 1mM



beta-mercaptoethanol. 2.6  $\mu$ l of SLAIN2c aliquots from the stirred syringe were injected 14-28 times into the sample cell. To determine the binding stoichiometry,  $N$ , and the equilibrium binding constant,  $K_D$ , of the binding isotherms were fitted using a nonlinear least squares minimization method provided with the ITC calorimeter. Exact concentrations of protein solutions were determined by absorbance at 280 nm in 6 M GuHCl for the CAP-Gly domains or by quantitative amino acid analysis for the SLAIN2c peptide.

#### *Crystal structure determination*

For crystallization, CLIP170CG1 and SLAIN2c in PBS were mixed in a 1:1.2 ratio to reach a final complex concentration of 24 mg/ml. Crystals were obtained at 20°C by the hanging-drop vapour-diffusion method from a 1:1 mixture of the complex solution and a reservoir composed of 36% PEG 6000, 100 mM citric acid pH 4.5.

X-ray diffraction data were collected at 100 K at beamline X06DA of the Swiss Light Source (Villigen PSI, Switzerland). The structure was solved by molecular replacement using the CLIP-170 CAP-Gly structure as a search model (PDB ID 2E3I). Data processing and refinement statistics are summarized in Table S1.

#### *Mass spectrometry*

GST pull-down assays followed by mass spectrometry and streptavidin bead pull-down assays from HeLa cells followed by mass spectrometry were carried out as described by (Grigoriev et al., 2007). 1D SDS-PAGE gel lanes were cut into 2-mm slices using an automatic gel slicer and subjected to in-gel reduction with dithiothreitol, alkylation with iodoacetamide and digestion with trypsin (Promega, sequencing grade), essentially as described by (Wilm et al., 1996). Nanoflow LC-MS/MS was performed on an 1100 series capillary LC system (Agilent Technologies) coupled to either an LTQ-Orbitrap or an LTQ linear ion trap mass spectrometer (Thermo) both operating in positive mode and equipped with a nanospray source. Peptide mixtures were trapped on a ReproSil C18 reversed phase column (Dr Maisch GmbH; column dimensions 1.5 cm  $\times$  100  $\mu$ m, packed in-house) at a flow rate of 8  $\mu$ l/min. Peptide separation was performed on another ReproSil C18 reversed phase column (column dimensions 15 cm  $\times$  50  $\mu$ m, packed in-house) using a linear gradient from 0 to 80% B (A = 0.1 % formic acid; B = 80% (v/v) acetonitrile, 0.1 % formic acid) in 70 min and at a constant flow rate of 200 nl/min using a splitter. The column eluent was directly sprayed into the ESI source of the mass spectrometer. Mass spectra were acquired in continuum mode; fragmentation of the peptides was performed in data-dependent mode. Peak lists were automatically created from raw data files using the Mascot Distiller software (version 2.1; MatrixScience). The Mascot search algorithm (version 2.2, MatrixScience) was used for searching against the IPI database (release IPI\_mouse\_20100507.fasta or IPI\_human\_20100507.fasta). The peptide tolerance was typically set to 10 ppm for Orbitrap data and to 2 Da for ion trap data. The fragment ion tolerance was set to 0.8 Da. A maximum number of 2 missed cleavages by trypsin were allowed and carbamidomethylated cysteine and oxidized methionine were set as fixed and variable modifications, respectively. The Mascot score cut-off value for a positive

protein hit was set to 60. Individual peptide MS/MS spectra with Mascot scores below 40 were checked manually and either interpreted as valid identifications or discarded. Proteins present in the negative controls (pull down assays with either GST or bioGFP alone) were omitted from the table.

Phosphorylated peptides were selectively enriched for in an offline chromatographic manner using a titanium dioxide (TiO<sub>2</sub>, Titansphere) packed fused silica capillary that is used as a trap and which acts as a first-dimension separation step in a two-dimensional chromatography system (Pinkse et al., 2004). Phosphorylated peptides were separated from non-phosphorylated peptides by trapping them under acidic conditions on the TiO<sub>2</sub> column and ultimately desorbed under alkaline conditions, dried and dissolved in 0.1 M formic acid. Subsequently, nanoflow LC-MS/MS was performed on an 1100 series capillary LC system (Agilent Technologies) coupled to an LTQ-Orbitrap mass spectrometer (Thermo) operating in positive mode and equipped with a nanospray source as described above. The Mascot search algorithm (version 2.2, MatrixScience) was used for searching against the IPI database (release IPI\_human\_20100507).

#### *Antibodies, immunofluorescent cell staining and image analysis*

Rabbit antibodies against SLAIN1/2 were raised against a bacterially purified GST-SLAIN2 N-terminus. We used rabbit polyclonal antibodies against GFP (Abcam), CLASP1 (Mimori-Kiyosue et al., 2005), CLASP2 and CLIP-170 (Akhmanova et al., 2001), EB3 (Stepanova et al., 2003), phosphorylated histone H3 (Ser 10) (Millipore), cyclin B1 (GNS1, Santa Cruz Biotechnology) and ch-TOG (Charrasse et al., 1998), a gift from L. Cassimeris (Lehigh University; Bethlehem, USA); mouse monoclonal antibodies against GFP and HA tag (Roche), EB1 (BD Biosciences),  $\beta$ -tubulin and acetylated tubulin (Sigma Aldrich), p150<sup>Glued</sup> (BD Biosciences), and actin (Chemicon); and rat monoclonal antibody against EB1/3, clone #15H11 (Absea) and HA tag (Roche). The following secondary antibodies were used; alkaline phosphatase-conjugated anti-rabbit, anti-mouse or anti-rat antibodies (Sigma-Aldrich), IRDye 800CW Goat anti-rabbit, anti-mouse and anti-rat IgG (Li-Cor Biosciences), Alexa-350, Alexa-488 and Alexa-598 conjugated goat antibodies against rabbit, rat, and mouse IgG (Molecular Probes),

Cultured cells were fixed with  $-20^{\circ}\text{C}$  methanol for 15 min in case of EB1/3, ch-TOG, CLASP1/2 and p150<sup>Glued</sup> labeling. In the case of EB1, SLAIN1/2, CLIP-170, acetylated tubulin and  $\beta$ -tubulin labeling, cells were fixed with  $-20^{\circ}\text{C}$  methanol for 15 min and post-fixed in 4% PFA in phosphate-buffered saline (PBS) for 15 min at RT. Cells were rinsed with 0.15% Triton X-100 in PBS; subsequent washing and labeling steps were carried out in PBS supplemented with 1% bovine serum albumin and 0.15% Tween-20. At the end, slides were rinsed in 100% ethanol, air-dried and mounted in Vectashield mounting medium (Vector laboratories).

#### *Image Acquisition and Processing*

Images of fixed cells were collected with a Leica DMRBE microscope equipped with a PL Fluotar 100x 1.3 N.A. or 40x 1.00-0.50 N.A. oil objectives, FITC/EGFP filter 41012 (Chroma) and Texas Red filter 41004 (Chroma) and an ORCA-ER-1394 CCD camera (Hamamatsu).

Live cell imaging was performed on an inverted research microscope Nikon Eclipse Ti-E (Nikon) with perfect focus system (PFS) (Nikon), equipped with Nikon CFI Apo TIRF 100x 1.49 N.A. oil objective (Nikon), QuantEM 512SC EMCCD camera (Roper Scientific) and controlled with MetaMorph 7.5 software (Molecular Devices). The 16-bit images were projected onto the CCD chip with intermediate lens 2.5X at a magnification of 0.065  $\mu\text{m}/\text{pixel}$ . To keep cells at 37°C we used a stage top incubator (model INUG2E-ZILCS, Tokai Hit). The microscope was equipped with a TIRF-E motorized TIRF illuminator modified by Roper Scientific France/ PICT-IbiSA, Institut Curie. For regular imaging we used the mercury lamp HBO-100W/2 (Osram) for excitation or 491nm 50mW Calypso (Cobolt) and 561nm 50mW Jive (Cobolt) lasers. We used an ET-GFP filter set (Chroma) for imaging of proteins tagged with GFP and an ET-mCherry filter set (Chroma) for imaging of proteins tagged with mCherry. For simultaneous imaging of green and red fluorescence we used an ET-mCherry/GFP filter set (Chroma) together with a DualView (DV2, Roper) equipped with dichroic filter 565dcxr (Chroma) and an HQ530/30m emission filter (Chroma).

The FRAP assay was carried out using FRAP scanning system I-Las/I-Launch (Roper Scientific France/ PICT-IBiSA, Institut Curie) installed on the same microscope and with the lasers mentioned above at 100% laser power. We performed imaging at different frame rates, varying from 2 to 30 frames per second, to avoid missing rapid transitions between growth and shortening, and found that the frame rate of 2 frames/s was optimal for measuring MT dynamics. Movies with the same frame rate (2 frames/s) were used for analysis; when movies obtained at higher frame rates were used for the final quantifications, averaging was performed to lower the frame rate. For imaging of mitotic cells we used a CSU-X1-A1 Spinning Disc microscope (Yokogawa), equipped with a 405-491-561 triple band mirror and GFP, mCherry and GFP/mCherry emission filters (Chroma) installed on an inverted research microscope Nikon Eclipse Ti-E (Nikon), which is almost identical to the one described above. The 16-bit images were projected onto the CCD chip with an intermediate lens 2.0X at a magnification of 0.068  $\mu\text{m}/\text{pixel}$ .

Images were prepared for publication using MetaMorph and Adobe Photoshop. All images were modified by adjustments of levels and contrast; for images of live cells, averaging of several consecutive frames was performed in some cases; in addition to adjustments of levels and contrast, Unsharp Mask and Blur filters (Photoshop) were applied to tubulin images. Maximum intensity projection, kymograph analysis and various quantifications were performed in MetaMorph. Statistical analysis was performed using non-parametric Mann-Whitney U-test in Statistica for Windows and SigmaPlot.

Data deposition: The atomic coordinates of the CLIPCG1-SLAIN2c complex have been deposited in the Protein Data Bank (PDB ID code 3RDV).

### **Supplemental Information.**

Supplemental Information in this paper contains five supplemental figures. Figure S1 provides details of the mass spectrometry data on the identification of SLAIN2 and ch-TOG as EB1 binding partners, and illustrates dimer formation by SLAIN2 N-terminus and the specificity of anti-SLAIN1/2

antibodies. Figure S2 provides additional data on the SLAIN2-CLIP-170 interaction. Figure S3 provides details of the mass spectrometry analysis of SLAIN binding partners, RT-PCR-based data on expression of SLAIN1 and 2, and characterization of SLAIN2-depleted cells. Figure S4 provides additional data on SLAIN2-mediated ch-TOG binding to EB1 and to MT tips, and the dominant negative properties of the ch-TOG C-terminus. Figure S5 shows MT density after depletion or disruption of SLAIN2-ch-TOG complex and MT organization and dynamics in SLAIN2 and ch-TOG-depleted cells. Supplemental Table 1 provides the details of the X-ray crystallography data. Supplemental Table 2 provides the values and statistical analysis of the MT dynamics parameters. Seven supplemental movies illustrate the dynamic behavior of SLAIN2 and ch-TOG at the MT plus ends, and MT dynamics in SLAIN2 and ch-TOG depleted cells.

### Acknowledgments

We are grateful to D. Meijer, E. Mientjes, R. Tsien, L. Wordeman, L. Cassimeris and Kazusa DNA Research Institute for sharing materials, R. van der Linden and E. Dzierzak for FACS of the stable cell lines. This study was supported by the Netherlands Organization for Scientific Research ALW open program and ALW-VICI grants to A.A, ZonMw-VIDI and European Science Foundation (EURYI) awards to C.C.H and the Swiss National Science Foundation grants to M.O.S.

### References

- Akhmanova, A., C.C. Hoogenraad, K. Drabek, T. Stepanova, B. Dortland, T. Verkerk, W. Vermeulen, B.M. Burgering, C.I. De Zeeuw, F. Grosveld, and N. Galjart. 2001. Clasps are CLIP-115 and -170 associating proteins involved in the regional regulation of microtubule dynamics in motile fibroblasts. *Cell*. 104:923-35.
- Akhmanova, A., and M.O. Steinmetz. 2008. Tracking the ends: a dynamic protein network controls the fate of microtubule tips. *Nat Rev Mol Cell Biol*. 9:309-22.
- Barr, A.R., and F. Gergely. 2008. MCAK-independent functions of ch-Tog/XMAP215 in microtubule plus-end dynamics. *Mol Cell Biol*. 28:7199-211.
- Bonfils, C., N. Bec, B. Lacroix, M.C. Harricane, and C. Larroque. 2007. Kinetic analysis of tubulin assembly in the presence of the microtubule-associated protein TOGp. *J Biol Chem*. 282:5570-81.
- Brouhard, G.J., J.H. Stear, T.L. Noetzel, J. Al-Bassam, K. Kinoshita, S.C. Harrison, J. Howard, and A.A. Hyman. 2008. XMAP215 is a processive microtubule polymerase. *Cell*. 132:79-88.
- Brummelkamp, T.R., R. Bernards, and R. Agami. 2002. A system for stable expression of short interfering RNAs in mammalian cells. *Science*. 296:550-3.
- Cassimeris, L., B. Becker, and B. Carney. 2009. TOGp regulates microtubule assembly and density during mitosis and contributes to chromosome directional instability. *Cell Motil Cytoskeleton*. 66:535-45.
- Cassimeris, L., and J. Morabito. 2004. TOGp, the human homolog of XMAP215/Dis1, is required for centrosome integrity, spindle pole organization, and bipolar spindle assembly. *Mol Biol Cell*. 15:1580-90.
- Charrasse, S., M. Schroeder, C. Gauthier-Rouviere, F. Ango, L. Cassimeris, D.L. Gard, and C. Larroque. 1998. The TOGp protein is a new human microtubule-associated protein homologous to the *Xenopus* XMAP215. *J Cell Sci*. 111:1371-83.
- De Zeeuw, C.I., C.C. Hoogenraad, E. Goedknegt, E. Hertzberg, A. Neubauer, F. Grosveld, and N. Galjart. 1997. CLIP-115, a novel brain-specific cytoplasmic linker protein, mediates the localization of dendritic lamellar bodies. *Neuron*. 19:1187-99.
- Desai, A., and T.J. Mitchison. 1997. Microtubule polymerization dynamics. *Annu Rev Cell Dev Biol*. 13:83-117.
- Gergely, F., V.M. Draviam, and J.W. Raff. 2003. The ch-TOG/XMAP215 protein is essential for spindle pole organization in human somatic cells. *Genes Dev*. 17:336-41.
- Grigoriev, I., D. Splinter, N. Keijzer, P.S. Wulf, J. Demmers, T. Ohtsuka, M. Modesti, I.V. Maly, F. Grosveld, C.C. Hoogenraad, and A. Akhmanova. 2007. Rab6 regulates transport and targeting of exocytotic carriers. *Dev Cell*. 13:305-14.
- Hirst, C.E., S.M. Lim, L.A. Pereira, R.A. Mayberry, E.G. Stanley, and A.G. Elefanty. 2010. Expression from a betageo gene trap in the *Slain1* gene locus is predominantly associated with the developing nervous system. *Int J Dev Biol*. 54:1383-8.
- Hirst, C.E., E.S. Ng, L. Azzola, A.K. Voss, T. Thomas, E.G. Stanley, and A.G. Elefanty. 2006. Transcriptional profiling of mouse and human ES cells identifies SLAIN1, a novel stem cell gene. *Dev Biol*. 293:90-103.
- Holmfeldt, P., S. Stenmark, and M. Gullberg. 2004. Differential functional interplay of TOGp/XMAP215 and the KinI kinesin MCAK during interphase and mitosis. *EMBO J*. 23:627-37.

- Honnappa, S., S.M. Gouveia, A. Weisbrich, F.F. Damberger, N.S. Bhavesh, H. Jawhari, I. Grigoriev, F.J. van Rijssel, R.M. Buey, A. Lawera, I. Jelesarov, F.K. Winkler, K. Wuthrich, A. Akhmanova, and M.O. Steinmetz. 2009. An EB1-binding motif acts as a microtubule tip localization signal. *Cell*. 138:366-76.
- Honnappa, S., O. Okhrimenko, R. Jaussi, H. Jawhari, I. Jelesarov, F.K. Winkler, and M.O. Steinmetz. 2006. Key interaction modes of dynamic +TIP networks. *Mol Cell*. 23:663-71.
- Hoogenraad, C.C., A. Akhmanova, F. Grosveld, C.I. De Zeeuw, and N. Galjart. 2000. Functional analysis of CLIP-115 and its binding to microtubules. *J Cell Sci*. 113:2285-2297.
- Howard, J., and A.A. Hyman. 2003. Dynamics and mechanics of the microtubule plus end. *Nature*. 422:753-8.
- Howard, J., and A.A. Hyman. 2007. Microtubule polymerases and depolymerases. *Curr Opin Cell Biol*. 19:31-5.
- Kinoshita, K., I. Arnal, A. Desai, D.N. Drechsel, and A.A. Hyman. 2001. Reconstitution of physiological microtubule dynamics using purified components. *Science*. 294:1340-3.
- Komarova, Y., C.O. De Groot, I. Grigoriev, S.M. Gouveia, E.L. Munteanu, J.M. Schober, S. Honnappa, R.M. Buey, C.C. Hoogenraad, M. Dogterom, G.G. Borisy, M.O. Steinmetz, and A. Akhmanova. 2009. Mammalian end binding proteins control persistent microtubule growth. *J Cell Biol*. 184:691-706.
- Komarova, Y., G. Lansbergen, N. Galjart, F. Grosveld, G.G. Borisy, and A. Akhmanova. 2005. EB1 and EB3 control CLIP dissociation from the ends of growing microtubules. *Mol Biol Cell*. 16:5334-45.
- Komarova, Y.A., A.S. Akhmanova, S. Kojima, N. Galjart, and G.G. Borisy. 2002. Cytoplasmic linker proteins promote microtubule rescue in vivo. *J Cell Biol*. 159:589-99.
- Kronja, I., A. Kruljac-Leticic, M. Caudron-Herger, P. Bieling, and E. Karsenti. 2009. XMAP215-EB1 interaction is required for proper spindle assembly and chromosome segregation in *Xenopus* egg extract. *Mol Biol Cell*. 20:2684-96.
- Lansbergen, G., Y. Komarova, M. Modesti, C. Wyman, C.C. Hoogenraad, H.V. Goodson, R.P. Lemaitre, D.N. Drechsel, E. van Munster, T.W.J. Gadella Jr., F. Grosveld, N. Galjart, G.G. Borisy, and A. Akhmanova. 2004. Conformational changes in CLIP-170 regulate its binding to microtubules and dynactin localisation. *J Cell Biol*. 166:1003-1014.
- Mimori-Kiyosue, Y., I. Grigoriev, G. Lansbergen, H. Sasaki, C. Matsui, F. Severin, N. Galjart, F. Grosveld, I. Vorobjev, S. Tsukita, and A. Akhmanova. 2005. CLASP1 and CLASP2 bind to EB1 and regulate microtubule plus-end dynamics at the cell cortex. *J Cell Biol*. 168:141-53.
- Mishima, M., R. Maesaki, M. Kasa, T. Watanabe, M. Fukata, K. Kaibuchi, and T. Hakoshima. 2007. Structural basis for tubulin recognition by cytoplasmic linker protein 170 and its autoinhibition. *Proc Natl Acad Sci U S A*. 104:10346-51.
- Montenegro Gouveia, S., K. Leslie, L.C. Kapitein, R.M. Buey, I. Grigoriev, M. Wagenbach, I. Smal, E. Meijering, C.C. Hoogenraad, L. Wordeman, M.O. Steinmetz, and A. Akhmanova. 2010. In Vitro Reconstitution of the Functional Interplay between MCAK and EB3 at Microtubule Plus Ends. *Curr Biol*. 20:1717-22.
- Olieric, N., M. Kuchen, S. Wagen, M. Sauter, S. Crone, S. Edmondson, D. Frey, C. Ostermeier, M.O. Steinmetz, and R. Jaussi. 2010. Automated seamless DNA co-transformation cloning with direct expression vectors applying positive or negative insert selection. *BMC Biotechnol*. 10:56.
- Peset, I., and I. Vernos. 2008. The TACC proteins: TACC-ling microtubule dynamics and centrosome function. *Trends Cell Biol*. 18:379-88.
- Pinkse, M.W., P.M. Uitto, M.J. Hilhorst, B. Ooms, and A.J. Heck. 2004. Selective isolation at the femtomole level of phosphopeptides from proteolytic digests using 2D-NanoLC-ESI-MS/MS and titanium oxide precolumns. *Anal Chem*. 76:3935-43.
- Rehberg, M., and R. Graf. 2002. Dictyostelium EB1 is a genuine centrosomal component required for proper spindle formation. *Mol Biol Cell*. 13:2301-10.
- Schuyler, S.C., and D. Pellman. 2001. Microtubule "plus-end-tracking proteins": The end is just the beginning. *Cell*. 105:421-4.
- Slep, K.C. 2009. The role of TOG domains in microtubule plus end dynamics. *Biochem Soc Trans*. 37:1002-6.
- Smith, B., J. Treadwell, D. Zhang, D. Ly, I. McKinnell, P.R. Walker, and M. Sikorska. 2010. Large-scale expression analysis reveals distinct microRNA profiles at different stages of human neurodevelopment. *PLoS One*. 5:e11109.
- Splinter, D., M.E. Tanenbaum, A. Lindqvist, D. Jaarsma, A. Flotho, K.L. Yu, I. Grigoriev, D. Engelsma, E.D. Haasdijk, N. Keijzer, J. Demmers, M. Fornerod, F. Melchior, C.C. Hoogenraad, R.H. Medema, and A. Akhmanova. 2010. Bicaudal D2, dynein and kinesin-1 associate with nuclear pore complexes and regulate centrosome and nuclear positioning during mitotic entry. *PLoS Biol*. 8:e1000350.
- Steinmetz, M.O., and A. Akhmanova. 2008. Capturing protein tails by CAP-Gly domains. *Trends Biochem Sci*. 33:535-45.
- Stepanova, T., J. Slemmer, C.C. Hoogenraad, G. Lansbergen, B. Dortland, C.I. De Zeeuw, F. Grosveld, G. van Cappellen, A. Akhmanova, and N. Galjart. 2003. Visualization of microtubule growth in cultured neurons via the use of EB3-GFP (end-binding protein 3-green fluorescent protein). *J Neurosci*. 23:2655-64.
- Tirnauer, J.S., and B.E. Bierer. 2000. EB1 proteins regulate microtubule dynamics, cell polarity, and chromosome stability. *J Cell Biol*. 149:761-6.
- Tournebise, R., A. Popov, K. Kinoshita, A.J. Ashford, S. Rybina, A. Pozniakovskiy, T.U. Mayer, C.E. Walczak, E. Karsenti, and A.A. Hyman. 2000. Control of microtubule dynamics by the antagonistic activities of XMAP215 and XKCM1 in *Xenopus* egg extracts. *Nat Cell Biol*. 2:13-9.
- van der Vaart, B., A. Akhmanova, and A. Straube. 2009. Regulation of microtubule dynamic instability. *Biochem Soc Trans*.

37:1007-13.

Watson, P., and D.J. Stephens. 2006. Microtubule plus-end loading of p150(Glued) is mediated by EB1 and CLIP-170 but is not required for intracellular membrane traffic in mammalian cells. *J Cell Sci.* 119:2758-67.

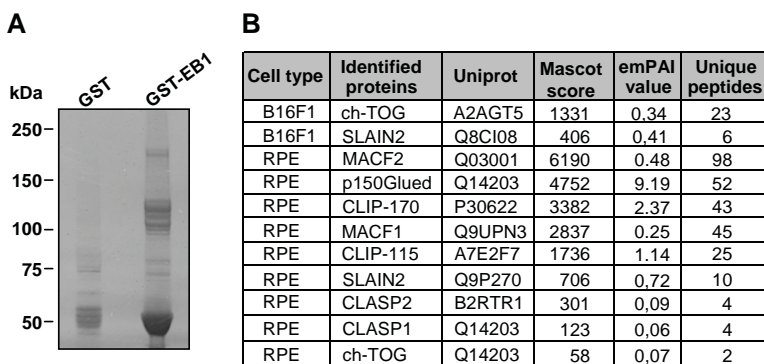
Weisbrich, A., S. Honnappa, R. Jaussi, O. Okhrimenko, D. Frey, I. Jelesarov, A. Akhmanova, and M.O. Steinmetz. 2007. Structure-function relationship of CAP-Gly domains. *Nat Struct Mol Biol.* 14:959-67.

Wilm, M., A. Shevchenko, T. Houthaeve, S. Breit, L. Schweigerer, T. Fotsis, and M. Mann. 1996. Femtomole sequencing of proteins from polyacrylamide gels by nano-electrospray mass spectrometry. *Nature.* 379:466-9.

Wittmann, T., A. Hyman, and A. Desai. 2001. The spindle: a dynamic assembly of microtubules and motors. *Nat Cell Biol.* 3:E28-34.

Wolyniak, M.J., K. Blake-Hodek, K. Kosco, E. Hwang, L. You, and T.C. Huffaker. 2006. The Regulation of Microtubule Dynamics in *S. cerevisiae* by Three Interacting Plus-End Tracking Proteins. *Mol Biol Cell.* 17:2789-98.

### Supplemental Information



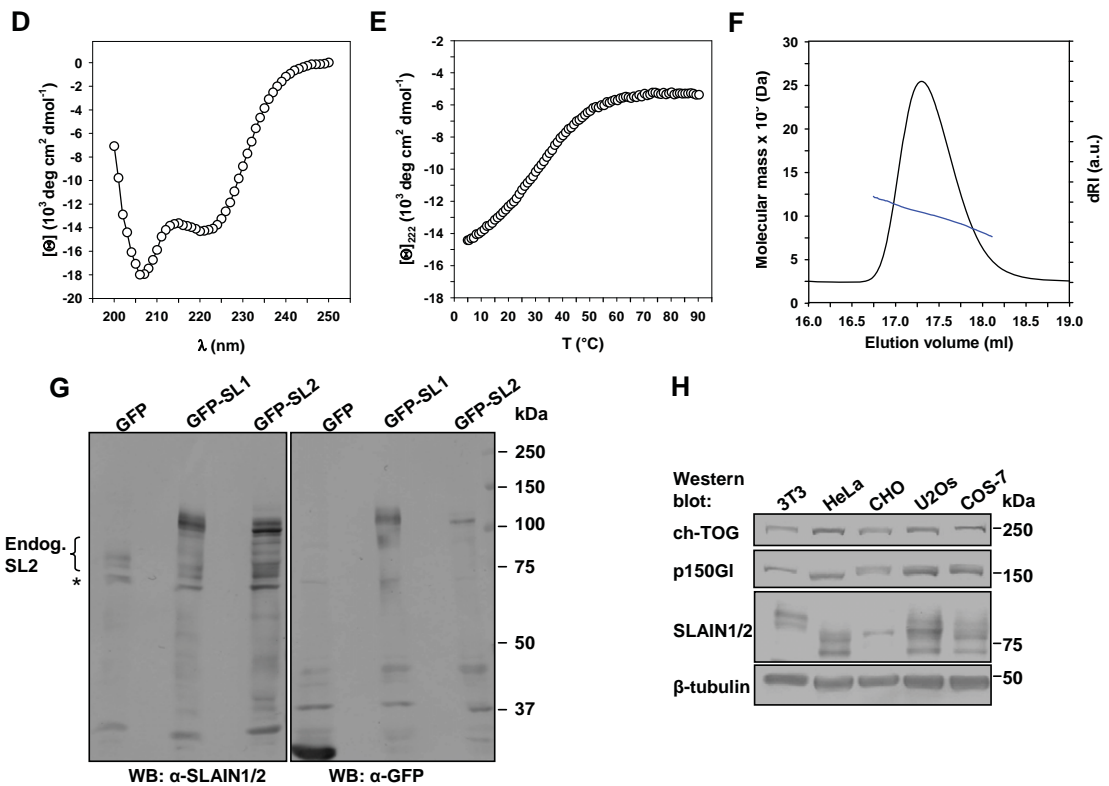
**C**

Hs SLAIN2 sequence:

```

1 MEDVNSNVNA DQEVKRLQEL VKKLEKQNEQ LRSRSGAVQG AGSLGPGSPV RAGASIPSSG
61 AASPRGFPLG LSSAKSGGGPG SGRRTSSEE LRDATSLAA GEGGLLDEVE PLRPDELERL
121 SGWEEEEESW LYSSPKKLLT PMQKSVSPLV WCRQVLDYPSS PDVECAKSL IHKLDQTMSA
181 LKRQNLNNP FNSMSYTSPYS SPNASSPYSS GFNSSPSTTPVS RPPIVKQLIL PGNSGNLKSS
241 DRNPPLSPQS SIDSELSASE LDEDSIGSNY KLNDVTDVQI LARMQEESLR QEYAATTSSR
301 SSGSSCNSTR RGTFSQEELD AQSLDEDDN MHHAVYPAVN RFSSPSPRNSPS RPSPKQSPRN
361 SPRSRSPARG IEYSRVSPQP MISRLQQPRL SLQGHPTDLQ TSNVKNEEKL RRSLPNLSRT
421 SNTQVDSVKS SRSDSNFQVP NGGIIPRMQPQ ASAIPSSPGKF RSPAAPSPLA LRQPVKAFSN
481 HGSGSPGSQE ITQLTQTSS PGPMVQSTV SANPPSNINS ATLTRPAGTT AMRSGLPRPFS
541 APSAGGIVP RSKLAQFVRRS SLPAKFKTYGS MKDDSWKDGC Y
    
```

SxIP-like motif: **S/G-x-I/L-P**  
 Mutated residues: **NN**  
**LP**  
 Minimal CDK1 consensus site:  
**S/T-P**  
 Major CDK1 consensus site:  
**S/T-P-x-K/R**  
 Phosphorylated serines  
 identified by mass spectrometry:  
**S**



**Supplemental Figure S1. Identification and characterization of SLAIN1 and SLAIN2 as EB1 partners.**

**A.** GST pull-down assays from B16F1 melanoma cells using GST alone or GST-EB1. Proteins were analyzed by Coomassie staining.

**B.** Identification of SLAIN2 and ch-TOG in GST-EB1 pull-down assays from B16F1 mouse melanoma and hTERT-RPE1 cell extracts by mass spectrometry.

**C.** Sequence of the human SLAIN2 protein. The IP/LP residues of the SxIP-like motifs are shown in blue, CDK1 major consensus sites (S/T-P-x-K/R) and other sites for proline-directed kinase sites (S/T-P) are shown in green, and phosphorylation sites confirmed by mass spectrometry are shown in red and underlined. Predicted coiled coil sequence is indicated by a box. Positions of the residues that were mutated to asparagines are indicated by an "N" above the sequence.

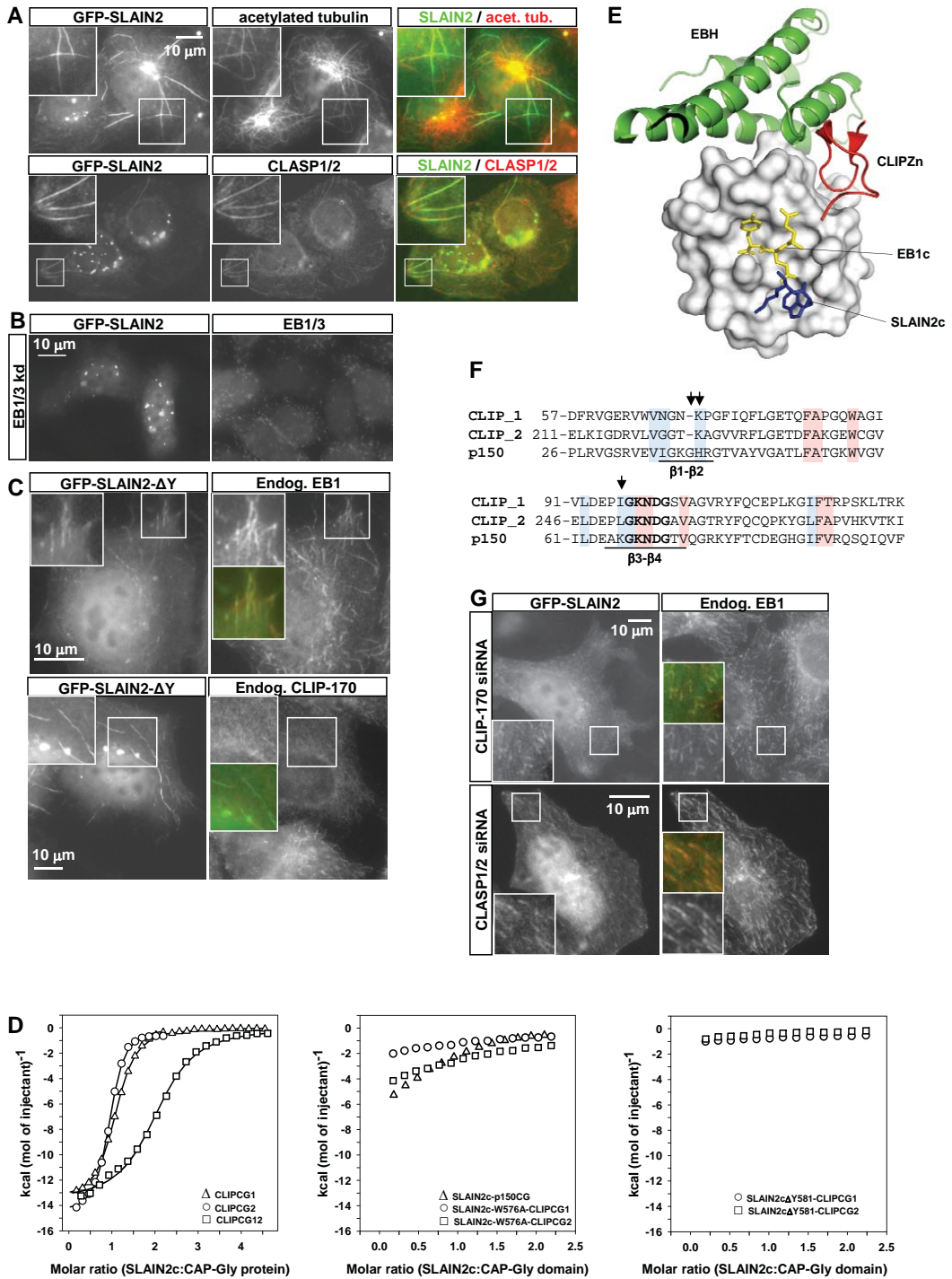
**D-F.** His6-tagged SLAIN2 (1-43) (His-SLAIN2cc) forms a two-stranded coiled-coil structure. **D.** Far-UV circular dichroism spectra of His-SLAIN2cc recorded at 5  $^{\circ}\text{C}$ . The spectrum with minima at 207 and 222 nm is characteristic of proteins with substantial  $\alpha$ -helical content.

**E.** Thermal unfolding profile of His-SLAIN2cc recorded by circular dichroism at 222 nm. The observed sigmoidal unfolding profile with a  $T_m$  of 37  $^{\circ}\text{C}$  is consistent with a cooperatively folded structure. The circular dichroism experiments were carried out at 50  $\mu\text{M}$  protein concentration in PBS.

**F.** Multi-angle light scattering analysis of His-SLAIN2cc. The blue line shows the molecular weight (see left Y axis) of the protein species measured at each point of the size exclusion chromatography elution profile, which was calculated using the static light scattering signal and the refracting index at each data point. The obtained molecular weight of His-SLAIN2cc is 10.4 kDa, which is consistent with the formation of a dimer (monomer molecular weight: 6.4 kDa). Together, these data are consistent with His-SLAIN2cc forming a moderately stable, two-stranded  $\alpha$ -helical coiled-coil structure.

**G.** Characterization of SLAIN1/2 rabbit polyclonal antibody. Extracts of HeLa cells expressing GFP, GFP-SLAIN1 or GFP-SLAIN2 were analyzed by Western blotting with anti-GFP or SLAIN1/2 antibodies. The bracket indicates endogenous SLAIN2 bands. The asterisk indicates an unspecific band cross-reacting with the SLAIN1/2 antibody.

**H.** Extracts of different cell lines analyzed by Western blotting with the indicated antibodies (p150GI stands for p150<sup>Glued</sup>).





**Supplemental Figure S2. SLAIN2 interaction with CLIP-170 depends on the SLAIN2 C-terminus.**

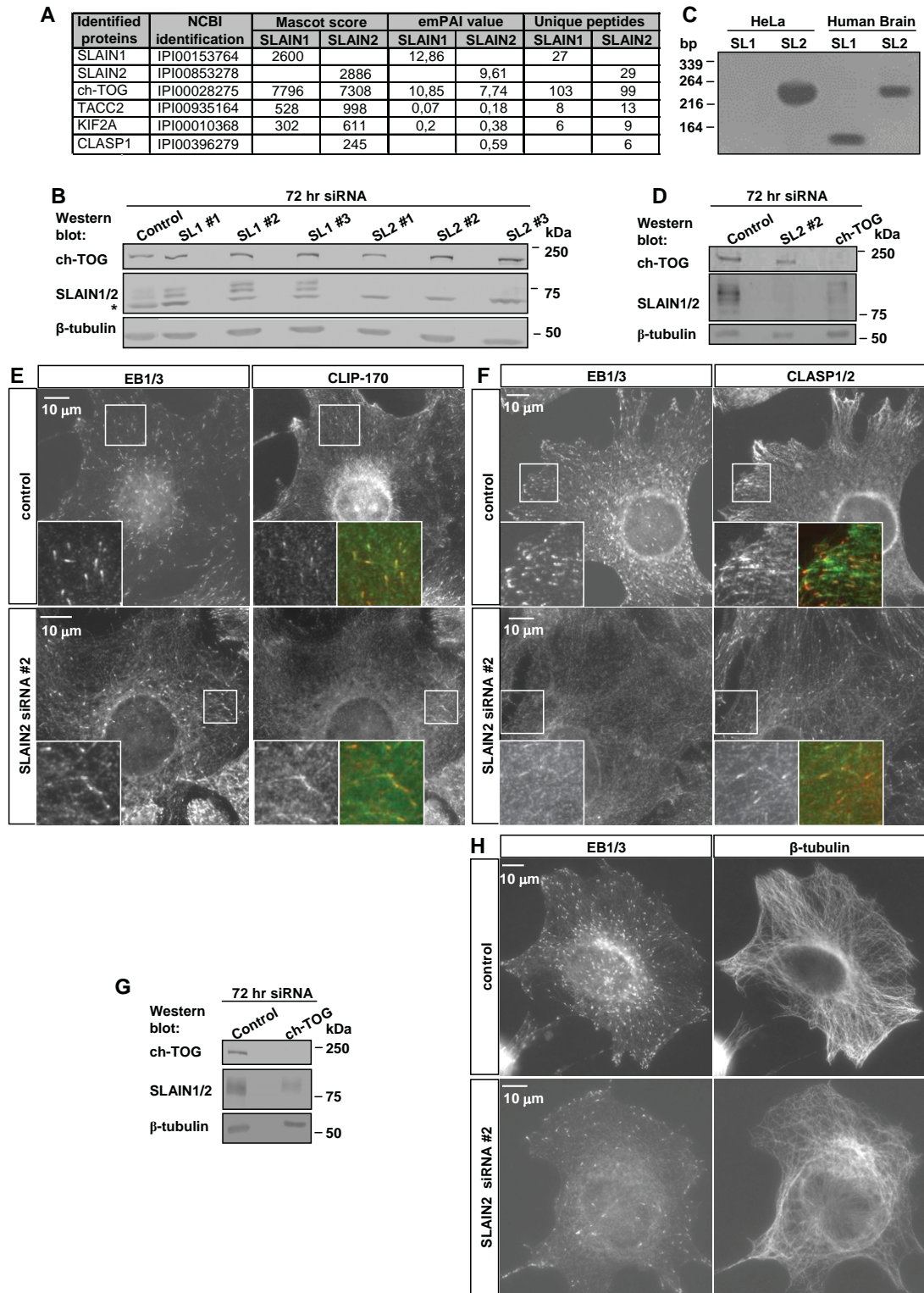
**A-C.** HeLa cells were transiently transfected with GFP-SLAIN2 or GFP-SLAIN2- $\Delta$ Y mutant, fixed and labeled with the indicated antibodies. In panel **B**, HeLa cells were transfected with siRNAs to deplete EB1 and EB3 two days before transfection with the GFP-SLAIN2 expression construct. In the overlay, GFP-tagged constructs are shown in green and acetylated tubulin, CLASPs, EB1 and CLIP-170 in red. Insets show enlargements of the boxed areas. Note that GFP-SLAIN2- $\Delta$ Y mutant colocalizes with EB1 but not with CLIP-170, which is displaced from the MTs. This experiment illustrates that when +TIPs such as SLAIN2 and CLIP-170 cannot bind each other, they instead compete with each other for the interaction with MTs.

**D.** Binding isotherms obtained by ITC. Left panel, SLAIN2c-CLIPCG1 (triangles), SLAIN2c-CLIPCG2 (circles), and SLAIN2c-CLIPCG12 (squares). Middle panel, SLAIN2c-p150CG (triangles), SLAIN2c-W576A-CLIPCG1 (circles), and SLAIN2c-W576A-CLIPCG2 (squares). Right panel, SLAIN2c- $\Delta$ Y581-CLIPCG1 (circles), and SLAIN2c- $\Delta$ Y581-CLIPCG2 (squares). Titration of CAP-Gly domains of CLIP-170 with SLAIN2c revealed binding isotherms consistent with the formation of complexes with a stoichiometry of one mole of SLAIN2c peptide per one mole of single CAP-Gly domain, and two moles of SLAIN2c peptide per one mole of tandemly arranged CAP-Gly domain (CLIPCG12) protein. The solid lines in the left panel represent the fit to the data. The data shown in the middle and right panels could not be subjected to rigorous analysis. However, the shape of the binding isotherms suggested that the  $K_d$ 's are in the millimolar range.

**E.** Overlay of the complexes formed between CAP-Gly domains and EBH (green), CLIPZnF (red), EEY of EB1 (yellow) and the LysTrp (KW) dipeptide of the C-terminal region of SLAIN2 (blue). The CAP-Gly domain is shown as grey surface representation; the ligands are shown as ribbon (EBH and ZnF) or stick (EEY and KW) representations.

**F.** Alignment of the sequence regions of the CLIP-170 and p150<sup>Glued</sup> CAP-Gly domains which form intermolecular contacts in the SLAIN2c-CLIPCG1 complex. Interacting residues of CLIPCG1 and the corresponding residues in CLIPCG2 and p150CG are highlighted in red (binding to SLAIN2c Y581) and blue (binding to SLAIN2c W576), respectively. Residues that differ in p150<sup>Glued</sup> are indicated by arrows. The  $\beta$ 1-  $\beta$ 2 and the  $\beta$ 3-  $\beta$ 4 loops are indicated.

**G.** HeLa cells stably expressing GFP-SLAIN2 were transiently transfected with the indicated siRNAs, fixed and labeled for EB1. Insets show enlargements of the boxed areas. In the overlay GFP-SLAIN2 is in green and EB1 in red. Note that GFP-SLAIN2 still localizes to EB1-positive MT tips in cells depleted of either CLIP-170 or CLASPs.



**Supplemental Figure S3. Identification of ch-TOG as SLAIN1 and SLAIN2 binding partner and characterization of SLAIN2-depleted cells.**

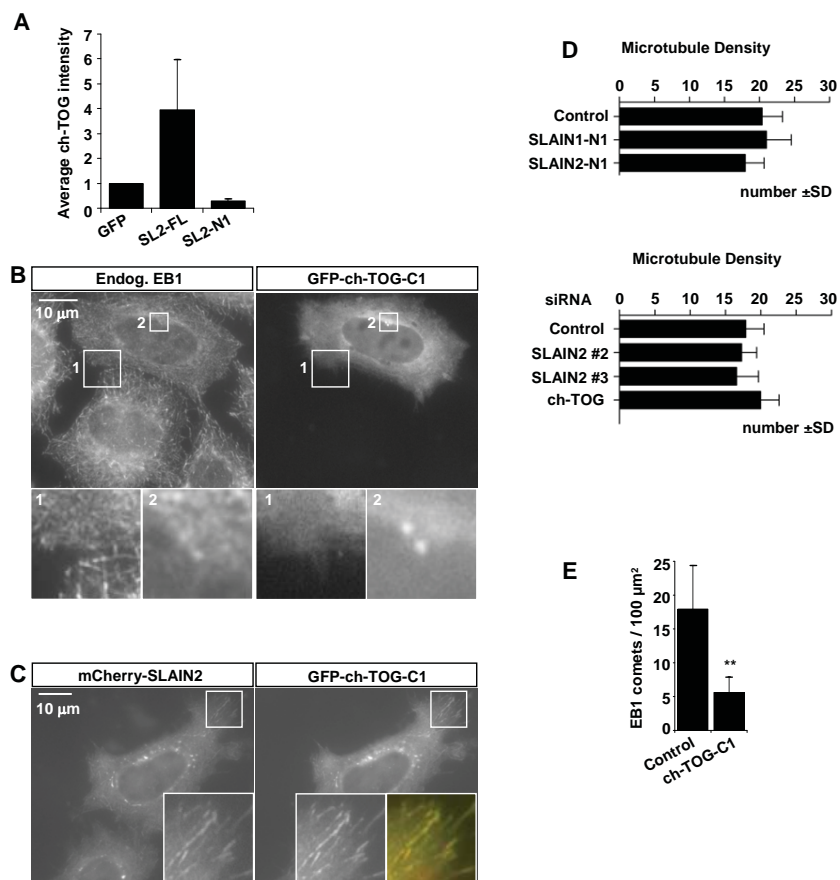
**A.** Mass spectrometry-based identification of SLAIN1 and SLAIN2 binding partners by streptavidin pull-down assays from HeLa cells. Note that in addition to ch-TOG and CLASP1, TACC2 was also recovered in SLAIN1/2 pull-downs in highly significant amounts. TACC proteins have been reported to bind to MT tips and to participate in subcellular targeting of XMAP215/Dis1 family proteins in different species (Peset and Vernos, 2008), and their potential involvement in the function of SLAIN2-ch-TOG complex needs further investigation. Another MT regulator present in SLAIN1/2 pull downs was the kinesin-13 KIF2A. Although it was absent in the negative control in this experiment, the specificity of its interaction with SLAINs or SLAIN-associated proteins is uncertain and needs to be further examined, because it is frequently found in preparations of various MT associated proteins from HeLa cells (A. Akhmanova, unpublished data).

**B,G.** Extracts of HeLa cells transfected with the indicated siRNAs analyzed by Western blotting with the indicated antibodies. The asterisk indicates an unspecific band cross-reacting with SLAIN1/2 antibody.

**C.** RT-PCR analysis of SLAIN1 and SLAIN2 expression in HeLa cells and human brain. Note that no SLAIN1-specific products could be obtained using HeLa cell cDNA, while the same cDNA sample yields strong amplification with SLAIN2-specific primers. Both SLAIN1 and SLAIN2 are expressed in human brain. This is in line with the data on SLAIN1 gene expression in the nervous system based on mouse gene trap analysis (Hirst et al., 2010).

**D.** Extracts of 3T3 cells transfected with the indicated siRNAs and analyzed by Western blotting with the indicated antibodies.

**E,F,H.** 3T3 cells were transiently transfected with control or SLAIN2 siRNAs, fixed and stained with the indicated antibodies. The insets show enlargements of the boxed areas. In the overlays EB staining is shown in green and other proteins in red.



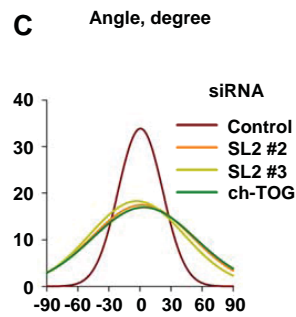
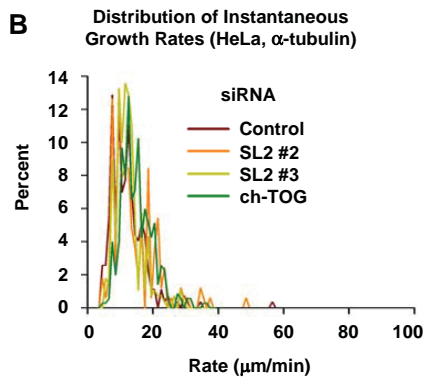
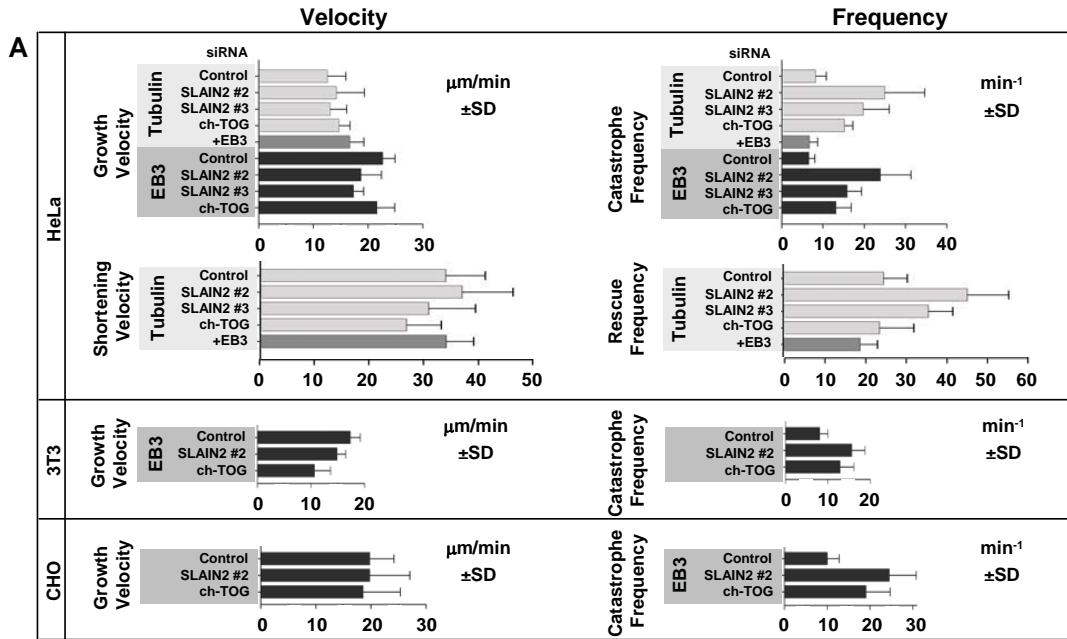
**Supplemental Figure S4. Recruitment of ch-TOG to MT tips and analysis of MT density in cells after the disruption of the SLAIN2-ch-TOG complex.**

**A.** Normalized average intensity of the ch-TOG band on Western blots of GST-EB1 pull downs from HEK293 cells expressing GFP, GFP-SLAIN2, or GFP-SLAIN2-N1 (Fig. 4E). Measurement was performed from three independent experiments with background subtraction using Metamorph. For each blot, values were normalized for the intensity observed for the GST-EB1 pull down from the extract of GFP-expressing cells.

**B,C.** HeLa cells were transfected with GFP-ch-TOG-C1 alone (**B**) or together with mCherry-SLAIN2 (**C**). In panel **B**, cells were stained for EB1. In the overlay in **C** mCherry-SLAIN2 is red and GFP-ch-TOG-C1 is green.

**D.** MT density determined as the number of MTs crossing a line of 7 μm width; the line was positioned parallel to the edge of the lamella at 5 μm distance from the edge. Analysis was performed one day after transfection with SLAIN1/2-N constructs or three days after transfection with the indicated siRNAs.

**E.** Quantification of the number of EB1/3-positive comets per 100 μm<sup>2</sup> surface area in control HeLa cells or cells expressing the C-terminal domain of ch-TOG (20 and 26 cells were analyzed for control and ch-TOG-C1, respectively). The number of comets was significantly lower in ch-TOG-C1-expressing cells,  $p < 0.001$ .



**Supplemental Figure S5. MT dynamics and organization in SLAIN2 and ch-TOG-depleted cells.**

**A.** Parameters of MT dynamic instability were determined in HeLa cells stably expressing GFP- or mCherry- $\alpha$ -tubulin (upper panels) and transfected with the indicated siRNAs (upper panels); in 3T3 cells stably expressing EB3-GFP and transfected with the indicated siRNAs (middle panels) and in CHO cells transiently transfected with EB3-GFP and the indicated shRNAs (bottom panels). In the upper panel, grey bars indicate parameters of MT dynamic instability in HeLa cells stably expressing GFP- or mCherry- $\alpha$ -tubulin. Statistical analysis showed no differences between these cell lines for the indicated parameters, and the data were pooled. Black bars indicate parameters of MT growth in HeLa cells stably expressing EB3-GFP and transfected with the indicated siRNAs. The actual values and statistical analysis of the data are shown in Table S2.

**B.** Distributions of instantaneous growth rates of MTs measured in HeLa cells stably expressing GFP- or mCherry- $\alpha$ -tubulin (for the number of measured MTs and cells, see Table S2).

**C.** MT organization in HeLa cells transfected with the indicated siRNAs. Cells were stained for  $\beta$ -tubulin, and the angles of MT segments in relation to the long axis of the lamella were measured; Gaussian fits of the angle distributions measured in 10 cells are shown for each condition.

<b>Structure</b>	<i>SLAINc-CLIPCGI</i>
<b>Data Collection</b>	
Space Group	P1
Unit cell a, b, c (Å)	38.21, 45.74, 49.36
$\alpha, \beta, \gamma$ (°)	100.06, 105.76, 108.38
Beamline	X06DA SLS
Wavelength (Å)	1
Resolution limits (Å)	45.5 – 1.75
High resolution shell (Å)	1.80 – 1.75
Reflections	
measured	178820
unique	28615
Completeness (%)	96.8 (95.1)*
$R_{\text{sym}}$ (%)	6.9 (34.9)*
Mean I / $\sigma$	17.56 (4.91)*
<b>Refinement</b>	
Reflections $R_{\text{cryst}} / R_{\text{free}}$	28600 / 1998
$R_{\text{cryst}}$ (%)	18.01
$R_{\text{free}}$ (%) <sup>†</sup>	22.88
Number of atoms	
Protein/Ligand	2476
Water	288
Average B factor (Å <sup>2</sup> )	
Protein	19.4
Ligand	44.6
Water	33.7
R.m.s.d. bond length (Å)	0.009
R.m.s.d. angles length (°)	1.150
Ramachandran plot (%)	
Favored	98.7
Outliers	0.0

\* Values in parentheses correspond to high resolution shell in data collection.

† 7 % of the reflections were set aside for an  $R_{\text{free}}$  test before initiating refinement.

**Supplemental Table 1. X-ray crystallographic data collection and refinement statistics**

	Instantaneous growth rate* $\mu\text{m}/\text{min} \pm \text{SD}$	Instantaneous shortening rate* $\mu\text{m}/\text{min} \pm \text{SD}$	Catastrophe Frequency $\text{min}^{-1} \pm \text{SD}$	Rescue Frequency $\text{min}^{-1} \pm \text{SD}$	cells / experiments
<b>HeLa, GFP-tubulin, mCherry-tubulin</b>					
Control	12.6 $\pm$ 3.4 n = 272	34.0 $\pm$ 7.3 n = 134	8.2 $\pm$ 2.5 n = 294	24.7 $\pm$ 5.8 n = 160	18 / 2
SLAIN2 siRNA#2	14.2 $\pm$ 5.1 n = 167, <i>p</i> < 0.5	40.0 $\pm$ 9.3 n = 90, <i>p</i> < 0.5	25.0 $\pm$ 9.7 n = 417, <i>p</i> < 0.001	45.3 $\pm$ 10.2 n = 214, <i>p</i> < 0.001	20 / 2
SLAIN2 siRNA#3	13.1 $\pm$ 3.0 n = 280, <i>n.s.</i>	30.8 $\pm$ 8.6 n = 124, <i>p</i> < 0.1	19.8 $\pm$ 6.3 n = 518, <i>p</i> < 0.001	35.7 $\pm$ 5.9 n = 270, <i>p</i> < 0.001	20 / 2
ch-TOG siRNA	14.7 $\pm$ 2.0 n = 352, <i>p</i> < 0.1	26.8 $\pm$ 6.3 n = 106, <i>p</i> < 0.01	15.2 $\pm$ 2.1 n = 425, <i>p</i> < 0.001	23.7 $\pm$ 8.5 n = 159, <i>p</i> < 0.5	15 / 2
<b>HeLa, mCherry-tubulin + EB3-GFP</b>					
Control	16.7 $\pm$ 2.6 n = 106, <i>p</i> < 0.1	34.0 $\pm$ 5.0 n = 60, <i>n.s.</i>	6.7 $\pm$ 2.0 n = 107, <i>p</i> < 0.5	18.9 $\pm$ 4.3 n = 68, <i>p</i> < 0.1	7 / 1
<b>HeLa, EB3-GFP</b>					
Control	22.7 $\pm$ 2.4 n = 202	–	6.6 $\pm$ 1.4 n = 202	–	15 / 2
SLAIN2 siRNA#2	18.7 $\pm$ 2.2 n = 341, <i>p</i> < 0.01	–	23.9 $\pm$ 7.4 n = 522, <i>p</i> < 0.001	–	20 / 2
SLAIN2 siRNA#3	17.4 $\pm$ 1.8 n = 368, <i>p</i> < 0.001	–	15.9 $\pm$ 3.4 n = 410, <i>p</i> < 0.001	–	17 / 2
ch-TOG siRNA	21.6 $\pm$ 3.3 n = 271, <i>p</i> < 0.5	–	13.2 $\pm$ 3.7 n = 292, <i>p</i> < 0.001	–	15 / 2
<b>3T3, EB3-GFP</b>					
Control	17.4 $\pm$ 1.8 n = 200	–	8.1 $\pm$ 1.9 n = 196	–	9 / 2
SLAIN2 siRNA#2	14.9 $\pm$ 1.6 n = 233, <i>p</i> < 0.1	–	15.7 $\pm$ 3.0 n = 154, <i>p</i> < 0.001	–	9 / 2
ch-TOG siRNA	10.7 $\pm$ 3.0 n = 186, <i>p</i> < 0.01	–	12.9 $\pm$ 3.2 n = 116, <i>p</i> < 0.01	–	9 / 2
<b>CHO, EB3-GFP</b>					
Control	19.8 $\pm$ 4.3 n = 323	–	10.1 $\pm$ 2.7 n = 312	–	17 / 2
SLAIN2 shRNA	19.9 $\pm$ 7.3 n = 539, <i>n.s.</i>	–	24.6 $\pm$ 6.2 n = 264, <i>p</i> < 0.001	–	12 / 2
ch-TOG shRNA	18.6 $\pm$ 6.8 n = 423, <i>n.s.</i>	–	19.1 $\pm$ 5.6 n = 277, <i>p</i> < 0.001	–	13 / 2

**Supplemental Table 2. Parameters of MT dynamics.**

Two HeLa cell lines, stably expressing GFP- or mCherry- $\alpha$ -tubulin were used for the analysis at 72 hr after transfection with SLAIN2 and ch-TOG siRNAs. The data were pooled since no significant differences were observed between the two lines for the measured parameters. Live cell images were collected with 30, 10 and 2 frames per second. Initial analysis revealed no significant differences in the measured values. Therefore, all the data were averaged to obtain movies with 0.5 s time interval for the final analysis. Parameters of MT growth were confirmed by independent measurements using HeLa cells stably expressing EB3-GFP. We applied kymograph analysis in order to distinguish very short episodes of growth and shortening, which are relevant for describing the phenotypes of SLAIN2 and ch-TOG depletion. This lead to much higher values for transition frequencies than those commonly determined using MT life history plots or particle tracking algorithms for EB-GFP movies.

For comparison, a similar analysis was performed in Swiss 3T3 fibroblasts stably expressing EB3-GFP after siRNA transfection, or in CHO cells after transient co-transfection of EB3-GFP and shRNA constructs. As we only focussed on MT dynamics in internal cell regions, we did not analyze the frequency and duration of pausing that is mostly associated with region-specific cortical MT stabilization. \* For measurements of instantaneous growth and shortening rates, the velocity of MT end displacements that were longer than 0.5  $\mu\text{m}$  were taken into account. Statistical analysis was performed using the Mann-Whitney U-test.







# Chapter 4

**Microtubule plus-end tracking  
proteins SLAIN1/2 and ch-TOG  
promote neurite extension**

Babet van der Vaart, Mariella A.M. Franker, Ilya Grigoriev,  
Casper C. Hoogenraad and Anna Akhmanova

*Manuscript in preparation*





## **Abstract**

The development, polarization, structural integrity and plasticity of neuronal cells critically depend on the microtubule (MT) network and its dynamic properties. Recently, SLAIN1 and SLAIN2 have been identified as regulators of MT dynamics. SLAIN1/2 are MT plus end tracking proteins (+TIPs), which are targeted to MT tips through interaction with End Binding (EB) family members. SLAINs promote persistent MT growth and suppress catastrophes by recruiting the MT polymerase ch-TOG to MT plus ends. Here, we show that SLAIN1/2 and ch-TOG proteins are highly enriched in brain and are expressed at constant levels during mouse brain development. Disruption of the SLAIN-ch-TOG complex in cultured primary hippocampal neurons affects MT growth similar to non-neuronal cells and inhibits neurite extension during neuronal development. Our study shows that proper control of MT dynamics is important for neuronal growth.

## **Introduction**

Neurons are highly specialized cells that form the major functional units of the nervous system. Through electrical and chemical signaling, they receive, process and transmit information. Most neurons are polarized cells with long extensions, neurites, which critically depend on the cytoskeleton for their development and maintenance. Until recently, it was thought that MTs play a secondary role in neuronal morphogenesis however, new insights have established a more pivotal role for MTs in controlling cell shape, actin organization and dynamics, and the polarized distribution of proteins, vesicles and other organelles in neurons (Conde and Caceres, 2009; Hoogenraad and Bradke, 2009; Poulain and Sobel, 2010).

The building blocks of MTs are the heterodimeric  $\alpha\beta$ -tubulin subunits, which polymerize in a head to tail fashion to form intrinsically polarized filaments. The  $\beta$ -tubulin subunit is projecting outward at the fast growing plus-end, whereas  $\alpha$ -tubulin is exposed at the minus-end, which is often stabilized and anchored at the MT organizing center (Jiang and Akhmanova, 2011). In both the axon and dendrites, bundles of highly stabilized MTs can be found that are crosslinked by the classical MT-associated proteins (MAPs) such as tau and MAP2, respectively. At the same time, a proportion of MTs remains dynamic and this is crucial for the functional and structural plasticity of neurons (Conde and Caceres, 2009; Hoogenraad and Bradke, 2009; Poulain and Sobel, 2010). Dynamic MTs are especially important in developing neurons, and even moderate changes in MT stability can affect neuronal polarity (Witte et al., 2008).

An important group of factors that regulate different aspects of MT plus end dynamics are the MT plus-end tracking proteins (+TIPs), a particular class of MAPs that associate specifically with growing MT plus ends (Akhmanova and Steinmetz, 2008; Schuyler and Pellman, 2001). End Binding (EB) proteins are considered to be core +TIP complex components as they can autonomously track growing MT plus ends and target many other +TIPs to them. In mammals, there are three EB family members: EB3 is a brain-enriched EB family member, whereas EB1 and EB2 are more widely expressed (Jaworski et al., 2009; Nakagawa et al., 2000). As principal +TIPs, EB proteins play important roles in neuronal function. The depletion of EB1 was shown to lead to shorter neurite-like extensions in neuroblastoma cells (Stepanova et al., 2010). Furthermore, EB1

is involved in the axonal targeting of Kv1 channels (Gu et al., 2006). In addition, in mature neurons dendritic spine morphology is regulated by the interaction of EB3 with the Src tyrosine kinase regulator p140Cap, linking MT dynamics to synaptic plasticity (Jaworski et al., 2009).

Other +TIPs and EB binding partners also play pivotal roles in neuronal development, maintenance and plasticity. Cytoplasmic linker proteins CLIP-115 and CLIP-170 are important regulators of axon induction and formation by stabilizing axonal MTs and regulating growth cone dynamics through a functional interplay with the actin cytoskeleton (Neukirchen and Bradke, 2011). CLASPs (CLIP-Associated Proteins), which interact with both CLIPs and EBs, are highly expressed in brain and are enriched in growth cones where they are thought to locally stabilize MTs and thereby regulate growth cone motility and navigation (Lee et al., 2004). Another important EB1-binding +TIP, Adenomatous Polyposis Coli (APC), participates in establishment of neuronal polarity, neurite outgrowth and formation of certain specialized synapses (Koester et al., 2007; Mattie et al., 2010; Rosenberg et al., 2008; Shi et al., 2004; Zhou et al., 2004).

Recently, we have identified the SLAIN family as novel +TIPs that interact with EBs. In mammals, two SLAIN homologues exist, SLAIN1 and SLAIN2 (Chapter 3). We showed that in 3T3 cells SLAINs are EB-dependent +TIPs that also interact with three other +TIP families, the CLIPs, CLASPs and XMAP215/ch-TOG. By binding to multiple +TIPs simultaneously, SLAINs can promote the formation of +TIP interaction networks while reducing the competition between proteins binding to growing MT tips. This property enables SLAINs to enhance the accumulation of the MT polymerase ch-TOG at the growing MT plus ends and in this way stimulate persistent MT growth by repressing catastrophes (switches from MT growth to depolymerization). The EB-SLAIN-ch-TOG complex is specific for interphase cells because its formation is inhibited by hyperphosphorylation of SLAINs during mitotic entry.

Neurons are post-mitotic cells and they often use the molecular machinery employed during mitosis (Baas, 1999). Since EB-SLAIN2-ch-TOG complex was only assembled in dividing cells during interphase it is important to investigate whether the complex also plays a role in neuronal development. This issue was particularly relevant because the function of ch-TOG, the only mammalian member of the XMAP215 family of MT polymerases, has never been properly investigated in the brain in spite of the fact that this is the only known factor responsible for high rates of MT polymerization *in vivo*.

In this study, we show that both ch-TOG and SLAIN1/2 are highly expressed in the mammalian adult brain. ch-TOG and SLAIN1/2 proteins are constantly expressed throughout development in various brain regions and are present at constant levels during the development of primary hippocampal neurons in culture. We use the latter model system to study the role of the SLAIN-ch-TOG MT regulating complex in neuronal development. Using immunofluorescent (IF) labeling we show that both SLAIN1/2 and ch-TOG are present throughout the cell body, axon and dendritic tree and are clearly detectable in neuronal growth cones. Disruption of the SLAIN-ch-TOG complex by depleting ch-TOG using short hairpin (sh) RNA or overexpression of a dominant-negative (DN) SLAIN2 construct caused a decrease in the number of EB1 comets in the cell bodies of young (DIV5) neurons and a reduction in processivity of MT growth. This is indicative

of a MT growth phenotype reminiscent to those seen in similar experiments using multiple cell-lines. On a morphological level, disruption of the complex leads to a decrease in total neurite length. These observations are consistent with the phenotypes observed after disruption of MT dynamics by applying low doses of the MT-depolymerizing drug nocodazole (Witte et al., 2008). We conclude that the SLAIN-ch-TOG complex plays an important role in neurite extension in primary hippocampal rat neurons. This study provides new molecular insights into the regulation of MT dynamics and its contribution to neuronal development.

## Results

### *Expression of ch-TOG and SLAIN/2 in brain*

Although initially identified in tumors, hence its name, colonic and hepatic tumor-overexpressed gene (ch-TOG), ch-TOG is ubiquitously expressed in healthy tissue, with elevated levels in brain (Charrasse et al., 1996; Charrasse et al., 1995). Using reverse transcriptase polymerase chain reaction (RT-PCR) it was previously shown that both SLAIN1 and SLAIN2 are expressed in the human brain (Chapter 3). In agreement, SLAIN1 expression is predominantly associated with the developing and adult nervous system as determined by a  $\beta$ geo gene trap mouse-line, whole mount *in situ* hybridization and the Allen Mouse Brain Atlas (Hirst et al.; Hirst et al., 2006; Lein et al., 2007).

Using Western blot (WB) analysis we first determined the protein levels of SLAIN1/2 and ch-TOG in different tissue extracts isolated from adult rat. We found that ch-TOG is highly enriched in a variety of different brain regions, in line with previous RT-PCR results (Fig. 1A) (Charrasse et al., 1996; Charrasse et al., 1995). This expression pattern correlates with the high levels of  $\beta$ -tubulin found in these regions, and is in agreement with the reported function of ch-TOG as a protein regulating MT dynamicity (Brouhard et al., 2008; Popov et al., 2001). Using a pan-SLAIN antibody that recognizes both SLAIN1 and SLAIN2 equally well on WB, we observed multiple positive bands that likely correspond to different splice isoforms and/or post-translational modification of SLAIN1/2 in the different tissues tested (Fig. 1A). In different brain regions, the double band pattern of SLAIN1/2 is similar to non-phosphorylated SLAIN2 seen in HeLa or 3T3 interphase cells, in line with the post-mitotic nature of the adult brain (Fig. 1A, Chapter 3).

Next, we looked in more detail at ch-TOG and SLAIN1/2 expression levels during brain development. Extracts from different mouse brain regions were prepared at multiple time points during brain development. Constant levels of ch-TOG and SLAIN1/2 throughout development were observed (Fig.1B). These data indicate that ch-TOG and SLAIN1/2 are expressed at continuous levels in the brain, suggesting that they participate in regulating MT dynamics at all stages of development.

In order to study the role of the SLAIN-ch-TOG complex in neuronal development we made use of postmitotic hippocampal neuronal cultures isolated from rat embryos undergoing terminal differentiation (Banker and Goslin, 1988). In agreement with the *in vivo* data, in neuronal cultures, SLAIN1/2 and ch-TOG are present at sustained levels throughout development and in mature neurons (Fig. 1C). Using IF labeling endogenous ch-TOG and SLAIN1/2 could clearly be

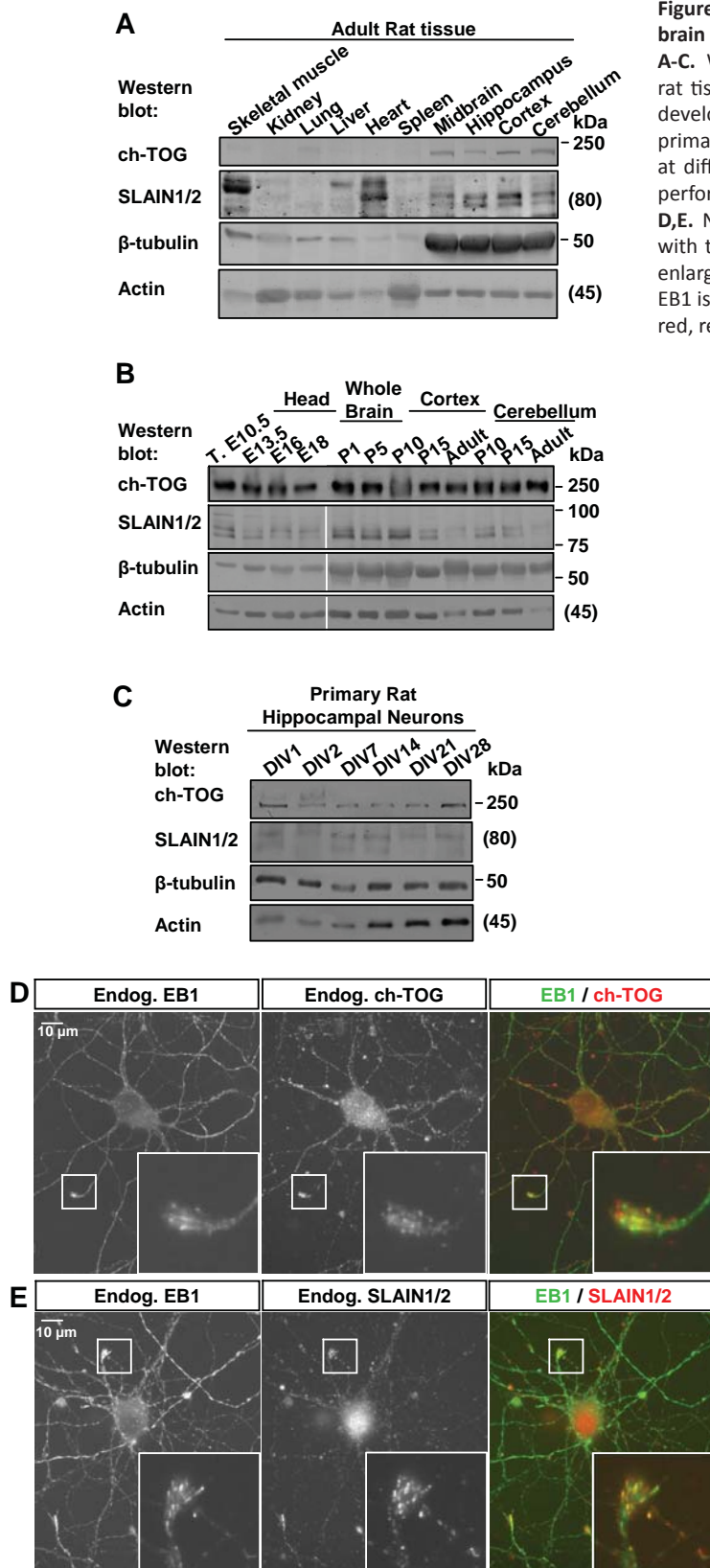


**Figure 1. ch-TOG and SLAIN1/2 are enriched in brain tissue**

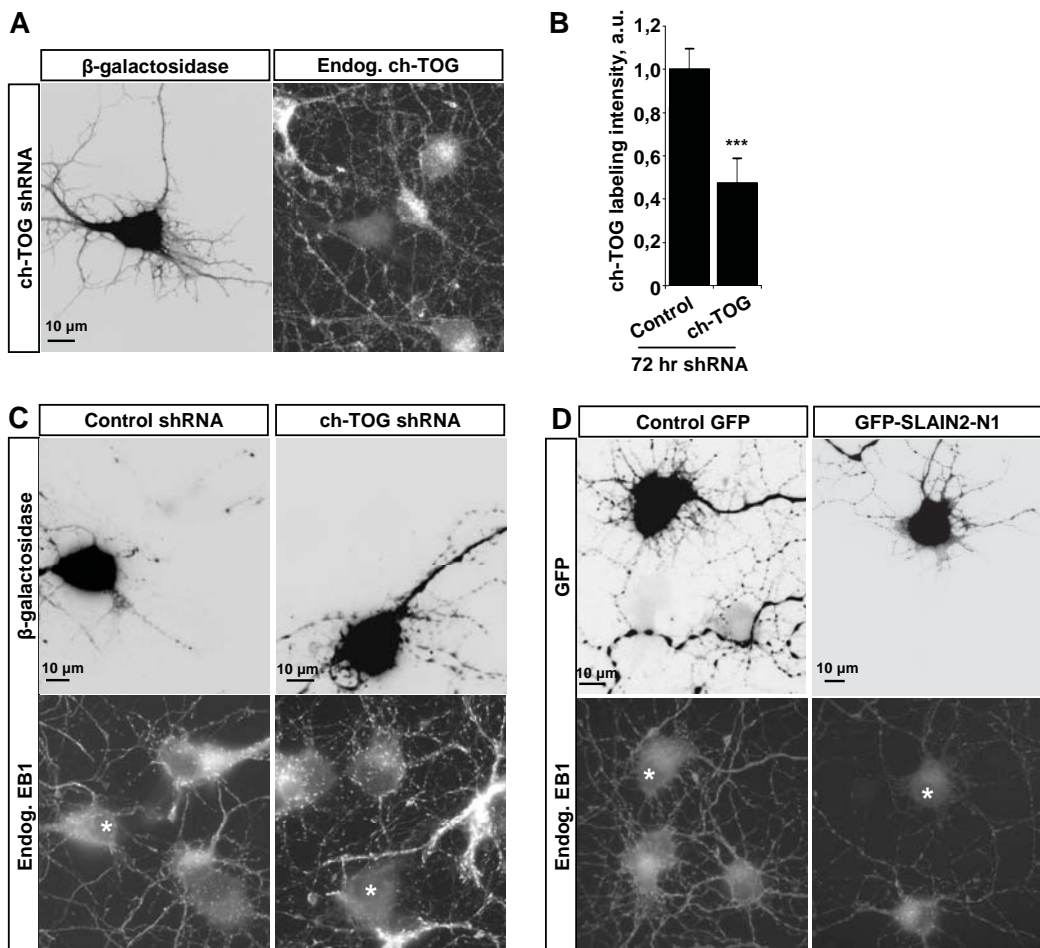
**A-C.** Western blot analysis of different adult rat tissues (**A**), mouse brain tissue of different developmental stages (**B**) and extracts of primary hippocampal neuron culture extracts at different stages of development *in vitro* (**C**) performed with the indicated antibodies.

**D,E.** Neurons were fixed on DIV5 and labeled with the indicated antibodies. The insets show enlargements of the boxed areas. In the overlay, EB1 is green and ch-TOG (**D**) and SLAIN1/2 (**E**) is red, respectively.

detected in the cell body, neurites and axonal growth cones of neurons at day 5 *in vitro* (DIV5) (Fig. 1D,E). Co-localization of SLAIN1/2 and ch-TOG with the plus-end marker EB1 was especially clear in the neuronal growth cones (Fig. 1D,E), which are the sites where highly dynamic MTs interact with the actin cytoskeleton to promote neurite outgrowth (Conde and Caceres, 2009; Hoogenraad and Bradke, 2009; Poulain and Sobel, 2010).

*Disruption of SLAIN-ch-TOG complex affects MT growth in neurons*

To assess the function of the SLAIN-ch-TOG complex during neuronal development, the complex was disrupted in two different ways. First, RNAi-mediated knockdown of ch-TOG was performed by transfection of a short hairpin (sh) RNA construct in DIV1 neurons. This construct has previously been shown to inhibit MT growth and nucleation in CHO cells (Chapter 3). ch-TOG was efficiently depleted with this construct because transfected neurons, identified by co-expression of  $\beta$ -galactosidase marker, showed a highly significant reduction of ch-TOG staining intensity (Fig. 2A,B). Secondly, the SLAIN-ch-TOG complex was disrupted by overexpression of dominant negative (DN) SLAIN2 (GFP-SLAIN2-N1) in DIV1 neurons. The expression of this SLAIN2 fragment, which can bind to ch-TOG but not to EBs, CLIPs or CLASPs, has previously been shown to disrupt



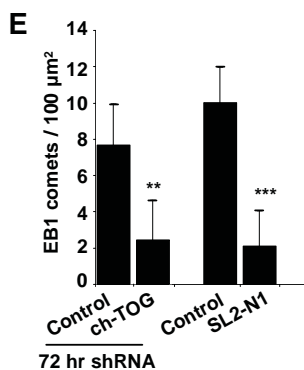


**Figure 2. Disruption of SLAIN-ch-TOG complex in neuronal cells**

**A,C,D.** Neurons transfected at DIV1 with indicated constructs (**A,C,D**) were fixed on DIV5 and labeled with indicated antibodies. Asterisk in lower panels in **C** and **D** indicate transfected cells. **B.** Quantification of the ch-TOG labeling intensities in control shRNA and ch-TOG depleted neurons (total number of analyzed cells was 10 and 12 respectively). The values for ch-TOG depleted cells were significantly different from control, \*\*\*  $p < 0.001$ . **E.** Quantification of the number of EB1 comets in the cell body per 100  $\mu\text{m}^2$  surface area in control shRNA, ch-TOG shRNA, GFP control and GFP-SLAIN2-N1 expressing neurons (total number of analyzed cells was 14, 10, 12 and 15 respectively). Statistically significant differences are indicated (\*\*  $p < 0.001$ , \*\*\*  $p < 0.001$ ).

MT plus-end recruitment of ch-TOG and inhibit MT growth similar to SLAIN2 knockdown in HeLa cells (Chapter 3).

Disruption of the SLAIN-ch-TOG complex in neurons using these two methods strongly affected the number of growing MTs as observed by IF labeling of DIV5 neurons with an EB1 antibody (Fig. 2C,D). The number of EB1-positive MT tips in the cell body was dramatically reduced (Fig. 2E). These results are similar to those seen in multiple different cell lines after the disruption of the SLAIN-ch-TOG complex (Chapter 3).

Next, we set out to investigate MT dynamics phenotypes in neuronal cells after disruption of the SLAIN-ch-TOG complex using Cherry-MT+TIP, a marker of growing MT ends based on the C-terminal MT plus end tracking fragment of the spectraplakine MACF2 (Honnappa et al., 2009; Kapitein et al., submitted). In control neurons robust plus-end tracking of Cherry-MT+TIP could be observed, as well as persistent outgrowth of MTs (Fig. 3A,B). In conditions where SLAIN-ch-TOG complex was disrupted by GFP-SLAIN2-N1 overexpression, Cherry-MT+TIP positive plus-ends were still visible but persistent MT growth was diminished due to increased catastrophes (Fig. 3A,B and Chapter 3). Reduction of persistent MT growth resulted in a 5-fold decrease in the mean MT growth velocity (Fig. 3C). In conclusion, the effect of disruption of the SLAIN-ch-TOG complex on MT dynamics is similar in neuronal and non-neuronal cells.

#### *SLAIN and ch-TOG play a role in neurite extension*

To access the morphological affect of disrupting MT dynamics by inhibiting SLAIN-ch-TOG complex formation, we analyzed the total neurite length at DIV5 in neurons that were transfected with the ch-TOG shRNA or GFP-SLAIN2-N1 at DIV1. Both the depletion of ch-TOG and the overexpression of GFP-SLAIN2-N1 caused a significant decrease in neurite length at DIV5 compared to control cells (Fig.4A-C). From these experiments we conclude that MT growth dynamics regulated by the SLAIN-ch-TOG complex is important for proper neurite extension during neuronal development.

#### **Discussion**

In this study, we showed that ch-TOG and SLAIN1/2 are highly expressed in the brain. The expression levels of these proteins are constant throughout mouse brain development and primary hippocampal neuron cultures of different developmental stages as determined by WB.

Disruption of the SLAIN-ch-TOG complex by ch-TOG depletion or overexpression of the



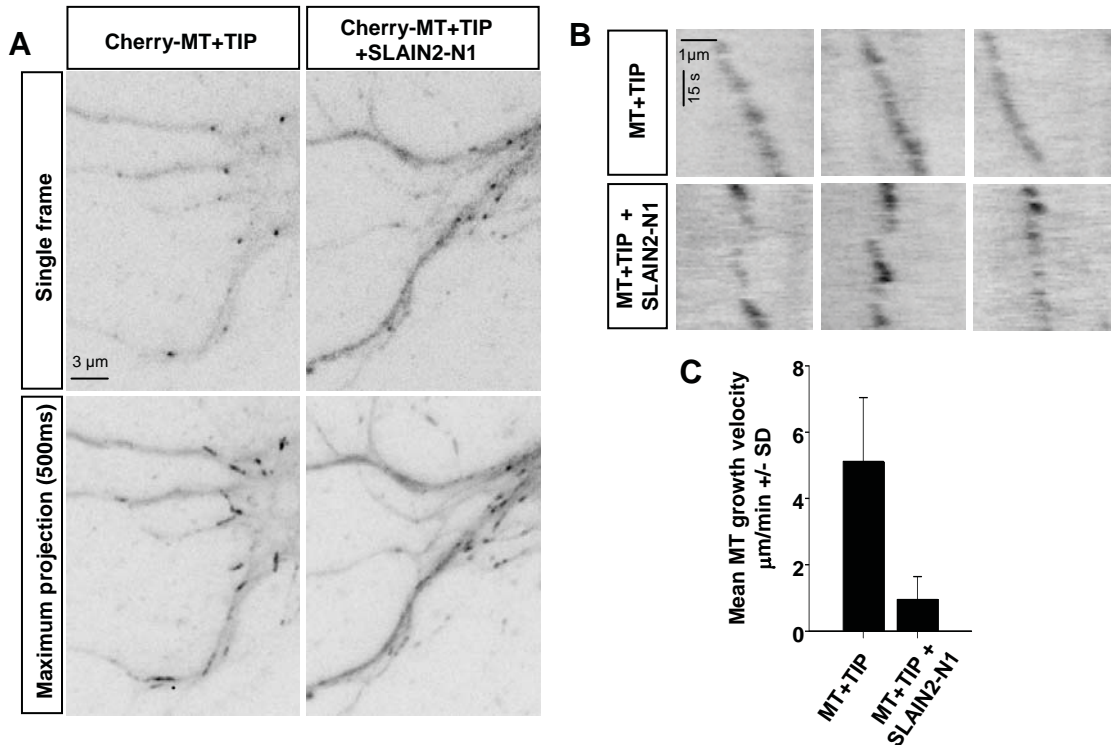
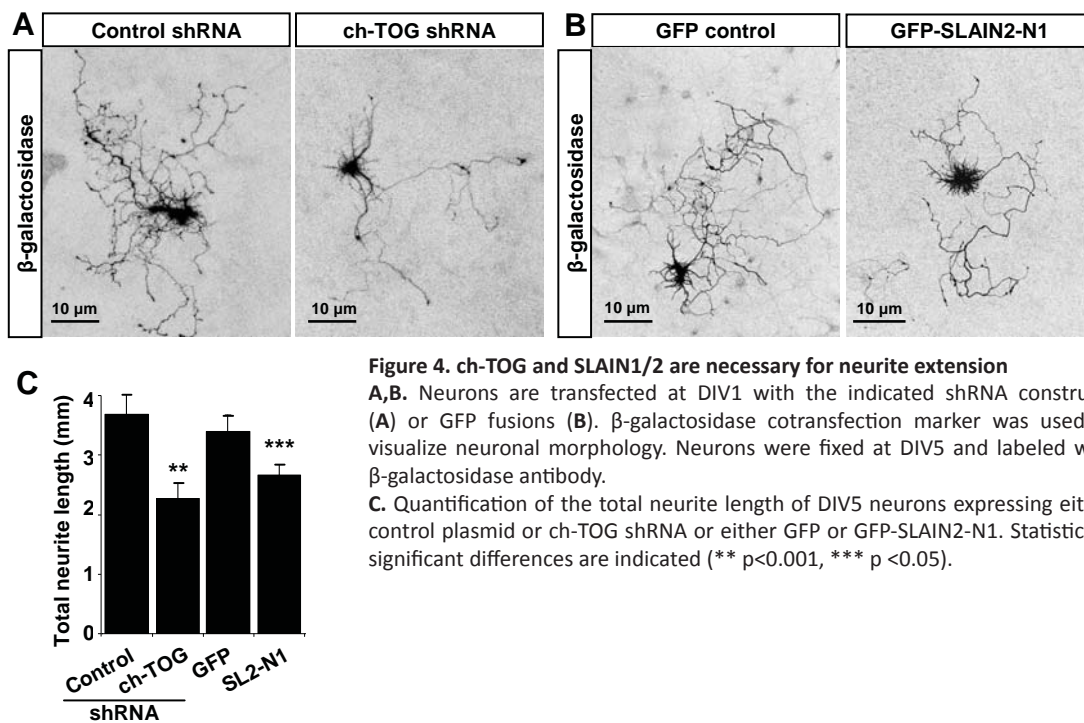


**Figure 3. SLAIN-ch-TOG complex promotes MT growth in neuronal cells**

**A.** Neurons were transfected at DIV1 with indicated constructs. Live images were collected at DIV5 with 0.5 s time interval. Single frames (top) and maximum intensity projections of 121 frames (bottom) are shown. **B.** Kymographs illustrating MT growth using Cherry-MT+TIP in neurons co-expressing GFP and Cherry-MT+TIP (control) or GFP-SLAIN2-N1 and Cherry-MT+TIP. **C.** Quantification of mean MT growth velocity based on the displacement of Cherry-MT+TIP comets in DIV5 neurons transfected with the indicated constructs at DIV1 (MT+TIP  $5.12 \pm 1.93$   $\mu\text{m}/\text{min}$ ,  $n = 70$ ; MT+TIP + SLAIN2-N1  $0.95 \pm 0.69$   $\mu\text{m}/\text{min}$ ,  $n = 8$ ).

dominant negative SLAIN2 strongly reduced the number of EB1 comets in neuronal cell bodies indicating that MT growth was inhibited. This suggests that the SLAIN-ch-TOG complex regulates MT dynamics in neurons and non-neuronal interphase cells in a similar manner. Disruption of the complex in neurons affects neuronal morphology, because neurite outgrowth was reduced.

In interphase non-neuronal cells SLAIN1/2 and ch-TOG together with EBs help to support frequent and rapid MT outgrowth, which is needed to maintain a radial MT array necessary for proper localization of membrane compartments and cell polarity. In neurons, regulation of MT dynamics by this complex is important for neuritogenesis. How could the SLAIN-ch-TOG complex play a role in this process? The initial steps in neurite outgrowth are the invasion of lamellipodia by MTs and subsequent elongation of the neurites (Conde and Caceres, 2009; Hoogenraad and Bradke, 2009; Poulain and Sobel, 2010); both steps require robust MT growth events (Fig. 5). By stimulating persistent outgrowth of MTs, the SLAIN-ch-TOG complex supports MT stability, which is important for the initial steps of neuritogenesis. In line with this view, cortical neurons treated with low concentration of nocodazole at one hour after plating have fewer MTs invading the lamellipodia resulting in a failure to extend neurites (Dent et al., 2007). It has also been shown that MT dynamics is essential for axon extension: application of low doses of nocodazole,



vinblastine or taxol has been shown to slow down axonal growth cone propagation (Gallo and Letourneau, 1999; Rochlin et al., 1996; Tanaka et al., 1995; Williamson et al., 1996; Yu and Baas, 1995). In our experiments, neurite extension was reduced but not abolished, most likely due to the timing of our inhibitory treatments (transfection at DIV1) or the incomplete disruption of ch-TOG function. Interestingly, the extent of reduction of neurite length in our experiments was similar to that observed in another study where hippocampal neurons were treated with low doses of nocodazole from DIV1 to DIV3 (Witte et al., 2008).

Recently, a general model of cell elongation showed that cell length can be controlled by parameters of MT growth dynamics, such as polymerization velocity and catastrophe frequency (Picone et al., 2010). Our results are in excellent agreement with this model because they show that disruption of processive MT polymerization leads to shorter MT-dependent cell processes.

The high enrichment of ch-TOG and SLAIN1/2 in neuronal growth cones suggests a role of this complex in growth cone dynamics similar to the roles of CLIPs and CLASPs (Lee et al., 2004; Neukirchen and Bradke, 2011). These protein families are also known SLAIN binding partners, and it remains to be determined whether SLAINs play a role in the accumulation of these proteins at the MT tips in growth cones.

In our studies we determined the role of SLAIN-ch-TOG complex in neuronal development, but they do not address a potential role for the complex in regulating MTs in mature neurons, which will require additional studies. Taken together, our study has identified the SLAIN-ch-TOG MT tip complex as an important regulator of neurite growth in primary hippocampal neurons.

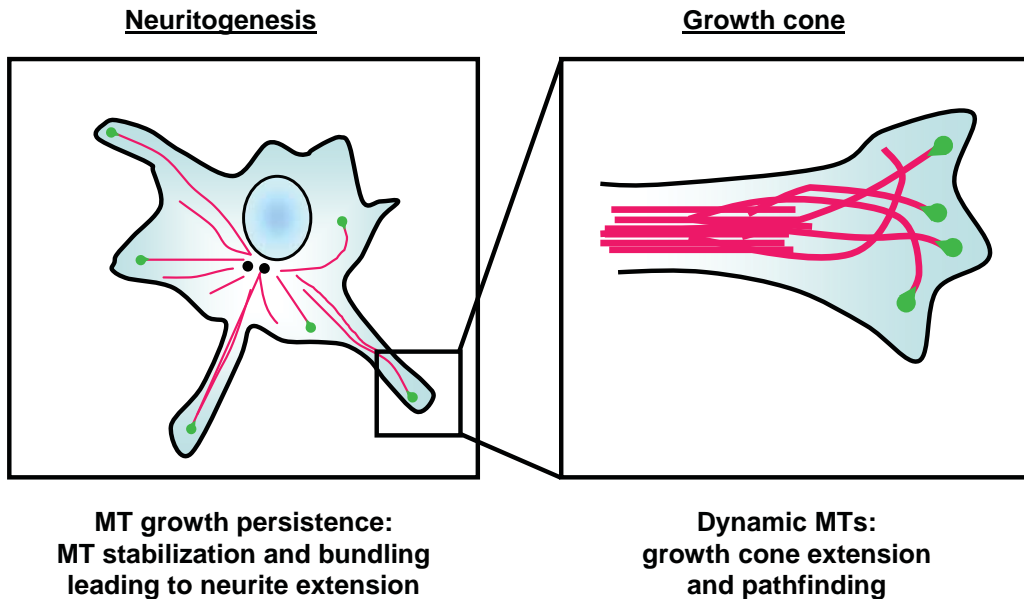


**Figure 5. A model for role of SLAIN-ch-TOG complex in neuronal development**

The EB1-SLAIN-ch-TOG complex is represented by a green comet. MT growth persistency controlled by the SLAIN-chTOG complex in the initial steps of neuritogenesis, growth cone extension and pathfinding.

### Experimental procedures

#### *Tissue extracts and primary hippocampal neuron cultures*

For WB, rat and mouse tissues were placed in ice-cold PBS. Samples were homogenized in homogenization buffer (150 mM NaCl, 50 mM Tris HCl, pH 8.0, 0.1% SDS, 0.5% NP-40, protease inhibitor cocktail (Complete, Roche)), briefly sonicated, centrifuged at 900 rcf, resuspended in SDS-PAGE sample buffer and boiled for 5 min. Protein concentrations were measured using a BCA protein assay kit (Pierce) and 50 µg of protein was loaded per lane. Hippocampal neuron cultures were directly lysed in SDS-PAGE sample buffer, briefly sonicated, boiled and subjected to Western blotting.

#### *Neuronal cultures and transfections*

Primary hippocampal cultures were prepared from embryonic day 18 (E18) rat brains as described by (Jaworski et al., 2009) and transfected using Lipofectamine 2000 (Invitrogen).

#### *Constructs*

pβactin-HA-β-galactosidase has been previously described (Hoogenraad et al., 2005), GFP-SLAIN2-N1 (Chapter 3) was re-cloned into neuronal GFP-GW1 expression vector (modified GW1-vector British Biotechnology) (Hoogenraad et al., 2005). The Cherry-MT+TIP construct (Kapitein et al., submitted) contains the two-stranded leucine zipper coiled-coil sequence corresponding to GCN4-p1 (RMKQLEDKVEELLSKNYHLENEVARLKKLVGER) fused to N-terminal 43 amino acid peptide (ETVPQTHRPTPRAGSRPSTAKPSKIPTPQRKSPASKLD KSSKR) of human MACF2 (E5455-R5497; NP\_899236), which binds to EB1 and tracks growing MT ends in an EB1-dependent manner

(Honnappa et al., 2009). A glycine rich-linker sequence (GAGG) was inserted between GCN4-pl and MACF43 and subcloned in pBactin-16-pl expression vectors (L. C. Kapitein et al., 2010) to generate pBactin-Cherry-GCN4-MACF43. Since we use Cherry-GCN4-MACF43 as a general marker to analyze the dynamics of growing MT plus-ends, we gave this construct a more general name - Cherry-MT+TIP. pSuper-based shRNA vector (Brummelkamp et al., 2002) was directed against the following target sequence: mouse/rat ch-TOG AGAGTCCAGAATGGTCCAA (Chapter 3).

#### *Antibodies and immunofluorescent cell staining*

Neurons were fixed with 4% PFA/4% sucrose in PBS for 10 minutes at room temperature to visualize neurite morphology, and with a combination of cold methanol and paraformaldehyde to stain for EB1 or SLAIN1/2.

We used rabbit polyclonal antibodies against SLAIN1/2 (Chapter 3),  $\beta$ -galactosidase (MP Biomedicals) and ch-TOG (Charrasse et al., 1998), a gift from L. Cassimeris (Lehigh University; Bethlehem, USA); mouse monoclonal antibodies against EB1 (BD Biosciences),  $\beta$ -tubulin, and actin (Chemicon). The following secondary antibodies were used; alkaline phosphatase-conjugated anti-rabbit, anti-mouse or anti-rat antibodies (Sigma-Aldrich), IRDye 800CW Goat anti-rabbit, anti-mouse and anti-rat IgG (Li-Cor Biosciences), Alexa-350, Alexa-488 and Alexa-598 conjugated goat antibodies against rabbit, rat, and mouse IgG (Molecular Probes),

#### *Image Acquisition and Processing*

Images of fixed cells were collected with a Leica DMRBE microscope equipped with a PL Fluotar 100x 1.3 N.A. or 40x 1.00-0.50 N.A. oil objectives, FITC/EGFP filter 41012 (Chroma) and Texas Red filter 41004 (Chroma) and an ORCA-ER-1394 CCD camera (Hamamatsu). Low magnification images of fixed cultured neurons were obtained using a LSM510 confocal microscope (Zeiss) equipped with a 20x air Plan-Apochromat N.A. 0.75 objective.

Time-lapse live-cell imaging of Cherry-MT+TIP was performed on the upgraded inverted research microscope Nikon Eclipse TE2000E (Nikon) with a CFI Apo TIRF 100x 1.49 N.A. oil objective (Nikon). It was equipped with Evolve 512 EMCCD camera (Photometrics, Roper) and controlled by MetaMorph 7.7 software (Molecular Devices). For excitation of GFP and mCherry we used 113 mW 488nm laser line of argon laser (Spectra-Physics Lasers) and 11 mW 561nm diode-pumped solid-state laser (Melles Griot), respectively. For GFP imaging we have used ET-GFP filter set (49002, Chroma). For mCherry-imaging we have used ET-mCherry filter set (49008, Chroma). The 16-bit images were projected onto the CCD chip with intermediate lens 2.5X (Nikon C mount adapter 2.5X) at a magnification of 0.067  $\mu\text{m}/\text{pixel}$ .

Images were prepared for publication using MetaMorph and Adobe Photoshop. All images were modified by adjustments of levels and contrast. Maximum intensity projection, kymograph analysis and various quantifications were performed in MetaMorph. Neurite length quantification was performed based on projections of stacks of 5 images (1  $\mu\text{m}$  between z-sections); neurites were measured from cell body to tip using MetaMorph. Statistical analysis was performed using non-parametric Mann-Whitney U-test in Statistica for Windows and SigmaPlot.

## Acknowledgments

We are grateful to L. Cassimeris for the ch-TOG antibody, N. Keijzer, M. Kuijpers, P. Wulf and V. van Dis for help with primary hippocampal neurons, and tissue and neuronal extracts. This study was supported by the Netherlands Organization for Scientific Research ALW open program and ALW-VICI grants to A.A, ZonMw-VIDI and European Science Foundation (European Young Investigators (EURYI)) awards to C.C.H.

## References

- Akhmanova, A., and Steinmetz, M.O. (2008). Tracking the ends: a dynamic protein network controls the fate of microtubule tips. *Nat Rev Mol Cell Biol* 9, 309-322.
- Baas, P.W. (1999). Microtubules and neuronal polarity: lessons from mitosis. *Neuron* 22, 23-31.
- Banker, G., and Goslin, K. (1988). Developments in neuronal cell culture. *Nature* 336, 185-186.
- Brouhard, G.J., Stear, J.H., Noetzel, T.L., Al-Bassam, J., Kinoshita, K., Harrison, S.C., Howard, J., and Hyman, A.A. (2008). XMAP215 is a processive microtubule polymerase. *Cell* 132, 79-88.
- Brummelkamp, T.R., Bernards, R., and Agami, R. (2002). A system for stable expression of short interfering RNAs in mammalian cells. *Science* 296, 550-553.
- Charrasse, S., Coubes, P., Arrancibia, S., and Larroque, C. (1996). Expression of the tumor over-expressed ch-TOG gene in human and baboon brain. *Neurosci Lett* 212, 119-122.
- Charrasse, S., Mazel, M., Taviaux, S., Berta, P., Chow, T., and Larroque, C. (1995). Characterization of the cDNA and pattern of expression of a new gene over-expressed in human hepatomas and colonic tumors. *Eur J Biochem* 234, 406-413.
- Charrasse, S., Schroeder, M., Gauthier-Rouviere, C., Ango, F., Cassimeris, L., Gard, D.L., and Larroque, C. (1998). The TOGp protein is a new human microtubule-associated protein homologous to the Xenopus XMAP215. *J Cell Sci* 111 ( Pt 10), 1371-1383.
- Conde, C., and Caceres, A. (2009). Microtubule assembly, organization and dynamics in axons and dendrites. *Nat Rev Neurosci* 10, 319-332.
- Dent, E.W., Kwiatkowski, A.V., Mebane, L.M., Philippar, U., Barzik, M., Rubinson, D.A., Gupton, S., Van Veen, J.E., Furman, C., Zhang, J., et al. (2007). Filopodia are required for cortical neurite initiation. *Nat Cell Biol* 9, 1347-1359.
- Gallo, G., and Letourneau, P.C. (1999). Different contributions of microtubule dynamics and transport to the growth of axons and collateral sprouts. *J Neurosci* 19, 3860-3873.
- Geraldo, S., Khanzada, U.K., Parsons, M., Chilton, J.K., and Gordon-Weeks, P.R. (2008). Targeting of the F-actin-binding protein drebrin by the microtubule plus-tip protein EB3 is required for neuritogenesis. *Nat Cell Biol* 10, 1181-1189.
- Hirst, C.E., Lim, S.M., Pereira, L.A., Mayberry, R.A., Stanley, E.G., and Elefanty, A.G. (2010). Expression from a betageo gene trap in the Slain1 gene locus is predominantly associated with the developing nervous system. *Int J Dev Biol* 54, 1383-1388.
- Hirst, C.E., Ng, E.S., Azzola, L., Voss, A.K., Thomas, T., Stanley, E.G., and Elefanty, A.G. (2006). Transcriptional profiling of mouse and human ES cells identifies SLAIN1, a novel stem cell gene. *Dev Biol* 293, 90-103.
- Honnappa, S., Gouveia, S.M., Weisbrich, A., Damberger, F.F., Bhavesh, N.S., Jawhari, H., Grigoriev, I., van Rijssel, F.J., Buey, R.M., Lawera, A., et al. (2009). An EB1-binding motif acts as a microtubule tip localization signal. *Cell* 138, 366-376.
- Hoogenraad, C.C., and Bradke, F. (2009). Control of neuronal polarity and plasticity--a renaissance for microtubules? *Trends Cell Biol* 19, 669-676.
- Hoogenraad, C.C., Milstein, A.D., Ethell, I.M., Henkemeyer, M., and Sheng, M. (2005). GRIP1 controls dendrite morphogenesis by regulating EphB receptor trafficking. *Nat Neurosci* 8, 906-915.
- Jaworski, J., Kapitein, L.C., Gouveia, S.M., Dortland, B.R., Wulf, P.S., Grigoriev, I., Camera, P., Spangler, S.A., Di Stefano, P., Demmers, J., et al. (2009). Dynamic microtubules regulate dendritic spine morphology and synaptic plasticity. *Neuron* 61, 85-100.
- Jiang, K., and Akhmanova, A. (2011). Microtubule tip-interacting proteins: a view from both ends. *Curr Opin Cell Biol* 23, 94-101.
- Koester, M.P., Muller, O., and Pollerberg, G.E. (2007). Adenomatous polyposis coli is differentially distributed in growth cones and modulates their steering. *J Neurosci* 27, 12590-12600.
- Lee, H., Engel, U., Rusch, J., Scherrer, S., Sheard, K., and Van Vactor, D. (2004). The microtubule plus end tracking protein Orbit/MAST/CLASP acts downstream of the tyrosine kinase Abl in mediating axon guidance. *Neuron* 42, 913-926.
- Mattie, F.J., Stackpole, M.M., Stone, M.C., Clippard, J.R., Rudnick, D.A., Qiu, Y., Tao, J., Allender, D.L., Parmar, M., and Rolls, M.M. (2010). Directed microtubule growth, +TIPs, and kinesin-2 are required for uniform microtubule polarity in dendrites. *Curr Biol* 20, 2169-2177.
- Nakagawa, H., Koyama, K., Murata, Y., Morito, M., Akiyama, T., and Nakamura, Y. (2000). EB3, a novel member of the EB1 family preferentially expressed in the central nervous system, binds to a CNS-specific APC homologue. *Oncogene* 19, 210-216.

- Neukirchen, D., and Bradke, F. (2011). Cytoplasmic Linker Proteins Regulate Neuronal Polarization through Microtubule and Growth Cone Dynamics. *J Neurosci* 31, 1528-1538.
- Picone, R., Ren, X., Ivanovitch, K.D., Clarke, J.D., McKendry, R.A., and Baum, B. (2010). A polarised population of dynamic microtubules mediates homeostatic length control in animal cells. *PLoS Biol* 8, e1000542.
- Popov, A.V., Pozniakovskiy, A., Arnal, I., Antony, C., Ashford, A.J., Kinoshita, K., Tournebize, R., Hyman, A.A., and Karsenti, E. (2001). XMAP215 regulates microtubule dynamics through two distinct domains. *Embo J* 20, 397-410.
- Poulain, F.E., and Sobel, A. (2010). The microtubule network and neuronal morphogenesis: Dynamic and coordinated orchestration through multiple players. *Mol Cell Neurosci* 43, 15-32.
- Rochlin, M.W., Wickline, K.M., and Bridgman, P.C. (1996). Microtubule stability decreases axon elongation but not axoplasm production. *J Neurosci* 16, 3236-3246.
- Rosenberg, M.M., Yang, F., Giovanni, M., Mohn, J.L., Temburni, M.K., and Jacob, M.H. (2008). Adenomatous polyposis coli plays a key role, in vivo, in coordinating assembly of the neuronal nicotinic postsynaptic complex. *Mol Cell Neurosci* 38, 138-152.
- Schuyler, S.C., and Pellman, D. (2001). Microtubule "plus-end-tracking proteins": The end is just the beginning. *Cell* 105, 421-424.
- Shi, S.H., Cheng, T., Jan, L.Y., and Jan, Y.N. (2004). APC and GSK-3beta are involved in mPar3 targeting to the nascent axon and establishment of neuronal polarity. *Curr Biol* 14, 2025-2032.
- Stepanova, T., Smal, I., van Haren, J., Akinci, U., Liu, Z., Miedema, M., Limpens, R., van Ham, M., van der Reijden, M., Poot, R., et al. (2010). History-dependent catastrophes regulate axonal microtubule behavior. *Curr Biol* 20, 1023-1028.
- Tanaka, E., Ho, T., and Kirschner, M.W. (1995). The role of microtubule dynamics in growth cone motility and axonal growth. *J Cell Biol* 128, 139-155.
- Williamson, T., Gordon-Weeks, P.R., Schachner, M., and Taylor, J. (1996). Microtubule reorganization is obligatory for growth cone turning. *Proc Natl Acad Sci U S A* 93, 15221-15226.
- Witte, H., Neukirchen, D., and Bradke, F. (2008). Microtubule stabilization specifies initial neuronal polarization. *J Cell Biol* 180, 619-632.
- Yu, W., and Baas, P.W. (1995). The growth of the axon is not dependent upon net microtubule assembly at its distal tip. *J Neurosci* 15, 6827-6833.
- Zhou, F.Q., Zhou, J., Dedhar, S., Wu, Y.H., and Snider, W.D. (2004). NGF-induced axon growth is mediated by localized inactivation of GSK-3beta and functions of the microtubule plus end binding protein APC. *Neuron* 42, 897-912.









# Chapter 5

## **Regulation of microtubule dynamics by a liprin- $\alpha$ 1/ $\beta$ 1-mediated cortical attachment complex of KANK2 and KIF21A**

Babet van der Vaart, Samantha A. Spangler, Ilya Grigoriev, Ka-Lou Yu, Phebe S. Wulf, Yuko Mimori-Kiyosue, Gideon Lansbergen, Jeroen Demmers, Casper C. Hoogenraad and Anna Akhmanova

*Manuscript in preparation*





## **Abstract**

Capture of distal microtubule plus ends at the cell cortex is established by the interplay between microtubule associated proteins (MAPs) and cortical factors. The CLASP family of plus-end tracking proteins (+TIP) regulates microtubule attachment and stabilization by interacting with the cortical complex of LL5 $\beta$  and ELKS. Here, we have identified distinct regulatory cortical components of the microtubule attachment complex. We show that scaffolding proteins liprin- $\alpha$ 1 and liprin- $\beta$ 1 colocalize with ELKS and LL5 $\beta$  in the vicinity of focal adhesions and are required for the organization of the cortical microtubule attachment complex which is required for microtubule stabilization. In addition, we show that the kinesin-4 family member KIF21A, which is mutated in congenital fibrosis of the extraocular muscle type 1 (CFEOM1), is linked to liprin proteins via the actin regulator KANK2. Depletion of KIF21A results in excessive growth and disorganization of cortical microtubules. These results indicate that KIF21A controls cortical microtubule dynamics, providing new insights into the molecular basis of CFEOM1 syndrome.

## **Introduction**

The microtubule (MT) cytoskeleton is an important regulator of cell morphology and motility. MTs are polarized tubes consisting of  $\alpha$ - and  $\beta$ -tubulin subunits. In typical interphase cells MTs form a radial array with the dynamic MT plus ends pointing outward exploring the cellular space whereas the minus ends are captured at the MT organizing center (MTOC) near the nucleus. MTs undergo phases of growth and shrinkage termed dynamic instability (Desai and Mitchison, 1997). Once the growing MT reaches the cell cortex, it can undergo a catastrophe and shrink back. Alternatively, the distal MT plus-end can be captured and stabilized by anchoring at the cortex, or the MT can bend and continue growing parallel to the plasma membrane.

Cortical capture of MTs is dependent on the interplay between MTs and the cortical actin cytoskeleton. Cross-talk between the two systems can be established by plus-end tracking proteins (+TIPs) (Akhmanova and Steinmetz, 2008; Schuyler and Pellman, 2001) such as spectraplakin/ACF7, APC, CLASPs, CLIP-170 and the dynein/dynactin complex (Dujardin and Vallee, 2002; Fukata et al., 2002; Kodama et al., 2003; Okada et al., 2010; Tsvetkov et al., 2007).

CLASPs act as rescue factors that locally stabilize MTs at the cell cortex by forming a complex with LL5 $\beta$  and ELKS (Lansbergen et al., 2006). LL5 $\beta$  and its homologue LL5 $\alpha$  are pleckstrin-homology (PH) domain containing proteins reported to bind preferentially to phosphatidylinositol-3, 4, 5-triphosphate (PIP3) lipids in the membrane (Paranavitane et al., 2003). In addition, LL5 $\alpha$ / $\beta$  bind to the actin filament crosslinking protein  $\gamma$ -filamin providing a link between actin and MT cytoskeletal networks (Paranavitane et al., 2003; Paranavitane et al., 2007), and accumulation of LL5 $\alpha$ / $\beta$  at the plasma membrane is controlled by integrins (Hotta et al., 2010). ELKS (also known as ERC1, CAST2 or Rab6IP2) is a coiled-coil scaffolding factor (Wang et al., 2002), which strongly interacts with LL5 $\beta$  (Lansbergen et al., 2006).

Another important player in cortical MT stabilization is ACF7 (also known as MACF1), a very large cytoskeletal linker protein, which can directly interact with actin and MTs (Kodama et al., 2003). Depletion of ACF7 from HeLa cells caused partial disappearance of CLASP2 from the

cortex, suggesting that ACF7 acts upstream of CLASPs (Drabek et al., 2006); however, the interaction between ACF7 and CLASPs is likely to be indirect (Wu et al., 2008).

Cortical MT stabilization helps to polarize the MT network, potentially providing means for asymmetric transport of cargo to particular cellular sites. This can help to generate and maintain cell polarity, a process potentially important both for cell migration in 2D (Gundersen et al., 1998) and cell morphogenesis in 3D environments (Hotta et al., 2010). During cell migration, cortical organization of MTs is important for regulation of actin polymerization dynamics and the appropriate turnover of focal adhesions (FA) (Akhmanova et al., 2009; Rodriguez et al., 2003). Interestingly, LL5 $\beta$  and ELKS can be found around FA sites suggesting their possible role in MT attachment near FAs (Lansbergen et al., 2006). Also ACF7 was directly implicated in regulation of FA dynamics (Wu et al., 2008), but the exact mechanism remains to be elucidated.

In this study we searched for novel components of the MT attachment complexes. We identified the scaffold proteins liprin- $\alpha$ 1 and liprin- $\beta$ 1 as a part of the same cortical complex as LL5 $\beta$  and ELKS. Liprin- $\alpha$ 1/ $\beta$ 1 represent a highly conserved protein family that was originally identified through an interaction with the receptor protein tyrosine phosphatase LAR near focal adhesion sites (Serra-Pages et al., 1998). In mammals, there are six liprin genes, encoding four liprin- $\alpha$  and two liprin- $\beta$  isoforms. Liprin- $\beta$ s and liprin- $\alpha$ 1 are broadly expressed whereas other liprin- $\alpha$  family members are enriched in brain (Serra-Pages et al., 1998, Spangler et al., submitted). Liprin proteins are characterized by the presence of an N-terminal coiled-coil region that mediates homo- and hetero-dimerization, and three sterile- $\alpha$ -motif (SAM) domains that form the liprin homology (LH) region (Serra-Pages et al., 1998). Liprin- $\alpha$ 1/ $\beta$ 1 are extensively studied in neurons, where they are recognized as highly conserved factors involved in pre- and post-synaptic development by recruiting synaptic proteins and regulating synaptic cargo transport (Spangler and Hoogenraad, 2007; Stryker and Johnson, 2007). Recent data also implicated liprin proteins in spreading and migration of non-neuronal cells, where they were proposed to affect the distribution of integrins at the cell surface (Asperti et al., 2010; de Curtis, 2011; Shen et al., 2007). Here, we show that in HeLa cells liprin- $\alpha$ 1/ $\beta$ 1 are key regulators of recruitment and clustering of cortical components involved in MT tip attachment and stabilization.

Further, we identified a novel liprin- $\alpha$ 1/ $\beta$ 1 binding complex consisting of the ankyrin repeat protein KANK2 and its interaction partner KIF21A of the kinesin-4 family (Hirokawa et al., 2009; Kakinuma and Kiyama, 2009; Kakinuma et al., 2009). We show that although KIF21A is an intrinsically motile motor, it accumulates at the cell edge through a liprin-dependent mechanism. We further show that KIF21A is required for the local regulation of MTs at the cortex, because knockdown of KIF21A results in excessive MT growth along the cell margin. Interestingly, heterozygous mutations in *KIF21A* have been implicated in the autosomal dominant syndrome congenital fibrosis of the extraocular muscle type 1 (CFEOM1) (Heidary et al., 2008; Yamada et al., 2003). Patients are characterized by the absence of the superior division of the oculomotor nerve resulting in innervation defects of the extraocular muscles leading to their degeneration. This causes the inability of the patients to elevate eyelids and eye globe. Previously, it was suggested that CFEOM1 is the result of defects in KIF21A-mediated cargo transport (Kakinuma and Kiyama,

2009), however, our findings support a model where KIF21A, similar to another kinesin-4, Xklp1 (Bieling et al., 2010), is a local regulator of MT growth. This is in line with reports that CFEOM1-related disease CFEOM3, which is caused by mutations in neuronal  $\beta$ -tubulin III (*TUBB3*) gene, is associated with defects of MT dynamics (Tischfield et al., 2010). Our study thus provides new molecular insights into the cause of CFEOM1 syndrome.

## **Results**

### *Identification of liprin- $\alpha$ 1 and liprin- $\beta$ 1 as LL5 $\beta$ and ELKS interaction partners*

To identify novel cortical components of the CLASP-LL5 $\beta$ -ELKS complex, we performed streptavidin pull-downs of BioGFP-LL5 $\beta$  and -ELKS from HEK293 cells and analyzed the resulting proteins using mass spectrometry (Fig. S1A,B). Both LL5 $\alpha/\beta$  and ELKS co-purified with BioGFP-ELKS and BioGFP-LL5 $\beta$  verifying our experimental approach. In addition, major hits in both experiments were proteins of the liprin family, particularly liprin- $\alpha$ 1 and liprin- $\beta$ 1. Liprin- $\alpha$ 1 was already known as an interaction partner of ELKS in neuronal cells (Ko et al., 2003).

The identification of liprin proteins was validated by endogenous co-immunoprecipitation (co-IP) from HeLa cells using LL5 $\beta$ , liprin- $\alpha$ 1 and liprin- $\beta$ 1 specific antibodies (Fig 1A,B). Since cortical complexes are difficult to dissolve, we lysed the cells in two different buffers, a relatively mild one, containing a nonionic detergent Triton X-100, or the more denaturing radioimmunoprecipitation assay buffer (RIPA), which contains a mixture of NP-40 and ionic detergents deoxycholate and sodium dodecyl sulfate (Fig. 1A,B). Liprin- $\alpha$ 1 and liprin- $\beta$ 1 could co-precipitate each other as expected and in addition both proteins could be co-precipitated with LL5 $\beta$  (Serra-Pages et al., 1998). LL5 $\beta$  co-precipitated ELKS, and also bound to liprin- $\alpha$ 1 and liprin- $\beta$ 1. ELKS was most efficiently co-precipitated with LL5 $\beta$  and liprin- $\alpha$ 1, in line with the fact that it binds to both proteins (Asperti et al., 2010; Ko et al., 2003; Lansbergen et al., 2006). The co-IP results were somewhat different in the two buffers, likely due to changes in solubility and partial disruption of some protein subcomplexes (Fig. 1A,B).

At the immunofluorescence level, liprin- $\alpha$ 1 and liprin- $\beta$ 1 strongly co-localized with endogenous LL5 $\beta$ , ELKS and ACF7 in patches at the free cell edges of HeLa cells (Fig. 1C-F). Liprin protein patches often accumulated around FA sites but never overlapped with them (Fig. 1G). When MTs were depolymerized with nocodazole, liprin- $\alpha$ 1/ $\beta$ 1 and LL5 $\beta$  strongly colocalized around enlarged FAs (Fig. S1C-E), in agreement with previous results obtained for LL5 $\beta$  and ELKS in these conditions (Lansbergen et al., 2006). Based on these data, we conclude that liprin- $\alpha$ 1 and liprin- $\beta$ 1 are interaction partners of LL5 $\beta$  and ELKS that colocalize with them in cortical patches at the free cell edges and around FA sites.

### *Dynamics of the liprin- $\alpha$ 1-LL5 $\beta$ -ELKS complex at the cell cortex*

Cortical localization of the endogenous liprin- $\alpha$ 1 and colocalization with LL5 $\beta$  was fully recapitulated using live cell imaging with Total Internal Reflection Fluorescence (TIRF) microscopy of HeLa cells expressing mCherry-liprin- $\alpha$ 1 and GFP-LL5 $\beta$  (Fig. 1H). Next, we performed fluorescent recovery after photobleaching (FRAP) experiments using fluorescently tagged LL5 $\beta$ , liprin- $\alpha$ 1 and ELKS. For

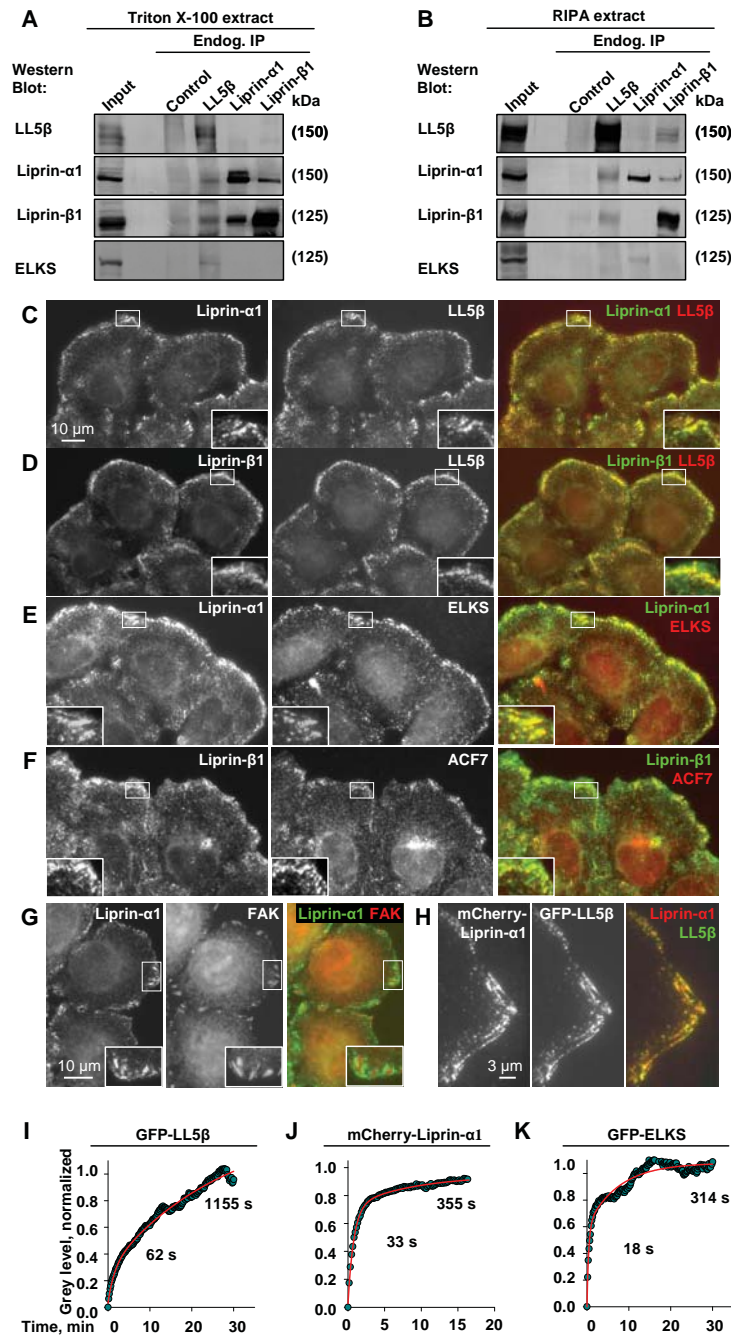


**Figure 1. Liprin-α1 and liprin-β1 interact with LL5β and ELKS and colocalize with them at the cell cortex**

**A,B.** HeLa cells were lysed with Triton X-100 (A) or RIPA (B) lysis buffers and IP experiments were performed with the indicated antibodies and analyzed by Western blotting.

**C-G.** HeLa cells were fixed and stained with the indicated antibodies. The insets show enlargements of the boxed areas. In the overlay in **C-F** liprin-α1/β1 are shown in red and LL5β (C,D), ELKS (E), ACF7 (F) in green. In **G** liprin-α1 is shown in green and FAK in red.

**H.** TIRF microscopy image (500 ms exposure) of a live HeLa cell transiently transfected with mCherry-liprin-α1 (red in overlay) and GFP-LL5β (green in overlay).

**I-K.** Analysis of GFP-LL5β (I), mCherry-liprin-α1 (J) and GFP-ELKS (K) turnover by FRAP in HeLa cells. The plots show processed FRAP data (green dots) and their fitting to a two-exponential model (red lines); see Experimental Procedures for details. 11-12 cells were analyzed in 3 experiments. The recovery halftimes for the two components are indicated.

all three proteins, the data could be fitted using a two-exponential model (Fig. 1I-K, Table S1). Fluorescence recovery halftimes ( $t_{1/2}$ ) were similar for ELKS and liprin- $\alpha$ 1 (with the  $t_{1/2}$  of the slower component on the order of  $\sim 350$ s), while the recovery of LL5 $\beta$  was much slower ( $t_{1/2}$  of the slower component on the order of  $\sim 1200$ s, in agreement with previously published data (Lansbergen et al., 2006)). Importantly, the recovery of all three proteins was faster than the dynamics of the cortical patches themselves, which remained stable for  $\sim 30$  min (Lansbergen et al., 2006). Taken together, our data indicate that cortical clusters of liprin proteins, LL5 $\beta$  and ELKS are relatively stable structures, which undergo a slow exchange with the cytoplasmic pool of their constituents. Liprin- $\alpha$ 1 and ELKS might be exchanging together, but independently of LL5 $\beta$ , which displays slower dynamics.

#### *Liprin- $\alpha$ 1/ $\beta$ 1 are required for organizing cortical MT attachment sites and stabilizing MTs*

To investigate the hierarchy of interactions between different cortical components, we performed knockdown experiments in HeLa cells using small interfering (si) RNAs. We could efficiently deplete LL5 $\beta$  and ELKS without affecting the expression of the two liprin proteins (Fig. S1F). LL5 $\beta$  depletion did not significantly affect the localization of liprin- $\alpha$ 1/ $\beta$ 1 or ACF7 (Fig. 2A-C). Also in nocodazole-treated cells where cortical proteins were accumulated in patches around FAs, liprin- $\alpha$ 1/ $\beta$ 1 were still concentrated at the cortex in the absence of LL5 $\beta$  (data not shown). In case of ELKS knockdown, the patches of both liprin- $\alpha$ 1 and - $\beta$ 1 had a more diffuse appearance, and the ACF7 labeling at the cell periphery was considerably reduced (Fig. 2D-F). Depletion of ACF7 using previously published siRNAs (Drabek et al., 2006) also did not affect the localization of liprin- $\alpha$ 1/ $\beta$ 1 or LL5 $\beta$  (Fig. 2G,H). In conclusion, liprin proteins can localize to peripheral cortical patches independently of LL5 $\beta$ , ELKS or ACF7.

Next, we tested whether liprin proteins act as upstream regulators of cortical proteins. Both liprin- $\alpha$ 1 and liprin- $\beta$ 1 could be efficiently depleted without affecting the expression of LL5 $\beta$  and ELKS (Fig. S1F). The depletion of liprin- $\alpha$ 1 had no strong effect on the localization of LL5 $\beta$  or liprin- $\beta$ 1, although LL5 $\beta$  was somewhat more diffuse (Fig. 3A,B). In contrast, the cortical localization of ELKS and ACF7 was very strongly reduced in the absence of liprin- $\alpha$ 1 (Fig. 3C-E). Liprin- $\beta$ 1 depletion greatly disrupted the localization of LL5 $\beta$ , liprin- $\alpha$ 1, ELKS and ACF7 (Fig. 3F-I). All cortical proteins tested were no longer concentrated at the cell periphery but instead were dispersed into small cortical clusters. In conclusion, liprin- $\alpha$ 1 participates in the cortical recruitment of ELKS and ACF7, while liprin- $\beta$ 1 is necessary for the clustering of LL5 $\beta$ , liprin- $\alpha$ 1, ELKS and ACF7 in cortical patches.

We have previously shown that the depletion of CLASPs, LL5 $\beta$  and ELKS from HeLa cells affects the stability and density of MTs at the cell cortex (Lansbergen et al., 2006). Cortical localization of liprin- $\alpha$ 1/ $\beta$ 1 and their upstream function in the localization of ACF7 and clustering of ELKS and LL5 $\beta$  suggested a possible role in regulating MT organization. Indeed, depletion of liprin- $\alpha$ 1 and - $\beta$ 1 diminished the number of MT ends at the cell periphery, similar to LL5 $\beta$  depletion (Fig. 4A-C)(Lansbergen et al., 2006). We conclude that liprin- $\alpha$ 1/ $\beta$ 1 participate in organization of the MT attachment sites and the regulation of MT density at the cortex of HeLa cells.

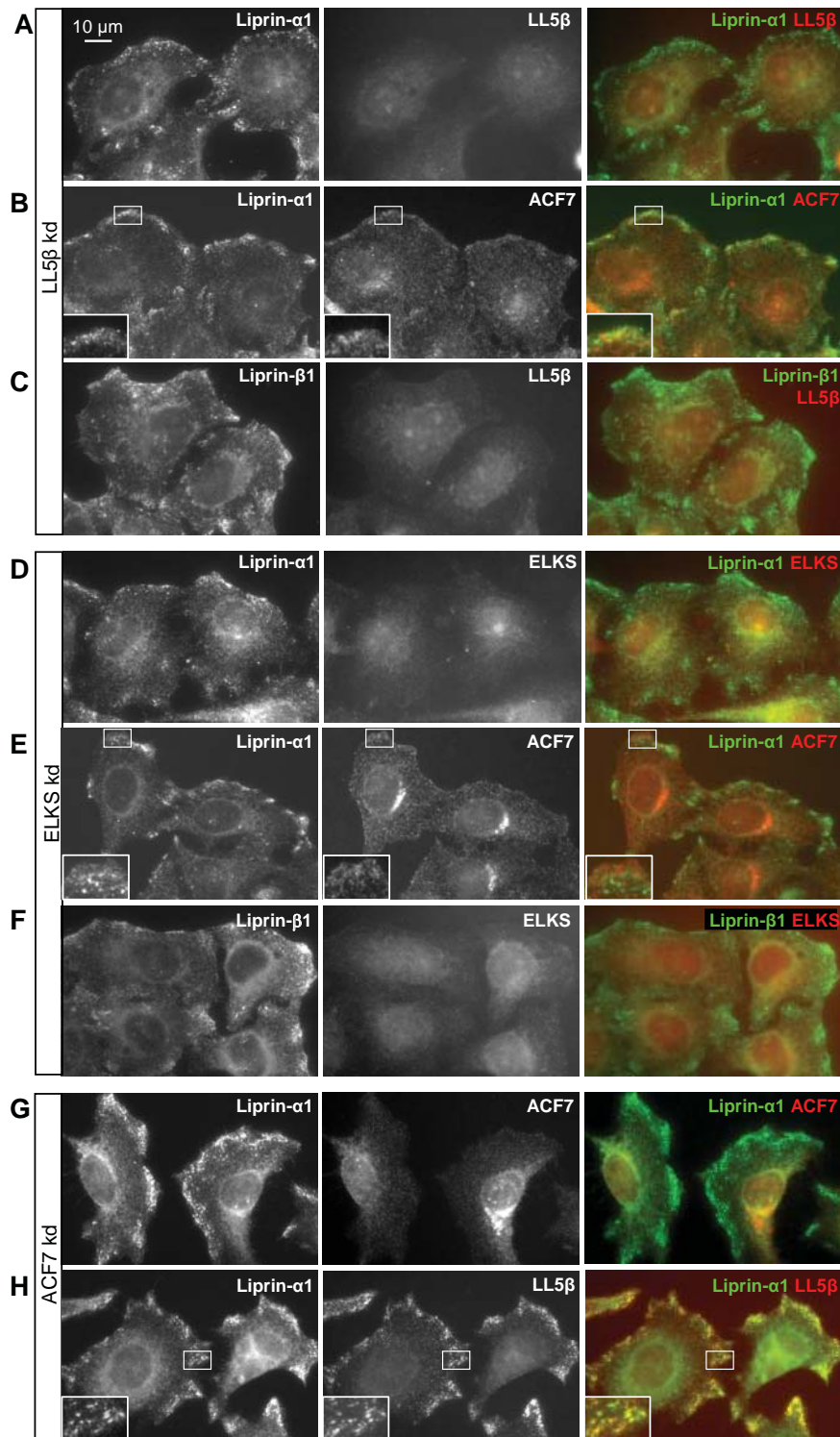


**Figure 2. Cortical accumulation of liprin- $\alpha$ 1 and liprin- $\beta$ 1 is independent from LL5 $\beta$ , ELKS and ACF7**

**A-H.** HeLa cells were transiently transfected with different siRNAs, fixed and stained with the indicated antibodies. The insets show enlargements of the boxed areas. In the overlays liprin proteins are shown in green and LL5 $\beta$  (A,H), ACF7 (B,E,G) and ELKS (D) in red.



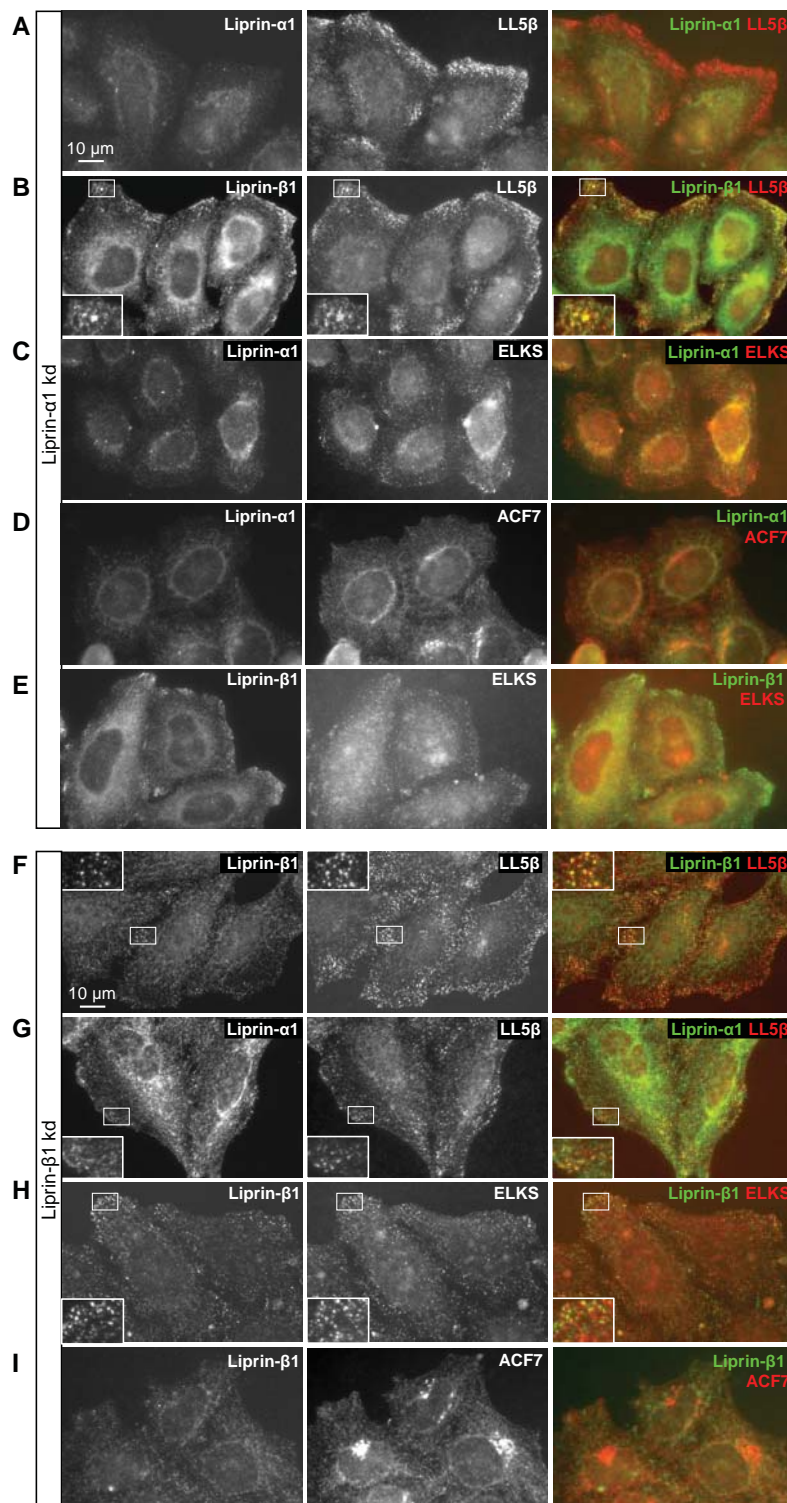


**Figure 3. Liprin- $\beta$ 1 is required for cortical clustering of liprin- $\alpha$ 1, LL5 $\beta$ , ELKS and ACF7**

**A-I.** HeLa cells were transiently transfected with liprin- $\alpha$ 1 or liprin- $\beta$ 1 siRNAs, fixed and stained with the indicated antibodies. The insets show enlargements of the boxed areas. In the overlays liprin proteins are shown in green and LL5 $\beta$  (A,B,F,G), ELKS (C,E,H) and ACF7 (D,I) in red.

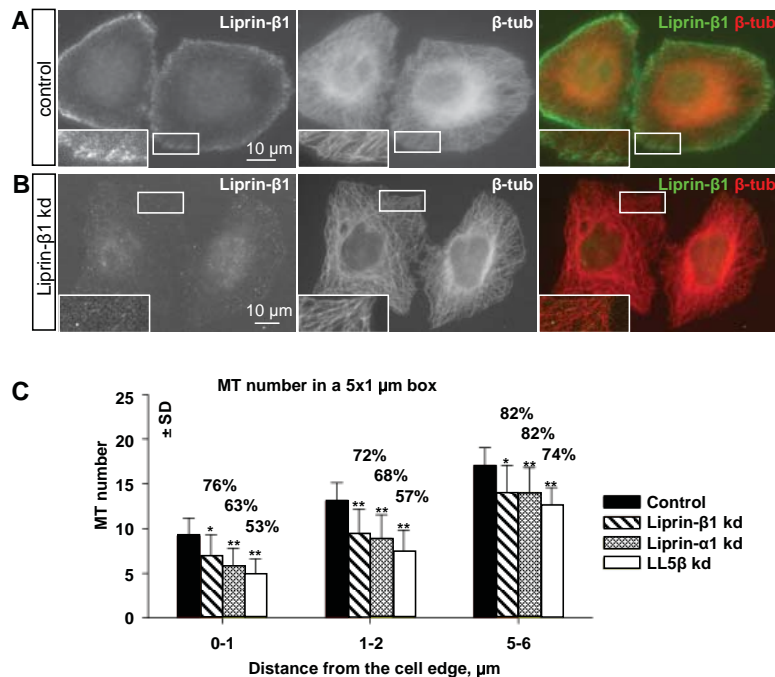


**Figure 4. Liprin- $\alpha$ 1 and liprin- $\beta$ 1 regulate of MT density at the cell cortex.**

**A,B.** HeLa cells were transiently transfected with control or liprin- $\beta$ 1 siRNAs, fixed and stained with the indicated antibodies. The insets show enlargements of the boxed areas. In the overlays liprin- $\beta$ 1 is shown in green and  $\beta$ -tubulin in red.

**C.** Plots show MT numbers in a 5 x 1  $\mu$ m box located at the indicated distance from the cell edge. Measurements were performed in 20 cells per siRNA. Numbers above the plots indicate the size of each bar in % compared to the adjacent control bar; values significantly different from control are indicated by asterisks (\*,  $p < 0.05$ ; \*\*,  $p < 0.001$ ).

#### Identification of KANK2 and a kinesin-4 family member KIF21A as liprin- $\alpha$ 1/ $\beta$ 1 binding partners

To further study the composition of the cortical MT attachment complex we set out to identify liprin- $\alpha$ 1/ $\beta$ 1 binding partners. We performed streptavidin pull-downs of BioHA-liprin- $\alpha$ 1 and BioGFP-liprin- $\beta$ 1 from HeLa cells and analyzed the resulting protein complexes by mass spectrometry (Fig. S2A,B). As expected, liprin- $\beta$ 1 peptides were found in liprin- $\alpha$ 1 pull-downs and visa versa, and LL5 $\beta$  and ELKS were present in both pull downs (Fig. S2A,B).

Interestingly, major hits for both liprin- $\alpha$ 1 and - $\beta$ 1 were KANK1 (ANKRD15), KANK2 (ANKRD25) and the known KANK1 interaction partner KIF21A (Fig. S2A,B). The family of KANK proteins (KANK1-4) regulates the actin cytoskeleton by controlling actin polymerization in part through PI3K/Akt effectors (Kakinuma et al., 2009). KANK proteins are characterized by an N-terminal coiled-coil region, the KN motif and the presence of ankyrin-repeats in the C-terminus (Kakinuma et al., 2009). This latter region is responsible for the interaction with KIF21A (Kakinuma and Kiyama, 2009). KIF21A is a member of the kinesin-4 family; it contains an N-terminal motor domain followed by a coiled-coil region necessary for dimerization and binding to KANK1, and a C-terminal WD-40 repeat domain (Fig. 5A). KIF21A is a brain enriched motor protein that is expressed at constant levels in cultured developing hippocampal neurons (Marszalek et al., 1999; Silverman et al., 2010). Heterozygous mutations in *KIF21A* cause the autosomal dominant syndrome congenital fibrosis of the extraocular muscles type 1 (CFEOM1) (Yamada et al., 2003). CFEOM1 patients suffer from degeneration of the muscles that control eye movement, because

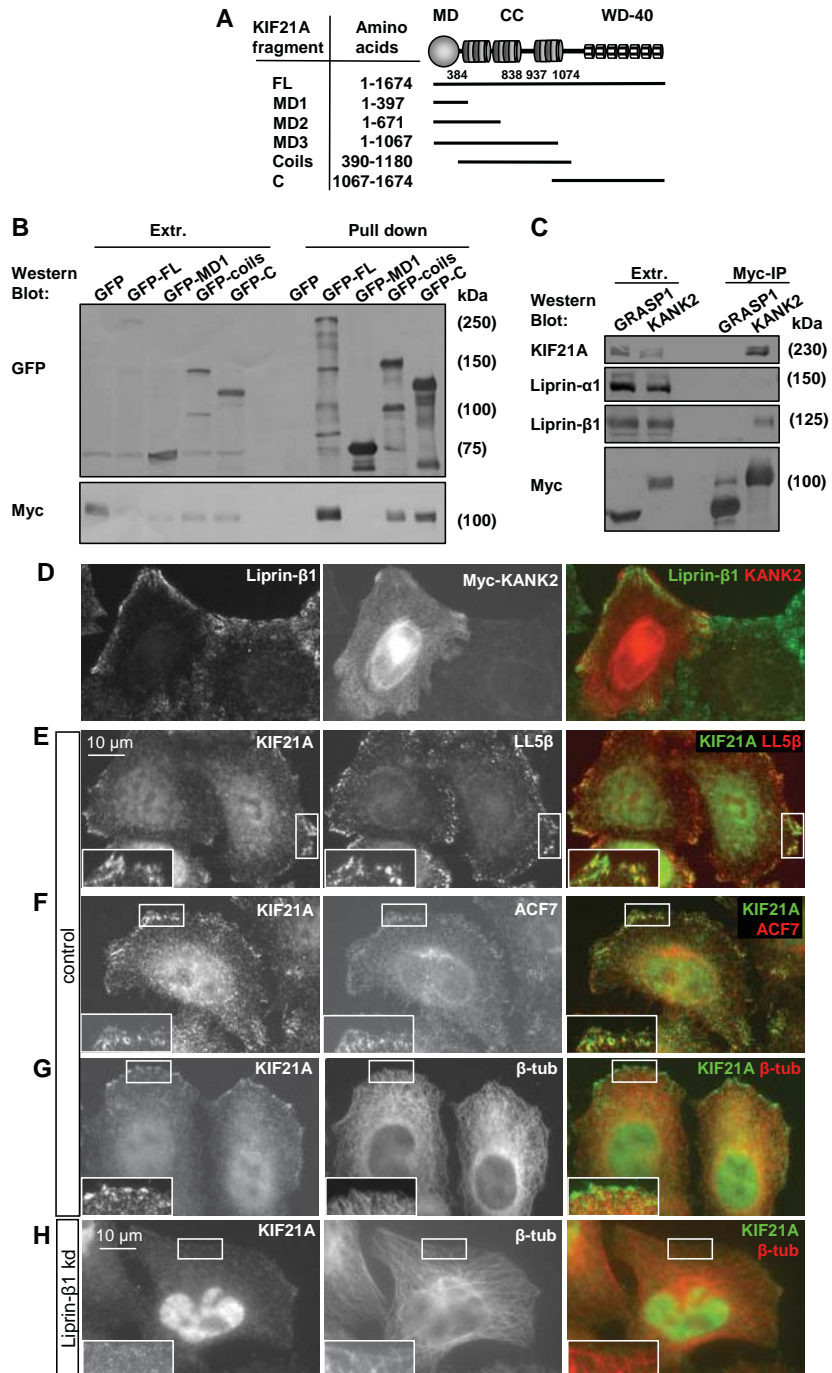


**Figure 5. KIF21A interacts with liprin- $\beta$ 1-binding protein KANK2 and localizes to the cell cortex**

**A.** A schematic overview of KIF21A deletion mutants used in this study. Abbreviations: MD, motor domain, CC, coiled-coil regions.

**B, C.** Streptavidin pull-down assay (**B**) or Myc-IPs (**C**) were performed with the extracts of HEK293 cells co-expressing BioGFP-KIF21A mutants, BirA and Myc-KANK2 (**B**) or expressing Myc-GRASP1 and Myc-KANK2 (**C**) and analyzed by Western blotting with the indicated antibodies.

**D-H.** HeLa cells were transiently transfected with Myc-KANK2 (**D**) or different siRNAs (**E-H**), fixed and stained with the indicated antibodies. The insets show enlargements of the boxed areas. In the overlays liprin- $\beta$ 1 (**D**) and KIF21A (**E-H**) are shown in green and Myc-KANK2 (**D**), LL5 $\beta$  (**E**), ACF7 (**F**) and  $\beta$ -tubulin (**G,H**) in red.

these muscles are not innervated properly. It is thought that mutations, which are mostly found in the coiled-coil region of KIF21A affect the cargo binding function of KIF21A rather than its motor activity. Surprisingly, CFEOM1-associated KIF21A mutations seem to increase KANK1-KIF21A binding efficiency (Kakinuma and Kiyama, 2009).

We have generated BioGFP-tagged KIF21A and several deletion mutants (Fig. 5A). By using streptavidin pull downs from HEK293 cells we show that Myc-tagged KANK2 binds to the full length KIF21A and the C-terminal part of its coiled-coil region (Fig. 5B).

The interaction between liprin- $\beta$ 1 and KANK2 was confirmed by co-IP of endogenous liprin- $\beta$ 1, but not liprin- $\alpha$ 1 with Myc-tagged KANK2 (Fig. 5C). Endogenous KIF21A also strongly co-precipitated with KANK2, but not with the negative control (Fig. 5C). The interaction between KIF21A and liprin- $\alpha$ 1/ $\beta$ 1 appears to be indirect and mediated by KANK2 as only weak co-IP of overexpressed liprin- $\alpha$ 1 and liprin- $\beta$ 1 with KIF21A-coil could be observed (Fig. S2C).

Immunofluorescent staining of HeLa cells expressing low levels of Myc-KANK2 showed cytosolic labeling and some accumulation around FAs (Fig. 5D). In highly expressing cells Myc-KANK2 forms aggregates that strongly recruited overexpressed KIF21A and endogenous liprin- $\alpha$ 1/ $\beta$ 1 (data not shown).

#### *KIF21A is a liprin- $\alpha$ 1/ $\beta$ 1-dependent component of the cortical MT attachment complex*

Endogenous KIF21A is present at the cell cortex where it colocalizes with LL5 $\beta$  and partially colocalizes with ACF7 (Fig. 5E-F), and with the distal MT stretches at the cell periphery (Fig. 5G). Colocalization of KIF21A with the distal MT ends is not dependent on their dynamics, because it is also observed in cells in which the MTs are stabilized with taxol (Fig. S2D). Depletion of the different components of the MT attachment complex resulted in a reduction of peripheral accumulation of KIF21A that was most prominent after the depletion of liprin- $\beta$ 1 (Fig. 5H, Fig. S2E-G). These data support an upstream role of liprin- $\beta$ 1 as assembly factor of the MT attachment complex, including KIF21A.

#### *KIF21A dynamics at the cell cortex and motility along MTs*

To further study the behavior of KIF21A in cells, we turned to live cell imaging experiments. Using TIRF microscopy, a significant co-localization of full-length GFP-KIF21A (KIF21A-FL) with RFP-LL5 $\beta$  and mCherry-liprin- $\alpha$ 1 could be observed at the peripheral cell cortex (Fig. 6A,B). The coiled-coil region of KIF21A, which links KIF21A to KANK2 based on our biochemical data (Fig. 5A-C) also localizes to the cortical sites positive for mCherry-liprin- $\alpha$ 1 (Fig. 6C). We also tested whether the substitution of arginine at the position 954 for a tryptophan (R954W), the most common KIF21A mutation found in ~70% of CFEOM1 patients (Chan et al., 2007) would affect the localization of the coiled-coil region of KIF21A, and found that this was not the case (Fig. 6D). We conclude that a defect in cortical association of KIF21A is unlikely to be the cause of CFEOM1.

Next, we used FRAP to investigate the turnover of GFP-KIF21A at the cortex (Fig. 6E, Table S1), and found that the  $t_{1/2}$  of the slower component was on the order of ~40s, almost 10 times faster than that observed for liprin- $\alpha$ 1 and ELKS (Fig. 1J,K). The coiled-coil region alone showed an

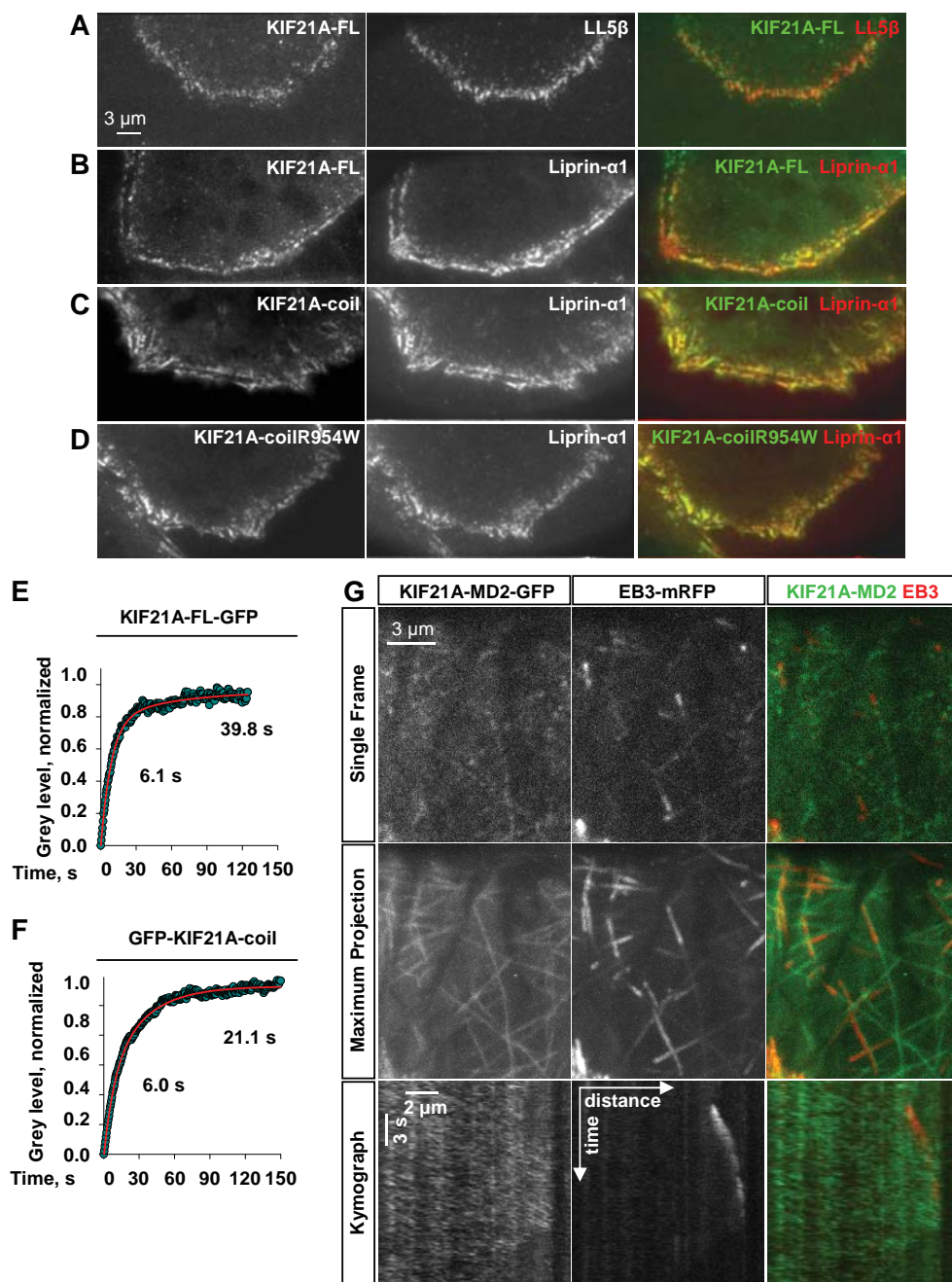


**Figure 6. Analysis of dynamics and motility of KIF21A and its mutants**

**A-D.** TIRF microscopy image (500 ms exposure) of live HeLa cells transiently co-transfected with GFP-tagged KIF21A-FL, KIF21A-coil and KIF21A-coilR954 (**A-D**, respectively) (green in overlay) together with RFP-LL5 $\beta$  (**A**) or mCherry-liprin- $\alpha$ 1 (**B-D**) (red in overlay).

**E-F.** Analysis of KIF21A-FL-GFP (**E**) and GFP-KIF21A-coil (**F**) turnover by FRAP in HeLa cells. The plots show processed FRAP data (green dots) and their fitting to a two-exponential model (red lines); see Experimental Procedures for details. 11-12 cells were analyzed in 3 experiments. The recovery halftimes for the two components are indicated.

**G.** TIRF microscopy live cell imaging of HeLa cells transiently transfected with KIF21A-MD2-GFP (green in overlay) and EB3-mRFP (red in overlay). Red and green images were collected simultaneously with a beam splitter and 0.1 s interval between frames. Top panel shows single frames, middle panel shows maximal projection of 250 frames, and bottom panel shows kymograph analysis along a single MT.

even faster recovery (Fig. 6F, Table S1), and similar values were obtained for the R954W mutant (data not shown). In conclusion, KIF21A has a relatively high turnover at the cell cortex.

Importantly, in these live imaging experiments, we observed no evidence of processive movement of the full-length GFP-KIF21A along MTs. We hypothesized that motility of this kinesin might be inhibited in the full-length molecule. To test this, we have generated C-terminal GFP-fusions of the KIF21A motor domain (MD) containing different portions of the coiled-coil region (MD1, 2 and 3, Fig. 5A). KIF21A-MD1 was largely diffuse, probably because it failed to dimerize. KIF21A-MD2-GFP, which is expected to be dimeric, appeared as small dots that displayed highly processive movement towards MT plus ends marked with EB3-mRFP (Fig. 6G). Using kymograph analysis we determined that the mean velocity of this movement was  $1.5 \pm 0.2 \mu\text{m/s}$  ( $n=55$ ), similar to the velocity of conventional kinesin. Interestingly, whereas the MD2 fragment showed processive motility, no movement of the full-length KIF21A could be observed in similar experiments, suggesting that processivity of the full-length protein is under tight regulatory control (data not shown). We also observed no motility of the KIF21A-MD3 fusion, suggesting that part of this control might be exerted by the C-terminal, KANK2 binding coiled-coil portion of the molecule. We analyzed the behavior of the C-terminal WD-40 repeat and found that it was diffusely distributed and showed no significant cortical association (data not shown).

#### *KIF21A regulates MT dynamics at the cell cortex*

To investigate the cellular function of KIF21A, we selected two different siRNAs that could deplete endogenous KIF21A from HeLa cells as shown by WB analysis and immunofluorescent labeling (Fig. 7A,C, siRNAs A and B). Although depletion of KIF21A did not strongly affect the cortical localization of liprin- $\alpha$ 1/ $\beta$ 1, ELKS, LL5 $\beta$ , ACF7 or CLASPs (Fig. 7D, Fig.S3) it strongly affected MT organization at the cell cortex (Fig. 7B-D). Instead of the typical interphase MT array with straight MTs that predominantly terminate at the cell cortex, the MTs in KIF21A depleted cells curved along the cell margin and often formed a circular bundle at the cell periphery (Fig. 7B-D). The plus ends of these MTs were often positive for EB1 indicating that these MT are in a growing state (Fig. 7E,F). This suggests that MT tips that reach the cortex continue growing, and this results in MT bending along the cell edge. These MTs show increased stability against disassembly by nocodazole, as compared to control cells (Fig. 7G,H), probably because they grow in a zone that is enriched in MT attachment complexes and MT stabilizing factors such as ACF7 and CLASPs (Fig S3). From these studies, we conclude that KIF21A is a cortical component of the MT attachment complex that is involved in restricting MT growth at the cell edge.

#### **Discussion**

In this study we have identified liprin- $\alpha$ 1 and liprin- $\beta$ 1 as distinct components and regulators of the cortical MT attachment complex. Depletion of liprin- $\alpha$ 1/ $\beta$ 1 results in reduced MT density at the cell cortex, similar to depletion of CLASPs, ELKS and LL5 $\beta$ . Interestingly, although liprin- $\alpha$ 1/ $\beta$ 1 are strongly colocalized with LL5 $\beta$ , their recruitment to the cortex is independent of this lipid-binding protein (Fig. 2A-C). Conversely, LL5 $\beta$  is still present in clusters at the plasma membrane

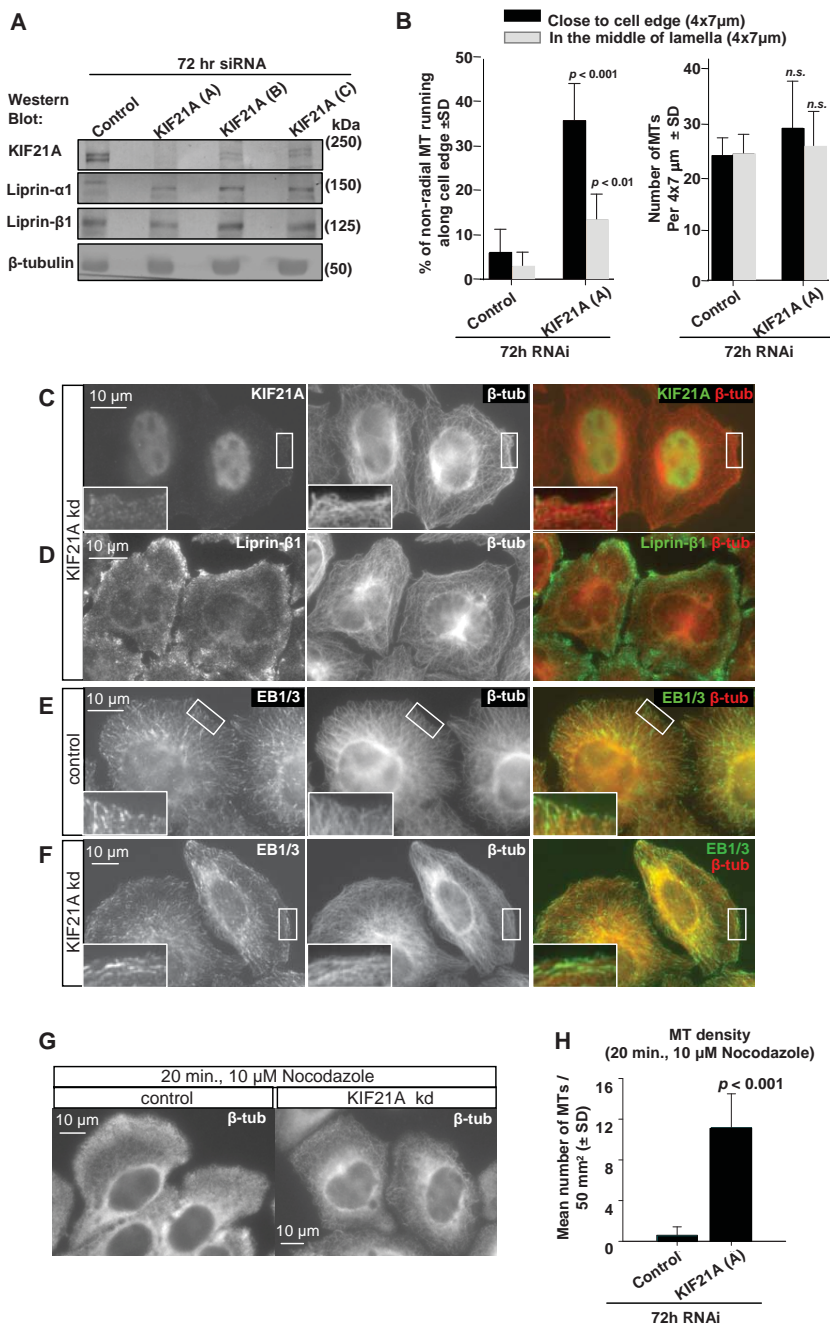


**Figure 7. KIF21A is required for regulation of MT dynamics at the cell cortex**

**A.** Extracts of HeLa cells transfected with the indicated siRNAs analyzed by Western blotting with the indicated antibodies.

**B.** Plots show percentage of non-radial MTs running along the cell edge in a 4 x 7  $\mu$ m box adjacent to the cell edge or in the same box but placed 4  $\mu$ m away from the cell edge. Measurements were performed in 10 cells per siRNA. Values significantly different from control are indicated.

**C-F.** HeLa cells were transiently transfected with control or KIF21A siRNAs, fixed and stained with the indicated antibodies. The insets show enlargements of the boxed areas. In the overlays KIF21A (C), liprin- $\beta$ 1 (D) and EB1/3 (E,F) are shown in green,  $\beta$ -tubulin in red.

**G-H.** HeLa cells transiently transfected with the indicated siRNAs were treated with nocodazole (10  $\mu$ M) for 20 min prior to fixation and labeling with  $\beta$ -tubulin antibodies (G). The mean numbers of MTs in a 50  $\mu$ m<sup>2</sup> box were counted (H). A value significantly different from control is indicated.

in liprin- $\alpha$ 1-depleted cells (Fig. 3A,B), although the clustering is strongly reduced after liprin- $\beta$ 1 knockdown (Fig. 3F,G). This suggests that LL5 $\beta$  and liprin proteins have independent means of interacting with the plasma membrane. The nature of this interaction is not completely clear: although LL5 $\beta$  can bind to PIP3, this interaction alone cannot explain the patchy distribution of LL5 $\beta$  at the plasma membrane (Lansbergen et al., 2006). Liprin proteins could in principle be targeted to the membrane through an interaction with transmembrane protein-tyrosine phosphatases such as LAR (Serra-Pages et al., 1998), but this notion has not been proven. It is noteworthy that the patches of LL5 $\beta$  and liprin- $\alpha$ 1/ $\beta$ 1 often form around FA sites, suggesting a connection to integrins, and both LL5s and liprin- $\alpha$ 1 were functionally linked to integrins (Asperti et al., 2010; Hotta et al., 2010).

Clustering of LL5 $\beta$  and liprin- $\alpha$ 1/ $\beta$ 1 partially depends on the coiled-coil protein ELKS (Fig. 2D-F). In addition to playing a role in MT attachment, this protein also participates in the docking and fusion of exocytotic vesicles (Grigoriev et al., 2007), making LL5 $\beta$ -liprin- $\alpha$ 1/ $\beta$ 1 patches at the cortex functionally similar to presynaptic sites, the cytomatrix at the active zone (Hida and Ohtsuka, 2010). Interestingly, liprin- $\alpha$ 1 seems to be a highly conserved upstream player in the assembly of both cortical structures (Spangler and Hoogenraad, 2007; Stryker and Johnson, 2007; this study).

The major function of the LL5 $\beta$ -liprin- $\alpha$ 1/ $\beta$ 1 patches is to attract MT-stabilizing factors, CLASPs and ACF7. CLASPs can directly bind to LL5 $\alpha$ / $\beta$  (Hotta et al., 2010; Lansbergen et al., 2006), but their cortical recruitment also depends on ACF7 (Drabek et al., 2006), although the biochemical mechanism is unknown. ACF7 does not critically depend on LL5 $\beta$  for its cortical targeting (Fig. 2B), but it does require liprin- $\alpha$ 1/ $\beta$ 1 (Fig. 3D,I). ACF7 is a very large protein of more than 7000 amino acids, making biochemical analysis of its binding to different partners challenging, and extensive additional efforts will be needed to elucidate its interactions with other components of the MT attachment complexes.

In spite of the high concentration of MT-stabilizing and rescue factors at the periphery of HeLa cells, most MTs terminate in close vicinity of the cell margin, and do not continue growing along the cell edge (Drabek et al., 2006; Lansbergen et al., 2006; Mimori-Kiyosue et al., 2005). Previously, we hypothesize that this was due to mechanical properties – MT attachment to the cell cortex close to the cell edge might physically hinder their elongation and promote catastrophes (Mimori-Kiyosue et al., 2005). This view was supported by *in vitro* experiments, which demonstrated catastrophe induction by a pushing force generated by a MT growing against an obstacle (Janson et al., 2003). Surprisingly, we now found that the restriction of MT growth at the edge of HeLa cells occurs predominantly due to a biochemical regulator, KIF21A. Depletion of this kinesin induced extensive MT growth along the cell margin, generating circular MT bundles at the cell periphery (Fig. 7B-D, Fig. 8). These bundles showed increased MT stability, indicating that KIF21A does not simply promote catastrophes like kinesin-13 family members (Moores and Milligan, 2006). We favor the idea that, similar to another kinesin-4, Xklp1, KIF21A acts as a context-dependent MT growth inhibitor. Xklp1 was shown to be a processive MT plus end directed motor that can reduce MT growth and shrinkage rates (Bringmann et al., 2004). It



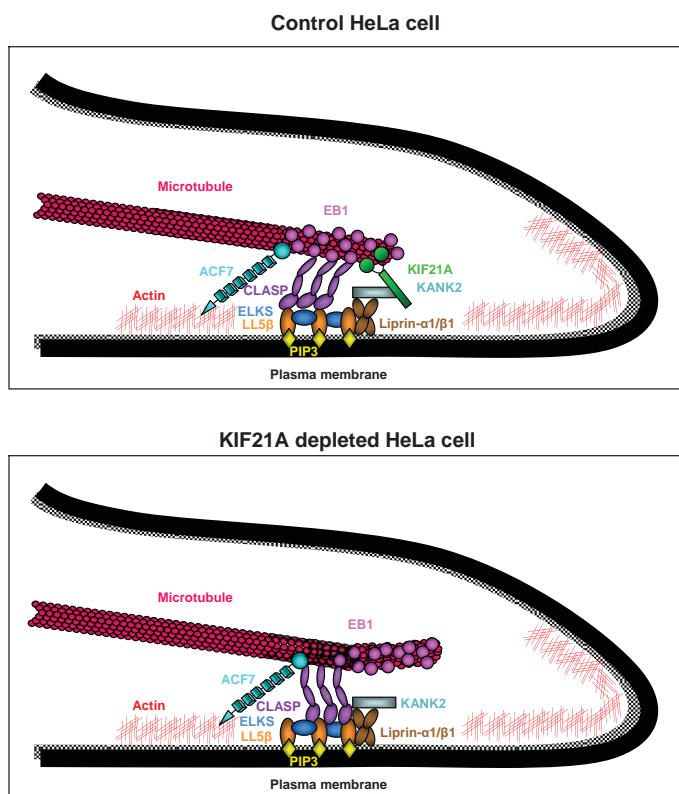


**Figure 8. Model for regulation of cortical MT dynamics by KIF21A**

In control cells the plus end of a growing MT makes contact with the cell cortex through the association of CLASPs with LL5 $\beta$ . ACF7 is an upstream regulator of CLASP-mediated cortical localization. The recruitment and clustering of LL5 $\beta$  at the cell cortex is mediated by PIP3 in the membrane and its association with ELKS. Liprin- $\alpha$ 1/ $\beta$ 1 act as upstream regulators of the cortical MT attachment complex. The actin modifying protein KANK2 was identified as a liprin- $\beta$ 1 interaction partner; it links KIF21A kinesin-4 family member to liprin- $\alpha$ 1/ $\beta$ 1. The depletion of KIF21A from HeLa cells disrupts cortical MT dynamics; MTs curve along the cell margin and form a circular bundle at the cell periphery.

is specifically recruited to overlapping MTs in the mitotic spindle midzone by its binding partner PRC1 and it can stabilize MT overlaps and restrict their length by inhibiting MT growth (Bieling et al., 2010). Our data indicate that KIF21A also contains a processive MT plus end directed motor domain (Fig. 6G). However, the full-length molecule seems to predominantly turn over on the LL5 $\beta$ -liprin- $\alpha$ 1/ $\beta$ 1 patches and displays no long runs along MTs (Fig. 6A, B,E). This could be due to some autoinhibitory mechanism that depends on the coiled-coil and the WD-40 repeat regions of the KIF21A molecule. We propose that KIF21A is activated by its recruitment to the cell cortex, where it restricts the growth of MTs with which it comes into contact. Detailed live cell imaging experiments using MT markers would be needed to prove this hypothesis.

The recruitment of KIF21A seems to require liprin- $\beta$ 1 (Fig.5H), and, based on our biochemical data, is possibly mediated by KANK2 (Fig. 5B,C). It should be noted that among liprin- $\alpha$ 1/ $\beta$ 1 binding partners we have also identified KANK1 (Fig.S2A,B), and it remains to be determined whether there is functional redundancy between KANK1 and KANK2.

Identification of KIF21A as a cortical regulator of MT dynamics provides a new insight into CFEOM1 syndrome. CFEOM1 is caused by abnormal innervation of extraocular muscles, a deficiency which is likely caused by axon guidance defects during development of the ocular motor neurons (Yamada et al., 2003). Axon guidance critically depends on the axonal growth cone dynamics, which is in turn determined by the functional cross-talk between MTs and the actin cytoskeleton (Conde and Caceres, 2009; Hoogenraad and Bradke, 2009; Poulain and Sobel, 2010). We have shown that KIF21A regulates MTs as part of a protein complex that has multiple direct

and indirect links to the actin cytoskeleton and adhesion sites. Abnormalities in this process, perhaps through strengthening of the KIF21A-KANK2 interaction (Kakinuma and Kiyama, 2009) or through some other as of yet unknown mechanisms seem to be a likely explanation of nerve misrouting observed in CFEOM1 patients. In line with this view, a related congenital syndrome, CFEOM3, is caused by mutations in the gene encoding a  $\beta$ -tubulin isotype, which result in MT dynamics defects (Tischfield et al., 2010). Understanding of the molecular role of KIF21A will provide a basis for unraveling how its mutated versions disrupt axonal pathfinding in ocular motor neurons and thus help to elucidate the mechanistic basis of CFEOM1 syndrome.

## Experimental procedures

### *Cell culture and transfection of DNA constructs*

HeLa and HEK293 were cultured as described previously (Akhmanova et al., 2001). PolyFect (Qiagen), FuGENE 6 (Roche) or Lipofectamine 2000 (Invitrogen) reagents were used for plasmid transfection.

### *Constructs*

(Bio)GFP-KIF21A and KIF21A-GFP expression constructs and their deletion mutants were generated using Flexi ORF clone pF1KA1708 human cDNA (Kazusa DNA Research Institute) in pEGFP-C1 and pEGFP-N3 by cloning- and PCR-based strategies. GFP-KIF21A-coilR954W mutation was introduced by overlapping PCR. In BioGFP fusions, a linker encoding the sequence MASGLNDIFEAQKIEWHEGGG which is the substrate of biotin ligase BirA is inserted into the NheI and AgeI sites in front of the GFP (pBioGFP-C1). BirA ligase expression construct was a gift from D. Meijer (Erasmus MC, Rotterdam, The Netherlands). Myc-GRASP1 (Hoogenraad et al., 2010), GFP-LL5 $\beta$ , RFP-LL5 $\beta$  and GFP-ELKS (Lansbergen et al., 2006), EB3-mRFP (Grigoriev et al., 2008) and HA-liprin- $\alpha$ 1 (S.A. Spangler et al., submitted) were described previously. BioHA-liprin- $\alpha$ 1 was generated by cloning a linker encoding the sequence MASGLNDIFEAQKIEWHEGGG into HA-liprin- $\alpha$ 1 construct. mCherry-liprin- $\alpha$ 1 was subcloned into GW1-mCherry vector. HA-liprin- $\beta$ 1 was generated using human cDNA (NM\_003622) in GW1-HA by cloning and PCR-based strategies and BioGFP-liprin- $\beta$ 1 was generated by re-cloning liprin- $\beta$ 1 in frame behind BioGFP vector. Myc-KANK2 was generated using clone KIAA1518 human cDNA (Kazusa DNA Research Institute) in GW1-Myc by cloning- and PCR-based strategies.

### *siRNAs*

siRNAs were synthesized by Ambion or Dharmacon; they were directed against the following target sequences: control: GCACUCAUUAUGACUCCAU (Mimori-Kiyosue et al., 2005), KIF21A (A): CACGUACUGUGAAUACAGA, KIF21A (B): GUAAGACCCAUGUCAGAU, KIF21A (C): CCCUACAGAAGCCCGAUA, human liprin- $\alpha$ 1: GGCUGAAAAAAUUCGUAAA, human liprin- $\beta$ 1: GAUUCGAGAUUUGGAGUUU, LL5 $\beta$ : GGAGATTTTGATCATCTA (Lansbergen et al., 2006), ELKS: GTAGGGAAAACCCTTCAAT (Lansbergen et al., 2006), ACF7 #A: UUGCAGCAGGUGAAUGGAC (Drabek et al., 2006), ACF7 #B: CCAAAGUGACUUGAAGGAU (Drabek et al., 2006). Synthetic

oligos were transfected using HiPerFect (Qiagen) at a concentration of 5 nM and cells were analyzed 72 hr after transfection.

#### *Antibodies and immunofluorescent cell staining*

We used rabbit polyclonal antibodies against GFP (Abcam), HA (Santa Cruz), LL5 $\beta$  (Lansbergen et al., 2006), rabbit IgG, ELKS (a gift from Dr. F. Melchior, ZMBH, University of Heidelberg, Germany), liprin- $\alpha$ 1 (S.A. Spangler et al., submitted), KIF21A (Tischfield et al., 2010) (a gift from Dr. E. Engle (Howard Hughes Medical Institute, Boston, USA)), used for immunofluorescent cell staining, or Upstate Biotechnology; used for Western blotting). Polyclonal rabbit antibodies against liprin- $\beta$ 1 were raised against GST fusion protein containing liprin- $\beta$ 1 amino acids 195-433. We used mouse monoclonal antibodies against GFP and HA tag (Roche), vinculin, Myc and  $\beta$ -tubulin (Sigma Aldrich), ACF7/MACF (Abnova), FAK (BD Biosciences), LL5 $\beta$  (Lansbergen et al., 2006) and rat monoclonal antibody against EB1/3, clone #15H11 (Absea). The following secondary antibodies were used; alkaline phosphatase-conjugated anti-rabbit and anti-mouse (Sigma-Aldrich), IRDye 800CW Goat anti-rabbit and anti-mouse (Li-Cor Biosciences), Alexa-350, Alexa-488 and Alexa-598 conjugated goat antibodies against rabbit and mouse IgG (Molecular Probes),

Cells were fixed with  $-20^{\circ}\text{C}$  methanol for 15 min in the case of liprin- $\alpha$ 1, LL5 $\beta$ , ELKS, ACF and vinculin staining. In case of liprin- $\beta$ 1, KIF21A, Myc and tubulin labeling, cells were fixed with  $-20^{\circ}\text{C}$  methanol for 15 min or fixed with  $-20^{\circ}\text{C}$  methanol for 15 min followed by a post-fix in 4% paraformaldehyde in phosphate-buffered saline (PBS) for 15 min at RT. Cells were rinsed with 0.15% Triton X-100 in PBS; subsequent washing and labeling steps were carried out in PBS supplemented with 1% bovine serum albumin and 0.15% Tween-20. At the end, slides were rinsed in 100% ethanol, air-dried and mounted in Vectashield mounting medium (Vector laboratories).

#### *Drug treatments*

MTs were depolymerized by a 1 hr or 20 min treatment with 10  $\mu\text{M}$  nocodazole (Sigma-Aldrich). To stabilize MTs, cells were treated for 1 hr with 200 nM Taxol (Sigma-Aldrich).

#### *Image Acquisition and Processing*

Images of fixed cells were collected with a Leica DMRBE microscope equipped with a PL Fluotar 100x 1.3 N.A. or 40x 1.00-0.50 N.A. oil objectives, FITC/EGFP filter 41012 (Chroma) and Texas Red filter 41004 (Chroma) and an ORCA-ER-1394 CCD camera (Hamamatsu). Live cell imaging was performed on an inverted research microscope Nikon Eclipse Ti-E (Nikon) with perfect focus system (PFS) (Nikon), equipped with Nikon CFI Apo TIRF 100x 1.49 N.A. oil objective (Nikon), QuantEM 512SC EMCCD camera (Roper Scientific) and controlled with MetaMorph 7.5 software (Molecular Devices). The 16-bit images were projected onto the CCD chip with intermediate lens 2.5X at a magnification of 0.065  $\mu\text{m}/\text{pixel}$ . To keep cells at  $37^{\circ}\text{C}$  we used stage top incubator (model INUG2E-ZILCS, Tokai Hit). The microscope was equipped with TIRF-E motorized TIRF illuminator modified by Roper Scientific France/ PICT-IbiSA, Institut Curie. For regular imaging we used mercury lamp HBO-100W/2 (Osram) for excitation or 491nm 50mW Calypso (Cobolt) and

561nm 50mW Jive (Cobolt) lasers. We used ET-GFP filter set (Chroma) for imaging of proteins tagged with GFP; ET-mCherry filter set (Chroma) for imaging of proteins tagged with mCherry. For simultaneous imaging of green and red fluorescence we used ET-mCherry/GFP filter set (Chroma) together with DualView (DV2, Roper) equipped with dichroic filter 565dcxr (Chroma) and HQ530/30m emission filter (Chroma).

FRAP assay was carried out using FRAP scanning system I-Las/I-Launch (Roper Scientific France/ PICT-IBiSA, Institut Curie) installed on the same microscope and with the lasers mentioned above at 100% laser power.

Images were prepared for publication using MetaMorph and Adobe Photoshop. All images were modified by adjustments of levels and contrast; for images of live cells, averaging of several consecutive frames was performed in some cases; in addition to adjustments of levels and contrast, Unsharp Mask and Blur filters (Photoshop) were applied to tubulin images. Maximum intensity projection, kymograph analysis and various quantifications were performed in MetaMorph. Data were averaged over multiple cells and experiments. Statistical analysis was performed using non-parametric Mann-Whitney U-test in Statistica for Windows and SigmaPlot.

#### *Protein purification, immunoprecipitation and Western blotting*

GST fusions were expressed in BL21 *E. coli* and purified with glutathione-Sepharose 4B (GE Healthcare). IPs and Western blotting were described previously (Lansbergen et al., 2004).

#### *Mass spectrometry*

1D SDS-PAGE gel lanes were cut into 2-mm slices using an automatic gel slicer and subjected to in-gel reduction with dithiothreitol, alkylation with iodoacetamide and digestion with trypsin (Promega, sequencing grade), essentially as described by (Wilm et al., 1996). Nanoflow LC-MS/MS was performed on an 1100 series capillary LC system (Agilent Technologies) coupled to either an LTQ-Orbitrap or an LTQ linear ion trap mass spectrometer (Thermo) both operating in positive mode and equipped with a nanospray source. Peptide mixtures were trapped on a ReproSil C18 reversed phase column (Dr Maisch GmbH; column dimensions 1.5 cm × 100 μm, packed in-house) at a flow rate of 8 μl/min. Peptide separation was performed on ReproSil C18 reversed phase column (Dr Maisch GmbH; column dimensions 15 cm × 50 μm, packed in-house) using a linear gradient from 0 to 80% B (A = 0.1 % formic acid; B = 80% (v/v) acetonitrile, 0.1 % formic acid) in 70 min and at a constant flow rate of 200 nl/min using a splitter. The column eluent was directly sprayed into the ESI source of the mass spectrometer. Mass spectra were acquired in continuum mode; fragmentation of the peptides was performed in data-dependent mode. Peak lists were automatically created from raw data files using the Mascot Distiller software (version 2.1; MatrixScience). The Mascot search algorithm (version 2.2, MatrixScience) was used for searching against the IPI database (release IPI\_mouse\_20100507.fasta or IPI\_human\_20100507.fasta). The peptide tolerance was typically set to 10 ppm for Orbitrap data and to 2 Da for ion trap data and the fragment ion tolerance was set to 0.8 Da. A maximum number of 2 missed cleavages by trypsin were allowed and carbamidomethylated cysteine and oxidized methionine were set as fixed and

variable modifications, respectively. The Mascot score cut-off value for a positive protein hit was set to 60. Individual peptide MS/MS spectra with Mascot scores below 40 were checked manually and either interpreted as valid identifications or discarded. Typical contaminants, also present in immunopurifications using beads coated with pre-immune serum or antibodies directed against irrelevant proteins were omitted from the table.

## **Acknowledgments**

We are grateful to D. Meijer, R. Tsien, R. Medema, M. Tanenbaum, E. Engle and F. Melchior for sharing reagents and E. de Graaff for technical assistance. This study was supported by the Netherlands Organization for Scientific Research ALW open program and ALW-VICI grants to A.A, ZonMw-VIDI and European Science Foundation (European Young Investigators (EURYI)) awards to C.C.H.

## **References**

- Akhmanova, A., Hoogenraad, C.C., Drabek, K., Stepanova, T., Dortland, B., Verkerk, T., Vermeulen, W., Burgering, B.M., De Zeeuw, C.I., Grosveld, F., et al. (2001). Clasps are CLIP-115 and -170 associating proteins involved in the regional regulation of microtubule dynamics in motile fibroblasts. *Cell* 104, 923-935.
- Akhmanova, A., Stehbens, S.J., and Yap, A.S. (2009). Touch, grasp, deliver and control: functional cross-talk between microtubules and cell adhesions. *Traffic* 10, 268-274.
- Akhmanova, A., and Steinmetz, M.O. (2008). Tracking the ends: a dynamic protein network controls the fate of microtubule tips. *Nat Rev Mol Cell Biol* 9, 309-322.
- Asperti, C., Pettinato, E., and de Curtis, I. (2010). Liprin-alpha1 affects the distribution of low-affinity beta1 integrins and stabilizes their permanence at the cell surface. *Exp Cell Res* 316, 915-926.
- Bieling, P., Telley, I.A., and Surrey, T. (2010). A minimal midzone protein module controls formation and length of antiparallel microtubule overlaps. *Cell* 142, 420-432.
- Bringmann, H., Skiniotis, G., Spilker, A., Kandels-Lewis, S., Vernos, I., and Surrey, T. (2004). A kinesin-like motor inhibits microtubule dynamic instability. *Science* 303, 1519-1522.
- Chan, W.M., Andrews, C., Dragan, L., Fredrick, D., Armstrong, L., Lyons, C., Geraghty, M.T., Hunter, D.G., Yazdani, A., Traboulsi, E.I., et al. (2007). Three novel mutations in KIF21A highlight the importance of the third coiled-coil stalk domain in the etiology of CFEOM1. *BMC Genet* 8, 26.
- Conde, C., and Caceres, A. (2009). Microtubule assembly, organization and dynamics in axons and dendrites. *Nat Rev Neurosci* 10, 319-332.
- de Curtis, I. (2011). Function of liprins in cell motility. *Exp Cell Res* 317, 1-8.
- Desai, A., and Mitchison, T.J. (1997). Microtubule polymerization dynamics. *Annu Rev Cell Dev Biol* 13, 83-117.
- Drabek, K., van Ham, M., Stepanova, T., Draegestein, K., van Horssen, R., Sayas, C.L., Akhmanova, A., Ten Hagen, T., Smits, R., Fodde, R., et al. (2006). Role of CLASP2 in microtubule stabilization and the regulation of persistent motility. *Curr Biol* 16, 2259-2264.
- Dujardin, D.L., and Vallee, R.B. (2002). Dynein at the cortex. *Curr Opin Cell Biol* 14, 44-49.
- Fukata, M., Watanabe, T., Noritake, J., Nakagawa, M., Yamaga, M., Kuroda, S., Matsuura, Y., Iwamatsu, A., Perez, F., and Kaibuchi, K. (2002). Rac1 and Cdc42 capture microtubules through IQGAP1 and CLIP-170. *Cell* 109, 873-885.
- Grigoriev, I., Gouveia, S.M., van der Vaart, B., Demmers, J., Smyth, J.T., Honnappa, S., Splinter, D., Steinmetz, M.O., Putney, J.W., Jr., Hoogenraad, C.C., et al. (2008). STIM1 is a MT-plus-end-tracking protein involved in remodeling of the ER. *Curr Biol* 18, 177-182.
- Grigoriev, I., Splinter, D., Keijzer, N., Wulf, P.S., Demmers, J., Ohtsuka, T., Modesti, M., Maly, I.V., Grosveld, F., Hoogenraad, C.C., et al. (2007). Rab6 regulates transport and targeting of exocytotic carriers. *Dev Cell* 13, 305-314.
- Gundersen, G.G., Kreitzer, G., Cook, T., and Liao, G. (1998). Microtubules as determinants of cellular polarity. *Biol Bull* 194, 358-360.
- Heidary, G., Engle, E.C., and Hunter, D.G. (2008). Congenital fibrosis of the extraocular muscles. *Semin Ophthalmol* 23, 3-8.
- Hida, Y., and Ohtsuka, T. (2010). CAST and ELKS proteins: structural and functional determinants of the presynaptic active zone. *J Biochem* 148, 131-137.
- Hirokawa, N., Noda, Y., Tanaka, Y., and Niwa, S. (2009). Kinesin superfamily motor proteins and intracellular transport. *Nat Rev Mol Cell Biol* 10, 682-696.
- Hoogenraad, C.C., and Bradke, F. (2009). Control of neuronal polarity and plasticity--a renaissance for microtubules?

- Trends Cell Biol 19, 669-676.
- Hoogenraad, C.C., Popa, I., Futai, K., Sanchez-Martinez, E., Wulf, P.S., van Vlijmen, T., Dortland, B.R., Oorschot, V., Govers, R., Monti, M., et al. (2010). Neuron specific Rab4 effector GRASP-1 coordinates membrane specialization and maturation of recycling endosomes. *PLoS Biol* 8, e1000283.
- Hotta, A., Kawakatsu, T., Nakatani, T., Sato, T., Matsui, C., Sukezane, T., Akagi, T., Hamaji, T., Grigoriev, I., Akhmanova, A., et al. (2010). Laminin-based cell adhesion anchors microtubule plus ends to the epithelial cell basal cortex through LL5alpha/beta. *J Cell Biol* 189, 901-917.
- Janson, M.E., de Dood, M.E., and Dogterom, M. (2003). Dynamic instability of microtubules is regulated by force. *J Cell Biol* 161, 1029-1034.
- Kakinuma, N., and Kiyama, R. (2009). A major mutation of KIF21A associated with congenital fibrosis of the extraocular muscles type 1 (CFEOM1) enhances translocation of Kank1 to the membrane. *Biochemical and biophysical research communications* 386, 639-644.
- Kakinuma, N., Zhu, Y., Wang, Y., Roy, B.C., and Kiyama, R. (2009). Kank proteins: structure, functions and diseases. *Cell Mol Life Sci* 66, 2651-2659.
- Ko, J., Na, M., Kim, S., Lee, J.R., and Kim, E. (2003). Interaction of the ERC family of RIM-binding proteins with the liprin-alpha family of multidomain proteins. *J Biol Chem* 278, 42377-42385.
- Kodama, A., Karakesisoglou, I., Wong, E., Vaezi, A., and Fuchs, E. (2003). ACF7: an essential integrator of microtubule dynamics. *Cell* 115, 343-354.
- Lansbergen, G., Grigoriev, I., Mimori-Kiyosue, Y., Ohtsuka, T., Higa, S., Kitajima, I., Demmers, J., Galjart, N., Houtsmuller, A.B., Grosveld, F., et al. (2006). CLASPs attach microtubule plus ends to the cell cortex through a complex with LL5beta. *Dev Cell* 11, 21-32.
- Lansbergen, G., Komarova, Y., Modesti, M., Wyman, C., Hoogenraad, C.C., Goodson, H.V., Lemaitre, R.P., Drechsel, D.N., van Munster, E., Gadella Jr., T.W.J., et al. (2004). Conformational changes in CLIP-170 regulate its binding to microtubules and dynactin localisation. *J Cell Biol* 166, 1003-1014.
- Marszalek, J.R., Weiner, J.A., Farlow, S.J., Chun, J., and Goldstein, L.S. (1999). Novel dendritic kinesin sorting identified by different process targeting of two related kinesins: KIF21A and KIF21B. *J Cell Biol* 145, 469-479.
- Mimori-Kiyosue, Y., Grigoriev, I., Lansbergen, G., Sasaki, H., Matsui, C., Severin, F., Galjart, N., Grosveld, F., Vorobjev, I., Tsukita, S., et al. (2005). CLASP1 and CLASP2 bind to EB1 and regulate microtubule plus-end dynamics at the cell cortex. *J Cell Biol* 168, 141-153.
- Moores, C.A., and Milligan, R.A. (2006). Lucky 13-microtubule depolymerisation by kinesin-13 motors. *J Cell Sci* 119, 3905-3913.
- Okada, K., Bartolini, F., Deaconescu, A.M., Moseley, J.B., Dogic, Z., Grigorieff, N., Gundersen, G.G., and Goode, B.L. (2010). Adenomatous polyposis coli protein nucleates actin assembly and synergizes with the formin mDia1. *J Cell Biol* 189, 1087-1096.
- Paranavitane, V., Coadwell, W.J., Eguinoa, A., Hawkins, P.T., and Stephens, L. (2003). LL5beta is a phosphatidylinositol (3,4,5)-trisphosphate sensor that can bind the cytoskeletal adaptor, gamma-filamin. *J Biol Chem* 278, 1328-1335.
- Paranavitane, V., Stephens, L.R., and Hawkins, P.T. (2007). Structural determinants of LL5beta subcellular localisation and association with filamin C. *Cell Signal* 19, 817-824.
- Poulain, F.E., and Sobel, A. (2010). The microtubule network and neuronal morphogenesis: Dynamic and coordinated orchestration through multiple players. *Molecular and cellular neurosciences* 43, 15-32.
- Rodriguez, O.C., Schaefer, A.W., Mandato, C.A., Forscher, P., Bement, W.M., and Waterman-Storer, C.M. (2003). Conserved microtubule-actin interactions in cell movement and morphogenesis. *Nat Cell Biol* 5, 599-609.
- Schuyler, S.C., and Pellman, D. (2001). Microtubule "plus-end-tracking proteins": The end is just the beginning. *Cell* 105, 421-424.
- Serra-Page, C., Medley, Q.G., Tang, M., Hart, A., and Streuli, M. (1998). Liprins, a family of LAR transmembrane protein-tyrosine phosphatase-interacting proteins. *J Biol Chem* 273, 15611-15620.
- Shen, J.C., Unoki, M., Ythier, D., Duperray, A., Varticovski, L., Kumamoto, K., Pedoux, R., and Harris, C.C. (2007). Inhibitor of growth 4 suppresses cell spreading and cell migration by interacting with a novel binding partner, liprin alpha1. *Cancer research* 67, 2552-2558.
- Silverman, M.A., Kaech, S., Ramser, E.M., Lu, X., Lasarev, M.R., Nagalla, S., and Banker, G. (2010). Expression of kinesin superfamily genes in cultured hippocampal neurons. *Cytoskeleton (Hoboken, NJ)* 67, 784-795.
- Spangler, S.A., and Hoogenraad, C.C. (2007). Liprin-alpha proteins: scaffold molecules for synapse maturation. *Biochem Soc Trans* 35, 1278-1282.
- Stryker, E., and Johnson, K.G. (2007). LAR, liprin alpha and the regulation of active zone morphogenesis. *J Cell Sci* 120, 3723-3728.
- Tischfield, M.A., Baris, H.N., Wu, C., Rudolph, G., Van Maldergem, L., He, W., Chan, W.M., Andrews, C., Demer, J.L., Robertson, R.L., et al. (2010). Human TUBB3 mutations perturb microtubule dynamics, kinesin interactions, and axon guidance. *Cell* 140, 74-87.
- Tsvetkov, A.S., Samsonov, A., Akhmanova, A., Galjart, N., and Popov, S.V. (2007). Microtubule-binding proteins CLASP1 and CLASP2 interact with actin filaments. *Cell Motil Cytoskeleton*.

- Wang, Y., Liu, X., Biederer, T., and Sudhof, T.C. (2002). A family of RIM-binding proteins regulated by alternative splicing: Implications for the genesis of synaptic active zones. *Proc Natl Acad Sci U S A* 99, 14464-14469.
- Wilm, M., Shevchenko, A., Houthaeve, T., Breit, S., Schweigerer, L., Fotsis, T., and Mann, M. (1996). Femtomole sequencing of proteins from polyacrylamide gels by nano-electrospray mass spectrometry. *Nature* 379, 466-469.
- Wu, X., Kodama, A., and Fuchs, E. (2008). ACF7 regulates cytoskeletal-focal adhesion dynamics and migration and has ATPase activity. *Cell* 135, 137-148.
- Yamada, K., Andrews, C., Chan, W.M., McKeown, C.A., Magli, A., de Berardinis, T., Loewenstein, A., Lazar, M., O'Keefe, M., Letson, R., et al. (2003). Heterozygous mutations of the kinesin KIF21A in congenital fibrosis of the extraocular muscles type 1 (CFEOM1). *Nat Genet* 35, 318-321.

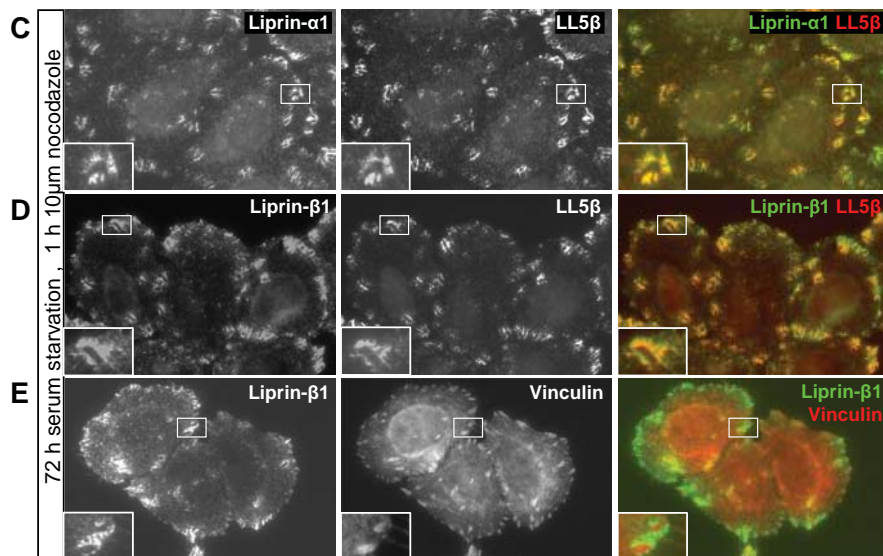
## Supplemental Information

A

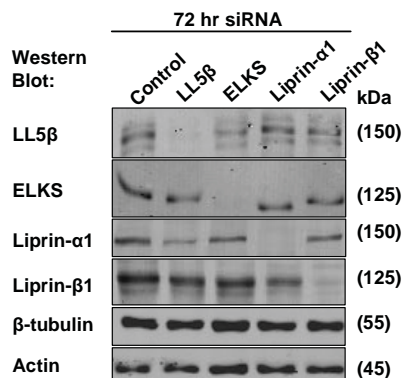
Identified proteins	Accession number	Mascot score	Unique peptides
LL5 $\beta$	IPI00410259	7839	109
ELKS	IPI00216719	5864	93
LL5 $\alpha$	IPI00413100	243	7
Liprin- $\alpha$ 1	IPI00163496	225	5
Liprin- $\alpha$ 2	IPI00795341	168	5
Liprin- $\alpha$ 4	IPI00397578	122	3

B

Identified proteins	Accession number	Mascot score	Unique peptides
ELKS	IPI00216719	7644	125
Liprin- $\beta$ 1	IPI00179172	924	5
LL5 $\alpha$	IPI00413100	243	7
KIF21A	IPI00410259	43	2



F

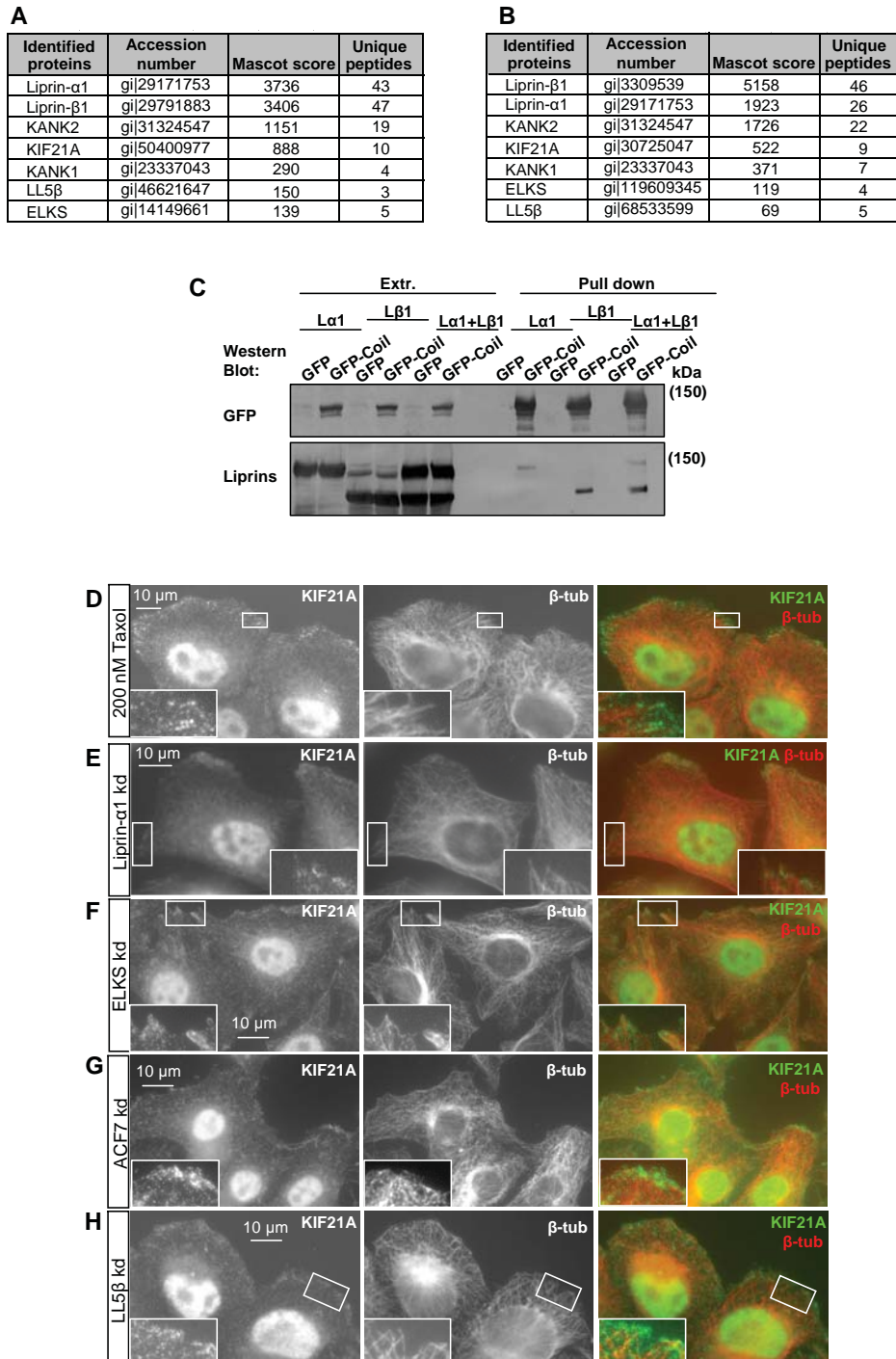
**Supplemental Figure S1. Identification of liprin- $\alpha$ 1 and liprin- $\beta$ 1 as LL5 $\beta$  and ELKS interaction partners**

**A,B.** Identification of liprin- $\alpha$ 1 and liprin- $\beta$ 1 in BioGFP-LL5 $\beta$  (A) and BioGFP-ELKS (B) streptavidin pull-down assays from HEK293 cell extracts by mass spectrometry.

**C-E.** HeLa cells were serum starved for 72h and treated with nocodazole (10  $\mu$ m) for 1h, prior to being fixed and stained with the indicated antibodies. The insets show enlargements of the boxed areas. In the overlay liprins are shown in green and LL5 $\beta$  (C,D) and vinculin (E) in red.

**F.** Extracts of HeLa cells transfected with the indicated siRNAs analyzed by Western blotting with the indicated antibodies.



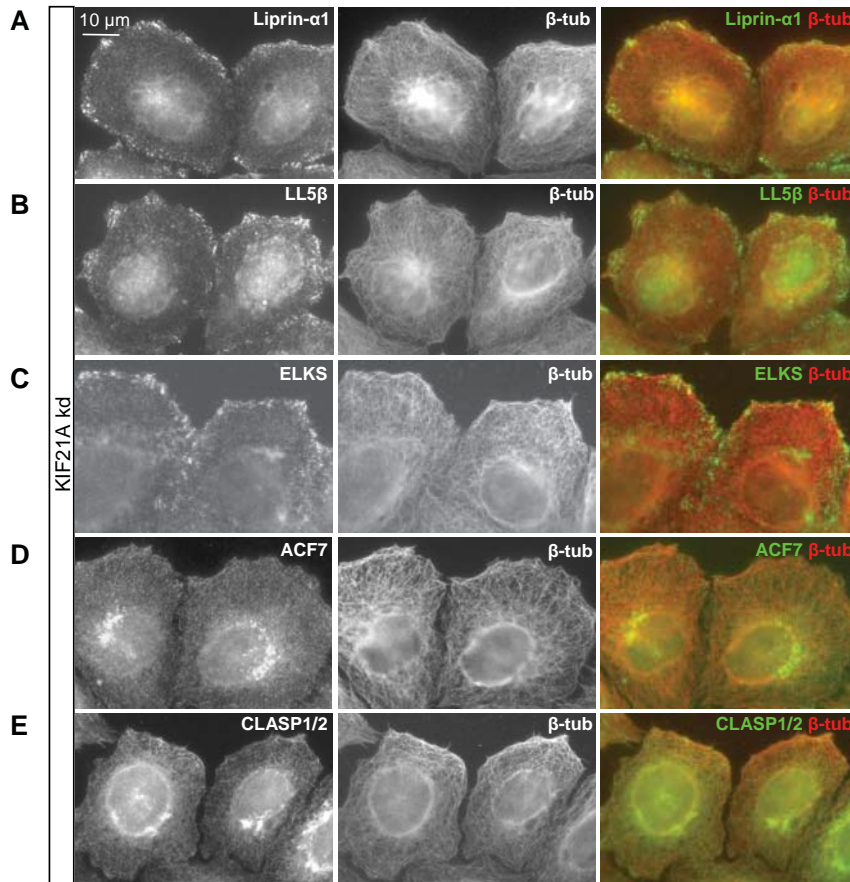


**Supplemental Figure S2. Identification of KANK1, KANK2 and KIF21A as liprin interaction partners**

**A,B.** Identification of KANK1, KANK2 and KIF21A in BioHA-liprin- $\alpha$ 1 (**A**) and BioGFP-liprin- $\beta$ 1 (**B**) streptavidin pull-down assays from HeLa cell extracts by mass spectrometry.

**C.** Streptavidin pull-down assay was performed with extracts of HEK293 cells co-expressing BioGFP-KIF21A mutants, BirA and HA-liprin- $\alpha$ 1 and HA-liprin- $\beta$ 1, and analyzed by Western blotting with the indicated antibodies.

**D-G.** HeLa cells were treated for 1h with taxol (200 nM) (**D**) or transiently transfected with different siRNAs (**E-F**) fixed and stained with the indicated antibodies. The insets show enlargements of the boxed areas. In the overlay KIF21A is shown in green and  $\beta$ -tubulin in red.



**Supplemental Figure S3. Cortical localization of liprin- $\alpha$ 1, LL5 $\beta$ , ELKS and ACF7 is independent from KIF21A**  
A-E. HeLa cells were transiently transfected with KIF21A siRNAs, fixed and stained with the indicated antibodies. The insets show enlargements of the boxed areas. In the overlay liprin- $\alpha$ 1 (A), LL5 $\beta$  (B), ELKS (C), ACF7 (D) and CLASP1/2 (E) are shown in green and  $\beta$ -tubulin (A-E) in red.

	1 <sup>st</sup> component			2 <sup>nd</sup> component		
	$t_{1/2}$ [s]	95% conf. int. [s]	Amount [%]	$t_{1/2}$ [s]	95% conf. int. [s]	Amount [%]
mCherry-liprin- $\alpha$ 1	33.3 s	(31.3, 35.6)	75	355.5 s	(275.1, 502.3)	25
GFP-ELKS	17.6 s	(13.7, 24.5)	56	313.6 s	(266.6, 380.9)	44
GFP-LL5 $\beta$	62.00 s	(45.9, 95.3)	19	1155.2 s	(912.04, 1540.32)	82
KIF21A-FL-GFP	6.1s	(5.6, 7.8)	81	39.8s	(24.4, 111.8)	19
GFP-KIF21A-coil	6.0 s	(5.1, 7.3)	44	21.1s	(19.5, 23.1)	56

**Supplemental Table S1. Analysis of the FRAP data**

Percentage and recovery half-time for each protein population were determined by fitting of a two-component model to FRAP curves. Half-time of fluorescence recovery  $t_{1/2}$ , 95% confidence interval (95% conf. int.) for each  $t_{1/2}$  and percentage of each protein population are indicated.





# Chapter 6

**General Discussion:  
Building protein interaction networks at microtubule tips**





## General Discussion: Building protein interaction networks at microtubule tips

Microtubules (MTs) are cytoskeletal structures that play pivotal roles in many cellular functions, such as control of cell shape, division, motility and intracellular cargo transport. The highly dynamic nature of MTs is essential for performing these tasks and is therefore tightly controlled. Failure to regulate the MT network properly has been associated with many diseases such as cancer, neurodegenerative disorders, mental retardation and ciliopathies. The fundamental understanding of the workings of MT networks is of importance to gain a basic insight into MT-related disorders and to provide tools for improving or developing treatments.

MT plus-end tracking proteins (+TIPs) encompass structurally unrelated protein families that associate with the plus ends of growing MTs and thereby regulate different aspects of MT dynamics (Akhmanova and Steinmetz, 2008; Schuyler and Pellman, 2001). Over the last decade approximately 20 different +TIP families have been identified that influence different aspects of MT behaviour, such as polymerization (XMAP215/ch-TOG and EBs), depolymerization (kinesin-8 and -13), rescue (CLIPs) or stabilization and attachment to intracellular organelles or other structures (STIM1, CLASPs, APC and ACF7).

In spite of the significant progress made in the MT research field, we are only beginning to understand how the association of such a huge variety of +TIPs with a relatively small contact area, the MT plus end, is regulated both in space and time and how this influences the dynamic behaviour of MTs and ultimately cellular functions.

### Autonomous +TIPs EB1 and XMAP215/ch-TOG: searching for connections

The first step in building a +TIP complex is the recognition of the growing MT plus end. Among the ~20 different +TIPs known today, only two protein families are autonomous +TIPs: the End Binding (EB) proteins and the *Xenopus* Microtubule Associated Protein of 215 kDa (XMAP215) family. The autonomous nature of these highly conserved families was determined using purified proteins in an *in vitro* MT polymerization setting (Bieling et al., 2008; Bieling et al., 2007; Brouhard et al., 2008). However, we have shown in this thesis that at least in mammalian interphase cells, the mammalian homologue of XMAP215, ch-TOG, does not efficiently accumulate at MT plus ends in the absence of EBs (Chapter 3).

ch-TOG and EB homologues colocalize at MT plus ends and centrosomes; they have been linked functionally as well as physically. Both proteins function in the regulation of MT dynamics and mitotic progression (Cassimeris et al., 2009; Cassimeris and Morabito, 2004; Howard and Hyman, 2009; Rehberg and Graf, 2002). A considerable effort has been put into demonstrating a direct interaction between EB and ch-TOG family members, with varying results.

Yeast-two-hybrid experiments using slime mold homologues of ch-TOG and EB, DdCP244 and DdEB1, respectively, did not show an interaction, although co-precipitation of endogenous proteins has been observed. However, this does not prove a direct interaction, a conclusion supported by the partial tip co-localization of DdCP244 with DdEB1 indicating that they might be linked by (an) additional partner(s) (Rehberg and Graf, 2002).

Evidence for an interaction between Stu2p and Bim1, the budding yeast homologues of ch-TOG and EB1, respectively, is based on a yeast two-hybrid assay (Wolyniak et al., 2006). Importantly, the use of this assay in budding yeast is complicated by the fact that endogenous proteins present in the same cell might mediate indirect binding. Co-immunoprecipitation of Stu2p and Bim1 could only be observed with overexpressed proteins, but not with the endogenous ones; however, this might be due to the low affinity of the interaction. Interestingly, no binding between Stu2p and Bim1 purified from *E. coli* could be detected using *in vitro* experiments, which again argues that these two proteins are linked by an additional factor or that some posttranslational modifications, which occur in yeast but not in bacteria, are involved (Wolyniak et al., 2006).

In *Xenopus* extracts, an interaction was detected between endogenous XMAP215 and EB1 in metaphase, but not interphase, using an unconventional VIP (visual immunoprecipitation) technique (Niethammer et al., 2007). The results could not be confirmed by regular immunoprecipitation, and also attempts to coprecipitate ch-TOG and EB1 from mitotic extracts of HeLa cells failed to reveal an interaction between either endogenous or overexpressed proteins (Barr and Gergely, 2008). In conclusion, a direct interaction between EB1 and ch-TOG has not convincingly been shown so far.

In search for novel MT tip associated proteins, we identified the SLAIN family as EB and ch-TOG interaction partners (Chapter 3). We showed that SLAINs are plus-end tracking proteins that provide a link between EBs and ch-TOG in mammalian interphase cells.

In our hands, co-immunoprecipitation of ch-TOG and EB1/3 could be observed under certain conditions (Chapter 3). In addition, GST-EB1 pull down experiments from HEK293 extracts showed that endogenous ch-TOG could bind to EB1. However, in both cases the interaction is likely mediated by the presence of endogenous SLAINs in the extracts. This is supported by the fact that GST-EB1 pull downs from mitotic extracts where SLAIN is not associated with EBs showed strongly diminished ch-TOG binding, which would most likely not be the case if the interaction between EBs and ch-TOG was direct and not via SLAINs. In *Xenopus*, the C-terminus of XMAP215 has been reported to bind to EB1 (Kronja et al., 2009). However, overexpression of the GFP-ch-TOG C-terminus together with EB1 in HeLa cells did not result in the plus-end tracking of the C-terminal fragment (our unpublished data). In contrast, this was observed after co-expression with SLAIN2 again supporting an indirect binding of EB to ch-TOG through SLAIN2 (Chapter 3).

### **Non-autonomous +TIPs: MT plus end targeting through EB proteins**

Most of the non-autonomous +TIPs identified so far target MT plus ends through their direct or indirect association with the EB proteins, a strategy named “hitchhiking” (Carvalho et al., 2003). EB-dependent +TIPs can be divided into two categories. The first group includes cytoskeleton-associated protein Gly-rich (CAP-Gly) domain containing proteins, represented by the cytoplasmic linker protein family (CLIPs) and the large subunit of the dynactin complex p150<sup>Glued</sup>, which primarily bind to the EEY/F motifs at the EB C-termini (Akhmanova and Steinmetz, 2008). The second category relies on the interaction of the short linear motif SxIP (where S is serine, x can be any amino acid, I is isoleucine and P is proline) embedded in a serine, proline and basic-rich



stretch with the hydrophobic C-terminal EB cavity (Honnappa et al., 2009).

Certain properties of +TIPs can regulate their targeting to plus ends and ultimately their role in controlling MT dynamics: (1) number of SxIP motifs and composition of flanking regions, (2) multi-merization, (3) reducing of competition by interaction with other +TIPs independently from EB binding, and (4) regulation in time and space.

### SLAIN proteins as master regulators of +TIP interaction networks

#### Expression and evolutionary conservation

Using biochemical approaches combined with mass spectrometry analysis, we have identified SLAIN1 and SLAIN2 as novel EB-dependent mammalian +TIPs. SLAIN1 and SLAIN2 share a high degree of homology (Figure 1); however, some divergence is observed especially in the N-terminal regions. The SLAIN2 N-terminus interacts with the MT polymerase ch-TOG and the overexpression of this SLAIN2 fragment has a dominant negative effect on ch-TOG binding to MT tips. The differences between SLAIN1 and SLAIN2 N-termini do not appear to determine the

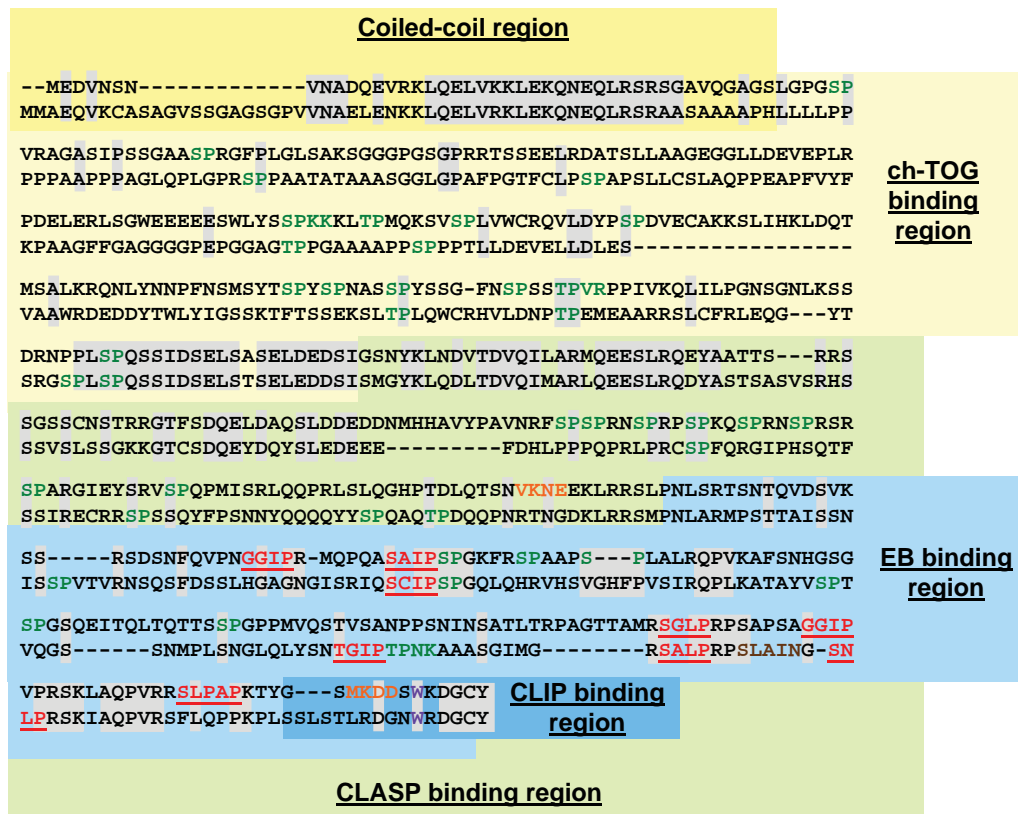


**Figure 1. Alignment of human SLAIN2 and SLAIN1**

Sequence homology between human SLAIN2 and SLAIN1 is marked in grey. The coiled-coil region of SLAIN2 is shown by a dark yellow box, whereas the ch-TOG binding region of SLAIN2 is highlighted in light yellow. The C-terminal part of SLAIN2 shown to interact with CLASPs is depicted in light green, the EB-binding region in light blue and the peptide binding to CLIP used in crystallography studies is shown in dark blue. Amino acids highlighted in dark green fall within CDK1 consensus sites (S/T-P-x-K/R and S/T-P), SxIP-like motifs and other important regions for plus-end tracking and EB binding are in red and underlined, the tryptophan residue important for CLIP CAP-Gly domain binding is in purple, the SLAIN2 sequences that match the sumoylation consensus motif ( $\Psi$ -K-x-D/E) are in orange, and finally, the amino acid sequence in SLAIN1 that reads SLAIN, from which the SLAIN family name is derived, is shown in brown.

binding specificity for ch-TOG because overexpression of the SLAIN1 N-terminus in HeLa cells affects MT dynamics in the same manner as the SLAIN2 dominant negative mutant, indicating that SLAIN1 N-terminus also binds to ch-TOG (Chapter 3).

SLAIN1 is highly expressed in undifferentiated embryonic stem cells (ESC) and its expression rapidly declines after induction of ESC differentiation (Hirst et al., 2006). Reverse transcriptase polymerase chain reaction (RT-PCR), Northern blot analysis and *in situ* hybridization showed that SLAIN1 is expressed in adult thymus, gut, brain, nervous system, tail bud, somites, testis, lung, bone marrow and kidney (Hirst et al., 2010; Hirst et al., 2006).

SLAIN2 appears to be a more widely expressed family member. RT-PCR and knockdown experiments show that in multiple experimental cell lines, such as HeLa, Swiss 3T3 and CHO cells, SLAIN2 is the only SLAIN family member expressed. In the brain and HEK293 cells both SLAIN1 and SLAIN2 proteins can be found as determined by RT-PCR and mass spectrometry analysis, respectively (Chapter 3 and our unpublished data).

It remains to be determined what, if any, functional differences exist between SLAIN1 and SLAIN2 in a cellular context. In this respect, it would be useful to generate SLAIN1 and SLAIN2 specific antibodies as all currently available antibodies recognize both variants equally well on Western blots.

SLAIN proteins are present in all mammals, zebrafish, *Xenopus* and the vase tunicate *Ciona intestinalis*, which is classified as an invertebrate. No proteins with clear sequence homology to SLAINs could be found in the genomes of yeast, *C. elegans* or *D. melanogaster*. This is surprising, as SLAINs play fundamental roles in mammalian interphase cells as regulators of MT dynamics by promoting ch-TOG accumulation at MT plus ends. The appearance of SLAINs might be an adaptation associated with a greater complexity of the +TIP network in higher organisms as compared to most invertebrates, plants and yeasts. Alternatively, it is possible that ch-TOG homologues are expressed in lower organisms at higher levels, making an accessory factor unnecessary. It is also possible that proteins with a function similar to SLAIN do exist in plants and invertebrates, but we cannot identify them as SLAIN counterparts because of a low degree or the complete absence of sequence conservation, especially as SLAINs, which encompass a short N-terminal coiled-coil sequence and unstructured basic, serine- and proline rich regions, contain no additional conspicuous domains.

As mentioned above, +TIPs make use of different properties to promote their access to MT plus ends. Below, we discuss the different strategies SLAINs might employ for targeting plus ends, as well as the interactions of SLAINs with other +TIPs and their role in the regulation of MT dynamics and neuritogenesis.

#### Multiple SxIP motifs and composition of flanking regions

SLAINs are EB-dependent +TIPs and their localization is mediated by their C-terminal part (Chapter 3 and Figure 1). SLAINs belong to the SxIP category of EB binders; SLAIN2 contains five tandemly arranged SxIP-(like)-motifs surrounded by serines, prolines and basic residues. Human SLAIN1 and SLAIN2 only contain one canonical SxIP motif (SCIP and SAIP, respectively), while the

other motifs are more variable. Mutagenesis of SAIP to SANN (where N is asparagine) in SLAIN2 did not abrogate plus-end tracking (our unpublished data) suggesting that the other SxIP-like-motifs can mediate plus-end tracking. This conclusion was supported by the plus-end tracking of a SLAIN2 deletion mutant containing the last three non-canonical SxIP-like-motifs, illustrating that the SxIP consensus allows significant sequence flexibility. Importantly, mutation of all five SxIP-like motifs as well as two additional, more divergent proline-containing sites strongly diminished plus-end tracking but did not abrogate it completely, and it also did not fully disrupt the capacity of the SLAIN2 C-terminus to bind to EBs (Chapter 3 and our unpublished data). This indicates that additional weak EB-interacting sites, which do not match the SxIP consensus are present in the C-terminal part of SLAIN2. The high affinity of SLAIN2 for EB1 might reflect the importance of accumulating SLAINs at the plus ends as a +TIP “glue” required for recruitment of the MT polymerase ch-TOG to MT tips.

#### Dimerization and multimerization

Another common feature of +TIPs, which contributes to their affinity for MT plus ends, is their capacity to dimerize and thus increasing the local concentration of EB binding sites. SLAIN1 and SLAIN2 both contain an N-terminal  $\alpha$ -helical region, which in case of SLAIN2 has been shown to be capable of folding into a dimeric coiled-coil structure (Chapter 3 and Figure 1). Based on the high sequence similarity between SLAIN1 and SLAIN2 in the first part of the N-terminus, it is possible that when the two SLAINs are co-expressed, not only homo- but also heterodimers could be formed. Dimerization of SLAINs is not necessary for plus-end tracking and EB binding as monomeric C-terminal SLAIN2 fragments still had a high affinity for EBs in GST pull down assays and showed robust plus-end tracking in live cell imaging experiments (Chapter 3). Along similar lines, dimer formation is also not required for the plus end accumulation of the EBs however, dimerization does make EBs more efficient plus-end trackers (Komarova et al., 2009). The same could be envisioned for SLAIN1/2 dimers.

Most other known +TIPs, such as CLIPs and MCAK are also dimers, although there are exceptions, such as CLASPs, which are monomers (Drabek et al., 2006). Importantly, while dimerization improves plus-end tracking behaviour, formation of higher order multimers can inhibit it, as we have shown for the transmembrane +TIP STIM1 (Chapter 2). After  $\text{Ca}^{2+}$  depletion from the endoplasmic reticulum (ER) STIM1 oligomerizes and this abrogates its plus-end tracking capacity. This is not because of disrupted EB1 binding, but is likely due to reduced diffusion rate in the membrane, as +TIPs need to diffuse in order to accumulate at the growing MT plus ends (Dragestein et al., 2008).

#### Redundant interactions as the building principle of +TIP networks

Most, if not all, identified +TIPs can track the growing MT ends through their association with EBs. All EB-dependent hitchhiking is mediated by the C-terminal region of EBs, for which numerous +TIPs have to compete. To reduce the competition and increase access to the MT tips, many +TIPs employ indirect, secondary means of accumulating at MT plus ends by associating with other

+TIPs besides EBs.

SLAINs interact not only with EBs, but also with three other +TIP families, CLIPs, CLASPs and ch-TOG. SLAINs utilize different properties to bind to these proteins, and thus their interactions with different +TIPs are not mutually exclusive. SLAIN2 (and most likely SLAIN1) form dimers through their N-terminus, and this region also interacts with ch-TOG. CLASPs bind to an undefined part of the SLAIN2 C-terminus (independently from EBs and CLIP-170) and CLIPs bind to the outmost C-terminal tail of SLAINs with its conserved tyrosine and tryptophan residues (Figure 1). SLAIN targeting to the growing MT tip would require at least one molecule of the SLAIN dimer to be associated with EB. The EB-SLAIN interaction would not necessarily preclude the binding of the same molecule to CLIP, because only the last ~10 amino acids of the SLAIN2 C-terminus are required for the association with CLIP, leaving the rest of the SLAIN C-terminus with its multiple SxIP-like motifs available for binding to EB. At the same time, the other half of the dimer might be free to associate with CLIP and/or CLASP. Currently, it is unknown if one SLAIN molecule can associate simultaneously with CLIP and CLASP as the SLAIN binding site for CLASP has not yet been unravelled. Given that CLIPs can also associate with CLASPs (Akhmanova et al., 2001), and that both of these +TIP families can directly bind to EBs (Komarova et al., 2005; Mimori-Kiyosue et al., 2005), a complex interaction network with multiple redundant nodes emerges from these studies. Most of the individual interactions within this network are of low affinity, a property that is important to ensure its “tracking” behaviour – rapid assembly and remodelling that enables these proteins to transiently concentrate at the polymerizing MT end.

#### Regulation and function of SLAIN interactions with other +TIPs

In interphase cells, SLAIN2 is strongly accumulated at MT plus ends in an EB-dependent manner. The localization of SLAIN to MT tips is necessary for the subsequent recruitment of ch-TOG. In Chapter 3, we have provided evidence suggesting that the triple EB-SLAIN2-ch-TOG complex is required for maintaining interphase MT dynamics by promoting persistent MT growth and suppressing catastrophes. As cells enter mitosis this complex is disrupted. Overexpression of the dominant negative SLAIN1/2 fragment in interphase cells is phenotypically similar to knockdown of SLAIN2 or ch-TOG; it results in more dynamic interphase MTs. Since MTs become more dynamic in mitosis (Saxton et al., 1984; Wittmann et al., 2001), disruption of the EB-SLAIN2-ch-TOG complex could, at least in part, contribute to this change when cells enter into mitosis (Figure 2).

How is the EB-SLAIN2-ch-TOG complex disrupted? SLAIN2 from mitotic extracts shows a strongly reduced mobility on SDS-PAGE gels (Chapter 3). The ~30 kDa increase in molecular weight can be attributed to phosphorylation. This is confirmed by both dephosphorylation experiments with lambda phosphatase as well as by mass spectrometry analysis. Using the latter method, 13 phosphorylated serines were detected in SLAIN2 isolated from mitotic cells; importantly, only ~50% of the protein was analysed in this experiment, and therefore additional phosphorylation sites are likely to exist in SLAIN2. The phosphorylation of many microtubule associated proteins (MAPs), including +TIPs, by mitotic kinases such as cyclin dependent kinase (CDK1)/cyclin B1, has been associated with mitosis-specific change of MT dynamics (Hong et al., 2009; Larsson et al.,

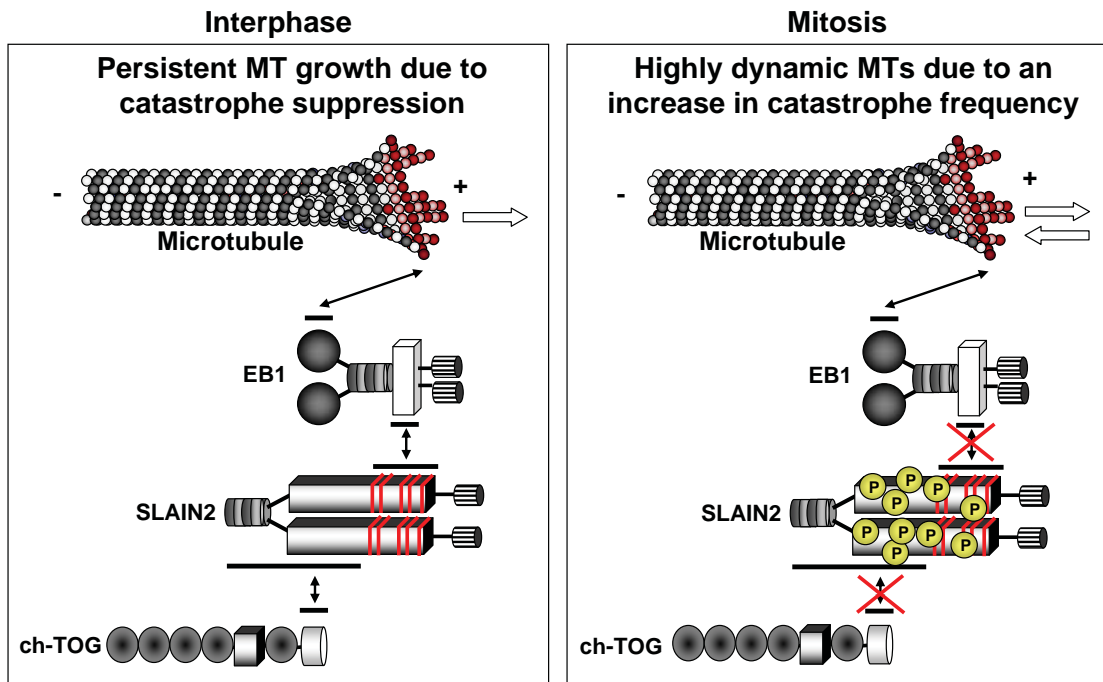


**Figure 2. EB-SLAIN2-ch-TOG complex in interphase and mitosis**

Growing MTs in interphase cells accumulate EB1 at their plus ends through a direct association of EBs with the MT tips. SLAIN2 is recruited to MT plus ends by associating with the EB C-terminus through the SxIP-like and additional proline-rich motifs. SLAIN2 in turn helps to accumulate ch-TOG at the MT plus ends by binding with its N-terminal region to the ch-TOG C-terminus. The EB-SLAIN2-ch-TOG complex promotes persistent MT growth by suppressing catastrophes. As cells enter mitosis, the triple complex is disrupted by the hyperphosphorylation of SLAIN2 by mitotic kinases such as CDK1. The increased dynamics of MTs in mitosis by the increased catastrophe rate could be in part explained by the disruption of the EB-SLAIN2-ch-TOG complex.

1995; Vasquez et al., 1999; Yang et al., 2009). SLAINs also contain many minor and major CDK1 consensus sites (Figure 1) and among the 13 identified phosphorylated serines in SLAIN2, 7 fit the CDK1 consensus. The other 5 identified phosphorylated serines are distinct from the CDK1 consensus, implicating additional, unidentified kinases in the phosphoregulation of SLAIN2.

Besides phosphorylation other posttranslational modifications such as sumoylation or (mono- and/or poly-) ubiquitination might also contribute to the molecular weight shift of SLAIN2 in mitosis. In line with this idea, two sumoylation consensus motifs ( $\Psi$ -K-x-D/E where  $\Psi$  is where  $\psi$  is Val, Leu, Ile, Phe, or Met, K is the lysine conjugated to SUMO, x is any amino acid) (Matic et al., 2008) are present in SLAIN2 (VKNE and MKDD), but not in SLAIN1 (Figure 1).

Could the large change in electrophoretic mobility of SLAIN2 in mitosis be due to sumoylation or ubiquitination? This possibility is attractive, because of the relatively large size of SUMO and ubiquitin proteins. However, this change could be fully reversed by lambda phosphatase treatment which argues against such a possibility. Still, sumoylation can be very unstable, so we cannot completely exclude that it would be lost during the lambda phosphatase treatment. In conclusion, it remains to be determined if SLAIN2 is indeed a target of sumoylation or any other posttranslational modifications in addition to phosphorylation.

Interestingly, SLAIN2 protein levels seem to be elevated in mitosis (Chapter 3). The

potential function of these increased levels is currently unknown, but it is possible that SLAINs play a role in mitosis by associating with other interaction partners besides +TIPs. This role is unlikely to be essential because the knockdown of SLAIN2 does not induce mitotic phenotypes or a cell-cycle arrest. Alternatively, SLAIN2 levels might be increased during mitosis in preparation for mitotic exit: in telophase SLAIN2 is released from its inhibited state by the dephosphorylating action of phosphatases, and the high concentration of SLAIN might be needed to re-establish interphase MT dynamics. This could explain why SLAIN2 is not degraded in mitosis but is instead retained in an inactive state so that it can quickly switch back to plus-end tracking during mitotic exit and help to promote the transition from mitotic to interphase MT dynamics.

The disruption of the EB-SLAIN2 complex in mitosis is probably due to the altered charge of the protein sequence surrounding SxIP-(like)-motifs upon phosphorylation, a common means of regulating the association of +TIPs and MAPs with the negatively charged MTs (Honnappa et al., 2009). How the increased phosphorylation status of the SLAIN2 N-terminus interferes with its ch-TOG-binding activity remains to be determined. Our efforts to narrow down the binding region of SLAIN2 to ch-TOG were unsuccessful, which made it difficult to dissect the involvement of phosphorylation in controlling of this interaction (Chapter 3). The phosphorylation status of mitotic ch-TOG could also provide an extra level of regulation. ch-TOG/XMAP215 family members are phospho-proteins: XMAP215 and its fission yeast homologue Dis1 are phosphorylated during mitosis by CDK1/CDC2 (Aoki et al., 2006; Vasquez et al., 1999). *In vitro* experiments indicate that phosphorylated XMAP215 showed a 50% reduction of its capacity to stimulate MT plus end elongation, whereas Dis1 phosphorylation by CDC2 is important for accurate chromosome segregation (Aoki et al., 2006; Vasquez et al., 1999). Interestingly, XMAP215, DdCP224, ch-TOG and to a lesser extent *A. thaliana* XMAP215 homologue and *Drosophila* Msps contain in their C-terminal regions a KXGS-motif which in other MAPs has been shown to be important for MT binding (Chapin and Bulinski, 1992; Drewes et al., 1997; Popov et al., 2001). This motif in Tau2, MAP4 and MAP2b is under phospho-control by MARKs (MAP/microtubule affinity regulating kinases) and phosphorylation reduces the affinity of these MAPs for the MT lattice (Ebner et al., 1999; Trinczek et al., 1995). It remains to be determined if the mammalian ch-TOG is also phosphorylated in the KXGS and/or other sites and how this interferes with SLAIN binding. The high conservation of the XMAP215 family and the large number of serine and threonine residues in mammalian ch-TOG suggest that it is a likely target of multiple kinases.

It has always been assumed that ch-TOG associates with MT plus ends not only in interphase, but also in mitosis however, this has not been shown convincingly. To date, only images of fixed mitotic cells labeled for ch-TOG have been published (Cassimeris and Morabito, 2004; Gergely et al., 2003). These images show that ch-TOG strongly associates with the spindle poles and the MT lattice of the spindle, but no convincing co-localization of ch-TOG with EBs at MT tips has been demonstrated.

Strikingly, in HeLa cells depleted of ch-TOG only a small reduction in MT spindle length and density has been observed indicating that ch-TOG is not a major player in regulating MT assembly in mitotic cells (Cassimeris et al., 2009; Cassimeris and Morabito, 2004); this would

correlate with the absence of MT tip-associated ch-TOG. Instead, in mitosis ch-TOG appears to strongly contribute to spindle bipolarity, which is in agreement with its presence at spindle poles and along the spindle MTs. It is possible that the disruption of the SLAIN and ch-TOG interaction in mitosis inhibits ch-TOG accumulation at MT plus ends, favoring the centrosomal and spindle localization of ch-TOG and promoting its role in spindle pole organization.

The inability of SLAIN2 to track growing MT ends in mitosis suggests that not only its interaction with EBs and ch-TOG is disrupted, but that it also no longer binds to CLIPs and CLASPs. Whether this is caused by the phosphorylation of SLAIN2 alone remains to be determined. Preliminary GST-pull down experiments using GST-CLIP-170 N-terminus and GFP-SLAIN2 from mitotic extracts indicate that phosphorylated SLAIN2 can still bind to the CAP-Gly domains of CLIP-170 (our unpublished data). However, it is still possible that the interaction is controlled in mitosis by the phosphorylation of CLIP-170, which is a known target of several mitotic kinases (Li et al., 2010; Yang et al., 2009).

In interphase cells, a significant pool of CLIP-170 is thought to be present in a folded back conformation (Lansbergen et al., 2004; Lee et al., 2010). The formation of the auto-inhibitory loop blocks the SLAIN-binding site in CLIP-170, explaining why endogenous CLIP-170 binds poorly to SLAIN2 in GST pull down and co-IP experiments (Chapter 3). The interaction between SLAINs and CLIP-170 requires an open CLIP-170 conformation, a process that is under tight phosphorylation-dependent control (Lee et al., 2010), and this might be a means to fine-tune the SLAIN-CLIP-170 interaction depending on the cell cycle, cellular or developmental process and subcellular localization.

Interestingly, CLIP-115 does not form an auto-inhibitory loop as it lacks the C-terminal zinc fingers and the EEY/F-like domain, and therefore the SLAIN-CLIP-115 interaction cannot be controlled by auto-inhibition (Lansbergen et al., 2004). This suggests that in the brain, where both CLIP-115 and SLAINs are enriched, the SLAIN-CLIP-115 interactions might be more unrestricted and this could reflect a specific, currently unknown, role for this complex in regulating MT dynamics in neuronal cells. It should be noted that it is unlikely that CLIP-115 is important for targeting the MT-growth promoting SLAIN2-ch-TOG complex to MT plus ends in neurons, because MTs grow faster, and not slower in hippocampal neurons lacking CLIP-115 (Stepanova et al., 2010).

What could be the role of the CLIP-SLAIN interaction, besides reducing competition levels? CLIPs influence MT dynamics by acting as rescue factors. The depletion of SLAIN2, but not ch-TOG from HeLa cells, results in an increase in the number of MT rescues (Chapter 3) and this might be related to the capacity of SLAINs to bind to CLIPs. However, it remains to be determined how exactly SLAIN can influence the MT rescue frequency, especially as it is still unclear how CLIP, which bind to polymerizing rather than shortening MT ends, can help to convert shrinking MTs to growing ones.

The interaction of CLIP-170 with  $\alpha$ -tubulin depends on the presence of the C-terminal tyrosine, which is under the control of modifying enzymes that can remove it (an unknown carboxypeptidase) or add it back (TTL; tubulin tyrosine ligase) (Arce et al., 1975; Argarana et al., 1977; Barra et al., 1973). Similarly, the interaction of EBs and the CAP-Gly domains of CLIPs

depends on the C-terminal tyrosine of EBs. So far, there are no strong indications that this tyrosine residue of EBs can be removed, and the EB mutants lacking this amino acid do not seem to be targeted by a tyrosine ligase (Komarova et al., 2005). Also for SLAINs, there are no indications that they can be substrates for tyrosine-modifying enzymes.

SLAINs are “scaffolding” proteins that provide a platform of binding sites for multiple MT plus end-associated proteins. Interestingly, while the C-terminus of SLAIN2 specifically binds to the CAP-Gly domains of CLIP-170, it has a very low affinity for the CAP-Gly domain of the dynein subunit p150<sup>Glued</sup>. Structural studies of the complex of the CLIP CAP-Gly domain with the C-terminal peptide of SLAIN2 uncovered a highly conserved tryptophan residue of SLAIN2 as a crucial specificity determinant for binding to CLIP and not to p150<sup>Glued</sup> (Chapter 3). The lack of SLAIN-p150<sup>Glued</sup> binding might be important for controlling the levels of dynein/dynein that is recruited to the MT plus ends. Excessive recruitment of p150<sup>Glued</sup> to MT tips by CLIP-170 has been shown to cause a significant delay in the reassembly of the Golgi apparatus after nocodazole-induced fragmentation, suggesting a defect in the kinetics of MT minus end directed membrane transport (Lee et al., 2010). Therefore, the low affinity of SLAIN for p150<sup>Glued</sup> might restrict the access of the highly abundant dynein complex to MT tips. This is in line with the fact that dynein recruitment to the growing MT ends critically depends on CLIP-170 (Lansbergen et al., 2004).

### Regulation in time and space

The dynamics of the MT network can vary depending on the cell type, subcellular localization and the specific time during the cell cycle or a developmental process. For example, mitotic MTs are much more dynamic than interphase ones; during mitosis MT turnover increases 18-fold (Saxton et al., 1984), which is essential for proper chromosome segregation. Above, we have already discussed how SLAINs can be controlled during the cell cycle.

In neuronal cells MT dynamics is differentially regulated in different parts of the cell: MTs are mostly stabilized in the shafts of the axon and dendrites, but remain highly dynamic in the growth cones. Another example of specific MT behaviour can be found in migrating cells, in which many MTs are oriented towards the leading edge of the cell where they can be stabilized by cortical attachment.

One means of changing MT dynamics is by altering the composition of the protein complexes at MT ends by excluding or promoting certain +TIPs from binding. In addition, MT nucleation and binding of MAPs along the MT lattice can also affect the formation of the MT network. Below, we discuss some examples of MT-related functions in which SLAINs might play a role.

### *MT nucleation*

Besides the association with growing MT plus ends, SLAIN2 and ch-TOG are also strongly enriched at the centrosome of interphase cells (Chapter 3). The recruitment of ch-TOG to centrosomes is mediated by its C-terminus (Popov et al., 2001) and does not depend on MTs (Cassimeris and



Morabito, 2004). As already mentioned, the C-terminus of ch-TOG contains a KXGS-motif that might be phospho-regulated. The mutation of the KKIGSK motif in XMAP215 showed a clear reduction of centrosomal targeting, suggesting that the association of ch-TOG with centrosomes can be regulated through phosphorylation by MARK kinases (Popov et al., 2001).

In some organisms, the C-terminus of XMAP215/ch-TOG homologues has been shown to interact with transforming acidic coiled-coil (TACC) proteins (Lee et al., 2001). Therefore, it was suggested that ch-TOG associates with centrosomes by interacting with TACCs (Figure 3). TACCs are highly acidic proteins conserved from yeast to mammals; they play essential roles in regulating MT dynamics and centrosome function during cell division (Peset and Vernos, 2008). In mammals, there are three TACC proteins, TACC1, -2 and -3. In mitosis, all TACC proteins are present in the centrosomal region, a localization dependent on the TTK kinase activity and, at least in *Drosophila*, on phosphorylation by Aurora A, but not on the presence of MTs (Barros et al., 2005; Dou et al., 2004; Giet et al., 2002; Kinoshita et al., 2005).

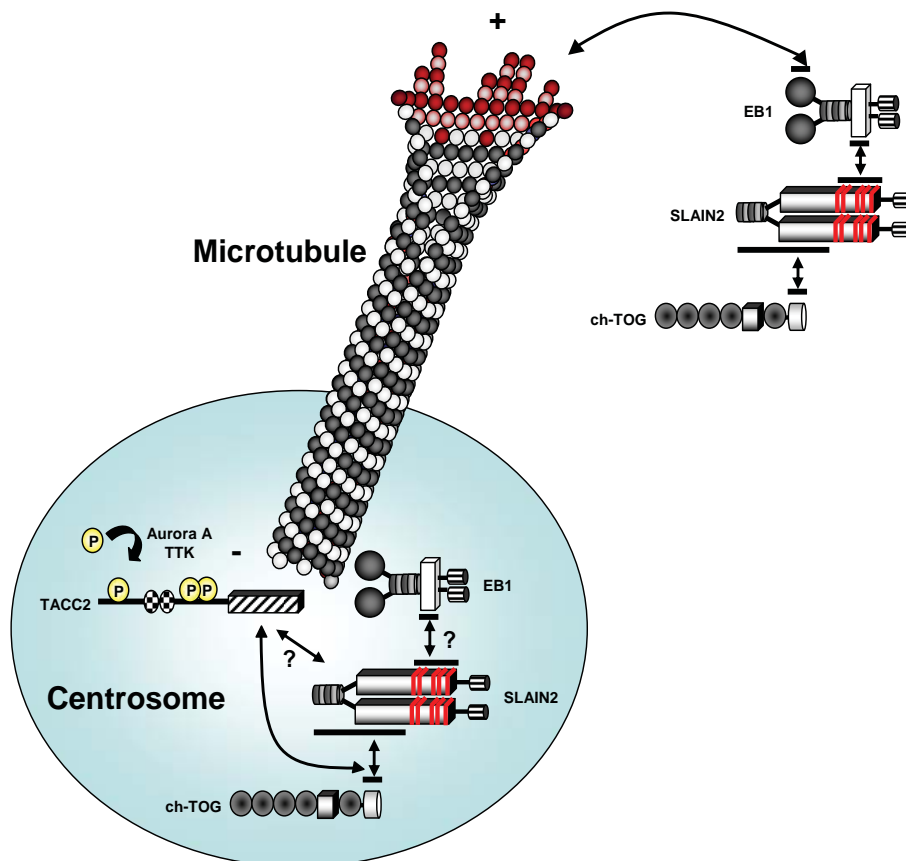


**Figure 3. Targeting of ch-TOG and SLAIN2 to centrosomes**

In interphase cells, both ch-TOG and SLAIN2 are accumulated at centrosomes. In case of ch-TOG this localization is independent from EBs, but is probably mediated by the interaction of the ch-TOG C-terminus with the C-terminus of the centrosomal protein TACC2, whose localization is thought to be regulated by Aurora A and TTK phosphorylation (Giet et al., 2002) (Dou et al., 2004). The centrosomal localization of SLAIN2 is possibly dependent on its interaction with the EB- or ch-TOG C-termini. However, a direct interaction with TACC2 cannot be excluded either, as TACC2 peptides were found in mass spectrometry analysis of streptavidin pull down of both SLAIN1 and SLAIN2 (see Chapter 3).

In interphase cells, both TACC1 and 3 are nuclear whereas TACC2 is localized to the centrosome and might be responsible for ch-TOG localization to this subcellular site (Gergely et al., 2000). Centrosome localization of ch-TOG does not require EBs, because ch-TOG is still present at the centrosome in EB1/3 depleted cells (Chapter 3). This is in line with the results from *Xenopus* cell extracts depleted of EB1, where XMAP215 could still be found associated with spindle poles, although to a slightly lesser extent (Kronja et al., 2009).

How are SLAIN proteins targeted to the centrosome? One possibility is that SLAINs are EB-dependent centrosomal proteins (Figure 3). Alternatively, SLAINs could bind to centrosomes by forming a complex with ch-TOG and TACC2. In line with this idea, TACC2 was found among the potential SLAIN binding partners in our mass spectrometry experiments (Chapter 3).

By using live imaging in CHO cells, we observed a defect in MT outgrowth from the centrosome in SLAIN2 and ch-TOG depleted cells, suggesting a role in MT nucleation. Furthermore, the MT network in cells where the SLAIN2-ch-TOG complex was disrupted showed a delayed recovery after depolymerization by nocodazole (Chapter 3). However, we cannot completely exclude that these phenotypes are related to defects in MT growth rather than MT nucleation, and additional experiments are needed to address this issue.

#### *SLAIN function in neuronal cells*

The brain is an organ with a high concentration of tubulin compared to other tissues. The MT network in neurons is of great importance for the proper functioning of the brain as reflected by the large number of neurological and neurodevelopmental disorders caused by abnormalities in the MT cytoskeleton due to mutations in genes encoding different MAPs (e.g. Tau, CLIPs, LIS1, Doublecortin (Dcx), APC, p150Glued) (Cahana et al., 2001; Dijkmans et al., 2010; Hoogenraad et al., 2004; Lim and Lu, 2005; Senda et al., 2005).

XMAP215/ch-TOG is the only vertebrate protein known to be able to strongly promote MT polymerization (Howard and Hyman, 2009). This fact, together with the observations that tubulin levels are extremely high in neurons and that both SLAIN1 and SLAIN2 are expressed in the brain, made it interesting to investigate the role of the SLAIN-ch-TOG complex in neuronal development (Chapter 4). We found that disruption of the SLAIN-ch-TOG complex affected neurite extension indicating a role of this complex in neuritogenesis. In fixed neuronal cells, SLAIN and ch-TOG appear to be enriched in the axonal growth cones suggesting a role for the complex in growth cone extension and/or pathfinding. This could possibly be related to the capability of SLAINs to bind to CLIPs and CLASPs, because both CLIPs and CLASPs are abundantly present in growth cones where they regulate MT extension into actin-rich protrusions (Lee et al., 2004; Neukirchen and Bradke, 2011), a process which is crucial for the growth cone dynamics (Poulain and Sobel, 2010). Live cell imaging showed that when the SLAIN-ch-TOG complex was disrupted in neurons by the overexpression of the dominant negative SLAIN2 fragment, MT growth was inhibited in the same way as in multiple different cell lines (Chapter 4). In agreement with this observation, depletion or disruption of the SLAIN2-ch-TOG complex resulted in a reduced number of EB1 comets in fixed neurons. It seems likely that MT polymerization defects in neurons lacking the SLAIN-ch-TOG

complex cause a less efficient MT extension in the growth cones, and, as a result, slower neurite extension, in line with the view that MT dynamics can directly affect cell length (Picone et al., 2010).

### **Regulation of the cortical MT attachment complex**

Interaction partners of +TIPs are not per definition also plus-end tracking proteins even if they can strongly associate with MT ends. Many +TIP interaction partners function in either nucleation of MTs (e.g. centrosomal proteins) or in attachment of MT tips to organelles or other intracellular structures (e.g. kinetochores, the cell cortex, cell-cell and cell-matrix contacts). This is illustrated by the cortically localized CLASP interaction partner LL5 $\beta$ : CLASP and LL5 $\beta$  directly bind to each other but LL5 $\beta$  does not track growing MT ends (Lansbergen et al., 2006). Although LL5 $\beta$  is a cytoplasmic protein, its stable association with the plasma membrane prevents its diffusion and thus precludes any plus-end tracking behaviour.

The attachment of MTs to the cell cortex not only depends on CLASPs and LL5 $\beta$  but also on other +TIPs, such as MACF/ACF7 (Drabek et al., 2006; Lansbergen et al., 2006), as well as additional cortical factors. The use of pull down experiments combined with mass spectrometry analysis has proven to be an effective strategy for the identification of cortical complex components. In Chapter 5 we identified liprin- $\alpha$ 1 and liprin- $\beta$ 1 as two upstream regulatory proteins of the cortical MT tip attachment network.

An important unanswered question that emerged from this study is how liprin proteins are organized at the cell cortex. A direct interaction of liprin- $\alpha$ 1/ $\beta$ 1 with membrane lipids might potentially target them to the plasma membrane however, no such interactions have been identified. Alternatively, liprin- $\alpha$ 1/ $\beta$ 1 might associate with some other cortical proteins. Hints on the nature of such proteins were provided by a mass spectrometry-based search for liprin partners. Immunoprecipitation of liprin- $\alpha$ 1/ $\beta$ 1 performed using RIPA lysis buffer in order to increase the solubility of membrane-associated proteins identified septins as potential liprin-interacting proteins. Septins are GTP-binding proteins that form hexameric assemblies and arrange into cytoskeletal filaments (Peterson and Petty, 2010; Spiliotis, 2010). They control many different cellular functions all of which are thought to be the result of their role in providing cortical rigidity. Preliminary protein localization studies, knockdowns and endogenous immunoprecipitations hint to a possible role of septin-mediated recruitment of liprin proteins to the cell edge (unpublished data). The reported roles of septins in controlling MT dynamics are in line with these findings (Spiliotis, 2010). Future experiments are needed to determine the exact relationship between liprin- $\alpha$ 1/ $\beta$ 1 and septins and their function in organizing cortical MT attachment sites and in regulating MT dynamics.

Dissecting the order of protein interactions at the cortex is key for understanding how the cortical patches of liprin- $\alpha$ 1/ $\beta$ 1 and LL5 $\beta$  are formed. The insoluble nature of many of the plasma membrane-associated proteins makes it difficult to show endogenous interactions by co-IP experiments and thus it has been challenging to uncover the protein interaction hierarchy. Another challenge lies in the structure of the proteins; many of them, like liprin- $\alpha$ 1/ $\beta$ 1 and

septins, function as multimers (Serra-Pages et al., 1998; Spiliotis, 2010). Multimerization of various structurally related subunits makes it difficult to define direct interactions and provides a source of functional redundancies, which necessitates double or even triple knockdowns in order to decipher protein interactions and functions. In addition, the complex structure of the proteins does not allow for overexpression studies or the use of deletion mutants, as proteins fragments often fail to fold properly making them useless for interaction mapping.

Another important question concerns the interplay between mechanical forces and biochemical regulators of MT dynamics at the cell cortex. For example, do MTs undergo catastrophes at the cell margin because the pushing force of their interaction with an obstacle (cortical cytoskeleton) is sufficient to induce a catastrophe? Or does the presence of specific cortical proteins actively induce MT destabilization or restrict MT growth? Our studies showed that liprin proteins promote clustering of positive regulators of MT polymerization, such as ACF7, as well as LL5 $\beta$  and ELKS, the factors acting upstream of CLASPs which are MT rescue factors. The activity of all these factors increases MT density and stability (Lansbergen et al., 2006; Mimori-Kiyosue et al., 2005). However, another component of the same cortical complex, KIF21A, seems to restrict MT growth at the cell periphery, because the depletion of KIF21A causes disorganization of cortical MTs resulting in MT buckling and excessive MT growth parallel to the plasma membrane (Chapter 5).

The cortical accumulation of KIF21A is dependent on liprin- $\beta$ 1 as the knockdown of this liprin reduced cortical accumulation of KIF21A. However, KIF21A does not seem to bind to liprin- $\alpha$ 1/ $\beta$ 1 directly but seems to be linked to them through the actin regulator KANK2 (Chapter 5, (Kakinuma and Kiyama, 2009)). Importantly, additional protein localization and depletion studies are needed to establish whether this hierarchy of interactions is indeed correct. In addition, the C-terminal WD-40 repeat region of KIF21A might also contribute to its cortical localization as it has been reported to have a significant affinity for acidic phospho lipids (Tsujita et al., 2010).

How does KIF21A control MT dynamics at the cell cortex? Two mechanisms could be proposed: first, KIF21A acts as a catastrophe factor that initiates MT depolymerization as soon as a MT hits the KIF21A-rich cell cortex. Second, KIF21A might regulate MTs by inhibiting their growth. This latter explanation seems more likely as the KIF21A family member Xklp1 has recently been shown to employ this mechanism to control MT overlap at the spindle midzone (Bieling et al., 2010).

The phenotype observed in HeLa cells depleted of KIF21A is reminiscent of the MT dynamics phenotype observed in cultured glial cells from Kif2A mutant mice (Homma et al., 2003). Kif2A belongs to the kinesin-13 family of MT depolymerases (including Kif2B and Kif2C (MCAK)) and it is thought that Kif2A suppresses growth cone advances in collateral branches by its MT-depolymerizing activity thereby promoting the arrival of the primary axons to their correct targets. Excessive cortical MT extension reminiscent of Kif2A and KIF21A knockout and knockdown phenotypes respectively, was also observed in the motile *Drosophila* D17 depleted of the MT severing enzyme katanin (Zhang et al., 2011). In D17 cells, depletion of katanin resulted in faster and more persistent, albeit less directional cell migration. This defect could be explained

by excessive MT-dependent stimulation of the small GTPase Rac at the leading edge of the cell, favouring formation and extension of cell protrusions. Similar to Kif2A, katanin appears to modulate cell migration by fine-tuning MT dynamics at the leading edge, which in turn is important for controlling actin-dependent cell protrusion. A similar mechanism could be envisioned for KIF21A: by controlling MT growth at the cortex, KIF21A could help to promote axonal pathfinding and thus direct the axons of oculomotor nerves to their correct target sites at the extraocular muscles (Figure 4). Mutation of KIF21A would cause MT disorganization at the cortex of axonal growth cones and this might give rise to abnormal axonal extension and the inability to find the target muscles. As a result, lack of proper innervation leads to fibrosis of the muscles that control certain aspects of eye movement. The role of KIF21A in controlling MT dynamics is in line with the recent data on CFEOM3, a genetic syndrome related to CFEOM1 where different heterozygous missense mutations in the human  $\beta$ -tubulin III (*TUBB3*) gene have been associated which increased MT stability and disrupted kinesin binding (Tischfield et al., 2010).

It remains to be determined how mutations in the coiled-coil region of KIF21A could be responsible for MT regulation defects, especially as the cortical localization of the mutant coil was not affected (Chapter 5) and its binding to KANK2 was even reported to be increased (Kakinuma and Kiyama, 2009). Possible explanation could be in the altered interplay between the actin and MT cytoskeleton in the growth cones of CFEOM1 patients (Figure 4). The interplay between the actin and MT networks is important in growth cone extension and turning (Conde and Caceres, 2009; Poulain and Sobel, 2010). KANK proteins as known effectors of actin polymerization could play important roles in these processes (Kakinuma et al., 2009).

In conclusion, liprin proteins are localized at the cell cortex, possibly via septins, and their presence is critical for the accumulation of other cortical proteins and the regulation of MT dynamics by providing cortical attachment sites but also by restricting MT growth. KIF21A is a part of the cortical complex, and the depletion of KIF21A results in disorganization of cortical MTs and excessive MT growth along the plasma membrane. These data provide new insights into the molecular mechanisms contributing to CFEOM1 syndrome.

### Future directions

With each newly identified +TIP the complexity of regulatory processes controlling MT dynamics seems to increase, making it more and more difficult to pinpoint the role of individual +TIPs in the cellular context. Therefore, the development of an *in vitro* MT plus end tracking assay that makes it possible to use purified proteins in an *in vitro* MT polymerization setting is a very important advance in the MT field (Bieling et al., 2007). *In vitro* experiments greatly contribute to elucidating +TIP behaviour and their role in the regulation of MT dynamics. They also make it possible to study the effects of cytostatics on MT dynamics, the hierarchy of protein interactions at the MT plus ends, and to perform detailed kinetic analysis of the protein association with the growing MT ends. The field is currently evolving towards *in vitro* reconstitution of more complex cellular behaviours. For example, it would be interesting to investigate whether the interaction of EB1-decorated MT tips with the transmembrane protein STIM1 is sufficient to cause membrane tubule

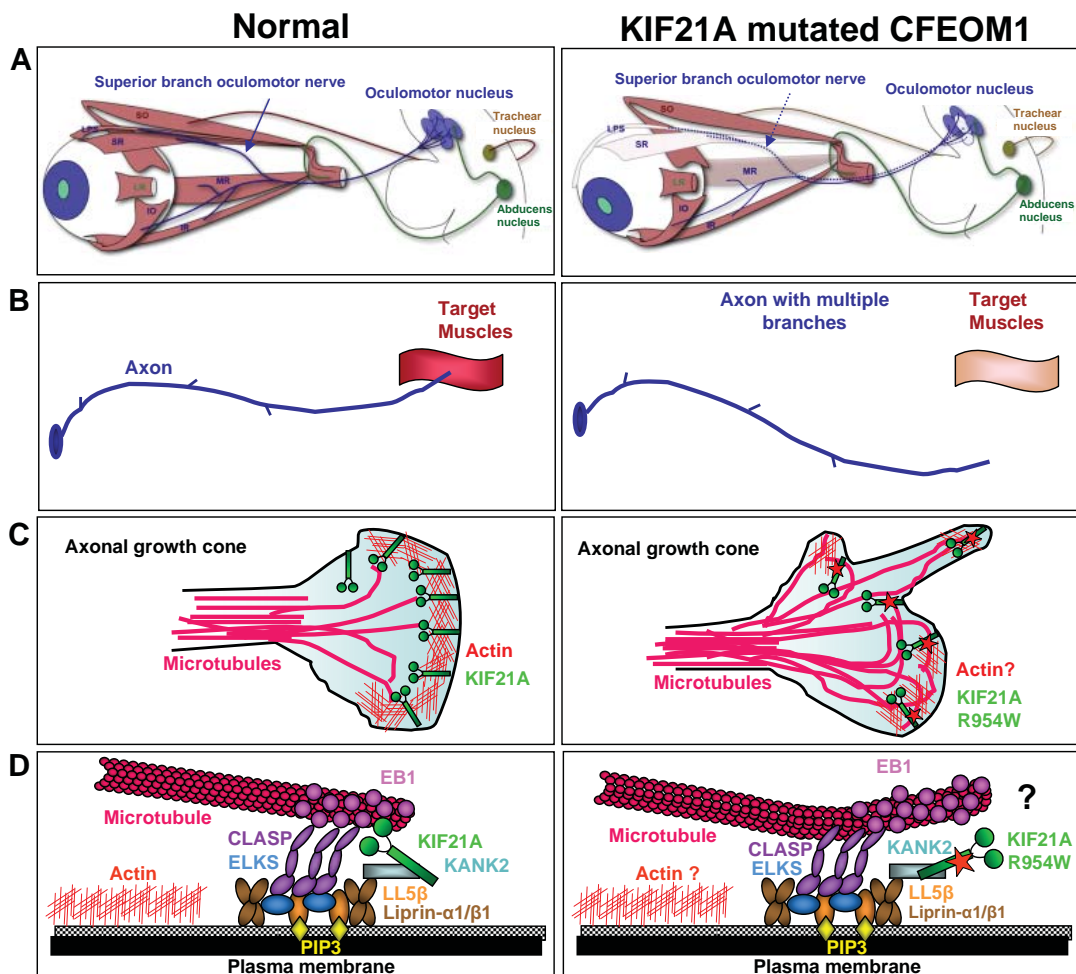


**Figure 4. Role of KIF21A in CFEOM1**

Congenital fibrosis of the extraocular muscle type I (CFEOM1) is caused by heterozygous mutations in the coiled coil region of KIF21A. (A) Normally, the oculomotor nucleus is located in the midbrain of the brainstem and its nerve (cranial nerve III) branches into an inferior and superior branch after exiting the brainstem. The superior branch innervates the levator palpebrae superioris (LPS, eyelid muscle) and superior rectus (SR, the eye muscle that pulls the eyeball upwards). In case of CFEOM1, the superior division of cranial nerve III is absent or underdeveloped (dotted lines). The motor neurons in the midbrain subnuclei whose axons make up the superior division of cranial nerve III are absent (depicted as absence of black outline of the tiny midbrain cranial nerve III subnuclei). The LPS and SR muscles that are normally innervated by the superior branch of cranial nerve III are abnormal or absent (as depicted by the lack of pink color). Dysfunction of the LPS results in bilateral ptosis (drooping of both upper eyelids), whereas dysfunction of the SR results in the downward fixation of the eyes and the inability to elevate the eye globe. These data indicate that CFEOM1 results from a neurogenic rather than a myopathic cause (picture adapted from (Tischfield et al., 2010))(Heidary et al., 2008). (B and C) The absence or underdevelopment of cranial nerve III superior division in CFEOM1 could be possibly similar to those seen in Kif2A deficient mice (Homma et al., 2003). This phenotype is caused by failure of the primary axons to extend to the target muscles. The formation of collateral branches might be caused by the unrestricted growth of MTs at the cortex of axonal growth cones. (D) MT overextension at the cortex is caused by defective KIF21A function. Although mutated KIF21A is still located at the cell cortex it is no longer able to control MT growth. It is possible that the interplay between MTs and actin is affected as the KIF21A interaction partner KANK2 is a known regulator of actin polymerization (Kakinuma and Kiyama, 2009; Kakinuma et al., 2009).

extension in *in vitro* experiments.

However useful the *in vitro* experiments are, it remains crucial to combine them with cellular localization studies, knockdown or knockout systems and biochemical approaches as not all aspects of protein *in vitro* activities fully reflect their physiological behaviour. This is nicely exemplified by XMAP215/ch-TOG family proteins: whereas purified XMAP215 is an autonomous +TIP *in vitro* (Brouhard et al., 2008), at least in some *in vivo* settings it requires the assistance of SLAIN proteins to accumulate at MT tips (Chapter 3).

When using a cellular approach to study +TIPs and their role in MT dynamics regulation and cell function it is important to carefully select the appropriate experimental set-up as not to omit any cellular activity; erroneous selection of a cell type or cell cycle stage could be the cause of overlooking critical experimental information. For example, the mitotic regulation of SLAIN2 plus-end tracking might have easily been missed, yet it is crucial for understanding all aspects of its cellular functions.

The use of model organisms to study MT regulation will also be of great help to uncover functional aspects of MT regulation. It is striking that to date no mouse models have been developed to study the function of ch-TOG. ch-TOG is the only known MT polymerase and a very important protein in promoting MT growth, as is reflected by its high conservation throughout eukaryotic evolution. Further, in spite of its important role in cells and its relatively large size (~250 kDa), only few ch-TOG binding proteins have been identified so far. These include tubulin, SLAIN, TACC, EBs, CDK1, ILK and the RNA trafficking protein hnRNP A2 (Aoki et al., 2006; Cassimeris and Morabito, 2004; Charrasse et al., 2000; Fielding et al., 2008; Kosturko et al., 2005; Kronja et al., 2009; Lee et al., 2001). This is in stark contrast to the high number of known interaction partners of the much smaller EB proteins. It seems likely that ch-TOG has additional partners that might be crucial for regulating its activity and thereby MT dynamics. These interaction partners will most probably include one or more kinases that can modulate ch-TOG function by phosphorylation.

Another development in the MT field has been the realization that not all +TIP interaction partners are in their turn also +TIPs even though they can indirectly associate with MT ends. Many proteins that fit into this category are important for the stabilization and attachment of MT tips to different organelles or the cell cortex. The identification of liprin proteins as upstream regulators of the cortical MT attachment complex is interesting, as these proteins were until recently mostly known in the neuronal field where they are involved in synapse formation. The overlap in composition of cortical MT attachment complexes and the synaptic cytomatrix at the active zone suggests that these structures might have a common evolutionary origin.

Also the identification of the KANK2-KIF21A complex as a novel cortical regulator of MT dynamics is of great importance, as it expands the number of factors controlling MT organization that are associated with human genetic diseases. It also illustrates how a defect in a widely expressed MT binding protein can specifically affect the development of a highly specialized subset of cells, such as oculomotor neurons. It would be interesting to reconstitute the activity of KIF21A, as well as other cortical MT regulators in an *in vitro* system. This might require the use of microfabricated chambers coated with certain proteins to mimic MT confinement within the cell

boundary (Holy et al., 1997; Romet-Lemonne et al., 2005).

In conclusion, the understanding of MT dynamics regulation by dissecting protein interaction networks at MT tips has been improved by the combination of genetic studies, cell biological approaches, structural biology as well as *in vitro* reconstitution and will continue to do so in future.

## References

- Akhmanova, A., C.C. Hoogenraad, K. Drabek, T. Stepanova, B. Dortland, T. Verkerk, W. Vermeulen, B.M. Burgering, C.I. De Zeeuw, F. Grosveld, and N. Galjart. 2001. Clasps are CLIP-115 and -170 associating proteins involved in the regional regulation of microtubule dynamics in motile fibroblasts. *Cell*. 104:923-35.
- Akhmanova, A., and M.O. Steinmetz. 2008. Tracking the ends: a dynamic protein network controls the fate of microtubule tips. *Nat Rev Mol Cell Biol*. 9:309-22.
- Aoki, K., Y. Nakaseko, K. Kinoshita, G. Goshima, and M. Yanagida. 2006. CDC2 phosphorylation of the fission yeast dis1 ensures accurate chromosome segregation. *Curr Biol*. 16:1627-35.
- Arce, C.A., J.A. Rodriguez, H.S. Barra, and R. Caputto. 1975. Incorporation of L-tyrosine, L-phenylalanine and L-3,4-dihydroxyphenylalanine as single units into rat brain tubulin. *Eur J Biochem*. 59:145-9.
- Argarana, C.E., C.A. Arce, H.S. Barra, and R. Caputto. 1977. In vivo incorporation of [<sup>14</sup>C]tyrosine into the C-terminal position of the alpha subunit of tubulin. *Arch Biochem Biophys*. 180:264-8.
- Barr, A.R., and F. Gergely. 2008. MCAK-independent functions of ch-Tog/XMAP215 in microtubule plus-end dynamics. *Mol Cell Biol*. 28:7199-211.
- Barra, H.S., J.A. Rodriguez, C.A. Arce, and R. Caputto. 1973. A soluble preparation from rat brain that incorporates into its own proteins ( 14 C)arginine by a ribonuclease-sensitive system and ( 14 C)tyrosine by a ribonuclease-insensitive system. *J Neurochem*. 20:97-108.
- Barros, T.P., K. Kinoshita, A.A. Hyman, and J.W. Raff. 2005. Aurora A activates D-TACC-Msps complexes exclusively at centrosomes to stabilize centrosomal microtubules. *J Cell Biol*. 170:1039-46.
- Bieling, P., S. Kandels-Lewis, I.A. Telley, J. van Dijk, C. Janke, and T. Surrey. 2008. CLIP-170 tracks growing microtubule ends by dynamically recognizing composite EB1/tubulin-binding sites. *J Cell Biol*. 183:1223-33.
- Bieling, P., L. Laan, H. Schek, E.L. Munteanu, L. Sandblad, M. Dogterom, D. Brunner, and T. Surrey. 2007. Reconstitution of a microtubule plus-end tracking system in vitro. *Nature*. 450:1100-5.
- Bieling, P., I.A. Telley, and T. Surrey. 2010. A minimal midzone protein module controls formation and length of antiparallel microtubule overlaps. *Cell*. 142:420-32.
- Brouhard, G.J., J.H. Stear, T.L. Noetzel, J. Al-Bassam, K. Kinoshita, S.C. Harrison, J. Howard, and A.A. Hyman. 2008. XMAP215 is a processive microtubule polymerase. *Cell*. 132:79-88.
- Cahana, A., T. Escamez, R.S. Nowakowski, N.L. Hayes, M. Giacobini, A. von Holst, O. Shmueli, T. Sapir, S.K. McConnell, W. Wurst, S. Martinez, and O. Reiner. 2001. Targeted mutagenesis of Lis1 disrupts cortical development and LIS1 homodimerization. *Proc Natl Acad Sci U S A*. 98:6429-34.
- Carvalho, P., J.S. Tirnauer, and D. Pellman. 2003. Surfing on microtubule ends. *Trends Cell Biol*. 13:229-37.
- Cassimeris, L., B. Becker, and B. Carney. 2009. TOGp regulates microtubule assembly and density during mitosis and contributes to chromosome directional instability. *Cell Motil Cytoskeleton*. 66:535-45.
- Cassimeris, L., and J. Morabito. 2004. TOGp, the human homolog of XMAP215/Dis1, is required for centrosome integrity, spindle pole organization, and bipolar spindle assembly. *Mol Biol Cell*. 15:1580-90.
- Chapin, S.J., and J.C. Bulinski. 1992. Microtubule stabilization by assembly-promoting microtubule-associated proteins: a repeat performance. *Cell Motil Cytoskeleton*. 23:236-43.
- Charrasse, S., T. Lorca, M. Doree, and C. Larroque. 2000. The Xenopus XMAP215 and its human homologue TOG proteins interact with cyclin B1 to target p34cdc2 to microtubules during mitosis. *Exp Cell Res*. 254:249-56.
- Conde, C., and A. Caceres. 2009. Microtubule assembly, organization and dynamics in axons and dendrites. *Nat Rev Neurosci*. 10:319-32.
- Dijkmans, T.F., L.W. van Hooijdonk, C.P. Fitzsimons, and E. Vreugdenhil. 2010. The doublecortin gene family and disorders of neuronal structure. *Cent Nerv Syst Agents Med Chem*. 10:32-46.
- Dou, Z., X. Ding, A. Zereshki, Y. Zhang, J. Zhang, F. Wang, J. Sun, H. Huang, and X. Yao. 2004. TTK kinase is essential for the centrosomal localization of TACC2. *FEBS Lett*. 572:51-6.
- Drabek, K., M. van Ham, T. Stepanova, K. Draegestein, R. van Horssen, C.L. Sayas, A. Akhmanova, T. Ten Hagen, R. Smits, R. Fodde, F. Grosveld, and N. Galjart. 2006. Role of CLASP2 in microtubule stabilization and the regulation of persistent motility. *Curr Biol*. 16:2259-64.
- Dragestein, K.A., W.A. van Cappellen, J. van Haren, G.D. Tsididis, A. Akhmanova, T.A. Knoch, F. Grosveld, and N. Galjart. 2008. Dynamic behavior of GFP-CLIP-170 reveals fast protein turnover on microtubule plus ends. *J Cell Biol*. 180:729-37.



- Drewes, G., A. Ebnet, U. Preuss, E.M. Mandelkow, and E. Mandelkow. 1997. MARK, a novel family of protein kinases that phosphorylate microtubule-associated proteins and trigger microtubule disruption. *Cell*. 89:297-308.
- Ebnet, A., G. Drewes, E.M. Mandelkow, and E. Mandelkow. 1999. Phosphorylation of MAP2c and MAP4 by MARK kinases leads to the destabilization of microtubules in cells. *Cell Motil Cytoskeleton*. 44:209-24.
- Fielding, A.B., I. Dobрева, P.C. McDonald, L.J. Foster, and S. Dedhar. 2008. Integrin-linked kinase localizes to the centrosome and regulates mitotic spindle organization. *J Cell Biol*. 180:681-9.
- Gergely, F., V.M. Draviam, and J.W. Raff. 2003. The ch-TOG/XMAP215 protein is essential for spindle pole organization in human somatic cells. *Genes Dev*. 17:336-41.
- Gergely, F., C. Karlsson, I. Still, J. Cowell, J. Kilmartin, and J.W. Raff. 2000. The TACC domain identifies a family of centrosomal proteins that can interact with microtubules. *Proc Natl Acad Sci U S A*. 97:14352-7.
- Giet, R., D. McLean, S. Descamps, M.J. Lee, J.W. Raff, C. Prigent, and D.M. Glover. 2002. Drosophila Aurora A kinase is required to localize D-TACC to centrosomes and to regulate astral microtubules. *J Cell Biol*. 156:437-51.
- Heidary, G., E.C. Engle, and D.G. Hunter. 2008. Congenital fibrosis of the extraocular muscles. *Semin Ophthalmol*. 23:3-8.
- Hirst, C.E., S.M. Lim, L.A. Pereira, R.A. Mayberry, E.G. Stanley, and A.G. Elefanty. 2010. Expression from a betageo gene trap in the Slain1 gene locus is predominantly associated with the developing nervous system. *Int J Dev Biol*. 54:1383-8.
- Hirst, C.E., E.S. Ng, L. Azzola, A.K. Voss, T. Thomas, E.G. Stanley, and A.G. Elefanty. 2006. Transcriptional profiling of mouse and human ES cells identifies SLAIN1, a novel stem cell gene. *Dev Biol*. 293:90-103.
- Holy, T.E., M. Dogterom, B. Yurke, and S. Leibler. 1997. Assembly and positioning of microtubule asters in microfabricated chambers. *Proc Natl Acad Sci U S A*. 94:6228-31.
- Homma, N., Y. Takei, Y. Tanaka, T. Nakata, S. Terada, M. Kikkawa, Y. Noda, and N. Hirokawa. 2003. Kinesin superfamily protein 2A (KIF2A) functions in suppression of collateral branch extension. *Cell*. 114:229-39.
- Hong, K.U., H.J. Kim, H.S. Kim, Y.S. Seong, K.M. Hong, C.D. Bae, and J. Park. 2009. Cdk1-cyclin B1-mediated phosphorylation of tumor-associated microtubule-associated protein/cytoskeleton-associated protein 2 in mitosis. *J Biol Chem*. 284:16501-12.
- Honnappa, S., S.M. Gouveia, A. Weisbrich, F.F. Damberger, N.S. Bhavesh, H. Jawhari, I. Grigoriev, F.J. van Rijssel, R.M. Buey, A. Lawera, I. Jelasarov, F.K. Winkler, K. Wuthrich, A. Akhmanova, and M.O. Steinmetz. 2009. An EB1-binding motif acts as a microtubule tip localization signal. *Cell*. 138:366-76.
- Hoogenraad, C.C., A. Akhmanova, N. Galjart, and C.I. De Zeeuw. 2004. LIMK1 and CLIP-115: linking cytoskeletal defects to Williams syndrome. *Bioessays*. 26:141-50.
- Howard, J., and A.A. Hyman. 2009. Growth, fluctuation and switching at microtubule plus ends. *Nat Rev Mol Cell Biol*. 10:569-74.
- Kakinuma, N., and R. Kiyama. 2009. A major mutation of KIF21A associated with congenital fibrosis of the extraocular muscles type 1 (CFEOM1) enhances translocation of Kank1 to the membrane. *Biochem Biophys Res Commun*. 386:639-44.
- Kakinuma, N., Y. Zhu, Y. Wang, B.C. Roy, and R. Kiyama. 2009. Kank proteins: structure, functions and diseases. *Cell Mol Life Sci*. 66:2651-9.
- Kinoshita, K., T.L. Noetzel, L. Pelletier, K. Mechtler, D.N. Drechsel, A. Schwager, M. Lee, J.W. Raff, and A.A. Hyman. 2005. Aurora A phosphorylation of TACC3/maskin is required for centrosome-dependent microtubule assembly in mitosis. *J Cell Biol*. 170:1047-55.
- Komarova, Y., C.O. De Groot, I. Grigoriev, S.M. Gouveia, E.L. Munteanu, J.M. Schober, S. Honnappa, R.M. Buey, C.C. Hoogenraad, M. Dogterom, G.G. Borisy, M.O. Steinmetz, and A. Akhmanova. 2009. Mammalian end binding proteins control persistent microtubule growth. *J Cell Biol*. 184:691-706.
- Komarova, Y., G. Lansbergen, N. Galjart, F. Grosveld, G.G. Borisy, and A. Akhmanova. 2005. EB1 and EB3 control CLIP dissociation from the ends of growing microtubules. *Mol Biol Cell*. 16:5334-45.
- Kosturko, L.D., M.J. Maggipinto, C. D'Sa, J.H. Carson, and E. Barbarese. 2005. The microtubule-associated protein tumor overexpressed gene binds to the RNA trafficking protein heterogeneous nuclear ribonucleoprotein A2. *Mol Biol Cell*. 16:1938-47.
- Kronja, I., A. Kruljac-Letic, M. Caudron-Herger, P. Bieling, and E. Karsenti. 2009. XMAP215-EB1 interaction is required for proper spindle assembly and chromosome segregation in *Xenopus* egg extract. *Mol Biol Cell*. 20:2684-96.
- Lansbergen, G., I. Grigoriev, Y. Mimori-Kiyosue, T. Ohtsuka, S. Higa, I. Kitajima, J. Demmers, N. Galjart, A.B. Houtsmuller, F. Grosveld, and A. Akhmanova. 2006. CLASPs attach microtubule plus ends to the cell cortex through a complex with L15beta. *Dev Cell*. 11:21-32.
- Lansbergen, G., Y. Komarova, M. Modesti, C. Wyman, C.C. Hoogenraad, H.V. Goodson, R.P. Lemaitre, D.N. Drechsel, E. van Munster, T.W. Gadella, Jr., F. Grosveld, N. Galjart, G.G. Borisy, and A. Akhmanova. 2004. Conformational changes in CLIP-170 regulate its binding to microtubules and dynactin localization. *J Cell Biol*. 166:1003-14.
- Larsson, N., H. Melander, U. Marklund, O. Osterman, and M. Gullberg. 1995. G2/M transition requires multisite phosphorylation of oncoprotein 18 by two distinct protein kinase systems. *J Biol Chem*. 270:14175-83.
- Lee, H., U. Engel, J. Rusch, S. Scherrer, K. Sheard, and D. Van Vactor. 2004. The microtubule plus end tracking protein Orbit/MAST/CLASP acts downstream of the tyrosine kinase Abl in mediating axon guidance. *Neuron*. 42:913-26.
- Lee, H.S., Y.A. Komarova, E.S. Nadezhkina, R. Anjum, J.G. Peloquin, J.M. Schober, O. Danciu, J. van Haren, N. Galjart, S.P. Gygi, A. Akhmanova, and G.G. Borisy. 2010. Phosphorylation controls autoinhibition of cytoplasmic linker protein-170. *Mol*

- Biol Cell. 21:2661-73.
- Lee, M.J., F. Gergely, K. Jeffers, S.Y. Peak-Chew, and J.W. Raff. 2001. Msps/XMAP215 interacts with the centrosomal protein D-TACC to regulate microtubule behaviour. *Nat Cell Biol.* 3:643-9.
- Li, H., X.S. Liu, X. Yang, Y. Wang, Y. Wang, J.R. Turner, and X. Liu. 2010. Phosphorylation of CLIP-170 by Plk1 and CK2 promotes timely formation of kinetochore-microtubule attachments. *Embo J.* 29:2953-65.
- Lim, J., and K.P. Lu. 2005. Pinning down phosphorylated tau and tauopathies. *Biochim Biophys Acta.* 1739:311-22.
- Matic, I., M. van Hagen, J. Schimmel, B. Macek, S.C. Ogg, M.H. Tatham, R.T. Hay, A.I. Lamond, M. Mann, and A.C. Vertegaal. 2008. In vivo identification of human small ubiquitin-like modifier polymerization sites by high accuracy mass spectrometry and an in vitro to in vivo strategy. *Mol Cell Proteomics.* 7:132-44.
- Mimori-Kiyosue, Y., I. Grigoriev, G. Lansbergen, H. Sasaki, C. Matsui, F. Severin, N. Galjart, F. Grosveld, I. Vorobjev, S. Tsukita, and A. Akhmanova. 2005. CLASP1 and CLASP2 bind to EB1 and regulate microtubule plus-end dynamics at the cell cortex. *J Cell Biol.* 168:141-53.
- Neukirchen, D., and F. Bradke. 2011. Cytoplasmic Linker Proteins Regulate Neuronal Polarization through Microtubule and Growth Cone Dynamics. *J Neurosci.* 31:1528-38.
- Niethammer, P., I. Kronja, S. Kandels-Lewis, S. Rybina, P. Bastiaens, and E. Karsenti. 2007. Discrete states of a protein interaction network govern interphase and mitotic microtubule dynamics. *PLoS Biol.* 5:e29.
- Peset, I., and I. Vernos. 2008. The TACC proteins: TACC-ling microtubule dynamics and centrosome function. *Trends Cell Biol.* 18:379-88.
- Peterson, E.A., and E.M. Petty. 2010. Conquering the complex world of human septins: implications for health and disease. *Clin Genet.* 77:511-24.
- Picone, R., X. Ren, K.D. Ivanovitch, J.D. Clarke, R.A. McKendry, and B. Baum. 2010. A polarised population of dynamic microtubules mediates homeostatic length control in animal cells. *PLoS Biol.* 8:e1000542.
- Popov, A.V., A. Pozniakovskiy, I. Arnal, C. Antony, A.J. Ashford, K. Kinoshita, R. Tournebise, A.A. Hyman, and E. Karsenti. 2001. XMAP215 regulates microtubule dynamics through two distinct domains. *Embo J.* 20:397-410.
- Poulain, F.E., and A. Sobel. 2010. The microtubule network and neuronal morphogenesis: Dynamic and coordinated orchestration through multiple players. *Mol Cell Neurosci.* 43:15-32.
- Rehberg, M., and R. Graf. 2002. Dictyostelium EB1 is a genuine centrosomal component required for proper spindle formation. *Mol Biol Cell.* 13:2301-10.
- Romet-Lemonne, G., M. VanDuijn, and M. Dogterom. 2005. Three-dimensional control of protein patterning in microfabricated devices. *Nano Lett.* 5:2350-4.
- Saxton, W.M., D.L. Stemple, R.J. Leslie, E.D. Salmon, M. Zavortink, and J.R. McIntosh. 1984. Tubulin dynamics in cultured mammalian cells. *J Cell Biol.* 99:2175-86.
- Schuyler, S.C., and D. Pellman. 2001. Microtubule "plus-end-tracking proteins": The end is just the beginning. *Cell.* 105:421-4.
- Senda, T., A. Shimomura, and A. Iizuka-Kogo. 2005. Adenomatous polyposis coli (Apc) tumor suppressor gene as a multifunctional gene. *Anat Sci Int.* 80:121-31.
- Serra-Pages, C., Q.G. Medley, M. Tang, A. Hart, and M. Streuli. 1998. Liprins, a family of LAR transmembrane protein-tyrosine phosphatase-interacting proteins. *J Biol Chem.* 273:15611-20.
- Spiliotis, E.T. 2010. Regulation of microtubule organization and functions by septin GTPases. *Cytoskeleton (Hoboken).* 67:339-45.
- Stepanova, T., I. Smal, J. van Haren, U. Akinci, Z. Liu, M. Miedema, R. Limpens, M. van Ham, M. van der Reijden, R. Poot, F. Grosveld, M. Mommaas, E. Meijering, and N. Galjart. 2010. History-dependent catastrophes regulate axonal microtubule behavior. *Curr Biol.* 20:1023-8.
- Tischfield, M.A., H.N. Baris, C. Wu, G. Rudolph, L. Van Maldergem, W. He, W.M. Chan, C. Andrews, J.L. Demer, R.L. Robertson, D.A. Mackey, J.B. Ruddle, T.D. Bird, I. Gottlob, C. Pieh, E.I. Traboulsi, S.L. Pomeroy, D.G. Hunter, J.S. Soul, A. Newlin, L.J. Sabol, E.J. Doherty, C.E. de Uzategui, N. de Uzategui, M.L. Collins, E.C. Sener, B. Wabbels, H. Hellebrand, T. Meitinger, T. de Berardinis, A. Magli, C. Schiavi, M. Pastore-Trossello, F. Koc, A.M. Wong, A.V. Levin, M.T. Geraghty, M. Descartes, M. Flaherty, R.V. Jamieson, H.U. Moller, I. Meuthen, D.F. Callen, J. Kerwin, S. Lindsay, A. Meindl, M.L. Gupta, Jr., D. Pellman, and E.C. Engle. 2010. Human TUBB3 mutations perturb microtubule dynamics, kinesin interactions, and axon guidance. *Cell.* 140:74-87.
- Trinczek, B., J. Biernat, K. Baumann, E.M. Mandelkow, and E. Mandelkow. 1995. Domains of tau protein, differential phosphorylation, and dynamic instability of microtubules. *Mol Biol Cell.* 6:1887-902.
- Tsujita, K., T. Itoh, A. Kondo, M. Oyama, H. Kozuka-Hata, Y. Irino, J. Hasegawa, and T. Takenawa. 2010. Proteome of acidic phospholipid-binding proteins: spatial and temporal regulation of Coronin 1A by phosphoinositides. *J Biol Chem.* 285:6781-9.
- Vasquez, R.J., D.L. Gard, and L. Cassimeris. 1999. Phosphorylation by CDK1 regulates XMAP215 function in vitro. *Cell Motil Cytoskeleton.* 43:310-21.
- Wittmann, T., A. Hyman, and A. Desai. 2001. The spindle: a dynamic assembly of microtubules and motors. *Nat Cell Biol.* 3:E28-34.
- Wolyniak, M.J., K. Blake-Hodek, K. Kosco, E. Hwang, L. You, and T.C. Huffaker. 2006. The regulation of microtubule dynamics

in *Saccharomyces cerevisiae* by three interacting plus-end tracking proteins. *Mol Biol Cell*. 17:2789-98.

Yang, X., H. Li, X.S. Liu, A. Deng, and X. Liu. 2009. Cdc2-mediated phosphorylation of CLIP-170 is essential for its inhibition of centrosome reduplication. *J Biol Chem*. 284:28775-82.

Zhang, D., K.D. Grode, S.F. Stewman, J.D. Diaz-Valencia, E. Liebling, U. Rath, T. Riera, J.D. Currie, D.W. Buster, A.B. Asenjo, H.J. Sosa, J.L. Ross, A. Ma, S.L. Rogers, and D.J. Sharp. 2011. *Drosophila* katanin is a microtubule depolymerase that regulates cortical-microtubule plus-end interactions and cell migration. *Nat Cell Biol*.





# Summary





## Summary

Microtubules are highly dynamic polarized tubular structures that assemble into a cytoskeletal network. This network plays a pivotal role in all eukaryotic cells; it is involved in the establishment and maintenance of the cell shape, separation of chromosomes during mitosis and the distribution of intracellular organelles and vesicles. Regulation of microtubule dynamics is mediated by the association of a distinct group of microtubule associated proteins with the plus ends of growing microtubules. These proteins are called plus-end tracking proteins or +TIPs.

EB proteins are autonomous plus-end tracking proteins that form the core subunits of the +TIP network. To identify new proteins that interact with microtubule tips, we made use of the unique ability of EBs to bind to practically all known +TIPs. Using biochemical approaches combined with mass spectrometry analysis, we have identified many novel EB interaction partners, two of which were investigated in detail in this thesis.

In **chapter 2** we focus on the identification of Stromal Interaction Molecule 1 (STIM1) as a new EB-binding protein and a +TIP. Interestingly, STIM1 is the first transmembrane protein shown to track growing MT plus-ends. The behavior of STIM1 is regulated by  $\text{Ca}^{2+}$  levels in the endoplasmic reticulum (ER). Using its cytoplasmic SxIP-motif, STIM1 directly interacts with EBs at the tips of polymerizing MTs that come into close proximity with the ER network. The overexpression of STIM1 has a strong effect on the extension of the ER through the “tip attachment complex” mechanism, whereby an ER tubule elongates together with the end of a growing microtubule. When  $\text{Ca}^{2+}$  is released from the ER, STIM1 oligomerizes and its plus-end tracking behavior is abrogated. We propose that the EB-STIM1 interaction plays an important role in the remodeling of the ER and that it might participate in regulation of  $\text{Ca}^{2+}$  signaling.

In **chapter 3** we discuss the identification and characterization of the two vertebrate +TIPs SLAIN1 and SLAIN2. We show that the plus-end tracking behaviour of SLAIN2 depends on EBs and is mediated by the SLAIN2 C-terminus, which contains several SxIP-like motifs surrounded by serines, prolines and basic residues. In addition, SLAIN2 also binds to CLASPs and CLIPs. SLAIN2 uses its C-terminal tyrosine and tryptophan residues to interact with the CAP-Gly domains of CLIPs but not p150<sup>Glued</sup>. Through its N-terminus, SLAIN2 interacts with ch-TOG, the mammalian homologue of the microtubule polymerase XMAP215. In interphase, SLAIN2 links ch-TOG to EBs and this triple complex promotes persistent microtubule growth by inhibiting catastrophes. Surprisingly, whereas ch-TOG knockdown causes severe mitotic defects, this is not the case in SLAIN2-depleted cells. During mitosis, SLAIN2 is hyperphosphorylated by CDK1 and other kinases, and its association with EBs and ch-TOG is disrupted. Dissociation of the triple EB-SLAIN-ch-TOG complex in mitosis can contribute to the dramatic increase in microtubule catastrophe frequency observed during mitotic entry. In addition, SLAINs act as ‘adhesive +TIP factors’ that enhance +TIP interactions and promote +TIP access to the microtubule ends.

In **chapter 4** we continue the analysis of the EB-SLAIN-ch-TOG complex, but this time in primary cultures of rat hippocampal neuron. Reverse transcriptase polymerase chain reaction and Western blot analysis showed high levels of ch-TOG, SLAIN1 and SLAIN2 in brain throughout

development. Disruption of the SLAIN-ch-TOG complex in neuronal cells by knockdown or dominant negative approaches affects microtubule dynamics similar to multiple cell lines. We show that the SLAIN-ch-TOG complex is involved in neurite extension providing new insights into the regulation of microtubule dynamics in neuronal cells and the role of microtubule dynamics in neuritogenesis.

In the second part of this thesis, we use biochemical approaches and mass spectrometry analysis to dissect the protein complex involved in the regulation of cortical microtubule dynamics and attachment of microtubule tips to the plasma membrane. Our findings provide insight into how the components of cortical microtubule attachment complex are assembled into a network and elucidate the role they fulfill in the local regulation of microtubule dynamics.

In **chapter 5** we identify liprin- $\alpha$ 1 and liprin- $\beta$ 1 as upstream interaction partners of ELKS and LL5 $\beta$ . We show that liprin proteins are important factors for the cortical organization of ELKS and LL5 $\beta$  and they are involved in regulating microtubule attachment and stability. In addition, liprin- $\alpha$ 1/ $\beta$ 1 indirectly associate with KIF21A, a member of the kinesin-4 family. KIF21A localizes to the cell cortex through the binding of its coiled-coil region to the actin remodeling protein KANK2, which in turn interacts with liprin- $\beta$ 1. Depletion of KIF21A by RNA-interference in HeLa cells resulted in increased microtubule density at the cell cortex and microtubule growth parallel to the plasma membrane. We hypothesize that KIF21A controls cortical microtubule dynamics by inhibiting microtubule polymerization. Our findings provide new insights into the molecular basis of congenial fibrosis of the extraocular muscle type I (CFEOM1) syndrome which is linked to heterozygous mutations in the coiled-coil region of KIF21A.

Finally, in **chapter 6** we discuss the experimental data presented in chapters 2 through 5 and provide an outlook on the future directions in the field of microtubule dynamics.





# Samenvatting





## Samenvatting

Microtubuli zijn zeer dynamische polaire buisjes die assembleren tot een cytoskelet netwerk. Dit netwerk speelt een cruciale rol in eukaryotische cellen; het is betrokken bij de formatie en in stand houding van de celvorm, het separeren van chromosomen tijdens de mitosis en de distributie van intracellulaire organellen en blaasjes. Regulatie van microtubuli dynamiek is afhankelijk van de associatie van een aparte groep van microtubuli geassocieerde eiwitten met de plus uiteinden van groeiende microtubuli. Deze eiwitten worden plus-uiteinde bindende eiwitten of +TIPs genoemd.

EB eiwitten zijn autonome plus-uiteinde bindende eiwitten die de kern onderdelen vormen van het +TIP netwerk. Om nieuwe eiwitten te identificeren die een interactie aangaan met de microtubuli uiteinden, hebben we gebruik gemaakt van de unieke eigenschap van EB eiwitten om aan praktisch alle +TIPs te binden. Door het gebruik van biochemische methoden in combinatie met massa spectrometrie analyse hebben we veel nieuwe EB interactie partners geïdentificeerd, waarvan er twee in detail worden bestudeerd in dit proefschrift.

In **hoofdstuk 2** richten wij ons op de identificatie van Stromal Interaction Molecule 1 (STIM1) als nieuw EB-bindend eiwit en een +TIP. Opvallend genoeg is STIM1 het eerste transmembraan eiwit waarvan aangetoond wordt dat het aan groeiende microtubuli plus-uiteinden bindt. Het gedrag van STIM1 wordt gereguleerd door  $Ca^{2+}$  niveau's in het endoplasmatisch reticulum (ER). STIM1 bindt met zijn cytoplasmatische SxIP-motief direct aan EBs die zich aan de uiteinden van polymeriserende microtubuli bevinden die in de nabijheid van het ER netwerk komen. De overexpressie van STIM1 heeft een sterk effect op de extensie van het ER door een "tip attachment complex" mechanisme, waarbij ER buisjes samen met groeiende microtubuli wordt verlengd. Wanneer  $Ca^{2+}$  vrijkomt uit het ER vormt STIM1 oligomeren en wordt zijn plus-uiteinde bindende gedrag verstoord. Wij stellen voor dat EB-STIM interactie een belangrijke rol speelt in het hervormen van het ER en dat het betrokken zou kunnen zijn bij de regulatie van  $Ca^{2+}$  signalering.

In **hoofdstuk 3** bediscussiëren we de karakterisatie van de twee vertebraten +TIPs SLAIN1 en SLAIN2. We laten zien dat het plus-uiteinde bindende gedrag van SLAIN2 afhangt van EBs en de SLAIN2 C-terminus, welke meerdere SxIP-achtige motieven heeft omgeven door serines, prolines en basische residuen. Daarnaast bindt SLAIN2 ook aan CLASPs en CLIPs. SLAIN2 gebruikt hiervoor zijn C-terminale tyrosine en tryptofaan residuen om aan de CAP-Gly domeinen van CLIPs, maar niet die van p150<sup>Glued</sup>, te binden. SLAIN2 gebruikt zijn N-terminus om een interactie aan te gaan met ch-TOG, de zoogdier homoloog van de microtubuli polymerase XMAP215. In interfase cellen, verbindt SLAIN2 ch-TOG aan EBs en dit trio complex zet aan tot persistente microtubuli groei door catastrofes te inhiberen. Verbazingwekkend genoeg resulteert SLAIN2 depletie uit cellen niet in ernstige mitotische defecten, terwijl dat wel het geval is in ch-TOG knockdown cellen. Tijdens de mitose wordt SLAIN2 sterk gefosforyleerd door CDK1 en andere kinases waardoor de interactie met EBs en ch-TOG wordt verbroken. Verbreken van het EB-SLAIN-ch-TOG complex in mitose kan bijdragen aan de dramatische toename in microtubuli catastrofe frequentie geobserveerd tijdens

intrede in mitose. Daarnaast werken SLAINs als “adhesie +TIP factoren” die de onderlinge +TIP interacties verhogen alsmede de toegang tot microtubuli uiteinden.

In **hoofdstuk 4** vervolgen we de analyse van het EB-SLAIN-ch-TOG complex, maar deze keer gebruiken wij primaire cultures van hippocampale ratten neuronen. Reverse transcriptase polymerase chain reaction en Western blot analyse laten hoge ch-TOG, SLAIN1 en SLAIN2 niveau's zien gedurende hersenontwikkeling. Verbreken van het SLAIN-ch-TOG complex in neuronale cellen door knockdown of dominant negatieve aanpak, verstoort microtubuli dynamiek in dezelfde mate als in verschillende cellijnen. We laten zien dat het SLAIN-ch-TOG complex betrokken is bij neuriten uitgroei en dit geeft nieuwe inzichten in de regulatie van microtubuli dynamiek in neuronale cellen evenals de rol van microtubuli dynamiek in neuritogenese.

In het tweede deel van dit proefschrift gebruiken wij biochemische middelen en massa spectrometrie analyse om de eiwitcomplexen te ontleden die betrokken zijn bij de regulatie van corticale microtubuli dynamiek en het koppelen van microtubuli uiteinden aan het plasma membraan. Onze bevindingen geven nieuw inzicht in hoe de componenten van het corticale microtubuli koppel complex tot een netwerk worden gevormd en het verheldert de rol die zij vervullen in de lokale regulatie van microtubuli dynamiek.

In **hoofdstuk 5** identificeren wij liprin- $\alpha$ 1 en liprin- $\beta$ 1 als interactie partners van ELKS en LL5 $\beta$ . Wij laten zien dat liprin eiwitten belangrijke factoren zijn voor de corticale organisatie van ELKS en LL5 $\beta$  en dat ze betrokken zijn bij de regulatie van de koppeling en stabiliteit van microtubuli. Daarnaast, associëren liprin eiwitten indirect met KIF21A, een lid van de kinesine-4 familie. KIF21A lokaliseert aan de cel cortex door de binding van zijn coiled-coil regio met het actine modulator eiwit KANK2, die op zijn beurt een interactie aan gaat met liprin- $\beta$ 1. Depletie van KIF21 door RNA-interferentie in HeLa cellen resulteert in de toename van microtubuli dichtheid aan de cel cortex en groei van microtubuli parallel aan het plasma membraan. Onze hypothese luidt dat KIF21A corticale microtubuli dynamiek reguleert door de inhibitie van microtubuli polymerisatie. Onze bevindingen geven nieuwe inzichten in de moleculaire basis van congeniale fibrose van de extraoculaire spieren type 1 (CFEOM1) syndroom dat gekoppeld is aan heterozygote mutaties in de coiled-coil regio van KIF21A.

Tenslotte bediscussiëren we in **hoofdstuk 6** de experimentele data zoals die gepresenteerd zijn in hoofdstukken 2 tot en met 5 en blikken we vooruit naar de toekomst van het microtubuli dynamiek veld.



# Portfolio







<p><b>International conferences</b></p> <ul style="list-style-type: none"> <li>- Marie Curie Research Institute (MCRI) Microtubule Dynamics Workshop, Oxted, UK (poster)</li> <li>- ASCB 48<sup>th</sup> annual meeting, San Francisco, USA (poster)</li> <li>- Mechanisms of cytoskeleton dynamics and intracellular trafficking, Warschaw, Poland (oral)</li> <li>- ASCB 50<sup>th</sup> annual meeting, Philadelphia, USA (poster)</li> </ul>	<p>May 2008</p> <p>December 2008</p> <p>October 2010</p> <p>December 2010</p>
<p><b>Seminars and workshops</b></p> <ul style="list-style-type: none"> <li>- 14<sup>th</sup> Medical Genetics Center (MGC) Graduate Student Workshop, Maastricht, The Netherlands (poster)</li> <li>- 15<sup>th</sup> MGC Graduate Student Workshop, Heidelberg, Germany (poster)</li> <li>- 16<sup>th</sup> MGC Graduate Student Workshop, Brugge, Belgium (oral)</li> <li>- 1<sup>st</sup> Intercity Young Scientist Meeting, Heemskerk, The Netherlands (oral)</li> <li>- 17<sup>th</sup> MGC Graduate Student Workshop, Cologne, Germany (oral)</li> </ul>	<p>May 2007</p> <p>June 2008</p> <p>June 2009</p> <p>November 2009</p> <p>June 201</p>
<p><b>Teaching</b></p> <ul style="list-style-type: none"> <li>- High school students participating in the Junior Science Programme</li> <li>- Master student</li> </ul>	<p>Two times one week</p> <p>January 2010</p>





# Curriculum Vitae





## Curriculum Vitae

### *Personal information*

Name: Babet van der Vaart

Born: 22 November 1982, Vlaardingen, The Netherlands

### *Education*

- 2007-present: PhD student, Department of Cell Biology, Erasmus MC, Rotterdam, The Netherlands
- 2004-2006: Master Developmental Biology and Biomedical genetics, University Utrecht, The Netherlands
- 2001-2004: Bachelor Biology, University Utrecht, Utrecht, The Netherlands
- 2002: Propedeuse Biology, University Utrecht, Utrecht, The Netherlands
- 1995-2001: Pre University Education, Christelijke Scholengemeenschap Aquamarijn afd. Groen van Prinsterer, Vlaardingen, The Netherlands





# Publications





**List of publications**

**van der Vaart B**, Manatschal C, Grigoriev I, Olieric V, Montenegro Gouveia S, Bjelić S, Demmers J, Vorobjev I, Hoogenraad CC, Steinmetz MO, Akhmanova A. SLAIN2 links microtubule plus-end tracking proteins and controls microtubule growth in interphase. *J Cell Biol.* 2011

Tanenbaum ME, Macurek L, **van der Vaart B**, Galli M, Akhmanova A, Medema RH. The kinesin-8 Kif18b acts together with MCAK to spatially and temporally control microtubule dynamics during cell division. *Submitted*

**van der Vaart B**, Akhmanova A, Straube A. (2009). Regulation of microtubule dynamic instability. *Biochem Soc Trans.* 2009 Oct;37(Pt 5):1007-13. Review.

Grigoriev I, Gouveia SM, **van der Vaart B**, Demmers J, Smyth JT, Honnappa S, Splinter D, Steinmetz MO, Putney JW Jr, Hoogenraad CC, Akhmanova A. (2008). STIM1 is a MT-plus-end-tracking protein involved in remodeling of the ER. *Curr Biol.* 18(3):177-82

Hajdo-Milasinović A, Ellenbroek SI, van Es S, **van der Vaart B**, Collard JG. (2007). Rac1 and Rac3 have opposing functions in cell adhesion and differentiation of neuronal cells. *J Cell Sci.* 2007 120(Pt 4):555-66.







Dankwoord





## Dankwoord

Toen ik bijna vier en een half jaar geleden begon in Anna's lab had ik nooit kunnen denken dat de tijd zo snel voorbij zou gaan. De afgelopen jaren heb ik heel veel geleerd, plezier gehad en typische aio frustraties ervaren. Ik ben mijn dank verschuldigd aan veel mensen die hebben bijgedragen aan mijn onderzoek dat uiteindelijk heeft geleid tot het tot stand komen van dit promotieboekje.

Als eerste wil ik graag mijn promotor Frank Grosveld bedanken voor de mogelijkheid om te promoveren in zijn fantastische departement. Tevens wil ik hem bedanken voor zijn vragen tijdens de werkbesprekingen die mij aanzette nog kritischer naar mijn eigen werk te kijken.

Mijn grootste dank gaat uit naar mijn mentor en tweede promotor Anna Akhmanova. Anna, ik wil je bedanken voor je goede begeleiding; niet alleen heb je me geleerd een wetenschappelijk experiment te ontwerpen, maar ook leerde je mij de technische snuffjes van goed labwerk en het daarna interpreteren van de resultaten. Ik herinner mij nog goed de eerste cel kleuring die ik gedaan heb onder jouw begeleiding en hoe je me hebt geholpen met het draaien van mijn eerste Western blots. Daarna zouden er nog vele volgen, sommige meer succesvol dan anderen... Ik ben je ook dankbaar voor je bereidheid om altijd naar mijn resultaten te kijken wanneer ik bij je langskwam als ik weer "iets leuks" had ontdekt. Daarnaast heb je mij ook helpen ontwikkelen op persoonlijk vlak door al je wijze levenslessen. Ik ben trots dat ik je eerste student mag zijn die promoveert met jou als promotor en ik wens je veel succes in Utrecht!

Ik ben ook Casper zeer dankbaar voor de afgelopen jaren. Je hebt me geleerd om kritisch te zijn over mijn eigen werk, maar ook standvastig te zijn in mijn conclusies en deze te verdedigen tijdens wetenschappelijke discussies. Ook wil ik je bedanken voor de mogelijkheid om te werken met de primaire neuron culturen die je zo succesvol hebt lopen in jouw lab. Hoewel het niet mijn favoriete bezigheid was, heb ik extra waardering gekregen voor jouw werk omdat ik heb gemerkt dat het knap lastige experimenten zijn! Bedankt dat je in mijn promotiecommissie wilt plaatsnemen en ik wens ook jou het allerbeste in Utrecht.

I would like to extend my gratitude to the other members of my promotion committee; Niels, Dies, Gert, René, Marcel and Michel. Niels, bedankt voor je vragen tijdens de werkbesprekingen en dat je in mijn leescommissie plaats wilde nemen. René en Marcel, bedankt dat jullie bereid zijn om naar Rotterdam te komen voor mijn promotie. Ook bedankt René en Marvin voor het sturen van verschillende siRNAs en inhibitors die ik in mijn onderzoek heb gebruikt. Special thanks to Michel for coming all the way from Switzerland for my promotion and being so kind to correct the first draft of my thesis. Michel; you introduced me into the interesting field of structural biology. I am very grateful for our nice collaborations and all the work that you and your lab performed to make the SLAIN-story even bigger and better. I wish to especially thank you, Cristina, for all your efforts and good work! I also enjoyed meeting you in person in Heidelberg and I hope we will meet again in future! To get the SLAIN-paper published was not easy and straightforward, but Michel, your kind emails after another rejection eased the pain a little and just as you said, everything turned out well in the end with the acceptance of the paper!

I also owe a big "thank you" to Anne Straub. We first met in Oxted at a great microtubule

meeting that you helped organize. This was my first big meeting and it was a fantastic experience for me; it really increased my enthusiasm for the microtubule-field. Since then we met on several occasions where we discussed the progressions of our research. You helped me a lot in my first writing experiences, which has led to a great review that I have used as the introduction of my thesis.

No PhD can be successful without the support and help of your lab-members. The core of the Akhmanova-lab, for me, will always consist of Ilya, Daniel, Susana and Carol with which I have spent most of my time. Ilya, thanks for your work on the live cell imaging and all the analysis on microtubule dynamics. You make it seem so effortless, which I know it is not! I also enjoyed the “borrels” we visited together as well as your (sometimes) weird e-mails and chats in the lab. Daniël; je bent al weer een tijdje weg, maar nog lang niet vergeten! Ik mis je nog steeds af en toe, vooral je vrolijkheid, onze gezamenlijke lunches (soms onverwachts buitenshuis), je unieke vaardigheid wat betreft het vinden van een bepaald “zeldzaam” voorwerp, maar vooral je klusvaardigheden als er iets stuk was of als ik iets stoms had gedaan en je mij uit de brand moest helpen (was er niet eens een bucket die vast zat in de rotor?). Dear Susana, you are truly unique and a very special person to me. Your help to me was not so much in terms of technical lab stuff, after all you are still an *in vitro*-girl and I am not (yet), but you mostly helped me to develop as a person. I am very thankful for all the (dinner) parties, trips and meetings you organized or attended with me. Particularly our trip to the ASCB in San Francisco was great! I also enjoyed my visit to Portugal together with Rick and Phebe where you showed us the beautiful spots of Porto and Lisbon. I will come back soon to visit you in Lisbon! I wish you all the best with your future work and all your world explorations! Carol; you were my neighbour for many years and at one point my only neighbour when we were together in Ee1063 when the rest of the lab had already moved to Ee1075. Thank you for your support and willingness to listen to all my lab frustrations or successes. I also appreciate all your efforts to organize the lab which I think you are quite successful at although it's never finished (I see new notes appearing every day)! Good luck in the last part of your promotion!

Also many thanks to the other (former) lab members of the Akhmanova-lab; Wim, Rick, Gert-Jan, Andrea, Renu, Kai, Benjamin and Kris. Andrea, thanks for the nice chats we had. You are very talented and motivated so don't worry so much and I am sure you are also going to be fine in Utrecht! Renu, thank you for your help with the MT pelleting assay; the centrifuge still scares me a bit...; Kai, I am amazed by your hard work and the great amount of success you have already achieved in such a short time in the lab. Thank you for your advice to improve my research and good luck with your own! Ben, thanks for taking over part of my research and all your jokes! Finally, Kris; thanks for your fun chats, discussions and organizing a barbeque with me. I am happy that you stayed true to your promise that I would see you around a lot in spite of your move to Niels' lab. All the best to you!

Daarnaast wil ik graag alle huidige en oud leden van de 12de bedanken voor de gezellige meetings, feestjes, weekendjes weg, etentjes, verjaardagen, etc.; Dick, Phebe, Marijn, Max, Myrre, Nanda, Esther, Kah Wai, Karin, Lukas, Vera, Robert, Marta, Mariella, Bjorn, Alexander,

Linde, Eva en Samantha. Jullie hebben me echt een beetje geadopteerd in het Casper-lab! Speciale dank gaat zeker ook uit naar Henk en Chris voor het nog gezelliger maken van de verschillende activiteiten (memorabele autoritten, zeiltochten en grot mountainbikeen).

Phebe en Marijn, onder het mom van een gezond avondje sporten, ging het ons natuurlijk ook om het gezellige kletsen in de kleedkamer! Over de onderwerpen van onze gesprekken werd sterk gespeculeerd door de squash-mannen, maar wat er in de kleedkamer wordt besproken, blijft in the kleedkamer, toch? Marijn, ik vond het altijd leuk om met je terug naar huis te fietsen na het werk of een feestje. Phebe, bedankt dat je er aan dacht me uit te nodigen als er iets werd georganiseerd met het Casper-lab. Ik heb ook goede herinneringen aan mijn trip met jou en Rick naar Portugal. Heel erg bedankt dat je mijn paranimf wilt zijn. Jij gaat nu ook een grote verandering tegemoet met het vertrek van het lab naar Utrecht en dat is niet altijd makkelijk voor jou, maar ik weet zeker dat het allemaal goed komt! Veel succes daar en ik zal je zeker missen!

Daarnaast wil ik ook Max, Nanda, Dick en Mariella bedanken voor hun hulp bij de verschillende neuron-gerelateerde proeven (kwantificaties, transfecties, confocal microscopie en live cell imaging). Volgende stap is het neuron-SLAIN paper gepubliceerd krijgen! Myrre en Karin, bedankt dat jullie mijn kamergenootjes waren op verschillende meetings. Ik vond het erg gezellig om (tot 's nachts laat) met jullie te kletsen over van alles en nog wat. Myrre, veel succes met de laatste loodjes en jij gaat zeker een mooi proefschrift afleveren.

Ook wil ik mijn (oud)-lunchgenoten bedanken voor hun goede gezelschap tijdens de gezellige onderbreking in de dag; Rick, Frank Sleutels, Jeffrey ("what's upppp"), Suzanne (nog bedankt dat ik je huisje kon overnemen), Michael, Dave en alle anderen...

Het belopen van een promotietraject wordt gemakkelijker gemaakt door de hulp van verschillende mensen die ik hier ook graag wil bedanken voor hun bijdragen; Jeroen voor zijn massa spectrometrie werk, Elaine en Reinier voor het FACS'en van verschillende cellijnen, Melle en Leo voor alle bestellingen, Martine en Siska voor hun hulp bij de ESC targeting, de secretaresses Marike, Jasperina en Bep, de dames van de spoelkeuken en de computer mannen.

Als laatste wil ik graag mijn familie bedanken voor hun interesse in mijn werk; bedankt oma's, tantes, ooms, neven en nichten. Mijn grootste dank gaat natuurlijk uit naar mijn ouders, Henk en Lisette, mijn broertje Rik en mijn zus Aniek. Pap en mam bedankt dat jullie mij altijd hebben gesteund ookal weten jullie niet zo veel af van het lab werk ("iets met celletjes, toch mam?") en waren jullie wel eens in de war wie nou waar werkte. Gelukkig heb ik jou, Aniek, altijd gehad om meer gedetailleerde problemen of successen betreffende het lab of andere onderwerpen te bespreken. Ik vind het ook heel leuk dat we een paar maandjes echte collega's zijn en ik wens je heel veel plezier en succes bij Gert. Bedankt ook dat je mijn paranimf wilt zijn. Rik, bedankt voor de ritjes naar de metro/huis en dat je het hebt uitgehouden met twee "geleerde" zussen! Ook bedankt voor je alternatieve stellingen, maar ze waren niet echt geschikt!

Dan is nu het moment gekomen om mijn tijd in Rotterdam af te sluiten en verder te gaan met het volgende hoofdstuk in mijn (wetenschappelijk) leven. Ik zal jullie missen....

Babet

